THE UNIVERSITY *of* EDINBURGH

Bridgehead Substituted Scorpionates providing Helically Chiral Complexes

Nicola Louise Bell MChem

A Thesis submitted for the degree of
Doctor of Philosophy
The University of Edinburgh
September 2012

Declaration

I hereby certify that this thesis has been entirely composed by myself and that the work described herein is my own except where clearly mentioned either in acknowledgement, reference or text. It has not been submitted, in whole or in part, for any other degree, diploma or qualification.

Nicola L. Bell

When I heard the learn'd astronomer;

When the proofs, the figures, were ranged in columns before me;

When I was shown the charts and the diagrams, to add, divide, and measure them;

When I, sitting, heard the astronomer, where he lectured with much applause in the lecture-room,

How soon, unaccountable, I became tired and sick;

Till rising and gliding out, I wander'd off by myself,

In the mystical moist night-air, and from time to time,

Look'd up in perfect silence at the stars.

– *Walt Whitman*

Acknowledgements

First and foremost I want to thank Dr. Phil Bailey for taking the chance on me, for encouraging me and giving me the freedom to follow my curiosity and make this project my own. I also want to take the opportunity to thank Dr Murray Low for his invaluable advice as my PhD Scholarship teaching mentor, and to the Department of Chemistry for the award of this scholarship. Special thanks go to Dr. Jason Love and Prof. Polly Arnold for adopting me into their group meetings and outings. All of your support has really made my PhD a wonderful experience.

Everyone whom I have worked with in the department has contributed substantially to this thesis and my enjoyment of my time at Edinburgh. My mean girls: R-Dubz, Iso-Bizzle, Chaz Bono, Anne, Turtle, Sarah and Anne-Fred have all made Lab 34 a fun place to work. I must also acknowledge the contribution of my project students: Li Gim, Denzyl, Kirsteen, Wojciech, Freda, Alison, Hannah and Li Ting for all their hard work. Thanks to Gary, Fraser and Guy for help with crystal structure refinement and Colin for help with electrochemistry. Jen & Tracy ran all my DFT calculations and explained the results to me, so thanks ladies, it really adds to my thesis. Also thanks to Stephen Mansell, who is a fount of knowledge; Aaron, who is crazy; as well as Andrew, Lorna, Nat, James, Emma, Mohammed and Rizwan for all their help along the way.

Francis Keppel famously stated “Education is too important to be left solely to the educators”. This thesis is dedicated, with my upmost gratitude, to all those who have educated me over the years. Firstly my mum, you are superwoman and my inspiration. Thank you for always listening & always understanding. Thank you to the sky & back down! Dad, you give the best

pep talks! Thank you for always telling me I could do anything I wanted, for supporting me when I found what that was and for helping me out with the tough bits of chemistry. I feel very lucky to have the most dedicated and loving stepparents in John & Gail as well as my extraordinary siblings Laura, Dani and Kieran who can always be relied upon to bring a smile to my face. I also want to thank Gran, Pop, Granny, Grandad & my Auntie Sandra; I would never be where I am today without your love, support, encouragement and wisdom. To John and Avyola, for always taking an interest and for giving me your son! Kathryn, Emma, Monica, Laura and Lesley: thank you for listening, for laughing, for drinks and shopping trips. You guys keep me (relatively) sane and I love you!

It is very difficult to articulate the depth of my gratitude to the one person who has been with me through this whole process. Jonny, you have been with me through all the excitement and all the stress, but you always know how to make me smile at the end of each day. Thank you for always challenging me and for encouraging me to challenge the world; for making me food and for learning about chirality for me. If for these reasons alone, I will love you endlessly!

Abstract

Tripodal borate ligands, including Tp and Tm, are some of the most widely used in organometallic chemistry and were originally prepared, as anions, from the reaction of the relevant heterocycle with an alkali metal borohydride. However, an alternate route, allowing access to zwitterionic, charge-neutral, scorpionates was recently developed within the Bailey group using tris(dimethylamino)borane as the boron source.

This thesis describes the expansion of the borane synthetic route to create new, charge-neutral, zwitterionic, tris(methimazolyl)borate (ZTm) ligands containing B-N, B-O and B-C coordinate bonds. Unusual reactivity with isonitrile donors is also presented which has allowed access to boron substituted anionic Tm ligands from the charge-neutral starting material, ($HNMe_2$)ZTm. Attempts to control the helical chirality of ZTm complexes, by using chiral imidazoline donors on the central boron are also described.

The borane synthetic route has allowed access to the novel ligand ZThp, the first example of a tripod based on 2-hydroxypyridine ligand arms. As with Tm, this ligand exhibits helical chirality upon complexation and demonstrates how individual atom hybridisation within the ligand arms affects the helicity and thus the chirality of flexible scorpionate ligands.

Coordination studies of both zwitterionic and boron-substituted anionic Tm ligands have shown a tendency for the formation of 'sandwich' complexes of the form L_2M with some metal precursors, whilst the formation of the corresponding 'half-sandwich' complexes of these ligands with ruthenium and rhodium was found to be disfavoured.

Abbreviations

2-^{i}Bu	2-*Iso*-butyl
Ar, ar	Aromatic
b.p.	Boiling point
Bn	Benzyl
Br	Broad
BuLi	Butyl Lithium
COD	1,5-Cyclooctadiene
Cp	Cyclopentadiene
d	Doublet
D	Lewis base donor
d.e.	Diastereomeric excess
d.r.	Diastereomeric ratio
DABCO	1,4-Diazabicyclo[2.2.2]octane
DBU	1,8-Diazabicyclo[5.4.0]undec-7-ene
DCM	Dichloromethane
DFT	Density functional theory
DMAP	*N,N*-Dimethylaminopyridine
DMF	Dimethylformamide
DMSO	Dimethylsulfoxide
e.e.	Enantiomeric excess
EI	Electron ionisation
ESI	Electrospray ionisation
Et	Ethyl
Et_2O	Diethylether
F*ac*	Facially capping
Fc	Ferrocene
Fc^{+}	Ferrocinium
HOMO	Highest fully occupied molecular orbital
Hz	Hertz
^{i}Pr	*Iso*-propyl, 2-propyl
IR	Infra-Red
J	Spin-spin coupling constant
kJ mol^{-1}	Kilojoules per mole
LUMO	Lowest unoccupied molecular orbital

m	Multiplet
M	Molar (mol^{-1})
Me	Methyl
Methimazole	2-Nercapto-1-methylimidazole
mmol	Millimoles (x 10^{-3} mol)
mt	Methimazole, 2-mercapto-1-methylimidazole
mV	Millivolts
mV/s	Millivolts per second
*n*Bu	*n*-Butyl
N-MeImid	N-Methylimidazole
NMI	N-Methylimidazole
NMR	Nuclear magnetic resonance
p	Para
p-cymene	*Para*-cymene, 1-methyl-4-iso-propylbenzene
Ph	Phenyl
ppm	Parts per million
q	Quartet
rac	Racemic
s	Singlet
SOMO	Singly occupied molecular orbital
t	Triplet
Tai	Hydrotris(7-azindolyl)borate
^{t}Bu	*Tert*-butyl
THF	Tetrahydrofuran
Tio	Hydrotris(imidazole-2-onyl)borate
Tm	Hydrotris(methimazolyl)borate
TMEDA	*N*,*N*,N'N'-Tetramethylethylenediamine
Tmp	Hydrotris(2-mercaptopyridyl)borate
To	Hydrotris(oxazolinyl)borate
Tp	Hydrotris(pyrazolyl)borate
UV	Ultraviolet
ZThp	Zwitterionic tris(2-pyridonyl)borate
ZTm	Zwitterionic tris(methimazolyl)borate
ZTmp	Zwitterionic tris(2-mercaptopyridyl)borate
ZTp	Zwitterionic tris(pyrazolyl)borate

Table of Contents

Chapter One

Chiral Homoscorpionates: Synthesis, Complexation and Applications

1.1 Introduction

Tripod ligands are used widely throughout organometallic chemistry to shape the reactivity of metals through their steric and electronic influence.[1,2] As face-capping, 6-electron donors, analogies are often drawn between tripods and commonly utilised aryl and cyclopentadienyl ligands (Figure 1.1). However, tripods have a number of advantages over aromatic ligands. The electronic properties of tripod ligands can be modified easily by simply altering the donor atoms or backbone structure. The ligands can also be either anionic or charge-neutral lending flexibility to the electronic structure of their complexes. In addition tripods allow greater possibility for substitution or alteration of the ligand architecture than in aromatic systems, thus facilitating tuning of the steric properties to suit specific applications.

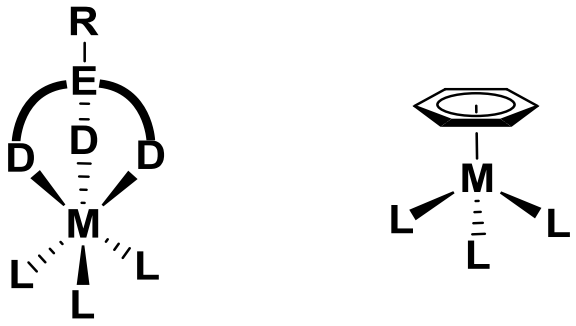

Figure 1.1: Comparison between tripod and arene ligands.

The ease with which chiral groups can be incorporated into the podand architecture means that enantiopure ligands and complexes are readily accessible for catalytic applications. Complexes of chiral tripods have already been utilised in asymmetric catalysis, with these ligands thus presenting

promising routes of inquiry for the development of new asymmetric syntheses.

Within this field complexes of, enantiopure, homotopic, C_3-symmetric ligands are of particular interest as asymmetric catalysts.[3,4] As first noted by Burk in 1990,[5] whilst C_2-symmetric ligands provide the ideal topology for square-planar catalysts they are less well suited for octahedral complexes. The reason for this lies in the nature of the metal sites not bound by the ligand (*i.e.* the sites opposite the ligand). Such 'free' sites are available for catalysis, and in a C_2-symmetric complex, are equivalent or homotopic (Figure 1.2). Contrastingly, in a C_2-symmetric octahedral complex there are two sets of equivalent sites which are mutually inequivalent or

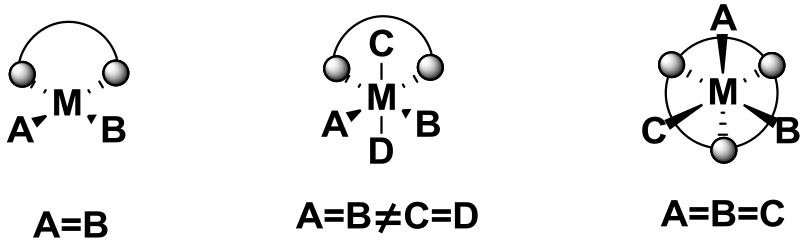

Figure 1.2: Comparison of the 'free sites' in complexes of C_2 and C_3 symmetric ligands.

diastereotopic. A C_3-symmetric octahedral complex contains three sites opposite the ligand which are homotopic. Catalysts are expected to give higher enantioselectivities when all 'free' sites are homotopic as there are a lower number of possible transition states through which the complex may pass during catalysis. Therefore, catalysts based on octahedral metal ions containing C_3-symmetric ligands are expected to give higher enantioselectivities than those containing C_2-symmetric ligands.

For these reasons, the synthesis of enantiomerically pure complexes of tripod ligands and investigation of their use as chiral catalysts has been the pursuit of a number of researcher groups in recent years. This chapter will discuss the development of chiral ligands as well as those ligands which exhibit helical chirality upon complexation. For each system the details of ligand synthesis, metal complexation and applications in asymmetric catalysis will be described. Other tridentate topologies, such as pincer ligands, have already been covered adequately in previous reviews notably those of Liang,[6] Danopoulos[7] and Zysman-Coleman[8] and therefore will not be covered here. In addition, the subject of chiral, tripodal, tetradentate ligands has been reviewed by Moberg[3] and Gibson[4] and will also not be discussed herein.

1.2 Homotopic Tripod Ligands

1.2.1 Chiral Tris(pyrazolyl)borates

The hydrotris(pyrazolyl)borate ligand (Tp) is arguably the most widely used tripod ligand in coordination chemistry.[9,10] First synthesised by Trofimenko in 1966 it is commonly prepared by heating pyrazole with an alkali metal tetrahydroborate in a solventless melt reaction (Scheme 1.2)[11] although a number of alternate synthetic routes have subsequently been reported.[12-14]

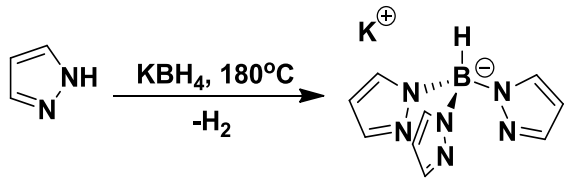

Scheme 1.2: Synthesis of hydrotris(pyrazolyl)borate by a borohydride melt. (Tp)

Although the Tp ligand is achiral a number of chiral derivatives have been developed by Tolman,[15-17] derived from chiral pyrazole derivatives which can be synthesised from chiral-pool aldehydes such as menthone or camphor (Scheme 1.1). The synthesis of *cis-(3R,6R)*-menthylpyrazole was achieved by formylation of commercially available (2*S*,5*R*)-(+)-menthone followed by subsequent heating with hydrazine to give the chiral pyrazole in a 13:1 diastereoisomer ratio (*d.r.*). Fractional crystallisation of the hydrochloride salt provided the enantiomerically pure pyrazole in 20% yield overall. Enantiomerically pure camphorylpyrazole was synthesised in 85% yield from (*R*)-(+)-camphor using a similar method. (*R*)-menthenylpyrazole could also be accessed from (*R*)-(+)-pugleone as a 2:1 ratio of *trans*:*cis* stereoisomers which were again separated by fractional crystallisation of their hydrochloride salts.

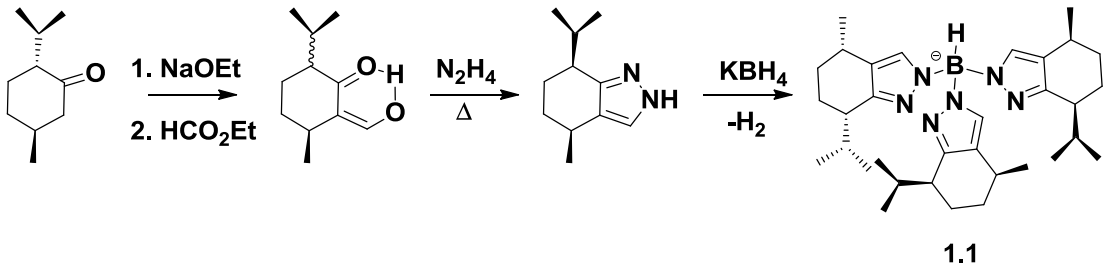

Scheme 1.1: Synthesis of chiral Tp ligand Tp^{men} (**1.1**).

These chiral pyrazoles, *cis-(3R,6R)*-menthylpyrazole and camphorylpyrazole, were used in the synthesis of the respective enantiopure C_3-symmetric ligands Tp^{men} (**1.1**) and Tp^{cam} (**1.2**) by melting the enantiopure heterocycles with potassium borohydride in a solventless reaction. Purification of the ligands proved difficult due to the presence of excess pyrazole in the reaction mixture, although pure complexes could be isolated by *in situ* coordination of the impure ligand to a metal centre. Treatment of the crude melt-reaction products with TlOAc in CH_2Cl_2 thus allowed the synthesis of the corresponding thallium salts $TlTp^{men}$ (**1.3**) and $TlTm^{cam}$ (**1.4**) (Figure 1.3). The ligand Tp^{memen} could not be accessed by this route, presumably as a consequence of the steric bulk of the *tert*-butyl group in *cis*-menth-4(8)-enylpyrazole as in all other ways it is analogous to *cis*-menthylpyrazole.

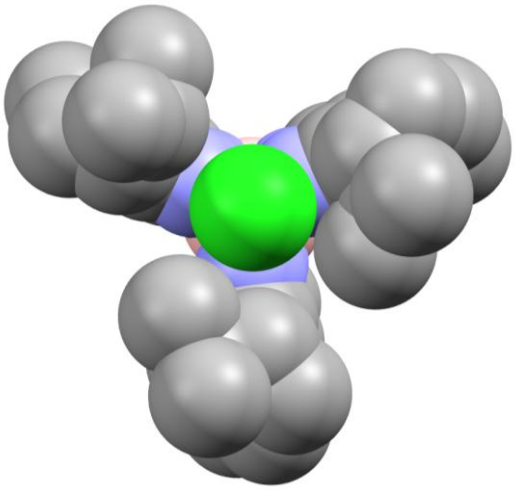

Figure 1.3: X-ray crystal structure of $Tp^{men}Tl$ (**1.3**) showing the C_3 symmetric environment of the metal centre.

A variety of transition metal complexes of Tp^{men} have been synthesised exhibiting κ^3-[*N*,*N*,N] coordination to the metal centre.[16] X-ray crystal structures of these complexes depicted single enantiomer complexes with C_3-symmetric pocket around the metal centres, ideal for asymmetric catalysis (Figure 1.3).[17] The complex [$Tp^{men}Rh(CO)_2$] (**1.5**) was found to undergo intramolecular C-H bond activation with a high degree of stereo- and regio- selectivity, although the corresponding intermolecular process was found to be disfavoured (Scheme 1.3).[18]

Chisholm later demonstrated the utility of complexes of chiral Tp

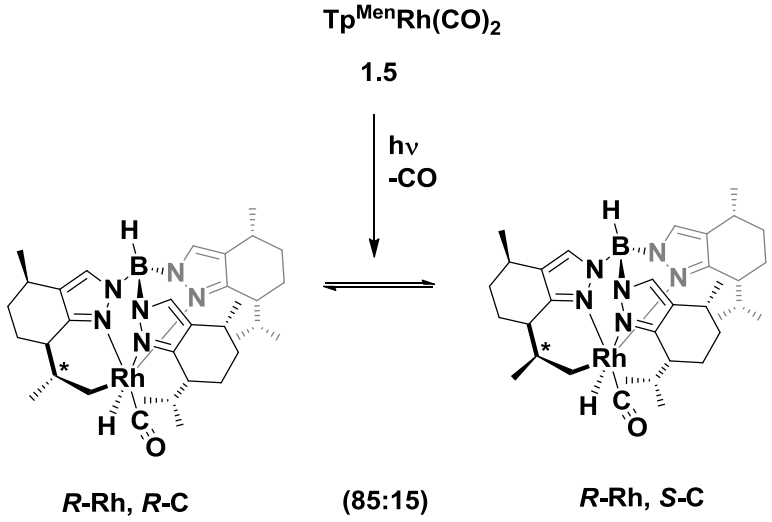

Scheme 1.3: Intramolecular CH activation in the complex $Tp^{men}Rh(CO)_2$ (**1.5**)

ligands in the asymmetric ring-opening polymerisation of lactides.[19] [Tp^{men}MgOPh] (**1.6**) showed clear diastereoselectivity for the polymerisation of *meso*-lactide over *rac*-lactide polymerising the former substrate exclusively when both were present in the mixture. Stereoselectivity of the polylactide

chain was however more moderate. In contrast, [Tp^{men}ZnOSiMe$_3$] (**1.7**) showed alternate behaviour polymerising both the *rac*- and *meso*-lactides at the same initial rate before preferentially polymerising *meso*-lactide in the latter two thirds of the reaction. This zinc complex also showed moderate enantioselectivity (up to 18.9%) in the polymerisation of L-lactide from *rac*-lactide.

Despite these successes, the scope of C_3-symmetric chiral Tp derivatives has been limited by a lack of synthetic routes to chiral pyrazole precursors. Therefore, it has not been possible to systematically probe the steric properties required for the application of such chiral Tp complexes in asymmetric catalysis.

1.2.2 Chiral Tris(oxazolinyl)methanes

Gade's 'trisox' ligands utilise readily available chiral oxazoline ligand arms, allowing such ligands to be systematically tuned to provide C_3-symmetric ligands with varying steric properties. In these ligands the oxazoline groups are linked via carbon bridgeheads giving charge-neutral [N]$_3$-donor ligands which contrast their anionic Tp derivatives.

Synthesis of the trisox ligand is achieved by deprotonation of the commonly used, enantiopure bis(oxazolinyl)ethane (BOX^R) precursor at the

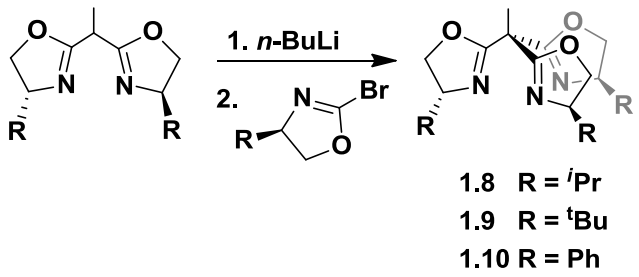

Scheme 1.4: Synthesis of trisox ligands (**1.8**-**1.10**).

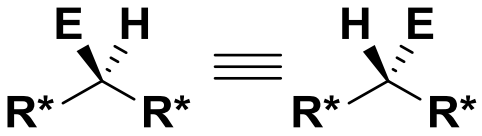

Figure 1.4: Formation of a prochiral centre.

bridgehead carbon with *n*-butyllithium (Scheme 1.4), taking advantage of the fact that substitution of a tetrahedral centre bound to two identical chiral groups results in the formation of a prochiral centre (Figure 1.4). The central carbon in the C_2-symmetric chiral bis(pyrazolyl)methane ligand can be considered to be just such a tetrahedral centre with substitution at this position yielding an enantiopure tripod ligand, negating the requirement for separation of stereoisomers. The resulting BOX carbanion can be treated with the relevant 2-bromooxazoline to yield the corresponding enantiopure C_3-symmetric 'trisox' ligand. This method has been utilised to develop the homoleptic ligands ^{i}Pr-trisox (**1.8**), ^{t}Bu-trisox (**1.9**) and Ph-trisox (**1.10**) from 4-isopropyl, 4-tert-butyl and 4-phenyloxazoline respectively in near-quantitative yields.[20,21]

Upon reaction with a metal cation many tripod ligands display the propensity to form homoleptic bis-ligand complexes of the form L_2M. Reaction of racemic ^{i}Pr-trisox (*rac*-**1.8**) with $[Co(ClO_4)_2]$ in a non-coordinating solvent such as dichloromethane gives bis-ligand $[Co(^{i}Pr\text{-trisox})_2][ClO_4]_2$ (**1.11**) (Scheme 1.5). The complex exists as the *meso*-diastereoisomer containing one (*R,R,R*)- and one (*S,S,S*)- ^{i}Pr-trisox and is therefore achiral. In acetonitrile, however, the same ligand displayed a preference towards the formation of the mono-ligand complex $[(^{i}Pr\text{-trisox})Co(MeCN)_3][ClO_4]_2$ (**1.12**).

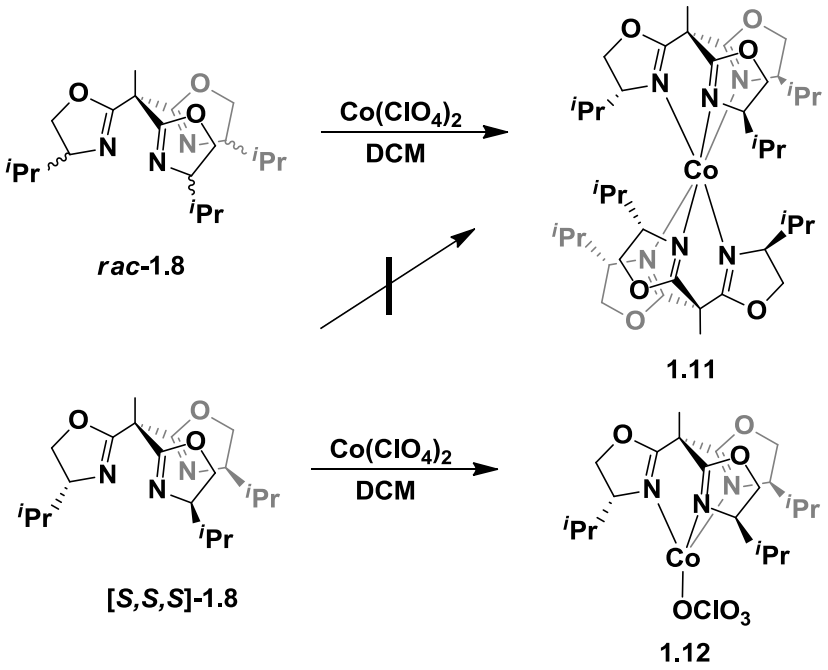

Scheme 1.5: Reaction of racemic and enantiopure ^{i}Pr-trisox with $Co(ClO_4)_2$ to give **1.11** and **1.12**.

Contrastingly, complexation of the enantiopure (*S,S,S*)-^{i}Pr-trisox ((*S,S,S*)-**1.8**) with cobalt resulted the formation of a mixture of products, one of which was identified as $[(trisox)Co(ClO_4)]^{+}$. Notably, no evidence was found for the presence of $[(trisox)_2Co]^{2+}$ in the mixture, demonstrating the strength of the repulsive interactions between the chiral substituents in the bis-ligand complex. Molecular mechanics simulations were used to study the energy difference between the (*R,R,R-S,S,S*) complex formed from racemic ligand and the hypothetical (*S,S,S-S,S,S*) which could theoretically be formed from enantiopure 'trisox'. The studies showed a large energy difference of 43 kcal mol^{-1} between these diastereoisomers. Strong chiral induction between the tripod and other metal substituents, namely catalytic intermediates, is crucial to the development of highly efficient asymmetric catalysts. Thus, the high barrier to formation of [((*S,S,S*)-^{i}Pr-trisox)$_2$Co] is indicative of the

potential of trisox complexes to act as highly stereodirecting asymmetric catalysts.

A variety of complexes of various trisox ligands have been described by Gade *et al.*, with many being tested as potential catalysts for a range of asymmetric transformations. The main catalysts studied are described below and summarised in Scheme 1.6.

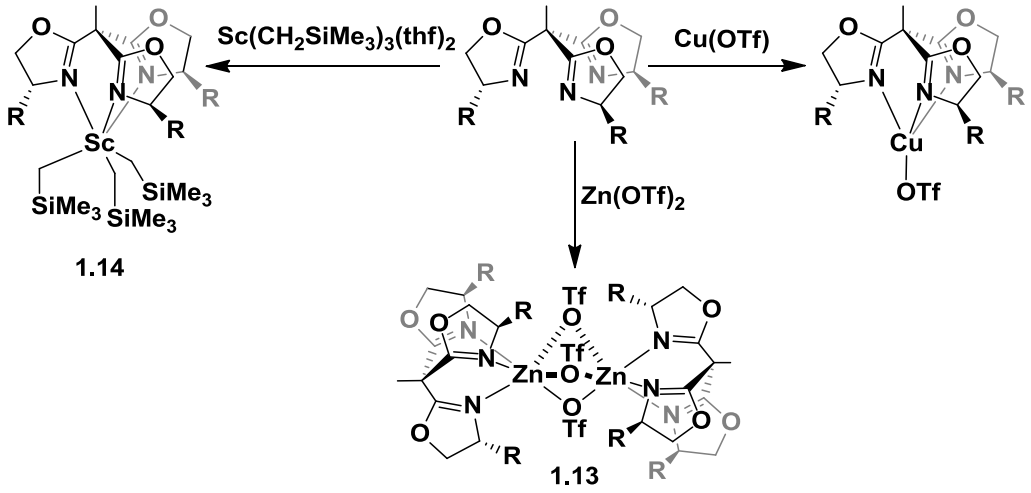

Scheme 1.6: Chiral catalysts synthesised from C_3 symmetric trisox ligands.

1.2.2.1 Cyclopropanation

The ligands ^{i}Pr-trisox (**1.8**) and ^{t}Bu-trisox (**1.9**) were reacted with Cu(I)OTf and tested *in situ* for activity in the asymmetric cyclopropanation of styrene with *tert*-butyl and ethyl diazoacetate. Both were shown to be effective precatalysts with moderate enantiomeric excesses of up to 73%, although with relatively poor diastereoselectivities (up to 81:19 *cis:trans*).[21]

1.2.2.2 Chiral resolution

Zinc complexes of ^{i}Pr-trisox (**1.8**) have also been shown to kinetically resolve chiral esters during transesterification reactions.[20] Coordination of

^{i}Pr-trisox to [Zn(OTf)$_2$] gave the triflate-bridged dimer [(^{i}Pr-trisox)$_2$Zn$_2$(μ^2-OTf)$_3$] (**1.13**) which showed modest enantioselectivity in this reaction (Selectivity factor up to 2.0). Complexes of [Zn(OAc)$_2$] and [Zn(OCOCF$_3$)$_2$] formed *in situ* prior to catalysis gave higher selectivity factors of up to 4.5 and 5.1 respectively.

1.2.2.3 Polymerisation

Tris(alkyl)scandium(III) complexes of ^{i}Pr-trisox (**1.8**) were shown to induce a high degree of tacticity in the polymerisation of 1-alkenes.[22-25] The complex [(^{i}Pr-trisox)Sc(CH$_2$SiMe$_3$)$_3$] (**1.14**) was accessed from the reaction of **1.8** with [Sc(CH$_2$SiMe$_3$)$_3$(thf)$_2$] and activated by treatment with 2 eq. of [Ph$_3$C][B(C$_6$F$_5$)$_4$] yielding [[(^{i}Pr-trisox)Sc(CH$_2$SiMe$_3$)(Solvent)$_n$][B(C$_6$F$_5$)$_4$)]$_2$ (**1.15**). At low temperature (-30^{o}C) the catalyst was highly active for the polymerisation of hex-1-ene (1938 kg mol^{-1} h^{-1}) and produced polymer with excellent isotacticity (99% *mmmm*) indicating a high degree of chiral induction from the *C*$_3$-symmetric ligand. Complexes of this ligand with other trivalent rare-earth elements (Y, Lu, Tm, Er, Ho and Dy) showed markedly lower activities than the scandium complex demonstrating an inverse relationship between the ionic radii of the metals and the catalytic activity of the trisox complex.[23,25]

1.2.2.4 Mannich reaction

Importantly, complexes of these ligands with non-deltahedral metals, where the ligand acts as a bidentate chelate, were also found to catalyse the Mannich reaction with a good degree of stereoselectivity.[26] Whilst the active species of [(^{i}Pr-trisox)Cu][ClO$_4$]$_2$ (**1.16**) contains a trisox ligand in the κ^2-[*N*,*N*] coordination mode the non-coordinating third arm was shown to facilitate rapid interconversion of the metal centre between the ligand arms resulting

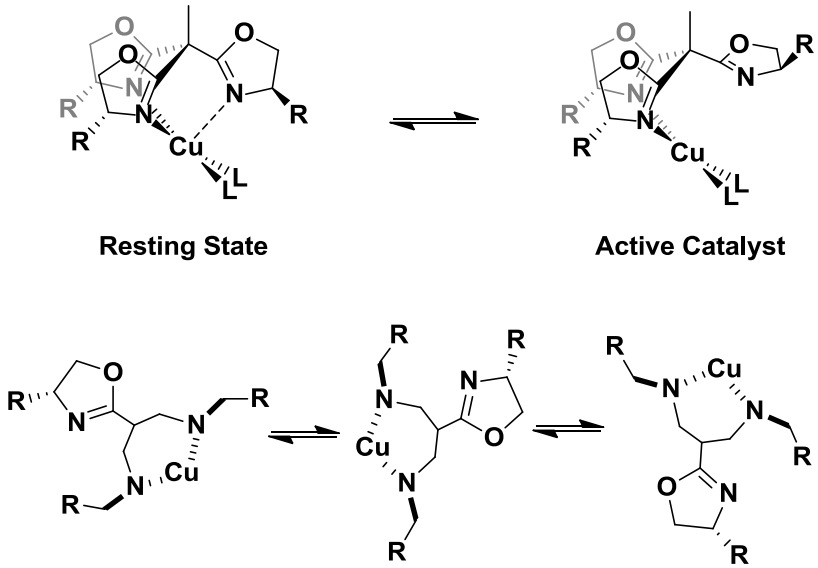

Figure 1.5: Equilibrium of trisox in square planar complexes. (**1.16**)

in the formation of three symmetry-equivalent active species (Figure 1.5). In the reaction between ethyl 2-methylacetoacetate and N-tosyl-α-imino methyl ester use of [(^{i}Pr-trisox)Cu][ClO_4]$_2$ (**1.16**) as the catalyst resulted in greater enantioselectivities (up to 91% *e.e.*) than the analogous [(^{i}Pr-BOX)Cu][ClO_4]$_2$ (up to 84% *e.e.*). In addition, the catalyst was found to be active at lower loading, with 90% *e.e.* obtained at 0.01% [(^{i}Pr-trisox)Cu][ClO_4]$_2$ catalyst loading compared to 66% *e.e.* at 0.01% [(^{i}Pr-BOX)Cu][ClO_4]$_2$ loading although the yields in both cases were low (36% and 35% respectively).

1.2.3 Chiral Tris(oxazolinyl)borates

More recently, Sadow has developed a boron-centred tris(oxazolinyl) ligand (To^R) as a monoanionic analogue of Gade's charge-neutral 'trisox'.[27] The increased electrostatic interaction between the anionic ligand and cationic metal centre facilitates metal coordination, whilst the presence of the boron bridgehead alters the donor properties of the ligand. Phenyltris(oxazolinyl)borate (To^P) (**1.17**) was accessed by deprotonation of

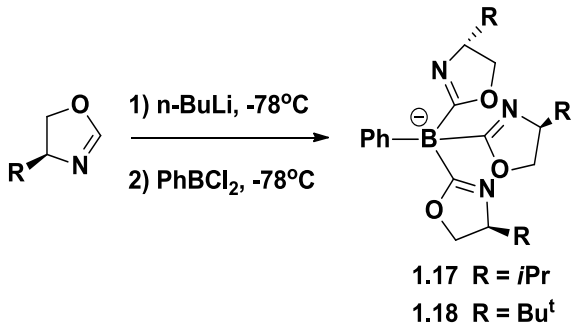

Scheme 1.7: Synthesis of To ligands from chiral oxazolines (**1.17**, R = ^{i}Pr) and (**1.18**, R = ^{t}Bu)

chiral oxazolines at the 2-position followed by reaction with $PhBCl_2$ (Scheme 1.7). Utilising 4-*iso*-propyloxazoline, 4-*tert*-butyloxazoline and 4,4-dimethyloxazoline precursors gave ligands (phenyl)tris(4-*iso*-propyloxazolinyl)borate (To^P) (**1.17**), (phenyl)tris(4-tert-butyloxazolinyl)borate (To^T) (**1.18**) and (phenyl)tris(4,4-dimethyloxazolinyl)borate (To^M) (**1.19**) respectively.

Complexation of the lithium salt of To^P (**1.17**) to iridium was initially disrupted due to side-reactions. Instead the thallium salt Tl[To^P] (**1.20**) was reacted with $[Rh(\mu\text{-}Cl)(CO)_2]_2$ to give [{To^P}$Rh(CO)_2$] (**1.21**). This complex was shown to undergo intermolecular oxidative-addition with a variety of substrates and a high degree of stereoselectivity.[28] In one example, treatment of this complex with $CHCl_3$ at room temperature gave the complex [To^PRh(CO)Cl($CHCl_2$)] as a 100:3 ratio of diastereoisomers. ^{1}H-NMR spectroscopy of **1.21** suggests equivalence of the oxazolinyl ligand arms, in agreement with the equilibrium model shown in Figure 1.5. Infra-red spectroscopy showed indicated the complex to be a mixture of the κ^3-*N,N*,N and κ^2-*N,N* isomers and that the isomers were interconverting rapidly on the NMR timescale. IR stretching frequencies of the metal-bound carbonyls also demonstrate that To^P (**1.17**) is a more electron donating ligand than Tp*.

The enantiopure To^P (**1.17**) and To^T (**1.18**) ligands and the achiral To^M (**1.19**) ligand all display analogous reactivity and a number of studies with To^M demonstrated the general potential of chiral To ligands as precatalysts for asymmetric hydroamination.[29-33] The enantiopure ligand To^T (**1.18**) was reacted with $[MgMe_2(O_2C_4H_8)]$ and $[Ca(C(SiHMe_2)_3)_2(thf)_2]$ to give the complexes $[To^TMgMe]$ (**1.22**) and $[To^TCa(C(SiHMe_2)_3)]$ (**1.23**) respectively. These were tested as catalysts in the asymmetric hydroamination/cyclisation of both 2,2-diphenyl-4-pent-1-amine and C-(1-allyl-cyclohexyl)-methylamine. Whilst full conversion was achieved with $[To^TCa(C(SiHMe_2)_3)]$ (**1.23**) extremely quickly, it afforded no stereoselectivity in the transformation of 2,2-diphenyl-4-pent-1-amine to 3,3-diphenyl-5-methylpyrrolidine which was isolated as a racemic mixture of stereoisomers. Conversion with $[To^TMgMe]$ (**1.22**) was much slower and no enantioselectivity was observed with this catalyst. In contrast, cyclisation of C-(1-allyl-cyclohexyl)-methylamine with $[To^TMgMe]$ (**1.22**) gave *R*-3,3-cyclohexyl-5-methyl-pyrrolidine in 36% *e.e.* The same reaction with $[To^TCa(C(SiHMe_2)_3)]$ (**1.23**) resulted in the formation of the opposite *S*- enantiomer in 14% *e.e.*

1.2.4 Chiral Tripodal Phosphines

Burk reported the first example of a chiral phosphine donor tripod ligand in 1991 (Figure 1.6).[5] Enantiopure phosphines were prepared by etherification of 2,5-hexanediol followed by reaction with Li_2PPh to give (*S*,*S*)-dimethylphospholane in 85% isolated yield. The lithium salt was accessed by reaction with elemental lithium but attempts to link three of the phosphine units to form a tripod ligand were less trivial. Reacting the phosphines with 1,1,1-tris(chloromethyl)ethane, which had been used previously with achiral phosphines to great effect, proved ineffective for this

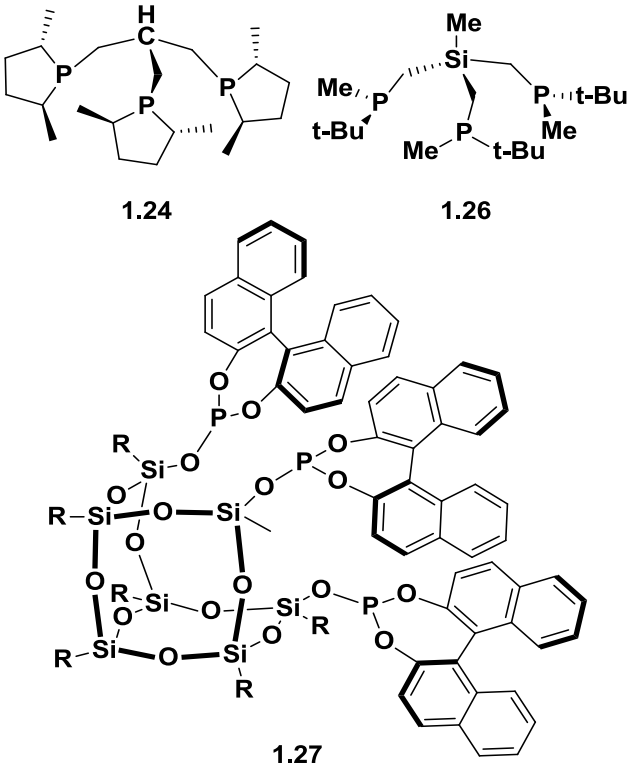

Figure 1.6: Chiral tripodal phosphine ligands (**1.24**, **1.26** and **1.27**).

reaction. Reaction with 1,3-dichloro-2-chloromethylpropane did however allow access to the tripod (**1.24**) in 63% yield.

A rhodium complex of **1.24** was prepared by reaction of the free ligand with $[Rh(COD)_2]^+[SbF_6]^-$ to give [κ²-[P,P]-{**1.24**}RhCOD] (**1.25**). This complex was tested for catalytic efficacy in the asymmetric hydrogenation of methylacetamidocinnamate (MAC) and dimethyl itaconate. In both cases the complexes of the tripod ligands gave improved enantioselectivities (94% *e.e.*) compared to their bidentate analogues (90% *e.e.*). The rates of these transformations were, however, slow at room temperature (20-72 h) compared to the bis-phosphine complexes (2-3 h) at RT. Upon heating to 50°C the reaction still required a 20-fold increase in reaction time to reach completion. Further increasing the reaction temperature was found to

increase the rate but resulted in a marked decrease in enantioselectivity (40% *e.e.* at 65°C). Burk hypothesised the presence of a stable five-coordinate 18-electron catalytic intermediate $[(MAC)Rh(L)]^+[SbF_6]^-$ which would necessitate the dissociation of one ligand arm to allow hydrogen oxidative-addition. The stability of the intermediate complex and the high barrier to dissociation of a tri-coordinate ligand was therefore proposed to limit the rate of conversion.

Very recently Glueck has developed a new route to a Siliphos ligand (**1.26**) with stereogenic phosphine donors.[34] Deprotonation of the commercially available phosphine borane $PMe_2(t\text{-Bu})(BH_3)$ in the presence of (-)-sparteine followed by treatment with $MeSiCl_3$ yielded the tripod as a 2.6:1 mixture of the C_3- and C_1-symmetric diastereoisomers. The major isomer could be preferentially enriched upon repeated crystallisations. Heating the enantiopure C_3-symmetric tris(phosphineborane) with morpholine gave the enantiopure tris(phosphine) **1.26**. This ligand was reacted with $Ru(DMSO)_4Cl_4$ yielding [κ^3-[P,P,P]-(**1.26**)$RuCl_2(DMSO)$]. Whilst at room temperature all three phosphines appear equivalent by ^{1}H-NMR spectroscopy low temperature studies of this complex indicated the presence of a fluxional 5-coordinate species formed by ligand arm dissociation, analogous to that proposed by Burk. The formation of this species, followed by pseudorotation at the metal centre, allows for interconversion of the ligand arms meaning they appear equivalent on the NMR timescale at room temperature.

Vogt has investigated an interesting class of tris(phosphite) ligands containing a silsesquioxane bridgehead (**1.27**).[34] *In situ* catalytic testing of a mixture of the ligand with $[Rh(acac)(CO)_2]$ yielded excellent conversions (99%) and moderate enantioselectivity (38% *e.e.*) in the asymmetric

hydroformaylation of vinyl acetate. In contrast [{**1.27**}Rh(COD)][BF_4] showed slightly improved enantioselectivity (up to 52% *e.e.*) in the hydrogenation of methyl-(*Z*)-2-acetamidocinnamate.

1.2.5 Chiral Tris(pyridine) ligands

Chiral tris(pyridyl) ligands have been synthesised by Moberg (Figure 1.7).[35,36] The C_3-symmetric chiral tris(pyridyl) ligand **1.28** was accessed in five steps from tris(pyridyl)methanol and isolated as a 97.5 : 2.5 mixture of diastereoisomers. In another synthetic route the tris(pyridyl)ligand **1.29** was obtained by treatment of chiral pyridine derivatives with $POCl_3$. The chiral pyridine ligand arms were synthesised in four steps from the chiral pool alcohol (1*R*,2*S*,5*R*)-(-)-menthol. Despite reports of the complexation of these

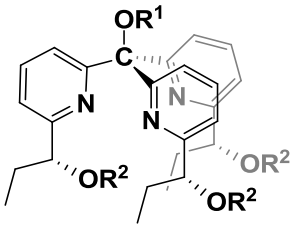

1.28a R^1=R^2=H
1.28b R^1=H R^2=Me
1.28c R^1=R^2=Me

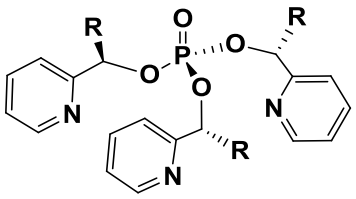

1.29
R = neomenthyl

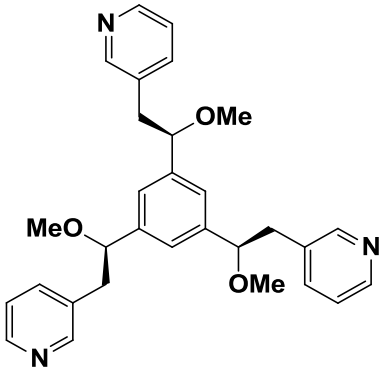

1.30

Figure 1.7: C_3 symmetric tris(pyridyl) ligands developed by Moberg and Gibson.

ligands, no information on the coordination mode of these novel ligands has been reported.

Gibson has also undertaken significant research in C_3-symmetric complexes, many of which are tetradentate and therefore out-with the remit of this review however; a number of tridentate examples have been synthesised. The enantiopure tris(pyridyl) ligand 1,3,5-tris(pyridyl)benzene **1.30** can be formed from a tricarbonylchromium complex of 1,3,5-tris(methoxymethyl)benzene.[37,38] Oxidative removal of the chromium fragment gave the free ligand **1.30** which was shown to form a homoleptic bis-ligand complex with ruthenium. In this complex the ligands adopt helicity, with each ligand assuming an alternate twist direction, indicating that the enantiopure groups on the ligand are too far removed from the metal centre to effect chiral induction (See Section 1.3).

1.2.6 Homoscorpionates with non-coordinating chiral groups.

There are few reports to date of the synthesis of tripod ligands with chiral substituents on the ligand bridgehead, a topic which will be addressed in Chapter Three. In 2003, the Bailey group reported the synthesis of an enantiopure Tp ligand with an isopinocampheyl (Ipc) substituent on the central boron (Scheme 1.8).[39] Hydroboration of (1*R*)-α-pinene (91% *e.e.*) with $H_2B{:}SMe_2$ followed by treatment with TMEDA gave the stable borate $[(Ipc)BH_2]_2$TMEDA in >99% *e.e.* after purification. This intermediate was then chlorinated by treatment with HCl in ether to give $[(Ipc)BCl_2]$. $Na[(Ipc)B(pz)_3]$ (**1.31**) was isolated in 87% yield as a hygroscopic white solid from reaction of $[(Ipc)BCl_2]$ with sodium pyrazolide in refluxing THF.

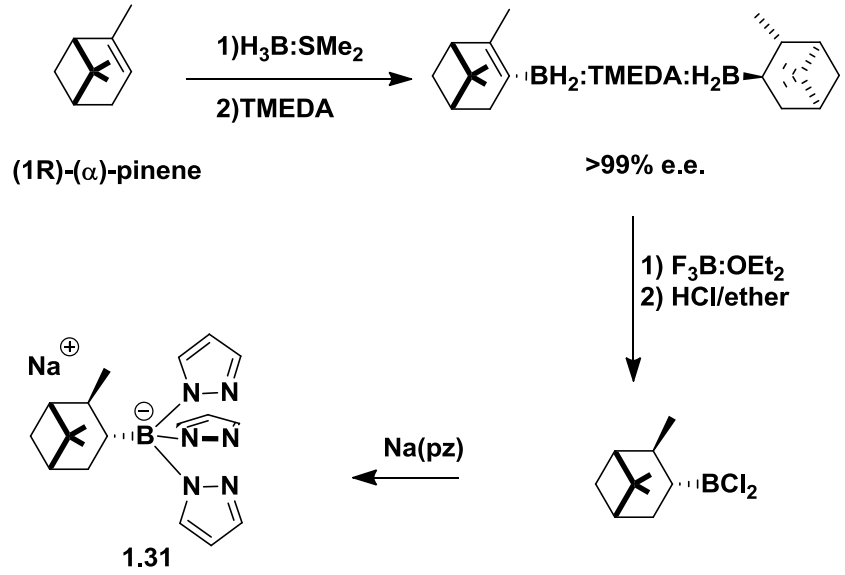

Scheme 1.8: Synthesis of $[(Ipc)B(pz)_3]^-$ (**1.31**).

Ligand **1.31** was reacted with $MnBr(CO)_5$ in refluxing acetonitrile to yield $[\{(Ipc)B(pz)_3\}Mn(CO)_3]$ (**1.32**). The FTIR spectrum of this ligand in toluene depicted two carbonyl stretching bands at 1927 and 2031 cm^{-1} consistent with local C_3v symmetry at the metal in solution. The solid state IR (KBr) spectrum showed splitting of the lower energy band (1934 and 1942 cm^{-1}) whilst the higher energy band remained unchanged, this being consistent with the X-ray crystal structure of the complex which contained two independent molecules in the asymmetric unit.

1.3 Helically chiral homoscorpionates

Alongside the aforementioned enantiopure ligands there is an important class of achiral ligands which form helically chiral complexes upon coordination to a metal centre. The helical structure of these complexes is a result of the torsional strain of bicyclic 8-membered rings which form upon κ^3-complexation of the ligands. 'Twisting' occurs when one of the atoms in the bicyclic ring system (*i.e.* in the ligand backbone) is able to adopt

sp^3 hybridisation to reduce strain. 'Twisting', in either a clockwise or anti-clockwise direction, gives the helical enantiomers denoted *P* for a positive twist and *M* for a negative twist respectively (Figure 1.8).

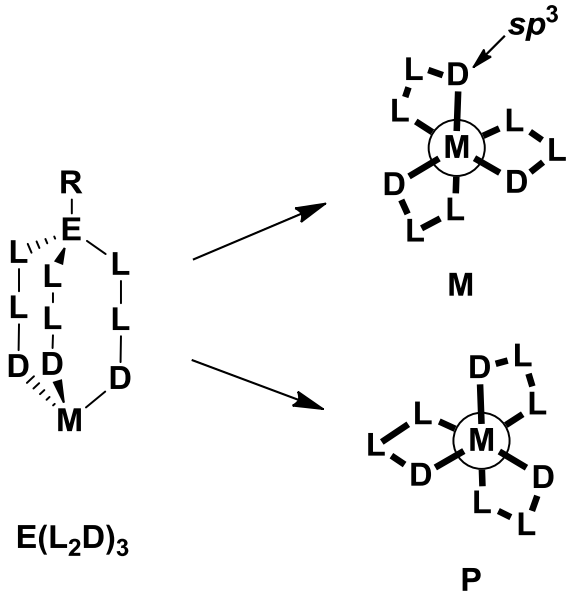

Figure 1.8: The Tm ligand can exhibit helical chirality upon complexation due to the presence of an sp^3-hybridised sulfur in the ligand backbone.

Helically chiral tripods have a number of advantages over enantiopure ligands which make them promising candidates as ligands for C_3-symmetric chiral catalysts. Firstly, the ligands could potentially be directed to form a single diastereoisomer using only one enantiopure chiral centre thus reducing the need for the expensive enantiopure precursors used in other homotopic tripods. In addition, the potential for full conversion of the ligand to a diastereomerically pure complex eliminates the necessity for separation of the stereoisomers, a costly and time consuming process thus improving experimental yields and leading to more economically viable catalytic processes.

1.3.1 Hydrotris(methimazolyl)borate

The helically chiral tripod hydrotris(methimazolyl)borate (Tm, **1.33**) was developed by Reglinski and Spicer in 1996 in an effort to synthesise complexes of tripod ligands with 'soft' metal centres.[40] The ligand was synthesised from the solventless melt reaction of commercially available methimazole with potassium tetrahydroborate (Scheme 1.9). The resulting monoanionic tripod was found to coordinate to a variety of soft metal centres which had been less reactive to the harder Tp ligand, as well as harder metal centres such as Ti(IV) and Zr(IV).[41,4243]

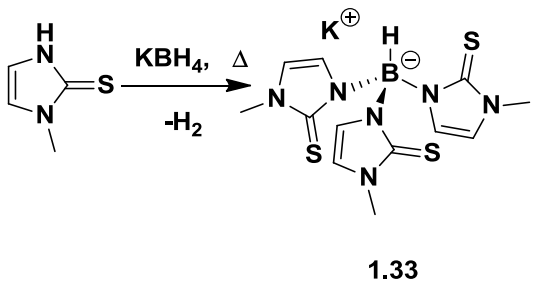

Scheme 1.9: Synthesis of hydrotrismethimazolyl borate (Tm, **1.33**)

X-ray crystal structures of these complexes show both the *P* and *M* enantiomers in the asymmetric unit. In order for the Tm ligand to coordinate in a κ^3-[S,S,S] mode and form a twisted 8-membered bicyclic ring system there must be a significant torsion angle resulting from the presence of at least one sp^3 hybridised atom in the bicyclic architecture. The heterocycle

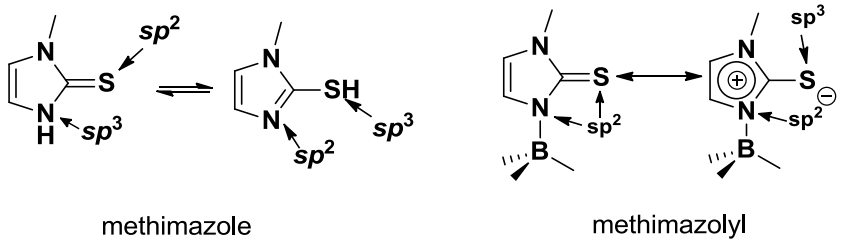

Figure 1.9: Hybridisation pattern of methimazole and the methimazolyl anion

methimazole is able to exist in two tautomeric forms (Figure 1.9) where the exocyclic sulphur is able to adopt either sp^2 or sp^3 hybridisation. The structural data suggests that the methimazolyl rings in Tm adopt the latter hybridisation pattern upon complexation, allowing the ligand to take on a helical structure.

In contrast, hydrotris(azaindolyl)borate (Tai) has no sp^3 hybridised atoms in the ligand arms and so does not exhibit helical chirality upon metal complexation, instead adopting a highly strained C_3v-symmetric structure upon tridentate coordination.[44] The lack of an sp^3 hybridised atom within the Tai backbone means that this ligand commonly coordinates in a bidentate κ^2-[*N,N*] mode (Figure 1.10) to relieve the angle strain which tridentate coordination involves. The 'twisting' of tripodal ligands to provide helically chiral complexes will be discussed further in Chapter 4.

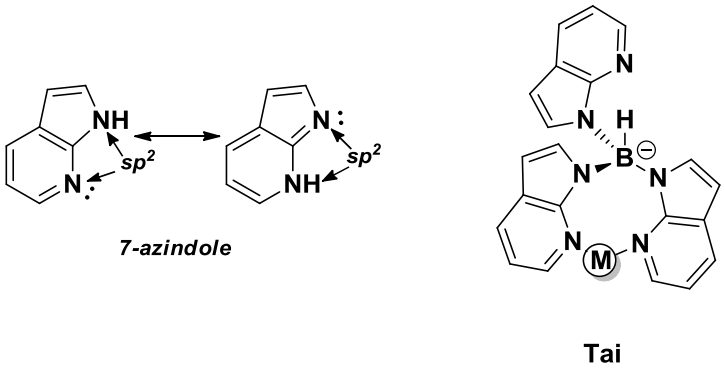

Figure 1.10: The Tai ligand does not adopt helical chirality because it contains no sp^3 hybridised atom in the ligand arms.

A large number of complexes of Tm have been synthesised in recent years. These have been described in some detail by Reglinski and Spicer and as such will not be covered in detail here.[45] However, it is worth noting a few

key points regarding their coordination chemistry. The IR spectrum of $TmMn(CO)_3$ indicates the ligand to be a more strongly donating tripod than Tp, with two lower energy carbonyl stretching bands (2003 / 1905 cm^{-1}) compared to those present in the spectrum of $TpMn(CO)_3$ (2036 / 1932 cm^{-1}). In addition, whilst only the κ^3-[*S,S,S*] coordination mode of Tm exhibits helicity, a number of other coordination modes have been observed, albeit less commonly. The ligand may act as a bidentate chelate with κ^2-[*S,S*] coordination or as a heterotopic tripod making an agostic bond between the metal centre and the boron bound hydride κ^3-[*S,S,H*] (Figure 1.11). One interesting coordination mode may arise upon oxidative addition of the metal across the B-H bond.[45-47] The resulting metallaboratranes have been shown to exhibit novel reactivity to give complexes of substituted (X)Tm ligands.[47]

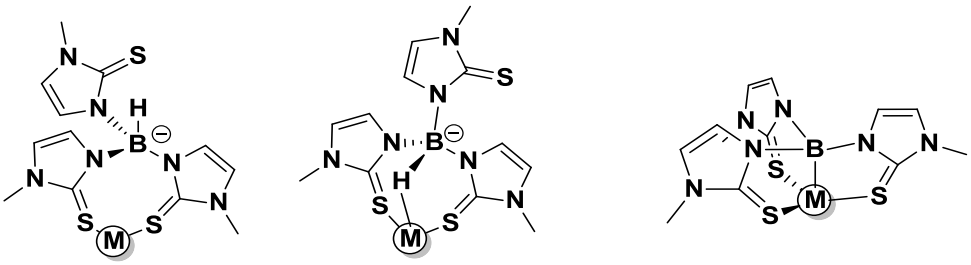

Figure 1.11: Some common binding modes of Tm.

Finally, Tm, like Tp, commonly forms homoleptic bis-ligand species of the type L_2M where the octahedral metal centre is ligated by two tripods. In these complexes each ligand adopts a different twist direction giving an inversion centre at the metal and the *meso-* diastereoisomer meaning that the complex is achiral overall. The pursuit of new heteroleptic complexes of

these ligands will be required in order to exploit helically chiral complexes containing this class of ligand in the future and will be discussed further in Chapter Five.

Since the development of Tm a variety of other tripod ligands providing helically chiral complexes with alternate heterocyclic ligand arms have been reported.

1.3.2 Hydrotris(N-tert-butylimidazole-2-one)borate

Parkin has described the synthesis of an oxygen donor analogue of Tm, hydrotris(N-tert-butylimidazole-2-one)borate (Tio)[i] (**1.34**), containing a 'hard' $[O]_3$ donor set (Scheme 1.10).[48] This ligand, prepared in a similar manner to Tm, was shown to complex to zirconium and rhenium giving

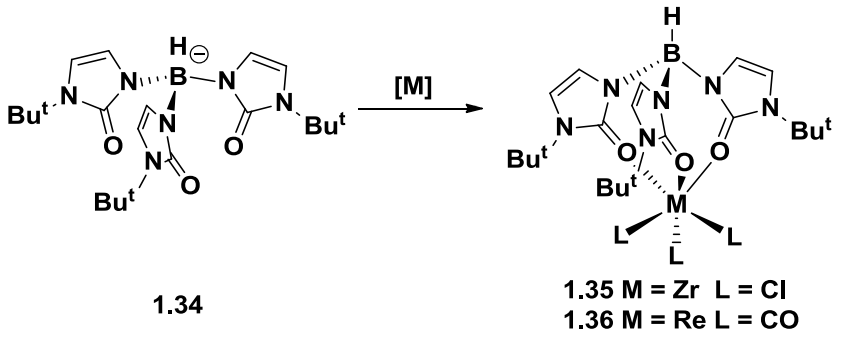

Scheme 1.10: Complexation of the Tio ligand **1.34**.

[{Tio}$ZrCl_3$] (**1.35**) and [{Tio}$Re(CO)_3$] (**1.36**) respectively. In these complexes Tio was found to be a stronger donor, but exhibit a larger cone-angle than the equivalent Tm^{tBu}. The helical twist of these complexes was found to be

[i] Both Sadow and Parkin have abbreviated their ligand systems as To in their own publications. In order to avoid confusion in this paper we will refer to the tris(oxazolinyl)borates as 'To' and the tris(imidazole-2-onyl)borates as 'Tio'.

significantly lower than for Tm with an average N-B-M-E torsion angle of 27.1° (E = O) compared to 48.6° in Tm complexes (E = S). This difference can be ascribed as a result of the difference in the angle about the sp^3 hybridised atom (i.e. the M-E-C angle) in each system. Tio has an average M-O-C angle of 140.5° whereas Tm complexes exhibit a lower average M-S-C angle in Tm (*ca.* 105°).

1.3.3 Pyridine-based helically chiral homotopic tripod ligands

Hydrotris(2-thiopyridone)borate (**1.37**) was developed by Owen and utilised 2-mercaptopyridine heterocycles as the ligand arms.[49] As with methimazole, 2-mercaptopyridine has two tautomeric forms which allows the exocyclic sulfur to adopt sp^3 hybridisation (Scheme 1.11). The alteration of the size of the heterocyclic ring increases the flexibility of this ligand as well as altering the steric environment around the metal centre.

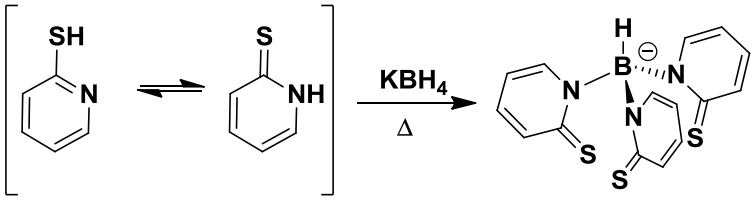

1.37

Scheme 1.11: Synthesis of the Tmp ligand **1.37**.

1.3.4 Enantiopure helically chiral scorpionates

In 2007, the Bailey group reported the first successful stereodirection of a helically chiral tripod ligand resulting in a complex in which the ligand cage is twisted in one direction exclusively (Scheme 1.12).[50] This was achieved by the inclusion of enantiopure α-methylbenzyl stereodirecting substituents of the methimazolyl ligand arms. Unfortunately the direct Tm analogue hydrotris(N-α-methylbenzylimidazolyl-2-thione)borate was

inaccessible by the traditional reaction of N-α-methylbenzylimidazol-2-thione with an alkali metal borohydride, so alternate routes were explored. Previous work by Niedenzu had described the synthesis of a charge-neutral zwitterionic analogue of Tp from the reaction of pyrazole with tris(dimethylamino)borane.[12] The resulting ligand, (dimethylamino)tris(pyrazolyl)borane (**1.38**),[ii] contained three pyrazole rings and a dimethylamino boron substituent. Expansion of this synthetic route

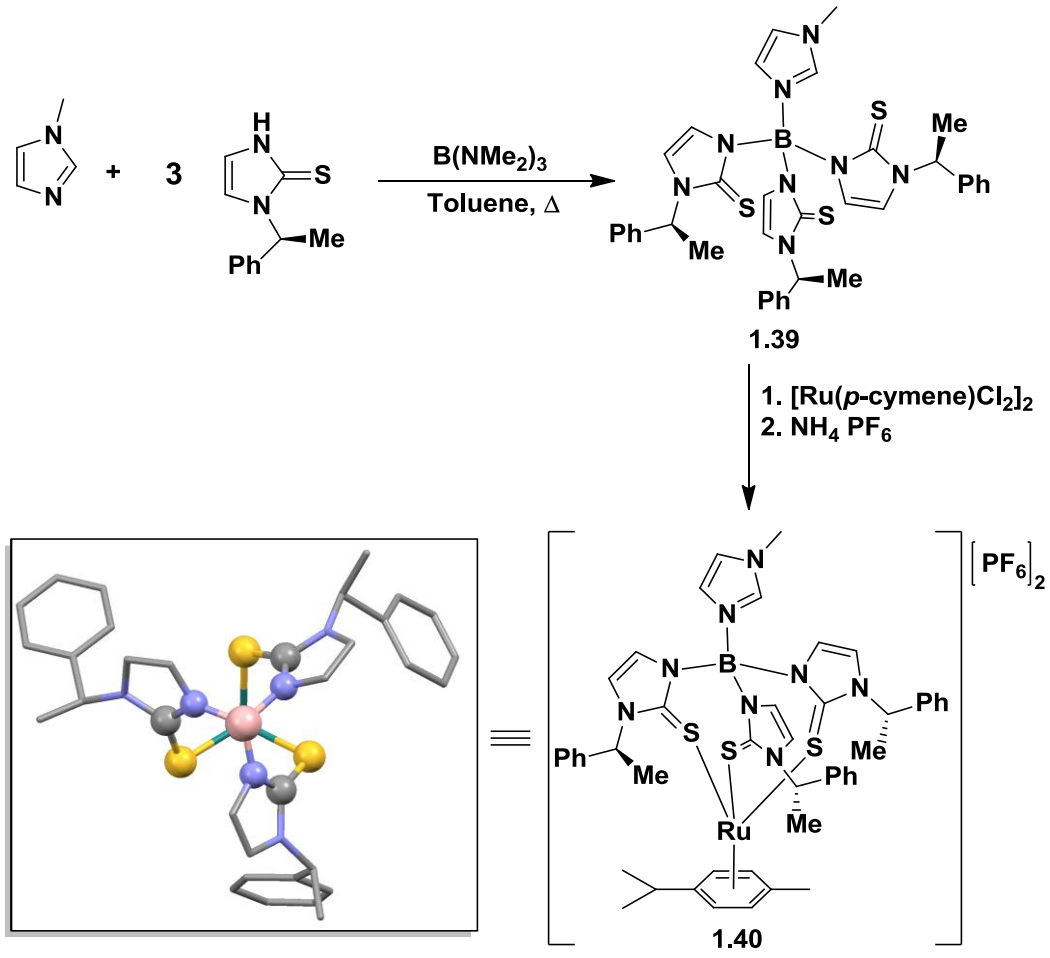

Scheme 1.12: The synthesis of ligand **1.39** and [{(NMI)Tmα-MeBz}Ru(p-cymene)] (**1.40**) along with the X-Ray crystal structure of the cation of **1.40** which exists as a single diastereoisomer.

[ii] These charge neutral zwitterionic scorpionates may also be described as the dimethylamine adducts of tris(pyrazolyl)borane giving 1.38 the alternate names (dimethylammonium)tris(pyrazolyl)borate or (dimethylamino)tris(pyrazolyl)borane. Both naming systems are equivalent and will be used interchangeably throughout this work.

has allowed the synthesis of a family of zwitterionic scorpionates which will be discussed further in Chapter 2. The dimethylammonium substituent in these zwitterionic ligands was also shown to be able to be substituted for a variety of other Lewis base donors.[51,52]

Using the above route, the chiral ligand **1.39** was accessible by reaction of N-α-methylbenzylimidazol-2-thione with tris(dimethylamino)borane and N-methylimidazole as the boron substituent (Scheme 1.12). Complexation of **1.39** to [Ru(*p*-cymene)Cl_2]$_2$ gave the single diastereoisomer complex [{(N-methylimidazolium)tris(N-a-methylbenzylimidazolyl-2-thione)borateruthenium(p-cymene)] (**1.40**). The solid state structure of **1.40**, determined by single crystal X-ray diffraction shows that the phenyl substituents of the α-methylbenzyl group interact with the adjacent methimazole sulfur thus inducing a single helical twist.

1.4 Conclusions

The development and application of chiral tripod ligands is a diverse and rapidly developing field of chemistry and a variety of methods have been described for the inclusion of chirality within the ligand architectures. Utilising inherently chiral starting materials, such as oxazolines, as the ligand arms has been shown to provide a facile route into C_3-symmetric enantiopure tripods. Ligands providing helically chiral complexes also represent a promising route of inquiry in the development of novel C_3-symmetric catalysts, although routes for synthesising stereochemically pure complexes require further study in order for the potential of these ligands to be realised.

Complexes of chiral tripod ligands have been utilised in a variety of catalytic processes including hydroformylation, hydrogenation, polymerisation and cyclopropanation. Although C_3-symmetric ligands are an ideal stereochemical match for metal coordination geometries containing a 3-fold axis (*i.e.* octahedral and tetrahedral), complexes of non-deltahedral metals with Gades enantiopure 'trisox' ligands have been shown to provide higher enantioselectivities than their bidentate analogue. However, enantioselectivities for many of these other applications described above have not been optimised and represent only moderate stereoselectivity at best. Further study of the structures of these complexes and the mechanism of catalysis operating in each case is required to improve the interplay between ligand chirality and catalytic intermediates in order for these ligands to be successfully utilised in asymmetric catalysis.

1.5 References

1. Trofimenko, S. *Poly(1-Pyrazolyl)Borates, their Transition-Metal Complexes, and Pyrazaboles*; McGraw-Hill, 1970.
2. Smith, J. M.; Scepaniak, J. J.; Vogel, C. S.; Khusniyarov, M. M.; Heinemann, F. W.; Meyer, K., *Science,* **2011**, *331*, 1049.
3. Moberg, C., *Angew. Chem. Int. Ed.,* **1998**, *37*, 248.
4. Gibson, S. E.; Castaldi, M. P., *Chem. Comm.,* **2006**, *29*, 1359.
5. Burk, M. J.; Feaster, J. E.; Harlow, R. L., *Tet. Asymm.,* **1991**, *2*, 569.
6. Liang, L. C., *Coord. Chem. Rev.,* **2006**, *250*, 1152.
7. Danopoulos, A. A.; Pugh, D., *Coord. Chem. Rev.,* **2007**, *251*, 610.
8. Zysman-Colman, E.; Denis, C., *Coord. Chem. Rev.*, *256*, 1742.
9. Trofimenko, S., *Chem. Rev.,* **1993**, *93*, 943.
10. Trofimenko, S., *Polyhedron,* **2004**, *23*, 197.
11. Trofimenko, S., *J. Am. Chem. Soc.,* **1966**, *88*, 1842.
12. Niedenzu, K.; Trofimenko, S., *Inorg. Chem.,* **1985**, *24*, 4222.
13. Reger, D. L.; Tarquini, M. E., *Inorg. Chem.,* **1982**, *21*, 840.
14. Reger, D. L.; Gardinier, J. R.; Gemmill, W. R.; Smith, M. D.; Shahin, A. M.; Long, G. J.; Rebbouh, L.; Grandjean, F., *J. Am. Chem. Soc.,* **2005**, *127*, 2303.
15. LeCloux, D. D.; Tolman, W. B., *J. Am. Chem. Soc.,* **1993**, *115*, 1153.
16. LeCloux, D. D.; Keyes, M. C.; Osawa, M.; Reynolds, V.; Tolman, W. B., *Inorg. Chem.,* **1994**, *33*, 6361.
17. Tolman, W. B.; LeCloux, D. D.; Tokar, C. J.; Osawa, M.; Houser, R. P.; Keyes, M. C., *Organometallics,* **1994**, *13*, 2855.
18. Keyes, M. C.; Young, V. G.; Tolman, W. B., *Organometallics,* **1996**, *15*, 4133.
19. Chisholm, M. H.; Eilerts, N. W.; Huffman, J. C.; Iyer, S. S.; Pacold, M.; Phomphrai, K., *J. Am. Chem. Soc.,* **2000**, *122*, 11845.
20. Bellemin-Laponnaz, S.; Gade, L. H., *Angew. Chem.,* **2002**, *114*, 3623.
21. Gade, L. H.; Bellemin-Laponnaz, S., *Angew. Chem. Int. Ed.,* **2002**, *41*, 3473.

22. Gade, L. H.; Dro, C.; Bellemin-Laponnaz, S.; Welter, R., *Angew. Chem. Int. Ed.,* **2004**, *43*, 4479.

23. Gade, L. H.; Ward, B. D.; Bellemin-Laponnaz, S., *Angew. Chem. Int. Ed.,* **2005**, *44*, 1668.

24. Gade, L. H.; Lukešová, L.; Ward, B. D.; Bellemin-Laponnaz, S.; Wadepohl, H., *Dalton Trans.,* **2007**, 920.

25. Gade, L. H.; Ward, B. D.; Lukešová, L.; Wadepohl, H.; Bellemin-Laponnaz, S., *Eur. J. Inorg. Chem.,* **2009**, *2009*, 866.

26. Gade, L. H.; Lukešová, L.; Ward, B. D.; Bellemin-Laponnaz, S.; Wadepohl, H., *Organometallics,* **2007**, *26*, 4652.

27. Sadow, A. D.; Baird, B.; Pawlikowski, A. V.; Su, J.; Wiench, J. W.; Pruski, M., *Inorg. Chem.,* **2008**, *47*, 10208.

28. Sadow, A. D.; Dunne, J. F.; Su, J.; Ellern, A., *Organometallics,* **2008**, *27*, 2399.

29. Sadow, A. D.; Pawlikowski, A. V.; Ellern, A., *Inorg. Chem.,* **2009**, *48*, 8020.

30. Sadow, A. D.; Dunne, J. F.; Fulton, D. B.; Ellern, A., *J. Am. Chem. Soc.,* **2010**, *132*, 17680.

31. Sadow, A. D.; Ho, H.-A.; Dunne, J. F.; Ellern, A., *Organometallics,* **2010**, *29*, 4105.

32. Sadow, A. D.; Neal, S. R.; Ellern, A., *J. Organomet. Chem.,* **2011**, *696*, 228.

33. Sadow, A. D.; Manna, K.; Xu, S., *Angew. Chem. Int. Ed.,* **2011**, *50*, 1865.

34. Ionescu, G., Thesis, Eindhoven University of Technology, 2004.

35. Adolfsson, H.; Wärnmark, K.; Moberg, C., *J. Chem. Soc., Chem. Commun.*, **1992**, 1054.

36. Adolfsson, H.; Nordström, K.; Wärnmark, K.; Moberg, C., *Tet. Asymm.,* **1996**, *7*, 1967.

37. Castaldi, M. P.; Gibson, S. E.; Rudd, M.; White, A. J. P., *Angew. Chem.,* **2005**, *117*, 3498.

38. Castaldi, M. P.; Gibson, S. E.; Rudd, M.; White, A. J. P., *Chem. Eur. J.,* **2006**, *12*, 138.

39. Bailey, P. J.; Pinho, P.; Parsons, S., *Inorg. Chem.,* **2003**, *42*, 8872.

40. Reglinski, J.; Garner, M.; Cassidy, I.; Spicer, M. D.; Kennedy, A. R., *Chem. Commun.*, **1996**, *17*, 1975.

41. Reglinski, J.; Slavin, P. A.; Spicer, M. D.; Kennedy, A. R., *Dalton Trans.*, **2000**, *2000*, 239.

42. Reglinski, J.; Spicer, M. D., *Eur. J. Inorg. Chem.*, **2009**, *2009*, 1553.

43. Reglinski, J.; Garner, M.; Spicer, M. D.; Kennedy, A. R., *J. Am. Chem. Soc.*, **1999**, *121*, 2317.

44. Song, D. T.; Jia, W. L.; Wu, G.; Wang, S. N., *Dalton Trans.*, **2005**, 433.

45. Hill, A. F.; Foreman, M. R. S. J.; Owen, G. R.; White, A. J. P.; Williams, D. J., *Organometallics*, **2003**, *22*, 4446.

46. Hill, A. F.; Owen, G. R.; White, A. J. P.; Williams, D. J., *Angew. Chem. Int. Ed.*, **1999**, *38*, 2759.

47. Parkin, G.; Pang, K.; Tanski, J. M., *Chem. Comm.*, **2008**, 1008.

48. Al-Harbi, A.; Sattler, W.; Sattler, A.; Parkin, G., *Chem. Comm.*, **2011**, *47*, 3123.

49. Owen, G. R.; Dyson, G.; Hamilton, A.; Mitchell, B., *Dalton Trans.*, **2009**, *2009*, 6120

50. Bailey, P. J.; McCormack, C.; Parsons, S.; Rudolphi, F.; Sanchez-Perucha, A.; Wood, P., *Dalton Trans.*, **2007**, 476.

51. Bailey, P. J.; Lorono-Gonzales, D.; McCormack, C.; Millican, F.; Parsons, S.; Pfeifer, R.; Pinho, P. P.; Rudolphi, F.; Sanchez Perucha, A., *Chem. Eur. J.*, **2006**, *12*, 5293.

52. Bailey, P. J.; Budd, L.; Cavaco, F. A.; Parsons, S.; Rudolphi, F.; Sanchez-Perucha, A.; White, F. J., *Chem. Eur. J.*, **2010**, *16*, 2819.

Chapter Two

Substituted Scorpionates: Reactivity at the Central Boron in Tris(methimazolyl)borate Ligand

2.1 Introduction

Scorpionates have traditionally been synthesised as anionic ligands from the solventless melt reaction between a protic heterocycle and an alkali metal borohydride.[1-4] In 1985, Niedenzu reported the synthesis of a charge-neutral zwitterionic analogue of Tp [$(HNMe_2)B(pz)_3$] in which the hydride is replaced with a dimethylamine moiety, achieved by reaction of pyrazole with tris(dimethylamino)borane.[5] Over recent years the Bailey group have developed this synthetic route to include other heterocyclic ligand donor arms.[6-8] Perucha studied the reactivity of a variety of heterocycles with tris(dimethylamino)borane and found that certain of these formed a $(HX)BX_3$ (b) species whilst others gave a ligand of the form $(HNMe_2)BX_3$ (a) regardless of the stoichiometries used (Scheme 2.1).[9]

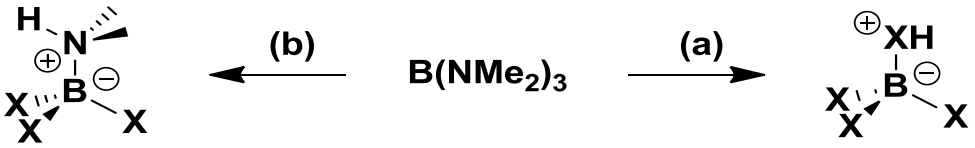

Scheme 2.1: Synthesis of scorpionates from tris(dimethylamino)borane (HX = protic heterocycle).

The formation of these two species was shown to be dependent upon the basic pK_a of the heterocycle used (Table 2.1). Thus, reaction between methimazole and tris(dimethylamino)borane yields $(HNMe_2)$ZTm (**2.1**), the charge neutral zwitterionic analogue of Tm. The dimethylamine in $(HNMe_2)B(methimazolyl)_3$ (**2.1**) may be substituted with a wide range of donors (D) to provide new ligands [(D)ZTm] (Scheme 2.2) providing these donors have a basic pKa greater than that approximately 3.0.

Table 2.1: pKa (in H_2O) of the heterocycles used in reaction with tris(dimethylamino)borane.

Heterocycle	Acidic pKa	Basic pKa	Product
Methimazole	12	-1.0	(a)
2-Nitroimidazole	7.5	-0.8	(a)
Pyrazole	14.0	2.8	(a)
2-Chloroimidazole	10.5	3.5	(b)
Benzimidazole	13.2	5.7	(b)
Imidazole	14.9	7.0	(b)
2-Methylimidazole	14.1	7.8	(b)

The initial mechanism proposed for this transformation involved the formation of an intermediate in which the boron centre was activated to reaction with weakly basic heterocycles by coordination of the strong donor to the $B(NMe_2)_3$. This was proposed to provide the tetrahedral adduct $[DB(NMe_2)_3]$ in which the basicity of the NMe_2 groups would be expected to be substantially increased by removal of the B-N π-bonding present in $B(NMe_2)_3$. This led to the early syntheses being carried out as 'one-pot' reactions between the borane, a heterocycle and a donor. However, no evidence for this activated tetrahedral species was found and it was subsequently demonstrated that reaction of a donor with $(HNMe_2)ZTm$ (**2.1**) gave the concordant substituted ligand via simple substitution of the $HNMe_2$ group. Thus, a second mechanism was proposed which allows for the

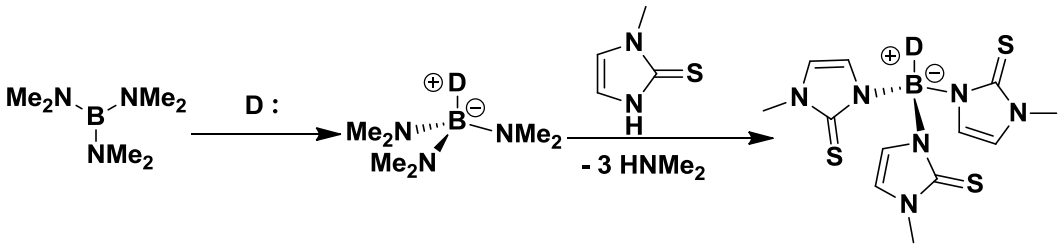

Scheme 2.2: Initially proposed mechanism for the formation of ligands of the type (D)ZTm.

substitution of the protonated dimethylamine group at any stage in the reaction (Scheme 2.3).

Substitution of the dimethylammonium group in **2.1** is aided by the loss of $HNMe_2$ gas from the reaction mixture which drives the equilibrium towards the right and enables the use of donors considerably less basic than $HNMe_2$. Studies with a variety of strong Lewis base donors demonstrated that the rate of substitution is dependent upon the basicity of the donor used. Strong Lewis bases such as DBU may coordinate to the boron centre before the formation of **2.1** as these reactions proceed more quickly than those

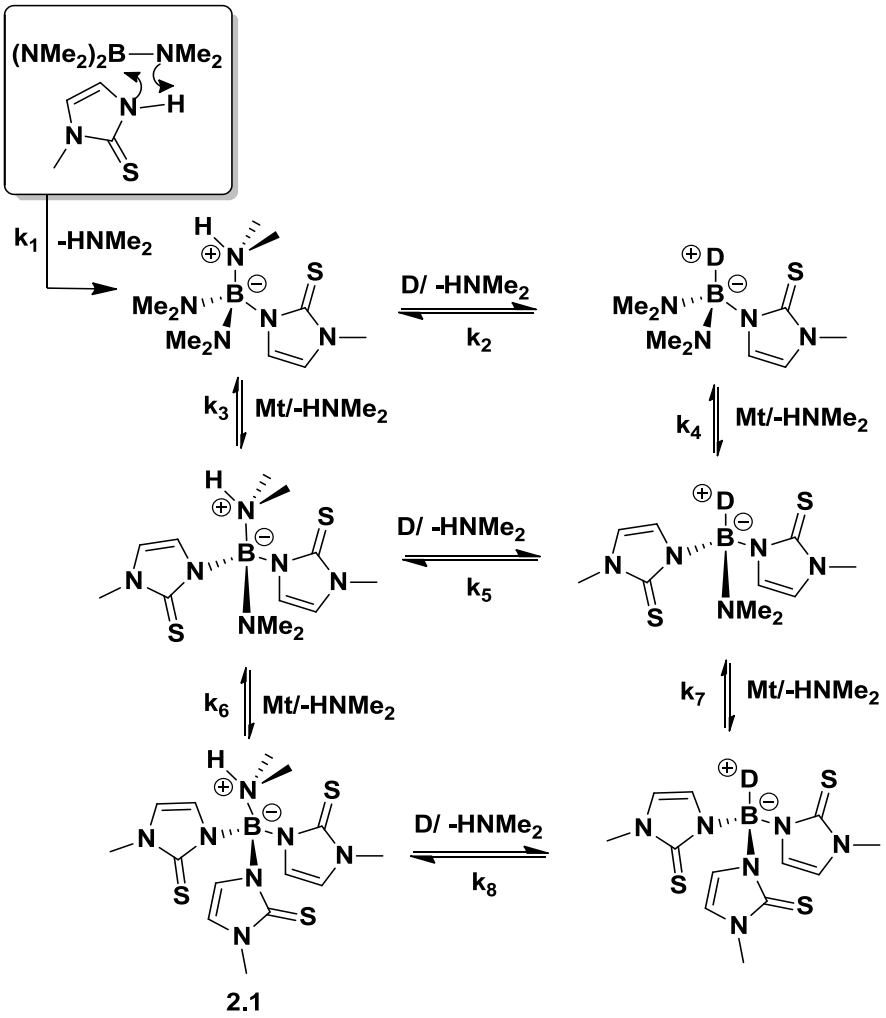

Scheme 2.3: Mechanism for the formation of zwitterionic charge neutral scorpionate ligands.

without added base. However, poorer bases such as 4-methoxypyridine likely substitute dimethylamine after formation of **2.1**.

In contrast to the amines shown in (Table 2.2), triethylamine was found to be unreactive towards substitution of the dimethylamine group despite its high basic pKa (18.4 in MeCN). The reasons for this were ascribed to the steric hindrance of the nitrogen ethyl groups meaning that steric requirements must also be considered when selecting donors for the boron centre in these systems.

Table 2.2: Donors used previously to substitute the dimethylamine group in **2.1.**

Donor	Basic pKa (MeCN)	Reaction Time
$HNMe_2$	10.73	2
4-Methoxypyridine	14.23	8
DMAP	17.95	6
1-methylimidazole	-	3
Triethylamine	18.4	-
DBN	23.79	1
DBU	24.34	1

2.2 Results and Discussion

2.2.1 Secondary Amines

Both tertiary and primary amines had previously been studied in both 'one-pot' (*vide supra*) and 'stepwise' reactions from **2.1**. Thus, reactions with secondary amines were studied to in order to complete the series.

2.2.1.1 Piperidine

Piperidine was selected due to its high basic pKa (H_2O) of 11.02 and low steric demand as a consequence of its cyclic nature. Thus, piperidine and tris(dimethylamino)borane were added to a suspension of three equivalents of methimazole in dry toluene (Scheme 2.4). The reaction mixture was heated to reflux for 6 hours forming a white precipitate after *ca.* 3 h. Upon cooling the precipitate was filtered and washed with toluene and diethyl ether. The target material, **2.2**, was isolated as a white powder in 79% yield.

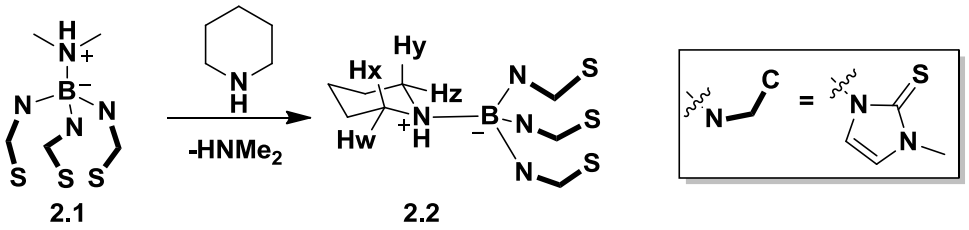

Scheme 2.4: Synthesis of (Piperidinium)tris(methimazolyl)borate **2.2**.

Due to the similarity in the structures of **2.2** and **2.1** the ^{1}H-NMR shifts of both ligands correlate closely. Resonances for the methimazolyl aromatic protons appear at 6.62 and 6.39 ppm while same protons in **2.1** resonate at 6.65 and 6.43 ppm. Similarly, the methimazolyl NCH_3 protons appear at 3.53 ppm compared with 3.56 ppm in **2.1**. However, there are also important differences in the spectra of these two ligands. The piperidinium NH proton appears at 8.81 ppm whereas the dimethylammonium proton in **2.1** appears at 9.77 ppm, although the shifts of these highly acidic protons are often concentration dependent. Intriguingly, the α-methylene protons of the piperidine ring appear as four very broad singlets at 4.42, 4.04, 2.77 and 2.28 ppm. The remaining piperidine protons appear as set of complex overlapping multiplets between 1.94 - 1.35 ppm.

The inequivalence of the piperidine α-methylene groups demonstrates that these protons are diastereotopic. Since there are no chiral centres in the molecule the diastereotopic nature of these protons suggests the stereoisomerism must be imparted by inherent helical chirality in the $B(mt)_3$ fragment.

The X-ray crystal structure of the analogous ligand $(HNMe_2)ZTm$ (**2.1**) in fact shows two enantiomers in the unit cell (Figure 2.1).[6] These arise because of the C_3-symmetric propeller conformation of the methimazole ligand arms which can either exhibit P or M axial chirality.[iii] The result of this axial chirality in the piperidine analogue (**2.2**) would be the inequivalence of the H_x/H_y and H_w/H_z protons which would otherwise be symmetry equivalent (Figure 2.2).

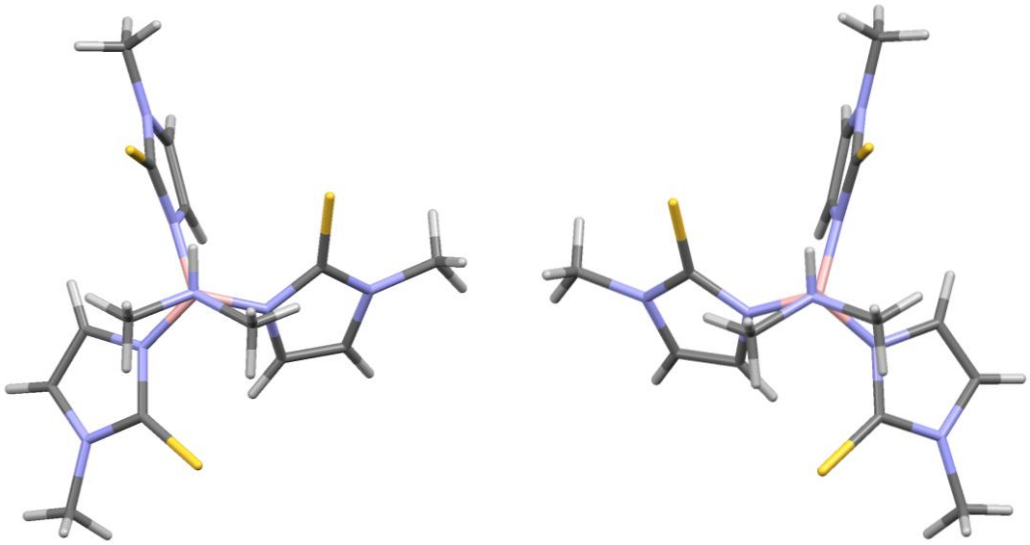

Figure 2.1: X-ray Crystal structure showing the two helical enantiomers of **2.1**.

[iii] Helical or Axial chirality is denoted as P (plus) or M (minus) for the relative twisting directions (clockwise or anticlockwise respectively). Therefore, the P enantiomer of these ligands have a positive value for the N-B-N-C torsion angle whilst those with a negative value are denoted M.

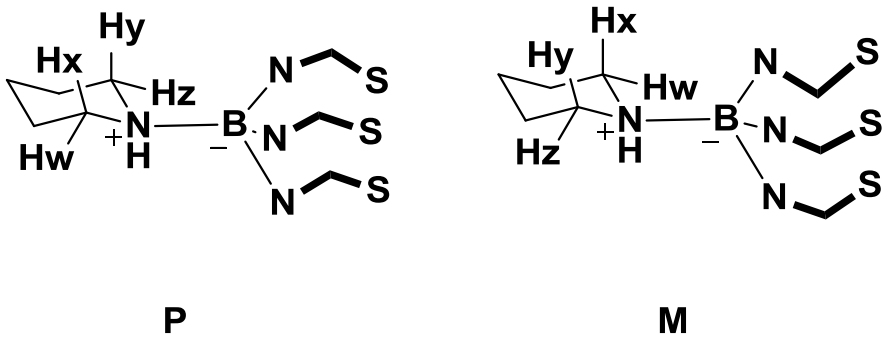

Figure 2.2: Model of the two enantiomers of **2.2.**

X-ray quality crystals of **2.2** were grown by slow cooling of a concentrated solution of the ligand in DCM (Figure 2.3). Unexpectedly, the ligand spontaneously resolves upon crystallisation giving a mixture of enantiopure crystals. The ligand crystallises in the chiral space group $P2_12_12_1$ and contains only one independent molecule in the asymmetric unit. In the

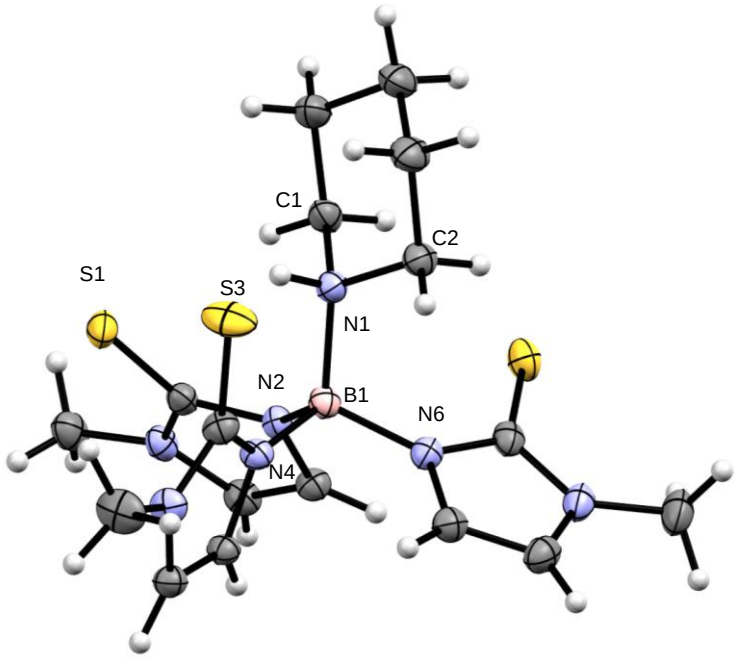

Figure 2.3: X-ray crystal structure of (piperidinium)tris(methimazolyl)borate (**2.2**). Selected bond lengths and angles are provided in Table 6.1. Displacement elipsoids have been drawn at 50% probablility .

crystal chosen, the structure shows the 'propeller' arrangement of the ligand arms from which chirality is derived but only in the P helical conformation. A hydrogen bond exists between the piperidinium proton and one of the methimazolyl sulfur atoms with a N1-S3 distance of 3.132 Å. The result is a much lower torsion angle for N1-B1-N4-C10 (-15.62°) compared with the other ligand arms (-64.29° and -64.81°).

Variable Temperature NMR studies were undertaken to ascertain the energy barrier to interconversion between the two enantiomers of **2.2** present in solution. Figure 2.4 shows the aliphatic region of the ^{1}H-NMR spectrum which contains resonances representing the protons of the piperidinium ring while Figure 2.5 shows only the region in which protons H_x (4.23 ppm) and H_y (3.88 ppm) resonate. At room temperature (303 K) these resonances

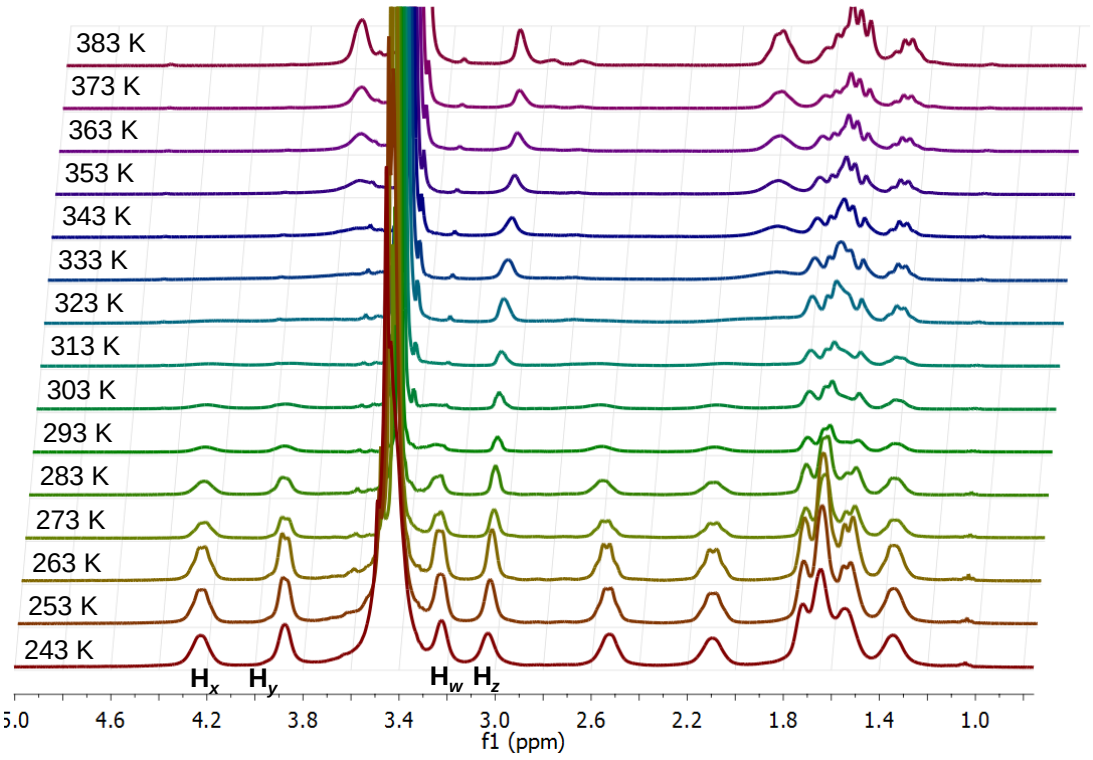

Figure 2.4: Aliphatic Region of the ^{1}H-NMR spectra of **2.2** in tetrachloroethane-d_2 between 243-383 K showing the coalescence of the resonances representing the diastereotopic protons H_w, H_x, H_y and H_z at high temperature.

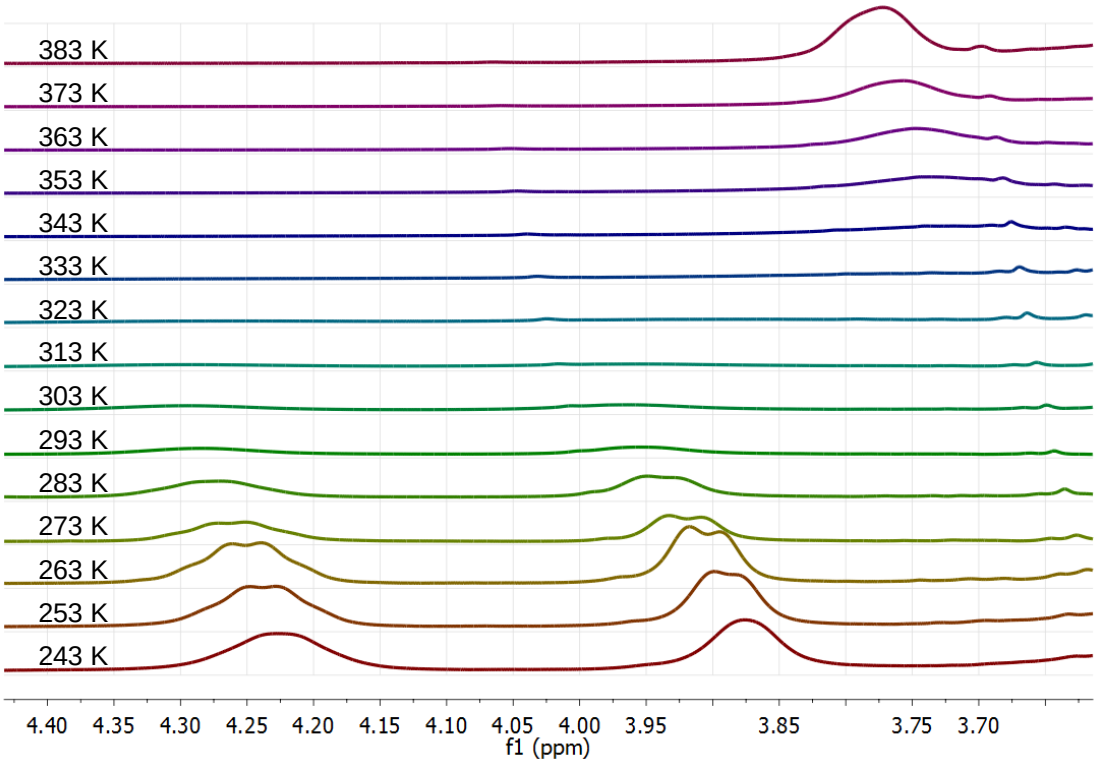

Figure 2.5: VT NMR of **2.2** showing the resonances relating to the diastereotopic piperidine protons H_x (4.23 ppm)and H_y (3.88 ppm) which coalesce to a single signal at 3.78 ppm above 343 K.

appear as two broad singlets. However, these signals become extremely broadened upon heating, coalescing at 343 K and giving a broad singlet (3.78 ppm) integrating for 2H at temperatures above 373 K. These data allow the calculation of the energy barrier to interconversion between these enantiomers using the Eyring equation (Equation 2.1).

At 243 K the separation of these resonances is 140.21 Hz and coalescence of these resonances occurs at 343 K. Using Equation 1, $\Delta G^{\ddagger}$ of interconversion was therefore calculated to be 68.0 kJ mol^{-1}. This activation energy suggests that the interconversion of helical enantiomers is relatively fast at room temperature (298 K) with a half-life of *ca.* 94 ms rising to *ca.* 1 minute at 243 K. Therefore, even if separation of these enantiomers was

possible (*e.g.* by chiral chromatography) racemisation would occur rapidly under ambient conditions.

Equation 2.1: Eyring equation.

$$k = \frac{RT}{N \cdot h} \cdot e^{\frac{-\Delta G}{RT}}$$

R = Universal Gas Constant = 8.314 J K^{-1} mol^{-1}

T = Temperature (K)

N = Avogadro's Number = 6.022 x 10^{23} mol^{-1}

h = Planck Constant = 6.626 x 10^{-34} J s

ΔG‡: Free Energy of Activation (kJ mol^{-1})

$$k = 2.22\Delta\nu$$

$\therefore$ Equation 1 can be simplified to:

$$\Delta G = R \cdot T_c \left[22.96 + \ln\left(\frac{T_c}{\Delta\nu} \right) \right]$$

T_c = Coalescence Temperature (K)

Δν: Separation of peaks in absence of exchange (Hz)

Δν = 140 Hz, T_c = 343 K

$\therefore$ **ΔG‡ = 68.02 kJ mol^{-1}**

2.2.1.2 Morpholine

Morpholine has two functional groups compared with piperidine's one. Although slightly less basic than piperidine, the amine group was expected to substitute the dimethylamine group in **2.1** relatively quickly based on previous trends. It was less certain whether the ether oxygen would attack a second boron centre. As a hard Lewis acid boron is highly oxophilic however ether oxygen atoms are poor Lewis bases.

Freshly distilled morpholine was added to a suspension of (dimethylammonium)tris(methimazolyl)borate (**2.1**) in toluene. The reaction mixture was heated to reflux for 12 h and formed a white precipitate upon cooling to room temperature. This precipitate was filtered, washed with toluene and diethyl ether and dried *in vacuo*. Mass spectrometry (EI) of the isolated material (**2.3**) showed a molecular ion peak at m/z = 437.2 indicating attack of only one boron centre by the morpholine amine functionality. In the ^{1}H-NMR spectrum the methimazolyl aromatic protons appear at 6.66 and 6.43 ppm integrating for 3H each. A broad resonance at 9.54 ppm was assigned as the morpholinium NH proton. As with **2.2** the morpholinium α-methylene protons are diastereotopic and appear as four broad resonances at 4.91, 4.28, 3.20 and 2.73 ppm. The protons of the β-methylene groups appear

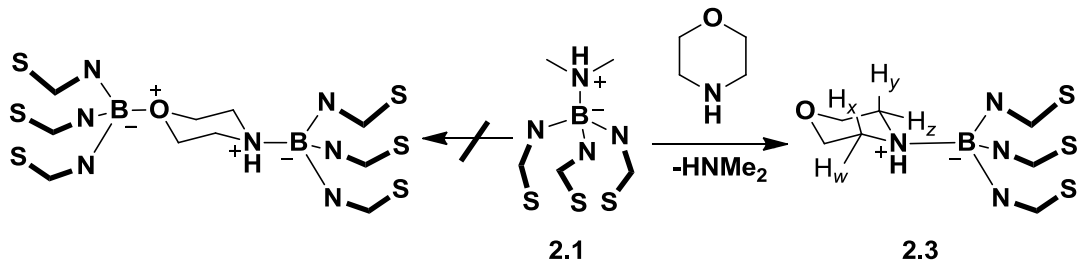

Scheme 2.5: Reaction of **2.1** with morpholine to give **2.3**.

as complex overlapping multiplets at 4.00 ppm.

2.2.1.3 Piperazine

Piperazine contains two amine functional groups and therefore was expected to coordinate to two boron centres giving **2.4a** (Scheme 2.6). Freshly sublimed piperazine[iv] and two equivalents of **2.1** were suspended in dry toluene and the reaction mixture refluxed for 4 h. After this time, a sample of the reaction mixture was subjected to ^{1}H-NMR spectroscopy. The spectrum indicated that the reaction mixture contained a mixture of **2.1**, free piperazine and a large proportion of methimazole. Continued heating of the reaction mixture resulted only in the continued degradation of the ligand yielding methimazole and piperazine upon workup after 72 h in refluxing toluene.

The degradation of the ligand in this reaction can be rationalised as a result of the bifunctionality of piperazine (Scheme 2.6). After piperazine

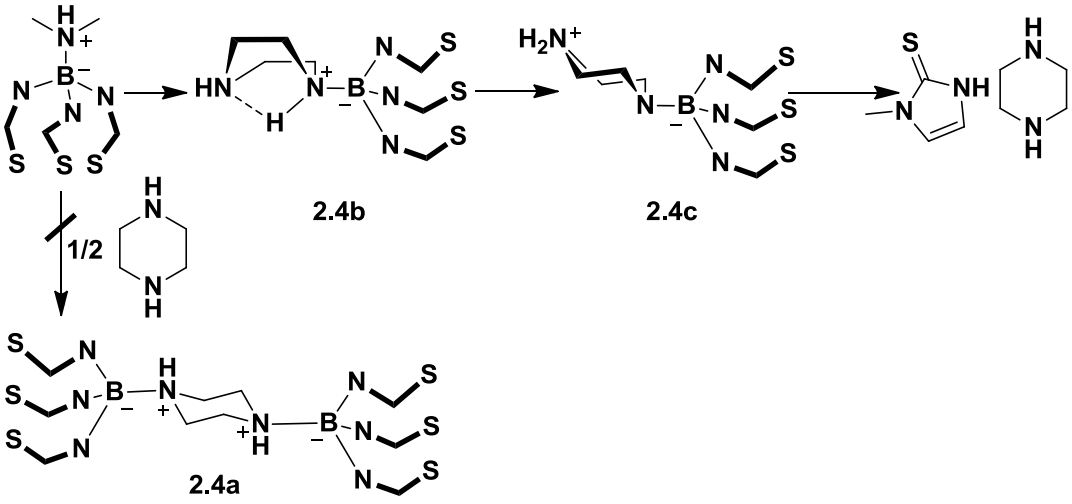

Scheme 2.6: Degradation of ZTm upon reaction with Piperazine.

[iv] In order to ensure that the highly hygroscopic piperazine remained completely dry the reagents were handled in the glovebox throughout.

substitutes the dimethylammonium group in **2.1** the proton bound to the positively charged nitrogen will become more acidic. Upon interconversion of the piperazine ring between the chair and boat conformation the strongly basic amine group is located proximate to this acidic proton (**2.4b**). Assuming intramolecular proton abstraction is faster than reaction with a second molecule of **2.1** this process may be favoured. Strong Bronsted bases have previously been shown to be able to deprotonate the dimethylammonium functionality in **2.1** resulting in complete degradation of the ligand to methimazole.[9] Therefore, ligand **2.4c** is likely to be highly unstable resulting in ligand degradation once the donor nitrogen is deprotonated.

2.2.1.4 Diisopropylamine

Triethylamine was previously shown to be unable to substitute the dimethylamine in **2.1**, an issue which was assigned to its relatively large steric bulk.[9] Diisopropylamine was used to further probe the steric requirements in these reactions. Thus, diisopropylamine was added to a suspension of (dimethylamino)tris(methimazolyl)borate in toluene and the reaction mixture heated to reflux for 72 h. After this time no reaction was detected by ^{1}H-NMR spectroscopy indicating that, similarly to NEt_3, diisopropylamine is sufficiently bulky to block its attack of the boron centre in **2.1**.

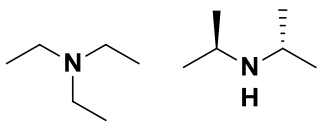

Figure 2.6: Preferred conformation of triethylamine and diisoproylamine

2.2.2 Other Amines

2.2.2.1 Ammonia

Ammonia was bubbled through a suspension of **2.1** in toluene and the reaction mixture heated to reflux for 1 h. After this time the solution was cooled and a white precipitate formed. Filtration and washing with toluene and diethyl ether yielded the ligand (ammonium)tris(methimazolyl)borate (**2.5**) as a white powder.

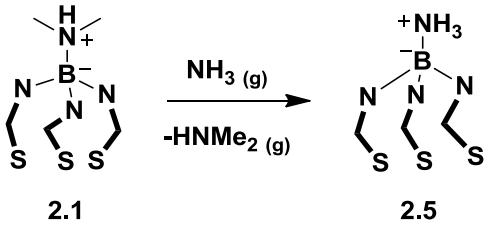

2.1 **2.5**

Scheme 2.7: Synthesis of (ammonium)tris(methimazolyl)borate (**2.5**).

The methimazole CH protons appear at 6.72 and 6.05 ppm in the ^{1}H-NMR spectrum. A very broad singlet at 8.58 ppm represents the acidic ammonium NH_3 protons. This signal is shifted to significantly higher frequency compared with ammonia borane $H_3N.BH_3$ (4 ppm)[10] suggesting that $B(mt)_3$ is a more electron deficient fragment than BH_3. This is reinforced by the ^{11}B-NMR spectrum where the boron resonance appears at -0.1 ppm (*cf.* H_3NBH_3 at -23.9 ppm). The electrophilicity of the boron centre in this ligand can be ascribed to the electron withdrawing effect of the aromatic methimazolyl rings.

X-Ray quality crystals of **2.5** were grown by slow diffusion of diethyl ether into a concentrated solution of the ligand in acetonitrile. The structure

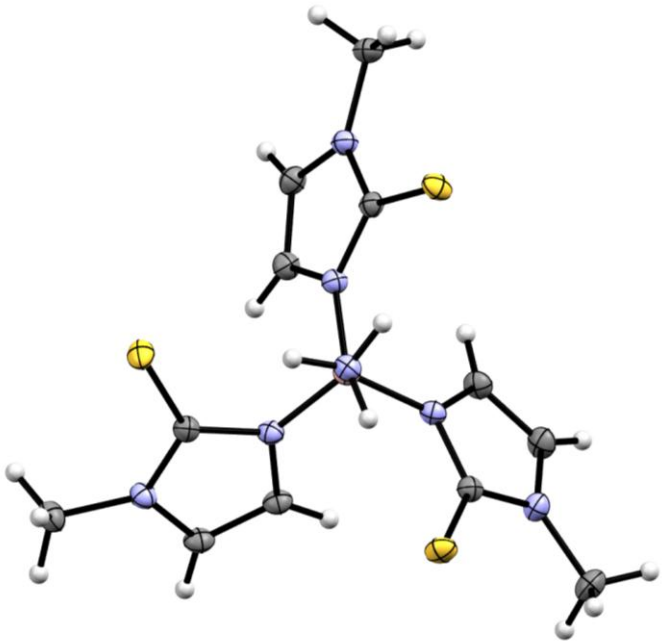

Figure 2.7: X-ray crystal structure of (NH_3)ZTm (**2.5**). Selected bond lengths and angles are provided in Table 6.2. Displacement elipsoids have been drawn at 50% probablility .

shows two independent molecules in the unit cell corresponding to the P and M axial isomers. Each molecule exhibs C_3-symmetry and the N-B-N-C torsion angles are 41.1°, 50.3° and 51.1°. In contrast, both **2.1** and **2.2** have two arms with torsion angles [*ca.* 65°] and one with a much smaller torsion angle [*ca.* 5-16°] in which the sulfur hydrogen bonds with the acidic dimethylammonium or piperidene proton. The average S-N(NH_3) distance in **2.5** is 3.164 Å and it can therefore be inferred that there is some degree of hydrogen bonding between the methimazolyl sulfurs and the ammonium protons in **2.5**.

2.2.2.2 Trimethylamine

Since only sp^2 hybridised tertiary nitrogen donors had been shown to substitute the dimethylamine group in **2.1** it was of interest to react **2.1** with a sp^3 hybridised tertiary nitrogen donor in order to investigate the steric limits of the substitution reaction. The simplest and least bulky of these was trimethylamine which has a basic pKa of 9.87. Trimethylamine was

synthesised by reaction of trimethylammonium chloride with calcium hydroxide, dried by passing over calcium oxide twice and bubbled through a solution of **2.1** in refluxing toluene. After 4 h the reaction mixture was cooled to room temperature. Despite the high basic pKa of trimethylamine no reaction was detected after this time with only the presence of **2.1** and free methimazole detected. Further reflux lead to complete degradation of the ligand to methimazole, presumably due to the presence of small quantities of water present in the gas despite the being passed over calcium oxide twice before reaction.

2.2.2.3 DABCO

1,4-Diazabicyclo[2.2.2]octane (DABCO) is a strong Lewis base, but due to its bicyclic nature it is less sterically demanding that NEt_3. DABCO is also easier to store and dry than trimethylamine and therefore **2.1** was not expected to degrade during the reaction. Freshly sublimed DABCO[v] and methimazole (3 eq.) were suspended in dry toluene (*ca.* 15 mL) and tris(dimethylamino)borane (1 eq.) were added and the suspension heated to reflux for 12 h. ^{1}H-NMR spectroscopy after this time showed no evidence of

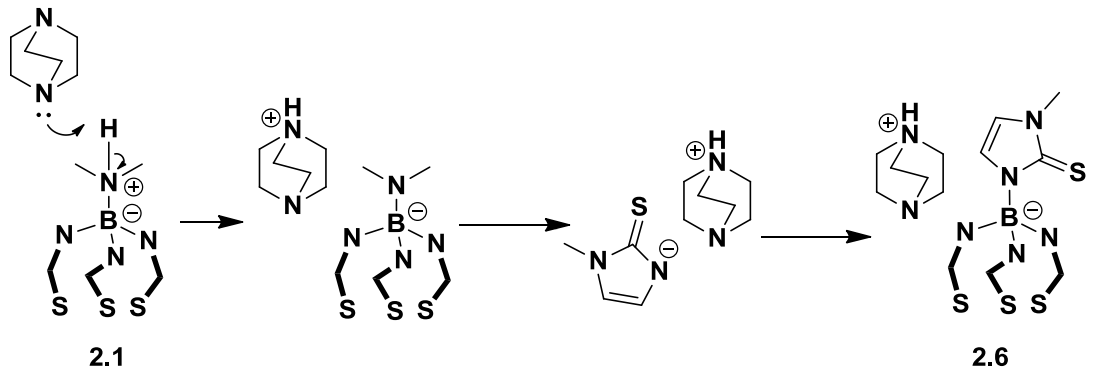

Scheme 2.8: Degradation of **2.1** to **2.6** in the presence of DABCO.

[v] As with piperazine DABCO was handled in the glovebox throughout.

reaction with only the presence of **2.1** and free DABCO detected. The reaction mixture was heated to reflux for a further 72 h, but the ^{1}H-NMR spectrum after this time showed no evidence of the target material. Small resonances at 6.65 and 7.21 indicated the presence of a new species, albeit in trace quantities. Mass spectrometry (ESI) of the reaction mixture indicated the presence of $[DABCOH]^{+}[B(mt)_4]^{-}$ (**2.6**) with a molecular ion peak at m/z = 463.09 in the negative ion spectrum. This salt may form if DABCO deprotonates the dimethylammonium moiety on **2.1** leading to degradation of the ligand to the methimazolate anion. This anion may then be able to attack another molecule of **2.1** upon extended heating yielding **2.6**. It is important to note that this material was only present in small quantities in the reaction mixture and only appears to form under forcing conditions.

2.2.3 Anionic Donors

Having demonstrated the broad scope of the synthesis of charge-neutral ZTm ligands by substitution of the dimethylamine in $(HNMe_2)$ZTm (**2.1**) with neutral donors,[4] it was of interest to explore the possibility of forming new anionic "XTm" ligands by similar substitution with anionic donors. Parkin has previously demonstrated that complexes of these ligands can be accessed by treating [TmNiX] (X = N_3, NCS, NCO) with iodine.[11] Thus the pseudohalides N_3^{-}, NCS^{-} and NCO^{-} were chosen as potential donors in this role. Due to the insolubility of the chosen $[PPN]^{+}$ and $[PPh_4]^{+}$ salts of these anions in toluene, the usual solvent for ligand substitution reactions, acetonitrile was employed as the reaction medium.

The $[PPN]^{+}$ salt of (thiocyanate)tris(methimazolyl)borate $[(SCN)Tm]^{-}$ (**2.7**) could be isolated in 51% yield after reflux of [PPN][NCS] with **2.1** for 24 hours in MeCN (Scheme 2.9).

The ^{1}H-NMR spectrum of **2.7** shows no signals due to N-H or NMe_2 groups indicating the loss of $HNMe_2$. The methimazolyl proton signals show small shifts relative to **2.1** reflecting minor changes in electronic structure between the neutral zwitterionic **2.1** and anionic **2.7**. Mass spectrometry (ESI) shows a molecular ion peak at m/z = 40 in the negative ion spectrum, consistent with the presence of the $[(SCN)B(methimazolyl)_3]^-$ anion. Additionally, the IR spectrum showed a strong absorption at 2158 cm^{-1} assigned to SCN C=N stretching (*c.f.* 2058 cm^{-1} in [PPN]SCN), thus indicating a strengthening of this bond upon coordination to the boron centre.

A complex of ligand **2.7** was obtained by reaction of [PPN][(SCN)B(mt)$_3$] with [(*p*-cymene)$RuCl_2]_2$ at room temperature in methanol for 2 hours followed by addition of sodium tetraphenylborate. After filtration of the precipitated salts and work-up of the solution the salt [(*p*-cymene)Ru{(SCN)B(mt)$_3$}][BPh_4] (**2.8**) was obtained as red needles in 30% yield.

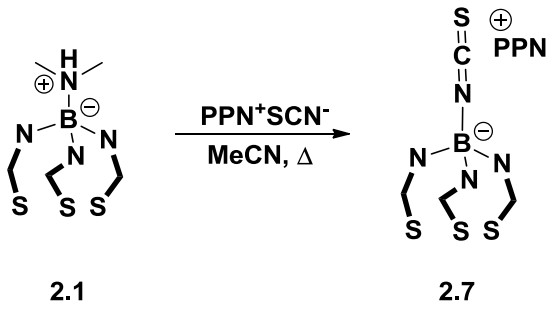

2.1 **2.7**

Scheme 2.9. Reaction of ZTm(**2.1**) with [PPN][NCS] to give **2.7**.

X-ray quality crystals of this complex were grown by slow diffusion of ether into a concentrated solution of the complex in chloroform. X-ray crystallography of this complex confirmed the structure of the ligand (Figure 2.8). The complex crystallises in space group I2/a with two independent molecules in the unit cell corresponding to the two helical enantiomers. Metric data for the two do not differ substantially and only those for the complex containing Ru1 (*i.e.* the M enantiomer) will be discussed. The B1A-N22A (NCS) bond [1.518(3)Å] is shorter than the other B-N bonds within this complex [1.542(4), 1.536(4), 1.545(3) Å] demonstrating its covalency. The N22A-C23A (NCS) bond [1.153(3) Å] is comparable with the same bond in KSCN [1.149(14) Å], although the C23A-S24A bond [1.597(3) Å] is slightly shorter than in the salt [1.689(13) Å].[12] The B1A-N22A-C23A is slightly bent

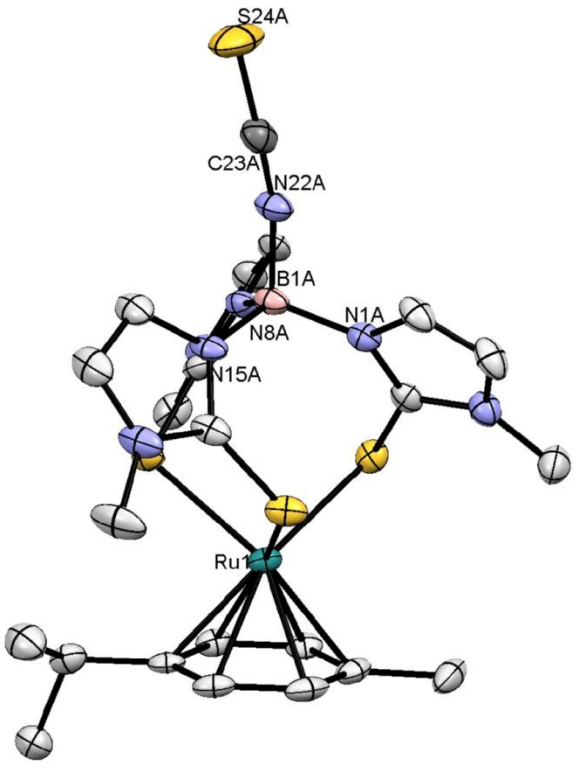

Figure 2.8. Structure of the cation of[(κ3-[S,S,S]-(thiocyanate)B(methimazolyl)3)Ru(p-cymene)][BPh_4](**2.8**). Hydrogen atoms and counter ion omitted for clarity. Displacement elipsoids have been drawn at 50% probablility .Selected bond lengths and angles are provided in Table 6.3.

[167.2(2)°], although the S24A-C23A-N22A bond angle is essentially linear [178.2(3)°].

In contrast to thiocyanate, reaction with both N_3^- and NCO^- resulted in the degradation of **2.1** to methimazolate (mt^-) after *ca.* 12 h in refluxing acetonitrile. Previous work has demonstrated that strong bases such as NaOH, NaOR and $NaNH_2$ cause degradation of **2.1** by deprotonation of the dimethylamine functionality leading to the anion $[(Me_2N)B(mt)_3]^-$ which appears to be unstable as only free methimazole is isolated in these reactions. However, N_3^- and NCO^- are not strong Brönsted bases and are in fact weaker Lewis bases than thiocyanate. Never-the-less, there are other important differences between these *pseudo*halides. Thiocyanate contains only one relatively hard donor nitrogen with the soft sulfur being unlikely to attack a second boron centre. In contrast, both azide and cyanate contain two hard donor atoms which may attack the hard Lewis acidic boron centre. This means that after initial substitution of **2.1**, **2.9a** may attack a second molecule of **2.1** forming the bis-ligand species , **2.9b**. If , **2.9b** were inherently thermodynamically unstable, with the *pseudo*halide unable to stabilise two Lewis acidic boron centres at once, then degradation may occur to give methimazolate.

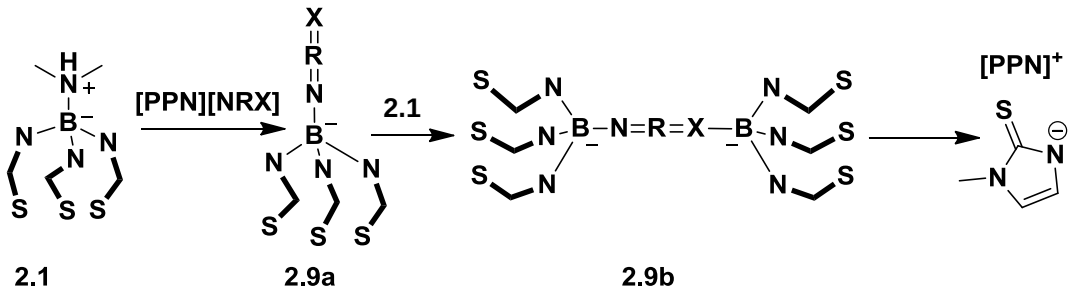

Scheme 2.10*:* Proposed reactivity of the pseudohalised N_3^- and OCN^- with **2.1** leading to ligand degradation. (R = C, N; X = O, N)

2.2.4 Unexpected reactivity

2.2.4.1 Acetonitrile

Analysis of samples of the reaction mixture during the synthesis of **2.7** by ^{1}H-NMR spectroscopy indicated the presence of an intermediate in the reaction. The origin of this species as a product of the reaction of **2.1** with the acetonitrile solvent was confirmed by heating a solution of **2.1** in acetonitrile to reflux which cleanly provided the same species (**2.10**). The ^{1}H-NMR spectrum of the reaction mixture showed no trace of **2.1** after 3 hours and EI-MS of the isolated colourless precipitate of the new species **2.10** showed a molecular ion at 436.1 *m*/*z*. The ^{1}H-NMR spectrum displayed three new resonances at 2.06, 3.05 and 3.29 ppm, each integrating as 3H. Similarly, the ^{13}C-NMR spectrum showed three new resonances in the alkyl region at 19.1, 40.6 and 41.2 ppm. An additional quaternary carbon resonance was also apparent at 167.3 ppm.

The spectra of **2.10** clearly indicate the retention of the dimethylamine group and the addition of a molecule of acetonitrile to **2.1**. Thus the acetonitrile does not substitute the $HNMe_2$ as observed with all other donors previously employed, but rather adds to the species, most likely through insertion into the B-N bond (Scheme 2.11). The 1,2-insertion of the nitrile into the B-N bond provides a species (**2.10b**) which tautomerises to provide a more stable secondary amidino moiety (**2.10**).

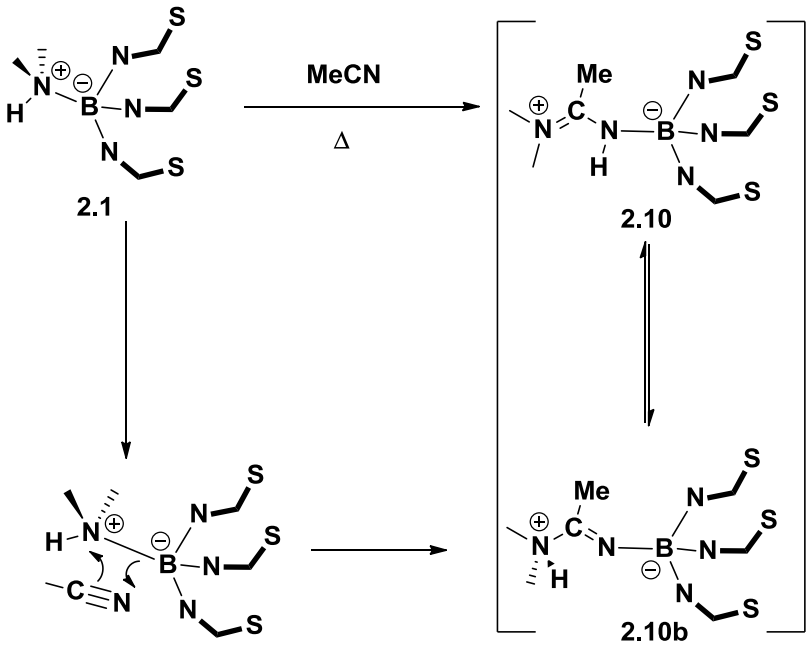

Scheme 2.11: Proposed mechanism for the reaction between the ($HNMe_2$)ZTm (**2.1**) and acetonitrile.

The inequivalence of the NMe_2 methyl groups in the ^{1}H-NMR spectrum of **2.10**, due to the presence of the C=N bond in the N, N'-dimethylacetamidino group, demonstrates the preference for tautomer **2.10** over **2.10b**. Such reactivity of **2.1** with MeCN, whilst somewhat unexpected, is not altogether unprecedented. Burger *et al.* have described a similar reaction between a boron analogue of cyclopropane with hydrogen cyanide or trimethylsilyl cyanide in the presence of acetonitrile which undergoes a ring expansion reaction via a similar mechanism.[13]

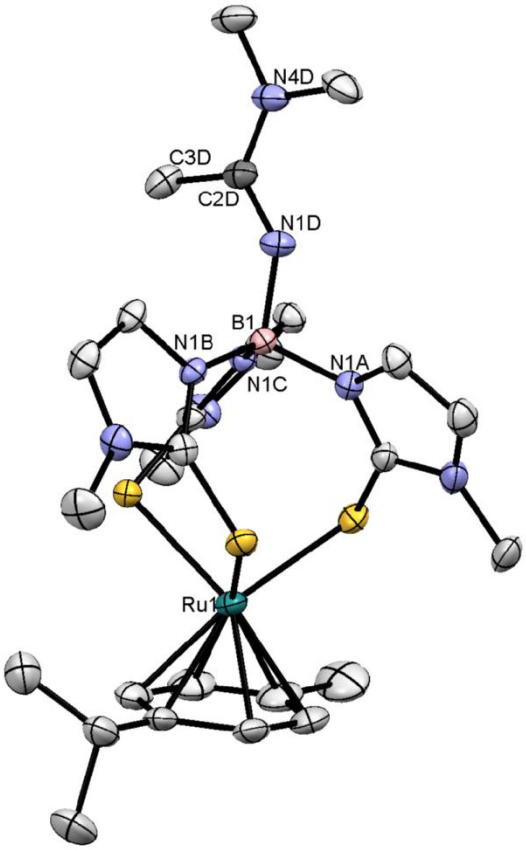

Figure 2.9: Structure of [κ^3-[S,S,S]-(*N*,*N*-dimethyl-acetamidine)B(methimazolyl)$_3$Ru(p-cymene)][PF_6]$_2$ (**2.11**). Hydrogens omitted for clarity. Displacement elipsoids have been drawn at 50% probablility .Selected bond lengths and angles are provided in Table 6.4.

A ruthenium complex, **2.11**, of ligand **2.10** was obtained by stirring a solution of the ligand in methanol with [(*p*-cymene)$RuCl_2$]$_2$ followed by precipitation by addition of [NH_4][PF_6]. X-ray quality crystals of **2.11** were grown from a slow diffusion of ether into a concentrated solution of the complex in acetonitrile. X-ray crystallography of this complex confirmed the predicted structure of the ligand (Figure 2.9). The angles around the NMe_2 group N(4D) (117.0, 120.7 and 122.3°) confirm its hybridisation as sp^2, and thus the ligand structure as **2.10** rather than **2.10b**. The C(2D)-N(4D) bond length to the NMe_2 group is shorter [1.315(3) Å] than the C(2D)-N(1D) bond [1.337(3) Å] pointing to the same conclusion and suggesting that the positive

charge resides on the NMe_2 nitrogen, although it is likely that there is some degree of delocalisation. The N-B bond length was found to be 1.545(3) Å which is concordant with typical B-N(sp^2) coordinate bonds.

2.2.4.2 Benzonitrile

Based on this unexpected result investigations were undertaken to determine whether other nitriles displayed similar reactivity with **2.1**. Despite its lower Lewis basicity, benzonitrile was also shown to insert into the B-N coordinate bond. This conversion proceeded more slowly than that with acetonitrile, despite the higher reflux temperature, providing the target species (**2.12**) after 8 hours at 110°C. EI-MS confirmed the expected formulation of **2.12** with a molecular ion peak at m/z = 498.2. The ^{1}H-NMR spectrum showed unusually broadened resonances for the methimazolyl protons at (6.39 and 6.84 ppm) which suggested possible restricted rotation about the B-N bond to the amidino group, due to steric interaction between the phenyl and methimazole rings, and consequent inequivalence of the methimazolyl rings. Additionally **2.12** displays a larger difference in the chemical shifts for the dimethyamine-derived methyl groups (2.83 and 3.57 ppm) which is attributed to ring-current effects of the phenyl ring which are absent in the methyl derivative **2.10**.

A ruthenium complex of this ligand (**2.13**) was synthesised and crystals were grown in a similar manner as for **2.11**. The crystal structure of **2.13** (Figure 2.10) shows that the phenyl ring resides between two of the methimazolyl arms of the ligand, approximately parallel to one of them, which may indicate some π-stacking interactions. The distance between the centroid of the phenyl ring and that of its nearest methimazolyl neighbour is 3.419 Å, and the angle between the two ring planes is 24.5°. The B-N(2) bond distance [1.544(5) Å] in this ligand is essentially the same as in **2.11** as is the

N(2)-C(3) bond to the NMe_2 group [1.340(5) Å]. The C(3)-N(1) bond, however, is slightly longer than in **2.11** [1.326(5) Å] indicating the effect of the phenyl ring on the resonance structure within the N-C-N unit. This observation is confirmed by the lower energy of the C=N bond stretching vibration in the IR spectrum which appears at 1608 cm^{-1} and compares with 1632 cm^{-1} in **2.11**.

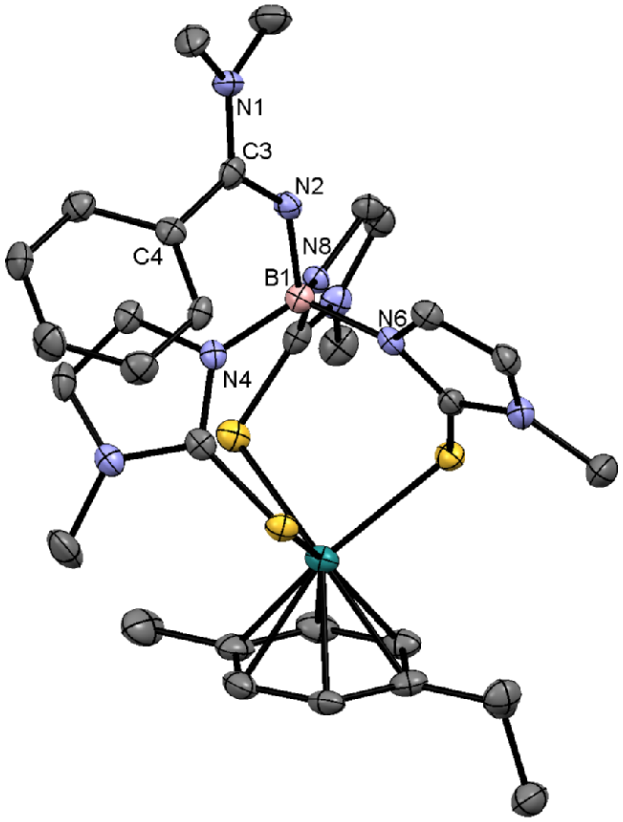

Figure 2.10: Structure of the dication in [κ^3-[S,S,S]-(*N,N*-dimethylbenzamidine)B(methimazolyl)$_3$Ru(p-cymene)][PF_6]$_2$ (**2.13**). PF_6 counterions and MeCN solvent omitted for clarity. Displacement elipsoids have been drawn at 50% probablility .Selected bond lengths and angles are provided in Table 6.5.

2.2.5 Oxygen Donors

Both ligands **2.10** and **2.12** are nitrogen analogues of the ligand characterised by Reglinski et al. in which a dimethylformamide molecule was found to coordinate to the boron fourth position, (DMF)ZTm.[14] The crystal structure of this ligand shows the expected oxygen coordination of

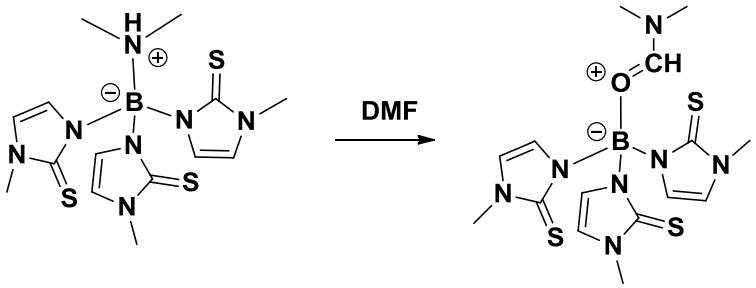

2.1 **2.14**

Scheme 2.12: Direct route to (DMF)ZTm (**2.14**).

the DMF to boron and adopting sp^2 hybridisation. It was therefore expected that reaction of **2.1** with DMF would yield the same ligand by substitution of the dimethylamine moiety. Reaction of **2.1** with one molar equivalent of DMF under reflux in toluene for 6 hours provided a colourless precipitate (Scheme 2.12). The ^{1}H-NMR spectrum of this material confirmed it to be (DMF)ZTm (**2.14**) with two resonances at 3.25 and 3.31 ppm (each 3H) representing NCH_3, as well as a singlet at 8.69 ppm integrating as 1H due to the formyl proton. Mass spectrometry (ESI) displayed a molecular ion peak at m/z = 423.9 consistent with this formulation. Finally, IR spectroscopy also agreed with reported data and displayed an absorbance at 1679 cm^{-1} assigned to the coordinated DMF C=O stretch. This reaction expands the range of available nucleophiles which are known to substitute the dimethylamine group in **2.1** to include oxygen donors.

2.2.6 Carbon Donors

2.2.6.1 Aryl Isonitrile

Having successfully exploited both nitrogen and oxygen donors it was of interest to investigate the coordination of a carbon donor to the boron centre. Thus, 2,6-dimethylphenyl isonitrile was stirred with **2.1** in toluene under reflux for 4 days providing a colourless solid upon work-up (Scheme 2.13).

Mass spectrometry (EI) of this material showed a peak at m/z = 481.1 indicating its formulation as the species formed from substitution of $HNMe_2$ by the isonitrile, (ArNC)ZTm. ^{1}H-NMR spectroscopy showed no resonances which could be assigned to an NMe_2 group indicating substitution of the dimethylamine group. However, a broad singlet integrating as 6H at 2.14 ppm, along with a multiplet (3H) in the aromatic region, confirmed the presence of the isonitrile aryl group. It should be noted that the three methimazolyl arms in this ligand appear equivalent by NMR spectroscopy at ambient temperature. However, IR spectroscopy showed no absorption corresponding to a CN triple bond, but an absorption was observed at 1660 cm^{-1} corresponding to a C=N stretch. Very weak and missing nitrile bands have been reported previously by Kitson and Griffith when the nitrile is bonded to electronegative groups.[15] Despite this fact, a similar boron compound, $Na[(cyano)B(pyrrolyl)_3]$, previously synthesised by Györi,[16] displayed the expected nitrile stretching frequency at around 2217 cm^{-1}, but no information was provided on the intensity of this band.

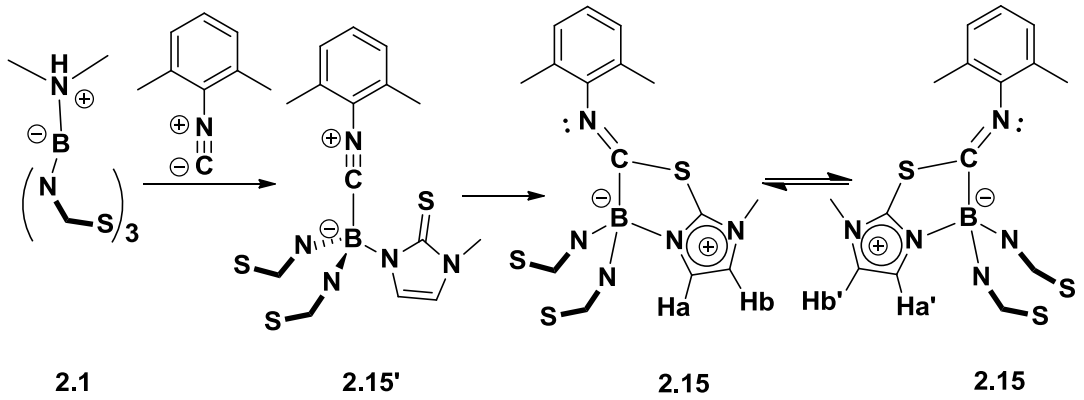

Scheme 2.13: Reaction of 1 with ArNC gives (ArNC)ZTm (**2.15'**) which is stabilised by the formation of the fluxional species **2.15**.

Variable temperature ^{1}H-NMR studies showed three resonances for H_a (Scheme 2.13) at 223 K indicating inequivalence of the methimazole rings at this temperature. Coalescence of these resonances occurred above 253 K. These data indicate that the isonitrile carbon is stabilized by a fluxional interaction (**2.15**) of the methimazole sulfur atoms which equilibrates between the three methimazolyl arms faster than the NMR timescale at room temperature.

X-ray quality crystals of this ligand were grown by slow diffusion of

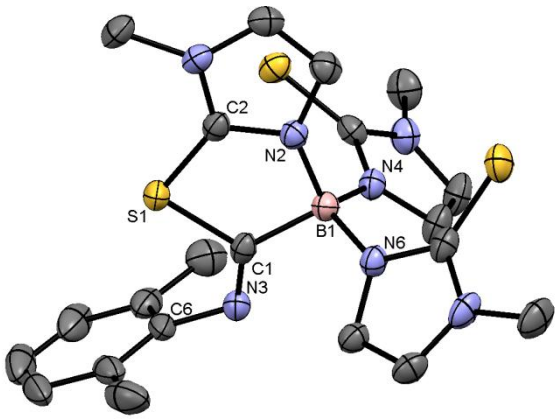

Figure 2.11: Structure of 3-bis(methimazolyl)-2-(2,6-dimethylphenylimino)-7-methyl-[1,4,3]-thiazaborolo[5,4-*b*]imidazolium (**2.15**). Hydrogen atoms have been omitted for clarity. Displacement elipsoids have been drawn at 50% probablility .Selected bond lengths and angles are provided in Table 6.6.

diethyl ether into a concentrated solution of the ligand in dichloromethane (Figure 2.11). The presence of a [1.4.3]-thiazaborolo-[5,4-b]-imidazolium ring formed by attack of the methimazole sulfur at the isonitrile carbon confirms the structure of the ligand as **2.15**.

There are few reports of thiazaborole rings in the literature; the only structurally characterized compound in the CCDC was reported by Carboni (Figure 2.12).[17] However, Carboni's system is fused to pyridine rather than an imidazole ring and contains a sp^3-hybridised carbon in the 2-position resulting in a partially unsaturated ring. These differences may contribute to a tighter thiazaborole ring in **2.15** demonstrated by the shorter bond lengths and smaller angles found in this complex. The thiazaborole S(1)-C(1) bond length [1.835(2) Å] is indicative of a relatively long C-S single bond and is slightly longer than in Carboni's system [1.805 Å]. However, the C(2)-S(1) bond [1.721(3) Å] is shortened compared with the reported thiazaborole [1.743 Å] and the C(1)-S(1)-C(2) angle (89.4°) is surprisingly small even compared with the literature value (94.9°). The B(1)-C(1)-S(1) angle in **2.15** is 112.6° compared with 108.5° in Carboni's species which is indicative of sp^2 hybridisation of the carbon in this position. The presence of an exocyclic C=N double bond is confirmed by the short C(1)-N(3) bond length of 1.255(3) Å.

It may be surmised that **2.15** arises because the donor properties of the *sp*-hybridized carbon donor are insufficient to stabilize the electron-deficient boron centre. The formation of this species illustrates the nucleophilic

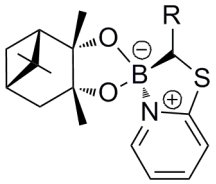

Figure 2.12: Carboni's thiazaborolo system

character of the methimazolyl sulfur atoms, something which has previously been observed to be responsible for the formation of ring-opened products on attempted coordination of oxazolines to the boron in **2.1** (See Chapter 3).[18] The structure of **2.15** confirms the presence of a B-C bond in the ligand, and thus by implication that substitution of the $HNMe_2$ moiety in **2.1** occurs by attack of the isonitrile carbon at the boron centre during the synthesis of ligand **2.15**.

The free ligand **2.15** was coordinated to Ru(II) by treatment with $[Ru(p\text{-cymene})Cl_2]_2$ in methanol and the resulting complex (**2.16**) precipitated after anion exchange with $[NH_4][PF_6]$. However, the ^{1}H-NMR spectrum indicated that the ligand in this complex did not coordinate in the expected κ^3-[S,S,S] mode. The aromatic region showed two different methimazolyl environments with a ratio of 2:1. Two broad resonances also appeared at 5.15 and 4.97 representing the *p*-cymene aryl protons which generally appear as a sharp $(AB)_2$ system in a κ^3-[S,S,S] coordinated ligand. Despite this result, ESI-MS showing a molecular ion peak at m/z = 358.3 corresponding to $M^+/2$ confirms the presence of complex of ligand **2.15** and ruthenium(p-cymene). The lack of a ruthenium-bound chloride in the molecular ion peak of the ESI-MS indicates that, in order for ruthenium to adopt the preferred octahedral geometry, the ligand must be coordinated in a κ^3-mode rather than a bidentate κ^2-[S,S] mode. Since NMR studies ruled out κ^3-[S,S,S] coordination it was assumed that the ligand adopted a κ^3-[N,S,S] coordination mode based on the ligand **2.15** rather than **2.15′**. Therefore, upon coordination of the two free methimazolyl arms to a metal centre the fluxional carbon-sulfur interaction observed in **2.15** becomes irreversible resulting in an [N,S,S] donor ligand.

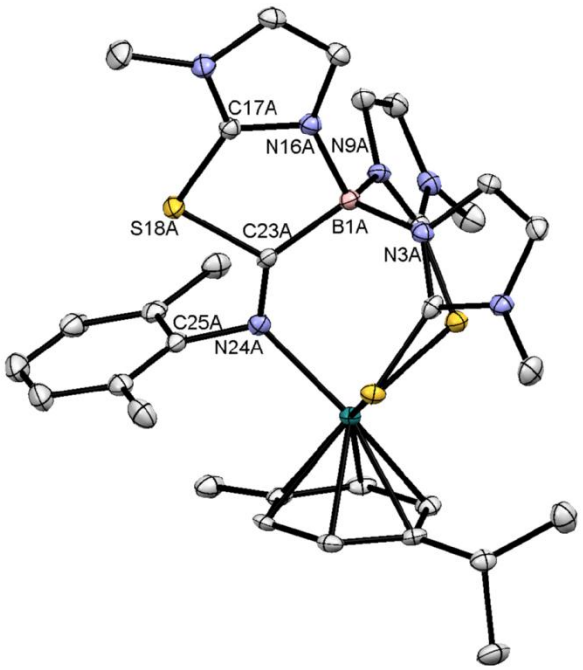

Figure 2.13: Structure of the dication in [κ^3[N,S,S]-3-bis(methimazolyl)-2-(2,6-dimethylphenylimino)-7-methyl-[1,4,3]-thiazaborolo[5,4-b]imidazolium)Ru(p-cymene)] $[PF_6]_2$ (**2.16**). Displacement elipsoids have been drawn at 50% probablility .Hydrogen atoms and PF_6^- counterions have been omitted for clarity. Selected bond lengths and angles are provided in Table **6.7**.

In order to establish the ligand coordination mode in **2.16**, X-ray quality crystals were grown by slow diffusion of ether into a concentrated solution of **2.16** in acetronitrile. The crystal structure confirms the above interpretation of the spectroscopic data and shows the ligand coordinating in a κ^3-[N,S,S] mode to give a complex with C_1-symmetry (Figure 2.13). The thiazaborole S(18A)-C(23A) bond length [1.791(2) Å] is shorter than in **2.15** [1.835(2) Å] reflecting a strengthening of this bond upon complexation. The C(17A)-S(18A) bond [1.731(2) Å] is essentially unchanged from the previous thiazaborole [1.721(3) Å] and the C(17A)-S(18A)-C(23A) angle (90.3°) is slightly larger (89.4°). The exocyclic C=N double bond C(23A)-N(24A) [1.283(3) Å] is also lengthened compared with **2.15** [1.255(3) Å] due to the coordination of the imine nitrogen to ruthenium. The B(1A)-N(16A) bond [1.561(3) Å] is lengthened relative to the other two B-N bonds [1.535(3) and

1.533(3) Å] in **2.16** and to the same bond in the free ligand **2.15** [1.544(5) Å] meaning that it is more comparable with a Lewis adduct type bond.

This structure gives an explanation of the broadening of the *p*-cymene arene resonances observed in the ^{1}H-NMR for this complex as a result of hindered rotation of the aryl ring due to interaction with the *o*-xylyl group, which is directed towards the *p*-cymene environment. The ^{13}C-NMR spectrum of the complex shows a resonance for the C-B carbon at 196.4 ppm which is significantly higher than the corresponding carbon in **2.15** at 177.2 ppm.

2.2.6.2 Aliphatic Isonitrile

The relatively electron-withdrawing nature of the aryl group in the isonitrile may contribute to the poor donor ability of the carbon centre and thus to the formation of ligand **2.15** and complex **2.16**. An aliphatic isonitrile was expected to be a stronger donor for the boron centre. To investigate this the readily available branched alkyl-isonitrile (1,1,3,3-tetramethylbutylisonitrile) was stirred with **2.1** in toluene under reflux for 12 hours. The colourless solids isolated after work-up were found to be an unexpected reaction product **2.17** (Scheme 2.14).

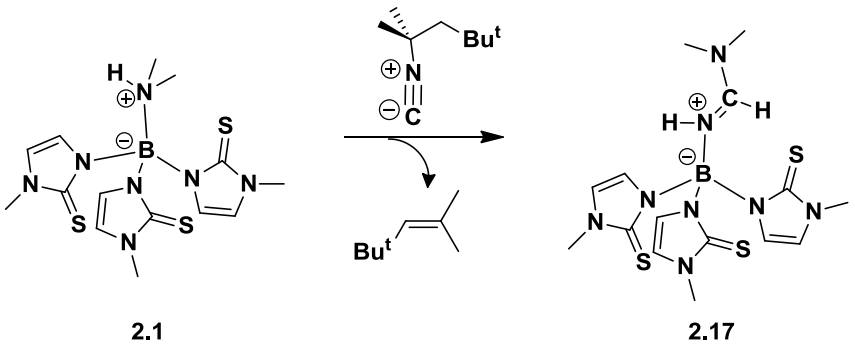

Scheme 2.14: Synthesis of **2.17** from treatment of **2.1** with 1,1,3,3-tetramethylbutylisonitrile.

^{1}H-NMR spectroscopy of **2.17** showed no resonances corresponding to the isonitrile alkyl group; however, two sharp singlets at 3.05 and 3.15 ppm which integrate as 3H each were present in the spectrum. The similarity of these signals to those of the NMe_2 protons in **2.10** and **2.12** suggested that the dimethylammonium group had been retained. Instead of the expected alkyl multiplets, two new doublets are present at 7.93 and 10.01 ppm which each integrate to 1H and display a coupling constant of 15.6 Hz indicative of a *trans*-relationship. ^{13}C-NMR DEPT experiments showed the presence of a tertiary carbon centre at 159.0 ppm; however, this carbon showed no C-B coupling indicating nitrogen-boron coordination. Isomerism of isonitriles to nitriles is known to occur over time at room temperature;[19] however, ^{13}C-NMR of the free isonitrile showed no evidence for this, even after 48 hours in toluene under reflux. Based on the spectroscopic evidence the structure of this ligand was thus assigned as that containing an *N,N'*-dimethylformamidino group attached to the boron (**2.17**).

^{1}H-NMR studies in deuterated toluene confirmed the formation of 2,4,4-trimethylpent-2-ene resulting from the intramolecular removal of the γ-proton in the alkyl moiety with concomitant elimination of the dimethylammonium cation (Scheme 2.15). The inherent stability of the trisubstituted alkene may contribute to its elimination in this process, and isonitriles not susceptible to this proton abstraction would necessarily provide a different product.

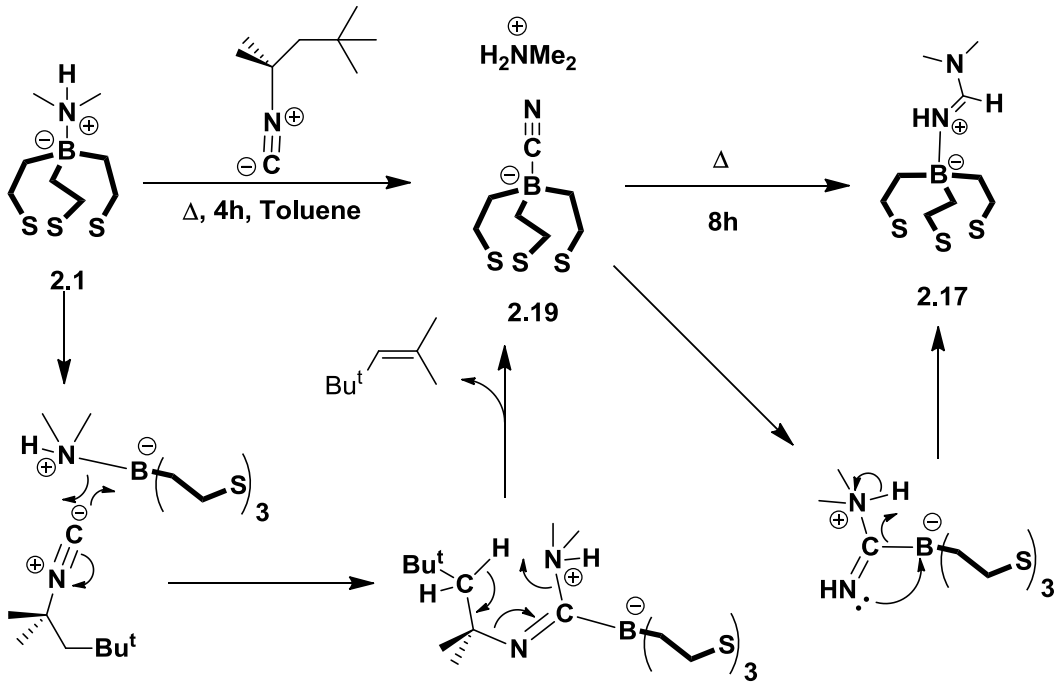

Scheme 2.15: Mechanism for the formation of **2.19** and **2.17** from reaction of **2.1** with 1,1,3,3-tetramethylbutylisonitrile.

Ligand **2.17** was complexed to Ru(II) as previously described for complexes of the related ligands. X-ray quality crystals of this complex (**2.18**) were grown by slow diffusion of ether into a concentrated solution of **2.18** in CH_2Cl_2. X-ray crystallography confirmed that the ligand contains a formamidino group bound to boron as indicated by the spectroscopic data (Figure 2.14), and this unexpected result indicates that this reaction does not proceed though the type of mechanism shown in Scheme 2.11. It is interesting to note, however, that the ligand **2.17**, formed by this elimination of the alkyl group from the alkylisonitrile, is the formamidino (CH) analogue of the acetamidino (CMe) and benzamidino (CPh) containing ligands (**2.10** and **2.12**), formed by treatment of ZTm (**2.1**) with acetonitrile and benzonitrile respectively. The B-N bond length in **2.18** [1.5210(16) Å] is rather shorter than that found in the ruthenium complexes (**2.11** and **2.13**) of the acetamidino and benzamidino analogues **2.10** and **2.12**. The N(23A)-C(24A)

(formamidino) bond length [1.323(6) Å] is slightly longer than the C(24A)-N(25A) bond length [1.306(6) Å] indicating a C=NMe_2 double bond as seen in **2.11** and **2.13**.

Further NMR investigation of the synthesis of **2.17** established the presence of an intermediate (**2.19**) in the reaction (Scheme 2.15). This cyano species could be isolated upon work-up of the reaction mixture after only 4 hours. Negative ion ESI-MS showed a molecular ion peak at m/z = 376.04 indicating that the ligand was no longer a charge-neutral zwitterion but instead an anionic species. The structure of the anionic ligand was therefore assigned as [(NC)Tm]$^-$. The ^{1}H-NMR spectrum of **2.19** contained a broadened

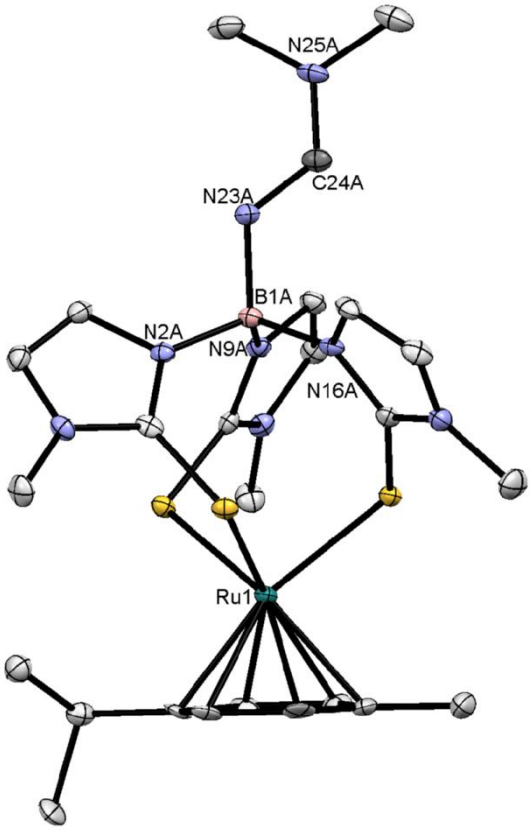

Figure 2.14: Structure of the dication in [κ^3-[S,S,S]- (*N,N*-dimethylformamidine)B(methimazolyl)$_3$Ru(*p*-cymene)][PF_6]$_2$ (**2.18**). PF_6 counterions and MeCN solvent are omitted for clarity. Displacement elipsoids have been drawn at 50% probablility .Selected bond lengths and angles are provided in Table 6.8.

triplet at 2.69 ppm (6H) and a broad singlet at 8.32 (2H) consistent with $[H_2NMe_2]^+$ as the counter ion to the anionic ligand. The ^{13}C-NMR spectrum of **2.19** contains a four line signal at 130.4 ppm confirming the presence of a quaternary C-B bond in this intermediate, in contrast to the corresponding singlet at 159.3 ppm in the spectrum of **2.17**. However, the expected IR absorption band for the nitrile functionality was not observed in the expected 2200-2260 cm^{-1} region of the spectrum. Elemental analysis confirmed the assigned formula of **2.17**, and it is therefore assumed that in this instance, as with **2.15**, the absorption due to C-N stretching is too weak to be detected.

A plausible mechanism for the formation of both **2.17** and **2.19** is shown in Scheme 2.15. Initial insertion of the isonitrile carbon into the B-N coordinate bond gives an intermediate species which may undergo 1,5-proton abstraction with loss 2,4,4-trimethyl-2-pentene to give **2.19**. Upon extended heating conversion of the salt **2.19** into the neutral zwitterionic ligand **2.17** occurs by insertion of the nitrile group into a dimethylammonium N-H bond, and subsequent isomerization provides **2.17**.

During the course of our mechanistic studies **2.1** was treated with two equivalents of 1,1,3,3-tetramethylbutylisonitrile in toluene under reflux (Scheme 2.16) which provided a further unanticipated outcome. Initially, after 4h, the intermediate **2.19** could be detected by ^{1}H-NMR spectroscopy. However, after further heating no resonances corresponding to **2.17** were detected, instead the salt **2.20** was isolated as a colourless powder after work-up.

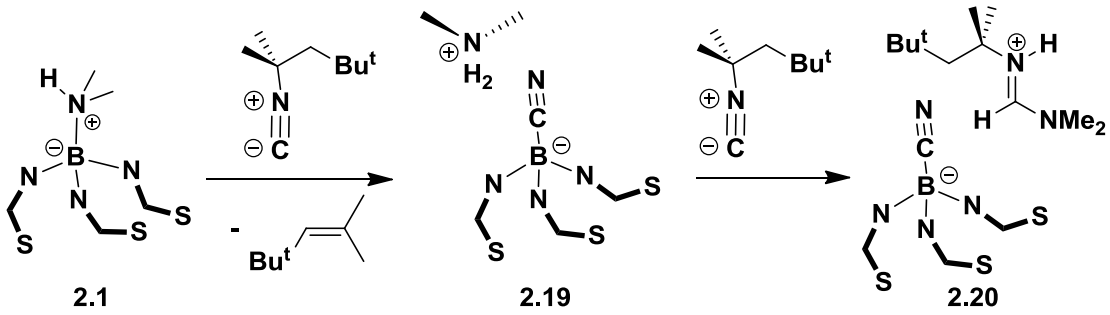

Scheme 2.16: Reaction of **2.1** with 2 equivalents of 1,1,3,3-tetramethylbutylisonitrile to yield **2.20**.

In contrast to **2.17** and **2.19**, ^{1}H-NMR spectroscopy of this compound showed three resonances at 0.97 (9H), 1.47 (6H) and 1.73 (2H) ppm corresponding to the 1,1,3,3-tetramethylbutyl group. Additionally, a resonance at 3.24 ppm (6H) indicated the presence of the dimethylamine group in the product. Finally, resonances at 8.52 and 7.52 ppm indicated the presence of amidinium NH and CH protons respectively. Although these resonances were too broad to determine the relationship between these protons, it was expected, based on the steric bulk of the other substituents, that the protons would exhibit a *trans*-relationship. Negative ion ESI-MS showed a molecular ion peak at m/z = 376.05, whereas the positive ion spectrum showed a molecular ion peak for the cation at m/z = 185.05. Thus, it is clear that the dimethylammonium cation of the salt **2.19** reacts preferentially with excess isonitrile over the boron-bound nitrile function.

Ligand **2.20** was coordinated to Ru(II) by treatment with [(*p*-cymene)$RuCl_2]_2$ in methanol, and the resulting complex (**2.21**) precipitated after anion exchange with ammonium hexafluorophosphate. As expected this complex showed no resonances for the 1,1,3,3-tetramethylbutyl group or the dimethylamine fragment. The positive ion electrospray mass spectrum contained a peak at m/z = 611.9 confirming the assigned formula of **2.21**. A very weak IR absorption band assigned to the cyano group C-N stretching

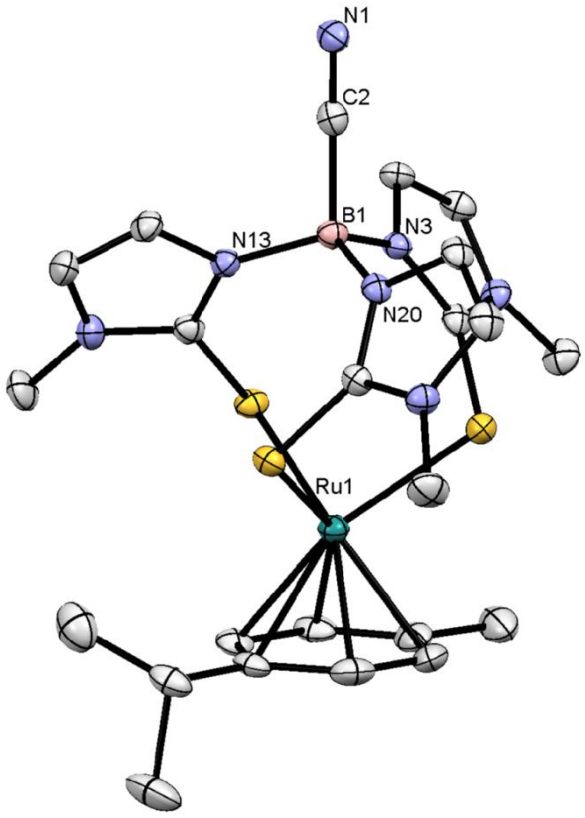

Figure 2.15: X-ray crystal structure of [κ^3-[S,S,S]-(cyano)B(methimazolyl)$_3$Ru(p-cymene)] [PF_6] (**2.21**). Hydrogens and an acetonitrile molecule were omitted for clarity. Displacement elipsoids have been drawn at 50% probablility .Selected bond lengths and angles are provided in Table 6.9.

vibration was present in the spectrum of this complex at 2218 cm^{-1} which agrees well with literature values for similar compounds.[16]

X-ray quality crystals of **2.21** were grown by slow diffusion of Et_2O into a concentrated solution of **2.21** in MeCN. The structure of the complex (Figure 2.15) confirms the presence of the predicted B-CN moiety inferring its presence in the free ligand **2.20**. The B(1)-C(2) bond length is significantly longer [1.624 (5) Å] than the corresponding B(1A)-N(1A) bond in **2.8** [1.542(4) Å] which supports the assignment as a C-bound cyano group in **2.21**, and by implication also in the free ligand **2.20**. This B-C bond length is comparable with that found in the previously reported [(PhTm)Mn(CO)$_3$] complex [1.634(5) Å].[20] The same bond is only slightly shorter than the B-C bond in

2.16 [1.658(3) Å] which was stabilized by attack of the methimazolyl sulfur. The C(2)-N(1) bond displays a typical nitrile bond length of 1.144(5) Å and does not deviate significantly from linear geometry with a B(1)-C(2)-N(1) angle of 178.5(3)°.

2.3 Conclusions

This chapter has demonstrated the reactivity of zwitterionic charge neutral tripodal borate ligands towards both substitution and insertion at the 4th position of the boron. Substitution of the dimethylammonium group in **2.1** with a piperidine donor gave a ligand with diastereotopic protons demonstrating the axial chirality of these tripods even as free ligands. The barrier to interconversion of these enantiomers (68 kJ mol^{-1}) demonstrates that these the helical enantiomers of these ligands will interconvert quickly at room temperature. Whilst reaction with morpholine gave the mono-ligand species **2.3**, the same reaction with piperazine which was expected to lead to the formation of a bis-ligand species, lead only to ligand degradation, presumably through deprotonation of the bound piperazinium nitrogen. The steric limits of this substitution reaction were probed with diisopropylamine, trimethylamine and DABCO and, based on their lack of reactivity, it must be concluded that tri-substituted *sp*^{3}-hybridised nitrogen donors are prevented from coordinating to the boron centre in these systems by their steric bulk.

This chapter has also demonstrated unanticipated reactivity of **2.1** with nitriles, isonitriles and *N,N*-dimethylformamide, these reactions resulting in charge-neutral ZTm species containing N-B, C-B and O-B coordinate bonds. Reaction of **2.1** with 2,6-dimethylphenylisonitrile gives ligand **2.15** which exhibits a relatively rapid fluxional interaction between the isonitrile carbon and the methimazolyl sulfur atoms resulting in a [1,4,3]-thiazaborolo-[5,4-*b*]imidazolium ring which can be trapped upon ligand complexation. In addition, anionic ligands have been accessed by substitution of the dimethylamine moiety in **2.1** with the thiocyanate anion and *via* the fragmentation of an alkylisonitrile to provide the cyano-substituted ligand system.

The common theme of the formation of boron-bound amidinato groups from the reaction with acetonitrile (to give acetamidinato), benzonitrile (to give benzamidinato) and an alkylisonitrile (to give fomamidinato) is striking and illustrates the stability of this particular functionality coordinated to boron in these systems. The use of the chemistry reported in the elaboration of this ligand system to incorporate further functionality at this boron fourth position may be envisaged.

2.4 References

1. Trofimenko, S., *J. Am. Chem. Soc.*, **1966**, *88*, 1842.
2. Trofimenko, S. *Poly(1-Pyrazolyl)Borates, their Transition-Metal Complexes, and Pyrazaboles*; McGraw-Hill, **1970**.
3. Trofimenko, S., *Chem. Rev.*, **1993**, *93*, 943.
4. Reglinski, J.; Garner, M.; Cassidy, I.; Spicer, M. D.; Kennedy, A. R., *Chem. Commun.*, **1996**, *17*, 1975.
5. Niedenzu, K.; Trofimenko, S., *Inorg. Chem.*, **1985**, *24*, 4222.
6. Bailey, P. J.; Lorono-Gonzales, D.; McCormack, C.; Millican, F.; Parsons, S.; Pfeifer, R.; Pinho, P. P.; Rudolphi, F.; Sanchez Perucha, A., *Chem. Eur. J.*, **2006**, *12*, 5293.
7. Bailey, P. J.; Budd, L.; Cavaco, F. A.; Parsons, S.; Rudolphi, F.; Sanchez-Perucha, A.; White, F. J., *Chem. Eur. J.*, **2010**, *16*, 2819.
8. Cavaco, F. A., PhD Thesis, University of Edinburgh, **2010**.
9. Perucha, A. S., PhD Thesis, University of Edinburgh, **2007**.
10. Shore, S. G.; Chen, X., WO2007120511A2, The Ohio State University, USA, **2007**.
11. Parkin, G.; Pang, K.; Tanski, J. M., *Chem. Comm.*, **2008**, 1008.
12. Willet, R. D.; Peterson, S. W.; Akers, C., *Acta Crystallogr., Sect. B: Struct. Sci.*, **1967**, 24.
13. Bürger, H.; Ansorge, A.; Brauer, D. J.; Hagen, T.; Pawelke, G., *J. Organomet. Chem.*, **1994**, *467*, 1.
14. Reglinski, J.; Spicer Mark, D.; Schwalbe, M.; Andrikopoulos, P.; Armstrong, D. R. C., *Eur. J. Inorg. Chem.*, **2007**, 1351.
15. Kitson, R. E.; Griffith, N. E., *Anal. Chem.*, **1952**, *24*, 334.
16. Györi, B.; Emri, J.; Szilágyi, L., *J. Organomet. Chem.*, **1978**, *152*, 13.
17. Carboni, B.; Ollivault, M.; Monnier, L., *Tet. Asymm.*, **1997**, *8*, 1955.
18. Bailey, P. J.; McCormack, C.; Parsons, S.; Rudolphi, F.; Sanchez-Perucha, A.; Wood, P., *Dalton Trans.*, **2007**, 476.
19. Naota, T.; Tannna, A.; Kamuro, S.; Murahashi, S. I., *J. Am. Chem. Soc.*, **2002**, *124*, 6842.

20. Rabinovich, D.; Graham, L. A.; Fout, A. R.; Kuehne, K. R.; White, J. L.; Mookherji, B.; Marks, F. M.; Yap, G. P. A.; Zakharov, L. N.; Rheingold, A. L., *Dalton Trans*., **2005**, 171.

Chapter Three

Stereodirecting Scorpionates: Towards the Synthesis of Single Diastereoisomer Complexes of Tris(methimazolyl)borate Ligands

3.1 Introduction

C_3-symmetric complexes of flexible tripod ligands, such as Tm, present an exciting prospect in asymmetric catalysis due to their inherent axial chirality. However, exploitation of helical complexes of tripod ligands in asymmetric catalysis requires the availability of routes to stereochemically pure complexes of these ligands. This chapter will discuss the efforts towards the synthesis of stereochemically pure complexes of charge-neutral zwitterionic tris(methimazolyl)borate ligands.

3.1.1 Barrier to Racemisation

In undertaking the synthesis of stereochemically pure compounds, it is important to ensure the stability of the species against racemisation. With conformational stereoisomers, such as the helix of Tm complexes, the energy barrier to racemisation must be sufficiently high to prevent interconversion of the stereoisomers under ambient conditions. The interconversion of the helical enantiomers of complexes of Tm was studied previously by Bailey and McCormack.[1,2] Variable-temperature NMR studies were carried out on both tetrahedral and octahedral complexes of Tm^{Et} and Tm^{Bn}, both of which contain diastereotopic methylene NMR 'handles'.

Four possible routes to interconversion of the enantiomers were postulated (Figure 3.1). The 'dissociative' routes **A**, **B** and **C** all involve decoordination of one ligand arm as the first step. After decoordination the method of interconversion depends upon the geometry of the metal centre. Interconversion by route **A** may occur in octahedral metal complexes where decoordination leads to a 5-coordinate intermediate which can undergo Berry pseudorotation before recoordination of the third ligand arm. Both

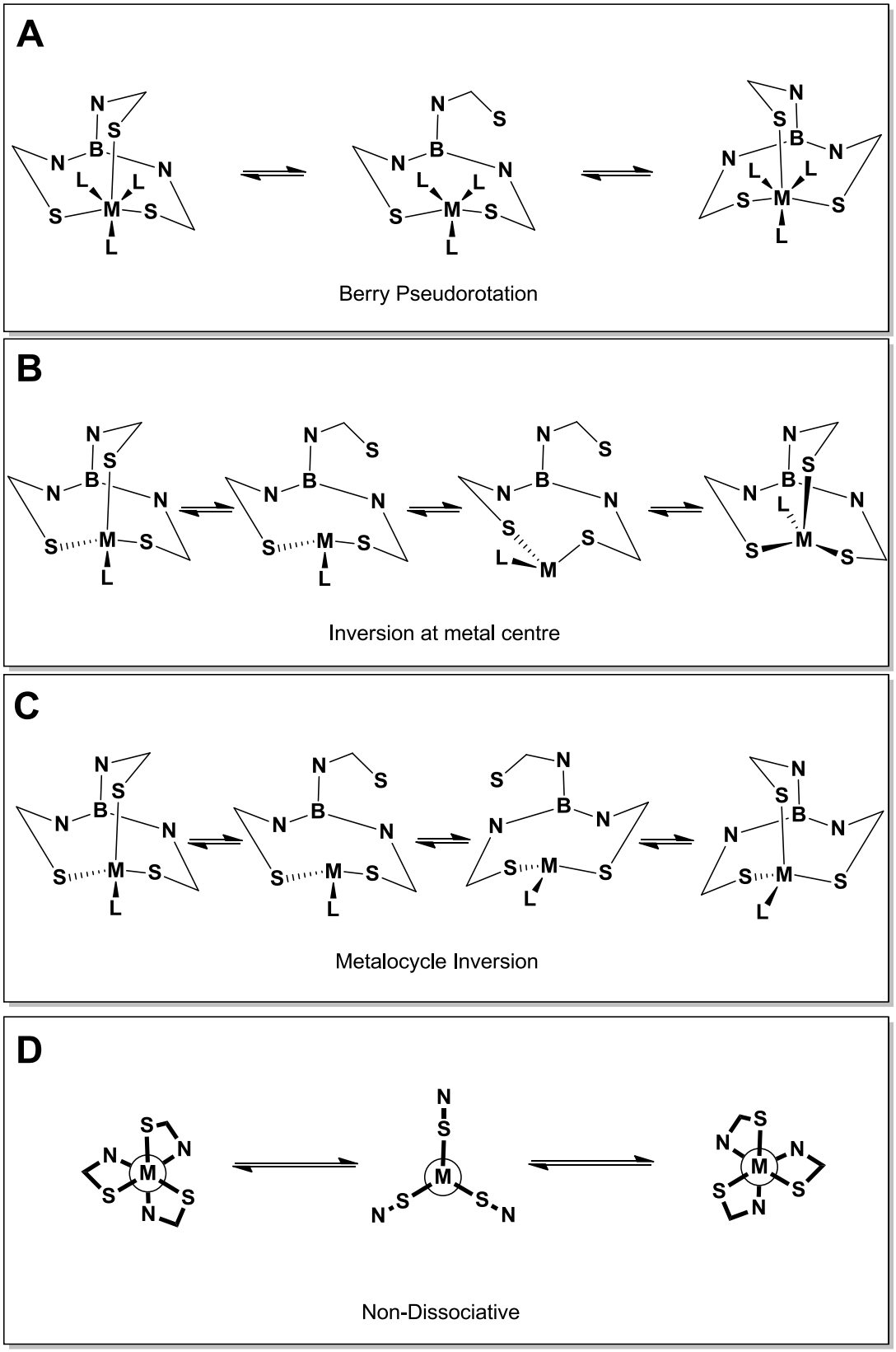

Figure 3.1: Mechanisms for interconversion of helical enantiomers of Tm proposed by Bailey and McCormack.

mechanisms **B** and **C** are possible in tetrahedral metal complexes. Mechanism **B** involves inversion at the metal centre after decoordination while route **C**, involves inversion of the metallocycle, before recoordination of the third ligand arm. Donor solvents are expected to promote these 'dissociative' routes by reducing the energy barrier to ligand arm dissociation by coordination to the 'free' metal site thus formed. The alternate 'non-dissociative' mechanism (**D**) requires the bicyclic ligand cage to 'twist' through a highly strained C_3v-symmetric transition state. DFT *Ab Initio* calculations were carried out to determine the barrier to interconversion by the 'non-dissociative' mechanism (**D**).

Activation energies calculated from the VT-NMR and the DFT studies for a variety of tetrahedral and octahedral complexes are shown in Table 3.1. For all complexes the activation energy for interconversion was found to be

Table 3.1: Barrier to racemisation in complexes of Tm^R (R = Et, Bn).

Complex	Activation Energy (kJ mol^{-1})			
	Non-coordinating	MeCN-d_3	DMSO-d_6	Calculated
$Tm^{Et}ZnCl$	>77	>72	60	121
$Tm^{Et}CdBr$	77	69	<61	
$Tm^{Et}HgCl$	68	57		
$Tm^{Et}CuPPh_3$	55	54		
$Tm^{Et}AgPPh_3$	53	45-50		
$Tm^{Bn}ZnCl$	>77		60	
$[Tm^{Et}Ru(p\text{-cymene})]^+$	>>79			
$Tm^{Et}Mn(CO)_3$	>>77		>>78	163

relatively high in both donor and non-donor solvents. In tetrahedral complexes the E_a in donor solvents was found to be slightly lower than in non-coordinating solvents indicating that the tetrahedral complexes may interconvert by one of the dissociative mechanisms (**B** or **C**). This was supported by the DFT calculations for [$Tm^{Et}ZnCl$] which calculated the activation energy by the non-dissociative mechanism (**D**) to be much higher than the experimentally determined value. Still, the calculated energy barrier was significantly lower for the tetrahedral complex [$Tm^{Et}ZnCl$] than the octahedral complex [$Tm^{Et}Mn(CO)_3$]. Analysis of the change in bond angles between the ground and transition state structures indicated that this difference arises as a result of angle strain at the metal centre in the C_3v-symmetric transition state. For example, at the transition state, the S-Zn-S angle was calculated to be almost ideal for a tetrahedron (109.9°). In contrast, whilst the ground state structure of $Tm^{Et}Mn(CO)_3$ contains nearly ideal octahedral S-Mn-S angles [93.9°], in the transition state structure this angle increases significantly [99.3°]. Therefore, the angle strain experienced by the metal centre in the transition state is larger in the octahedral Mn(I) complex than in the tetrahedral Zn(II) species.

The experimental activation energy for octahedral complexes was also found to be higher than for tetrahedral complexes in both coordinating and non-coordinating solvents. However, exact values were impossible to obtain as coalescence in the VT-NMR spectra of these complexes was not observed even at the highest temperatures (373 K). In order to calculate the activation energy using the Eyring equation the temperature at which coalescence occurs must be known. When coalescence does not occur below the boiling point of the solvent or the operational limits of the NMR spectrometer only the minimum possible value for the E_a can be reported. Therefore, the barrier

to interconversion, and thus the rate of racemisation, of octahedral complexes was not able to be determined accurately. However, the E_a is likely to be significantly higher than for tetrahedral complexes as no multiplet broadening (a precursor to coalescence) was observed even at the highest temperatures. The DFT calculations suggest that if octahedral complexes interconvert by the non-dissociative mechanism (**D**) they will be stable to interconversion at room temperature. In contrast, the experimentally determined activation energies in tetrahedral complexes are sufficiently low that interconversion may occur quickly at room temperature.

In light of these results, octahedral complexes of Tm were expected to be relatively stable to interconversion between their helical enantiomers. However, application of these complexes as asymmetric catalysts required the isolation of a single helical isomer (*P* or *M*). Chiral substituents, appended to the ligand, may direct the twist of the ligand upon complexation and thus effect the preferential synthesis of a single diastereoisomer complex.

3.1.2 Chiral Induction

There are two ways which a stereochemical preference could be induced in the helix. Substitution of the ligand arms is possible at a variety of positions on the heterocyclic rings and enantiopure substituents may effect

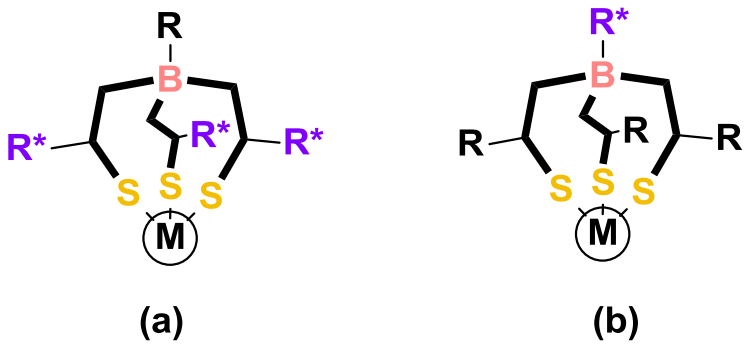

Figure 3.2: Stereoselective induction of chirality in helical tripod complexes.

the formation of a single diastereoisomer complex (Figure 3.2(a)). Alternatively, substitution of the boron bridgehead with a chiral donor may allow for stereodirection of the ligand arms upon complexation if the chiral group is sufficiently bulky for adequate chiral induction (Figure 3.2(b)).

The former was achieved previously within the Bailey group by using enantiopure N-(S)-α-methylbenzylimidazole-2-thione as the ligand arms.[3,4] The resulting ligand (**1.39**) was shown to form a single diastereoisomer complex (**1.40**) upon coordination to [Ru^{II}(*p*-cymene)] (Scheme 3.1). However, this ligand requires the use of three enantiopure groups and it would be preferable to direct the helicity of the ligand using only one enantiopure

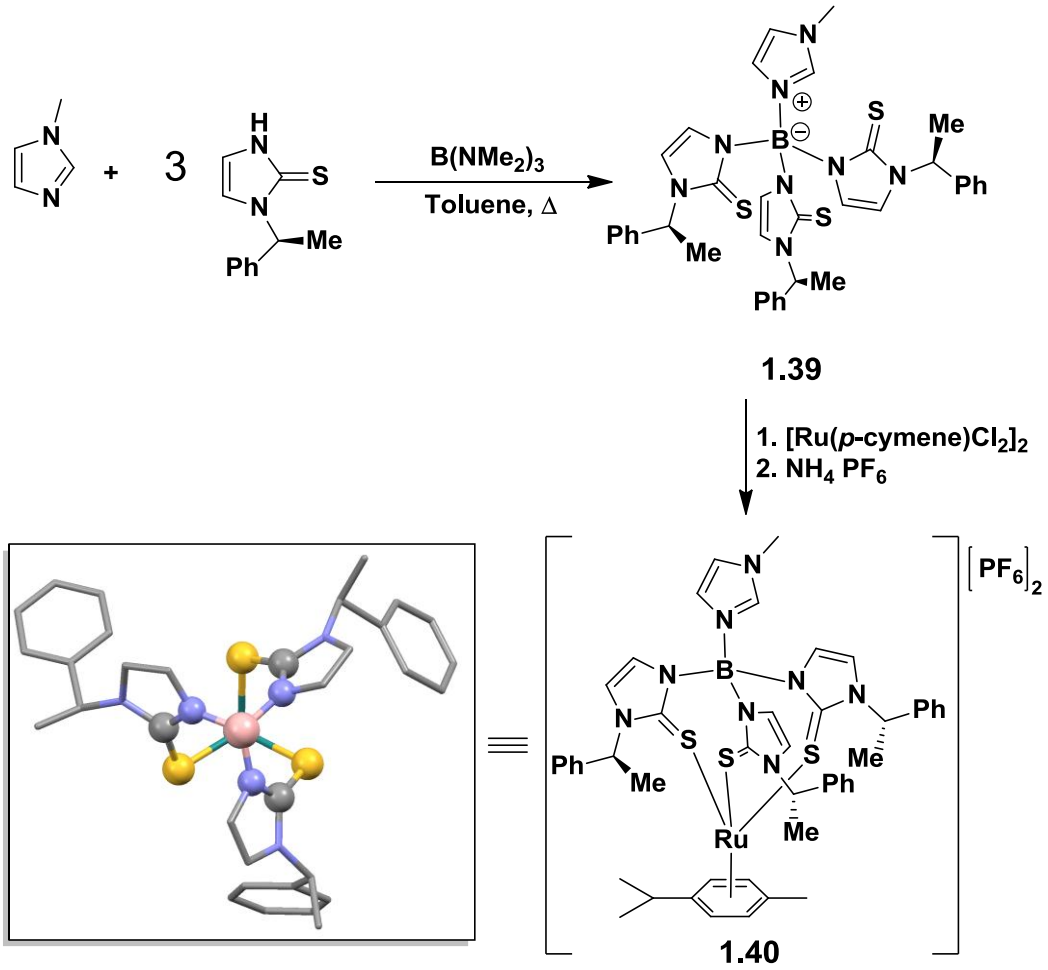

Scheme 3.1: The synthesis of ligand **1.39** and [{(N-MeImid)Tm$^{(S)\text{-}\alpha\text{-}MeBz}$}Ru(*p*-cymene)] (**1.40**) along with the X-Ray crystal structure of the cation of **1.40** which exists as a single diastereoisomer in which the metal-ligand cage adopts the *M*-conformation.

substituent. In addition, the α-methylbenzyl groups in this ligand are situated proximal to the metal centre. Whilst this may improve the enantioselectivity of any catalyst derived from this ligand, the presence of these groups will also prevent steric tuning of the metal centre which may be possible if these sites were free for the inclusion of alternative substituents.

In order to achieve stereodirection by use of a chiral boron donor a fine balance must be struck. The donor used must have a stereogenic directing group which is not only sterically large enough to induce asymmetry, but is also located close to the methimazole ligand arms in a complex. Chiral oxazoline donors were tested previously within the Bailey group for this purpose. A variety of enantiopure oxazolines were reacted with methimazole and tris(dimethylamino)borane in the 'one-pot' ligand synthesis. The product of all of these reactions was an oxazoline ring-opened compound (**3.1**) and forms when one of the nucleophilic methimazole sulphur atoms attacks the relatively electrophilic oxazoline C5 carbon centre. Scheme 3.2 shows the proposed mechanism for (4*R*, 5*S*)-4-methyl-5-phenyloxazoline, although ring-opening was found to occur in all the chiral oxazolines tested

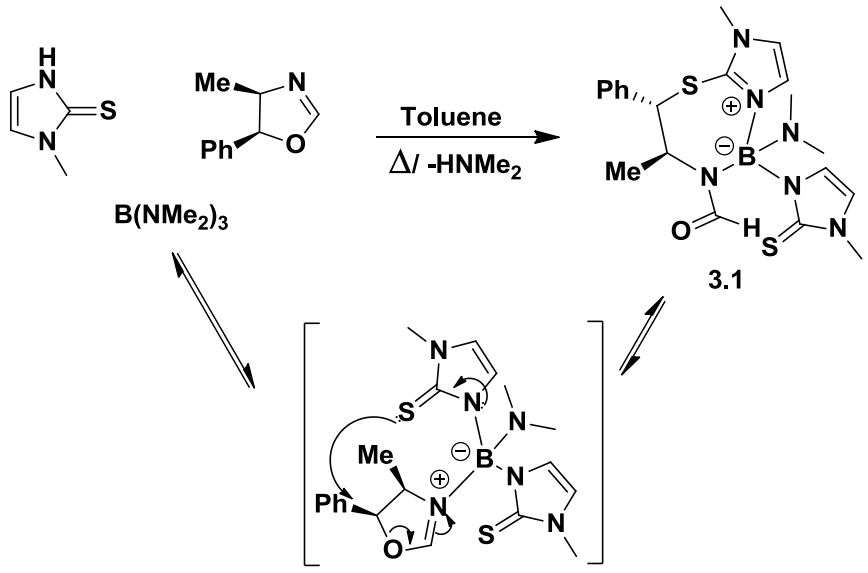

Scheme 3.2: Formation of the oxazoline ring-opened product (**3.1**).

regardless of the nature of the C5 substituent.

In contrast, the commercially available chiral base (+)-tetramisole was shown to be a good donor for these systems giving the ligand ((+)-tetramizolium)tris(methimazolyl)borate (**3.2**) upon reaction with methimazole and tris(dimethylamino)borane.[4] Complexation of **3.2** to [Ru(*p*-cymene)Cl_2]$_2$ yielded **3.3** as a mixture of the two diastereoisomers (*S,P*) and (*S,M*) in a *ca.* 2:1 ratio as demonstrated by ^{1}H-NMR spectroscopy.

This indicates a moderate degree of chiral induction between the phenyl substituent of the tetramisole donor and the methimazole ligand

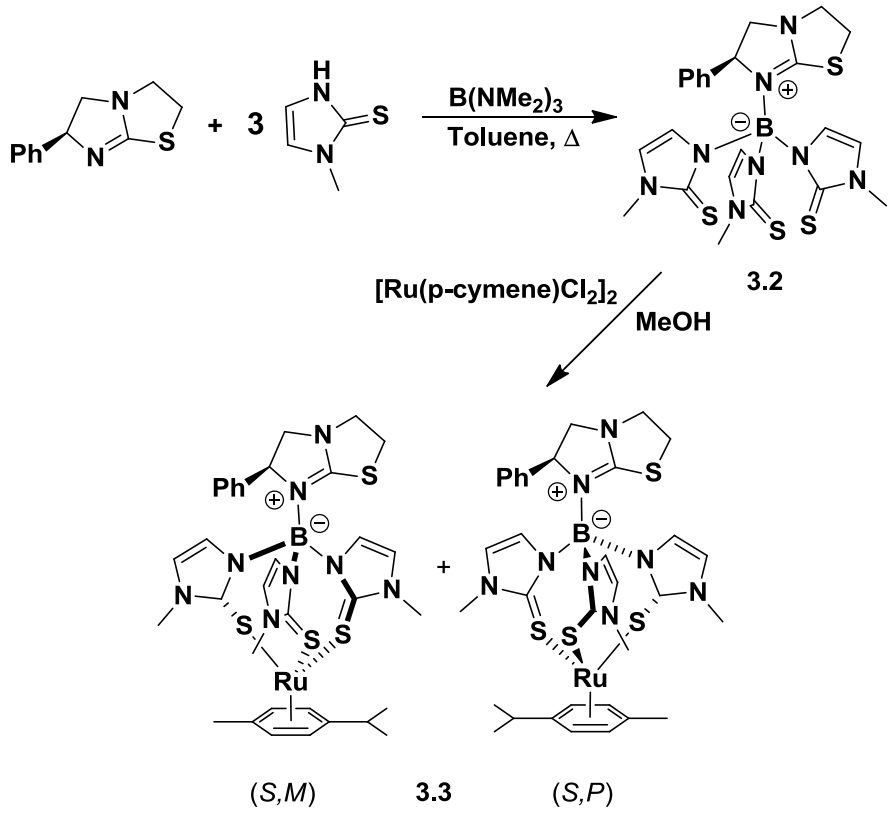

Scheme 3.3: Synthesis of complex **3.3** as a mixture of diastereoisomers (*S,P*) and (*S,M*) in a *ca.* 2:1 ratio.

arms. The work presented in this chapter will describe the efforts towards improving chiral induction in these complexes using alternative chiral boron substituents.

3.2 Results and Discussion

3.2.1 Chiral DBU donor

It was shown previously that 1,8-diazabicycloundec-7-ene (DBU) substitutes the dimethylamine group in ($HNMe_2$)ZTm (**2.1**) very rapidly due to its strong Lewis basicity.[4,5] The X-ray crystal structure of a complex of (DBU)ZTm shows that the methylene group at C6 lies close to the methimazolyl ligand arms (Figure 3.3). This methylene group is in the α-position relative to the amidine functionality and thus contains relatively acidic protons. Substitution of one of these acidic protons with a methyl group would therefore create the chiral Lewis base donor 6-methyl-1,8-diazabicycloundec-7-ene (6-Me-DBU, **3.4**). Coordinating **3.4** to the boron centre was then expected to allow translation of the donor group chirality to

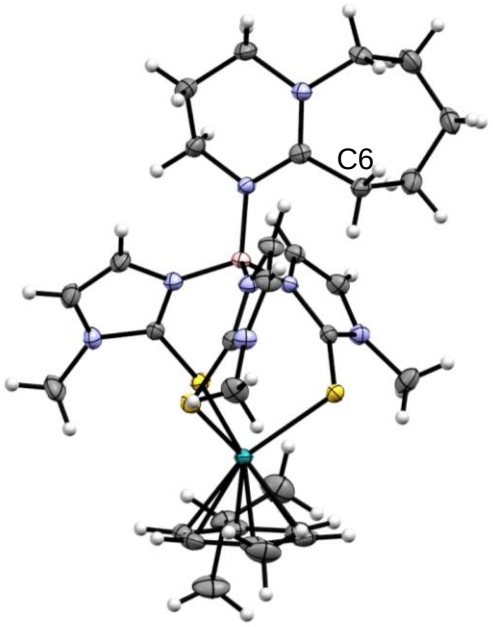

Figure 3.3: X-ray crystal structure of the cation of [{(DBU)B(mt)$_3$}Ru(*p*-cymene)]. Counterions and solvent molecules removed for clarity. Displacement elipsoids have been drawn at 50% probablility .

the ligand arms providing a single-diastereoisomer complex of **3.5**.

To this end 1,8-diazabicycloundec-7-ene (DBU) was reacted with *n*BuLi in THF at -78°C. Subsequent addition of iodomethane and warming to room temperature provided racemic 6-Methyl-1,8-diazabicycloundec-7-ene (**3.4**) after basic workup (Scheme 3.4). A doublet at 1.14 ppm was assigned as the exocyclic methyl group whilst the ring protons appeared as complex multiplets between 3.55 and 1.41 ppm. Mass spectrometry (ESI) confirmed the formulation of the product with a molecular ion peak at *m*/*z* = 166.1 corresponding to 6-MeDBU$^+$.

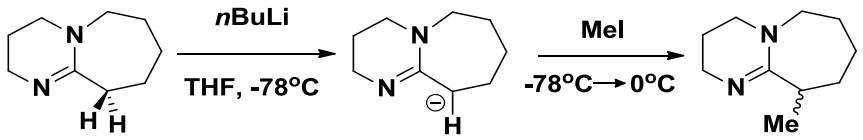

Scheme 3.4: Synthesis of 6-Methyl-1,8-diazabicycloundec-7-ene (**3.4**)

In the first instance **3.4** was synthesised as a racemic mixture as the ^{1}H-NMR spectrum of a complex of the target ligand (6-MeDBU)ZTm was expected to give an indication of the extent of chiral induction from this group. In the absence of strong chiral induction the ^{1}H-NMR spectrum was predicted to show resonances corresponding to four diastereomers (*R,P*), (*S,P*), (*S,M*) and (*R,M*). However, full chiral induction from the donor to the ligand arms was expected to result in a spectrum containing only resonances corresponding to the (*R,P*) and (*S,M*) isomers. These constitute the diastereoisomers in which the methyl group was expected to be subject to the

least steric crowding based on careful study of the X-ray crystal structure shown in Figure 3.3.

Therefore, 6-Methyl-1,8-diazabicycloundec-7-ene was added to a suspension of (dimethylamino)tris(methimazolyl)borane (**2.22**) in toluene and the mixture was heated to reflux. After 72 h the reaction mixture was cooled to room temperature and the precipitate which had formed filtered and washed with toluene and diethyl ether and dried *in vacuo* to give **3.6** as a pale blue powder (Scheme 3.5).

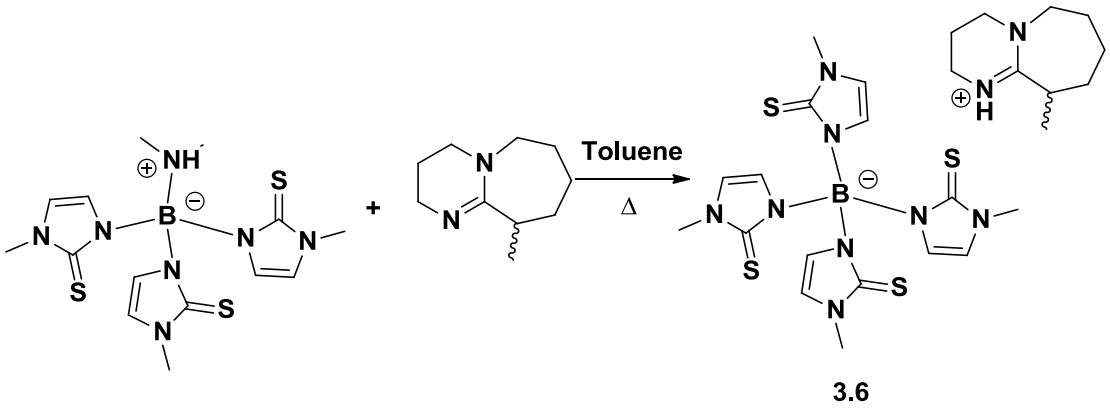

Scheme 3.5: Synthesis of $[6\text{-MeDBUH}]^{+}[B(mt)_4]^{-}$ (**3.6**).

Mass spectrometry (ESI) of the isolated material showed peaks at *m*/*z* = 167 corresponding to protonated 6-Methyl-1,8-diazabicycloundec-7-ene (**3.4**) and *m*/*z* = 463 corresponding to a tetra(methimazolyl)borate anion along with a molecular ion peak at *m*/*z* = 631 consistent with $[6\text{-MeDBUH}^{+}][B(mt)_4^{-}]$ as the formulation of **3.6**. ^{1}H-NMR spectroscopy confirmed this assignment with a doublet at 1.17 ppm (3H) corresponding to the 6-MeDBU methyl group which appears at 1.14 ppm in **3.4**. The methimazolyl NCH_3 protons appear as a singlet (3.35 ppm) which integrates for 12H demonstrating the symmetry equivalence of all four methimazolyl groups. Two singlets at 6.67 and 6.83 ppm correspond to the methimazolyl aromatic protons and

integrate for 4H each. These resonances are shifted to high frequency from the same protons in both the charge-neutral ligand ($HNMe_2$)ZTm (**2.1**) and the anionic ligand (NC)Tm (**2.19**) suggesting a more electron-deficient boron centre in **3.6**. Similarly, in the ^{13}C-NMR spectrum the methimazolyl ring carbon atoms are equivalent, appearing at 124.2 and 115.0 ppm, whilst the NCH_3 carbon resonance appears at 33.8 ppm.

X-ray quality crystals of **3.6** were grown by slow diffusion of diethyl ether into a concentrated solution of the ligand in dichloromethane. The refined structure confirms the formulation of the product as [6-MeDBUH]$^+$[B(mt)$_4$]$^-$ with a hydrogen-bonding interaction between S1 and N1 [2.505 Å]. As a result the C(16)-S(1) bond-length is slightly longer [1.703(2) Å] than those for the other three methimazolyl rings [avg. 1.693 Å]. All of the B-N bonds in this structure are equivalent within experimental error [avg. 1.554 Å].

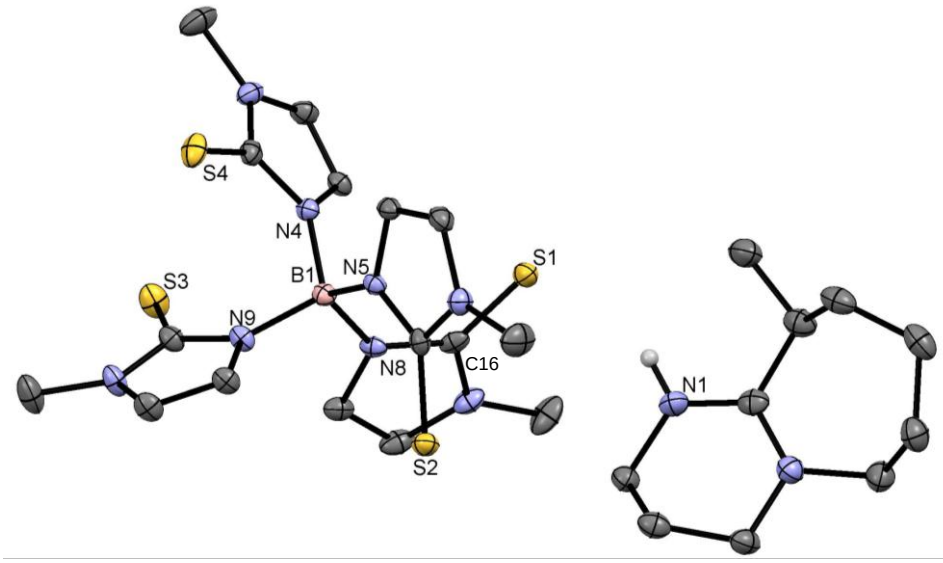

Figure 3.4: X-ray crystal structure of [6-MeDBUH][B(mt)$_4$] (**3.6**). Hydrogen atoms except for that on N1 have been omitted for clarity. Displacement elipsoids have been drawn at 50% probablility . Selected bond lengths (Å) and angles (°) are presented in Table 6.10.

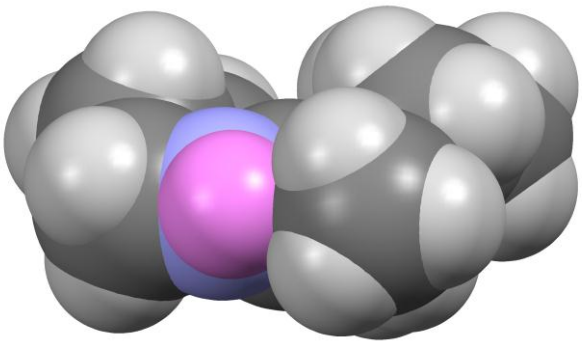

Figure 3.5: Spacefill X-ray crystal structure of the cation of (**3.6**) showing the partial blocking of the nitrogen lone pair (shown in pink) by the 6-methylsubstituent.

The structure shows that the C6-methyl group on the DBU points towards the donor nitrogen, blocking the approach of all but the smallest acids (*i.e.* H^+). Since the donor nitrogen in 6-MeDBU is sterically hindered, but remains strongly basic deprotonation of ($HNMe_2$)ZTm (**2.1**) competes with the substitution of the $HNMe_2$ group (which is known to occur with the unsubstituted DBU) upon extended heating leading to ligand degradation. The free methimazolate anion resulting from this degradation is then able to substitute the dimethylammonium group in **2.1**. The synthesis of the lithium salt of this tetra(methimazolyl)borate anion from the reaction of $Li[BH_4]$ with methimazole has been reported previously, although significantly higher temperatures (200°C) were required for this preparation.[6] The formation of this anion was also postulated as a trace product of reaction between **2.1** and DABCO, which was also deemed too sterically demanding to attack the boron centre (See Chapter 2).

3.2.2 Chiral imidazoline donors

Chiral imidazolines are structurally similar to the chiral oxazolines tested previously, although they are expected to be more stable to nucleophilic ring-opening by the methimazolyl sulfur. Previous attempts to substitute ZTm with a 2-phenylimidazoline donor were unsuccessful due to steric blocking of the nitrogen lone pair which prevented coordination to the boron centre.[4] However, the high basic pKa of imidazolines means they are strong donors and in the absence of a substituent in the 2-position they were expected to substitute the dimethylamine group in **2.1**.

To test the ability of imidazolines to coordinate to the boron, 1-methylimidazoline and tris(dimethylamino)borane were added to a suspension of methimazole (3 eq.) in toluene, which was subsequently heated to reflux for *ca.* 6 h. Upon cooling the imidazoline functionalised ligand **3.7** was isolated in 46% yield after workup (Scheme 3.6). The ^{1}H-NMR spectrum of this ligand showed two resonances at 6.73 and 6.69 ppm (H_a/H_b) with the former appearing as a very broad singlet. A resonance at 8.38 ppm was assigned to the acidic imidazoline proton (H_i) which is highly shifted

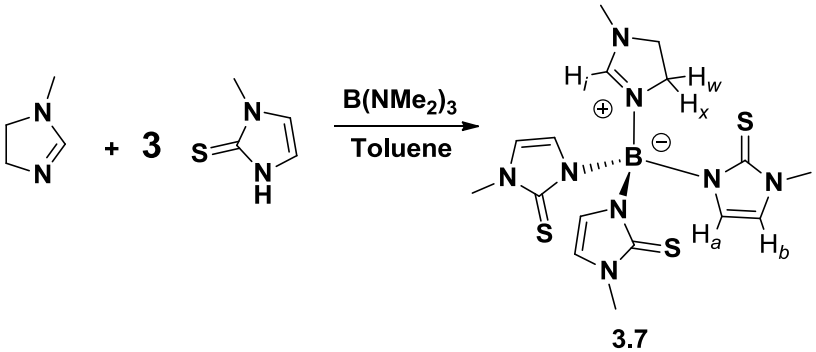

3.7

Scheme 3.6: Synthesis of (1-methylimidazolinium)tris(methimazolyl)borate (**3.7**).

from the free imidazoline (6.70 ppm) and reflects the proximity of this proton to a cationic nitrogen centre. The α-methylene protons (H_w/H_x) on the imidazoline ring are diastereotopic, appearing as two broad singlets at 4.29 and *ca.* 3.8 ppm, indicating the presence of axial chirality in this ligand as seen for **2.2**.

This ligand was added to a solution of [Ru(*p*-cymene)Cl_2]$_2$ in methanol and stirred for 1 h. After this time, ammonium hexafluorophosphate was added causing immediate precipitation of the complex [{**3.7**}Ru(*p*-cymene)][PF_6]$_2$ (**3.8**) as an orange powder (54%) (Scheme 3.7). Mass

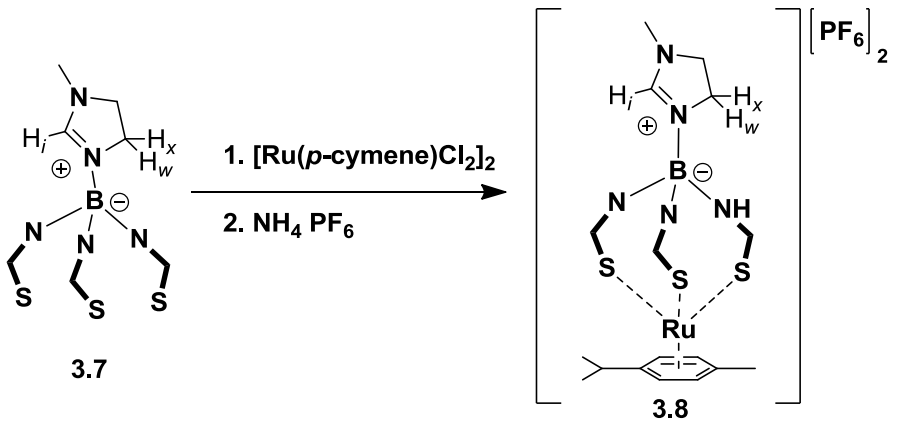

Scheme 3.7: Synthesis of complex [(1-methylimidazolinium)tris(methimazolyl)borato}ruthenium(II)para-cymene]bis(hexafluorophosphate) (**3.8**).

spectrometry (ESI) showed a molecular ion peak at m/z = 355 representing [$M^+/2$] and confirming this formulation. Two sharp resonances at 7.18 and 6.91 ppm appear in the ^{1}H-NMR spectrum representing the methimazolyl CH protons (H_a/H_b). The acidic imidazoline proton (H_i) appears shifted to lower frequency from the free ligand at 7.70 ppm, although this spectrum

was run in d_3-MeCN rather than $CDCl_3$ due to the poor solubility of the complex in the latter.

X-ray quality crystals of this complex were grown by slow diffusion of diethyl ether into a concentrated solution of the complex in dichloromethane. It is instructive to compare the structure of this complex to that of [{(1-methylimidazole)ZTm}Ru(*p*-cymene)][PF_6]$_2$ (**3.9**) which has been previously reported (Figure 3.7).[7] The B1-N23 coordinate bond in **3.8** [1.551(3) Å] is equivalent to that in **3.9** [1.567(12) Å]. However, the B1-N23-C24 angle [123.7(2)°] is significantly smaller than in the previously published structure [129.2(7)°]. Correspondingly, the B1-N23-C28 angle [128.7(2)°] is larger than that in **3.9** [125.3(8)°] indicating a degree of repulsion between the C28 methylene group and the ligand arms. The introduction of chiral substituents in this position may therefore result in favourable chiral induction and lead

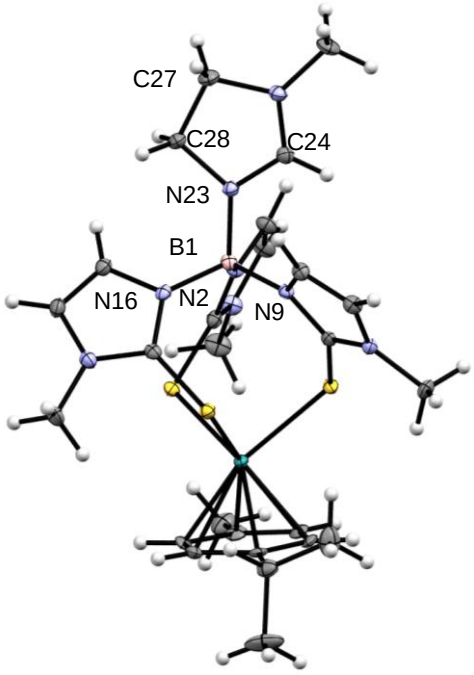

Figure 3.6: X-Ray crystal structure of the cation of **3.8**. Hydrogens and counterions removed for clarity. Displacement elipsoids have been drawn at 50% probablility. Selected bond lengths and angles shown in Table 6.11.

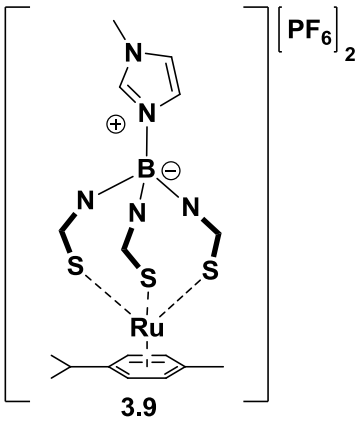

3.9

Figure 3.7: [(N-MeImid)ZTmRu(p-cymene)] (**3.9**).

to the isolation of a single diastereoisomer complex.

To this end the synthesis of a family of chiral imidazoline functionalised ligands was undertaken in order to assess their ability to induce the formation of a single helix upon complexation. A number of multi-step synthetic routes to these chiral imidazolines have been described in the literature.[8,9] However, for these purposes it was found that the imidazolines could be accessed in five steps from enantiopure amino acids (Scheme 3.8).[10,11]

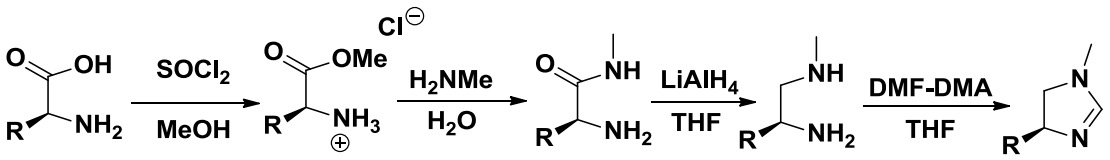

Scheme 3.8: Synthetic route to the synthesis of the enantiopure 1-methylimidazolines *S-3.10* (R = Bn), *S-3.11* (R = Ph), *S,S-3.12* (R = 2-^{i}Bu) and *S-3.13* (R = ^{i}Pr).

Four enantiopure imidazolines with substituents of differing steric bulk were synthesised starting from *L*-phenylalanine, *L*-phenylglycine, *L,L*-isoleucine and *L*-valine. Esterification of these commercially available

enantiopure amino acids with thionyl chloride in methanol gives the hydrochloride salt of the amino acid methyl ester in quantitative yields. For the amino esters with aromatic substituents, treatment of this salt with aqueous methylamine gave the amide after *ca.* 12 h at rt. In contrast, the amino esters with aliphatic substituents required some heating to promote reaction with the dimethylamine over ester hydrolysis. These amides were isolable after *ca.* 4 h at 40°C, however yields for this step for all amines were moderate at best. These amides were reduced with lithium aluminium hydride in refluxing THF for 48 h and worked up by the Fieser method.[12] The corresponding diamines were cyclised by reaction with *N,N*-dimethylformamide-dimethylacetal in refluxing toluene for 8 h and purified by Kugelrohr distillation. The enantiopure imidazolines *S*-**3.10** (R = Bn), *S*-**3.11** (R = Ph), *S,S*-**3.12** (R = 2-^{i}Bu) and *S*-**3.13** (R = ^{i}Pr) were isolated as colourless oils and characterised by NMR spectroscopy and high resolution mass spectrometry.

The corresponding imidazoline substituted ligands were synthesised by addition of the respective enantiopure imidazoline to a suspension of methimazole (3 eq.) in toluene. Tris(dimethylamino)borane was added and the reaction mixture heated to reflux for *ca.* 12 h. Ligands **3.14** (R = Bn), **3.15** (R = Ph), **3.16** (R = 2-^{i}Bu) and **3.17** (R = ^{i}Pr) were all isolated as colourless powers after standard workup (Scheme 3.9).

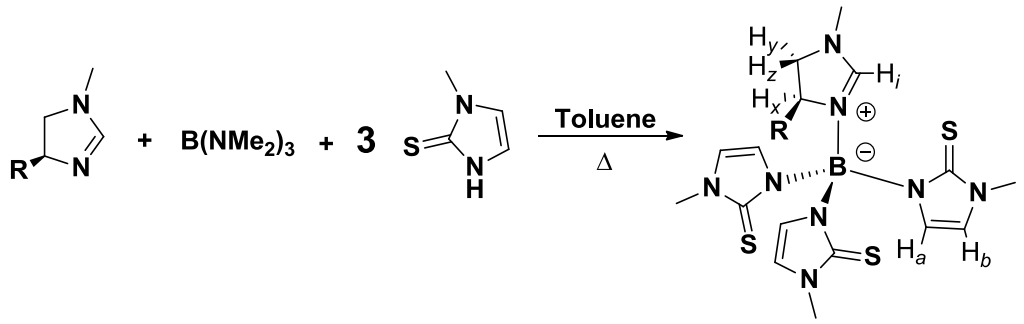

Scheme 3.9: Synthesis of the chiral (imidazoline)ZTm ligands *S*-**3.14** (R = Bn), *S*-**3.15** (R = Ph), *S,S*-**3.16** (R = 2-^{i}Bu) and *S*-**3.17** (R = ^{i}Pr).

Mass spectrometry (EI) of these ligands confirmed the formation of each with peaks representing [M^+] at m/z = 524 for **3.14** (R = Bn), m/z = 510 for **3.15** (R = Ph), m/z = 490 for **3.16** (R = 2-^{i}Bu), and m/z = 476 for **3.17** (R = ^{i}Pr). The ^{1}H-NMR spectra of these ligands all showed resonances between 6.64 – 6.69 ppm relating to the methimazolyl CH protons (H_b). While these resonances were relatively sharp, those representing H_a (6.74 – 7.83 ppm) and H_i (7.59 – 8.08 ppm) were significantly broadened compared with those in the parent system **3.7** (R = H). For example, the H_i signal in **3.16** (R = 2-^{i}Bu) has a width of *ca.* 242 Hz at half height whilst in the same spectrum the *protio* solvent signal had a width of *ca.* 4 Hz at half height. This broadening indicates hindered rotation about the B-N coordinate bonds in each of these ligands due to the steric bulk of the imidazoline substituents. The ^{1}H-NMR spectrum of **3.14** (R = Bn) and **3.15** (R = Ph) both showed large sharp multiplets between 7.15 and 7.48 ppm corresponding to their aryl protons. The spectrum of **3.14** also contained broad resonances at 2.94 and 2.37 ppm representing the diastereotopic benzyl protons. The imidazoline protons in **3.16** (R = 2-^{i}Bu) and **3.17** (R = ^{i}Pr) were more clearly visible each showing two sharp resonances at 3.82 / 3.85 (t, J = 10.8 Hz, 1H) and 3.45 / 3.47 ppm (dd, J = 10.7, 4.4 Hz, 1H) for the diastereotopic imidazoline protons (H_y and H_z) along with sharp multiplets representing the protons of the 2-^{i}Bu / ^{i}Pr substituent. In **3.14** (R = Bn), **3.16** (R = 2-^{i}Bu) and **3.17** (R = ^{i}Pr) the H_x proton appears as a very broad singlet between 4.61 and 5.39 ppm however in **3.15** (R = Ph) the same proton appears only slightly broadened as a triplet at 4.34 ppm (J = 11.0 Hz).

Each of the ligands **3.14**-**3.17** were reacted with [Ru(*p*-cymene)Cl_2]$_2$ (0.5 eq.) in methanol followed by salt metathesis with ammonium hexafluorophosphate (2 eq.). The precipitate which formed in each case was

filtered, washed with MeOH and dried *in vacuo* to yield the complexes **3.18** (R = Bn), **3.19** (R = Ph), **3.20** (R = 2-^{i}Bu) and **3.21** (R = ^{i}Pr) as red/orange powders. The ^{1}H-NMR spectra of these complexes differ so each will be discussed separately.

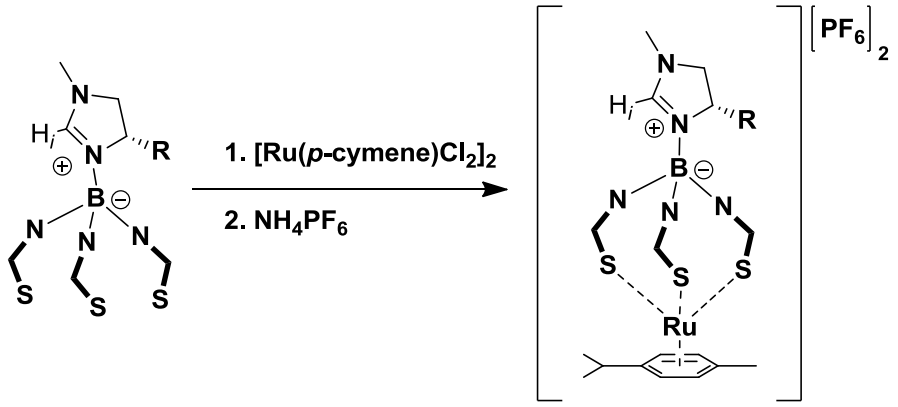

Scheme 3.10: Complexation of ligands **3.14-3.17** (R = Bn, Ph, 2-^{i}Bu, ^{i}Pr) to give **3.18-3.21** (R = Bn, Ph, 2-^{i}Bu, ^{i}Pr).

The acidic imidazoline proton (H_i) in **3.18** (R = Bn) (Scheme 3.10) appears as two resonances at 7.82 and 7.77 ppm which integrate in the ratio *ca.* 2.3 : 1 indicating this to be the ratio of the diastereoisomers *(S, P)*:*(S, M)*. Similarly, resonances at 7.05 and 7.03 ppm integrate overall to 3H and represent one set of methimazolyl ring protons in each of the diastereoisomers. Therefore a benzyl substituent on the imidazoline ring was found to promote some degree of stereodirection of the metal-ligand cage, although its steric bulk is not sufficient to promote the formation of a single diastereoisomer. A model of this complex was generated based on the crystal structure of **3.8** and the geometry optimised using density functional theory (DFT) calculations as approximated by the B3LYP functional and employing the 3-21G* basis set (Figure 3.8). In the lowest energy conformation the phenyl ring is positioned far from the methimazolyl groups and thus the

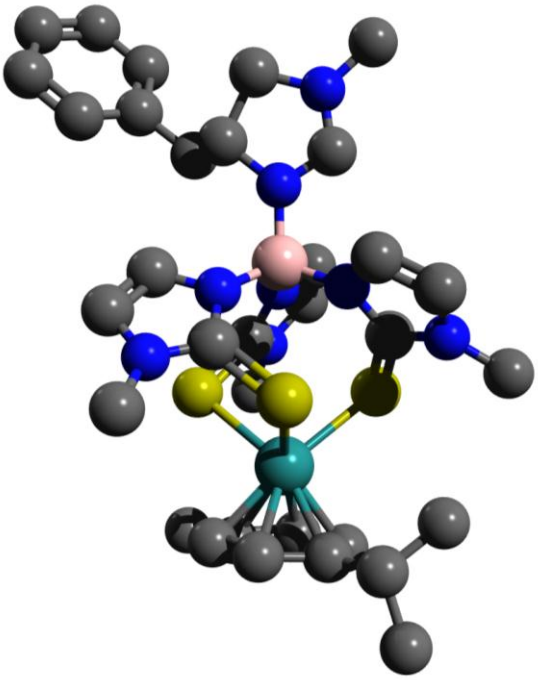

Figure 3.8: DFT Geometry optimised structure for (*R,M*-**3.18**) based on DFT calculations (B3LYP/3-21G*).

steric interaction between this enantiopure group and the ligand arms is reduced.

In light of this, an imidazoline such as *S*-**3.11**(R = Ph) in which the bulky substituent is located proximate to the ligand arms should promote improved stereodirection. However, in **3.19** (R = Ph) the acidic imidazoline proton (H_i) appears as two resonances at 8.03 and 7.99 ppm with a *ca.* 1.5 : 1 ratio. Similarly, two resonances at 7.13 and 7.06 ppm represent the methimazolyl ring protons and integrate in a *ca.* 1.5 : 1 ratio. This represents a decrease in stereodirection using the phenyl-substituted imidazoline *S*-**3.11** relative to *S*-**3.10**. Whilst the phenyl substituent is bulky in two dimensions it is free to rotate and may adopt an orientation which minimises interaction with the methimazolyl ligand arms resulting in poor chiral induction. Therefore, aliphatic substituents which contain more three-dimensional steric bulk were explored.

The imidazoline *S,S*-**3.12** (R = 2-^{i}Bu) contains two chiral centres and therefore ligand **3.16** (R = 2-^{i}Bu) was expected to have improved stereodirection upon complexation. Unlike in the previous examples, the ^{1}H-NMR spectrum of **3.20** (R = 2-^{i}Bu) shows the acidic imidazoline proton (H_i) as one resonance at 7.72 ppm. However, a set of resonances at 6.87 and 6.82 ppm represent the H_a protons in each of the diastereoisomers *S,S,P* and *S,S,M* (Figure 3.9). These signals have a relative ratio of *ca.* 2.5 : 1 indicating an improvement in stereodirection over **3.19** (R = Ph) but similar to **3.18** (R = Bn).

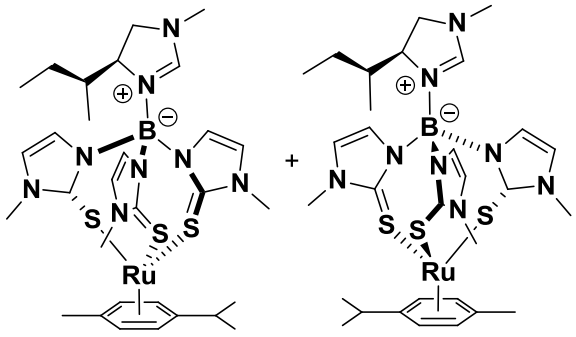

Figure 3.9: Two diastereoisomers of **3.20** (R = 2-^{i}Bu).

Finally, the ^{1}H-NMR spectrum of **3.21** (R = ^{i}Pr) in MeCN-d_3 showed a single resonance at 7.75 ppm representing the acidic imidazoline protons of both diastereoisomers. However, a set of resonances at 6.90 and 6.85 ppm represent the methimazolyl H_a protons and indicate the presence of two diastereoisomers in the ratio *ca.* 2 : 1.

An NMR sample of the isolated complex **3.21** was prepared in $CDCl_3$ to test solubility in non-donor solvents. Although solubility was very poor, a ^{1}H-NMR spectrum was collected which showed the presence of only one diastereoisomer. Resonances at 7.07 and 6.82 ppm represent the H_a and H_b

protons of the methimazole ligand arms and these shifts correspond to those of the major diastereoisomer in the MeCN-d_3 spectrum. Therefore, it was proposed that the major diastereoisomer could be selectively extracted from the reaction mixture using chloroform. A sample of **3.21** (*ca.* 50 mg) was extracted with $CHCl_3$ (10 x 5 mL) before the solvent was removed *in vacuo*. The residue was dissolved in MeCN-d_3 and subjected to ^{1}H-NMR spectroscopy. However, the complex began to racemise immediately upon dissolution in the donor solvent, reaching a constant ratio of *ca.* 2 : 1 after *ca.* 20 h at rt (Figure 3.10). The same extraction procedure was repeated followed by dissolution in DCM- d^2. However, rapid racemisation to the equilibrium diastereomer ratio was also found to occur in this solvent, perhaps aided by the presence of trace quantities of D_2O which could act as a donor towards the ruthenium centre and therefore lower the barrier to dissociative interconversion (**A,** Figure 3.1) between the two diastereoisomers of **3.21**.

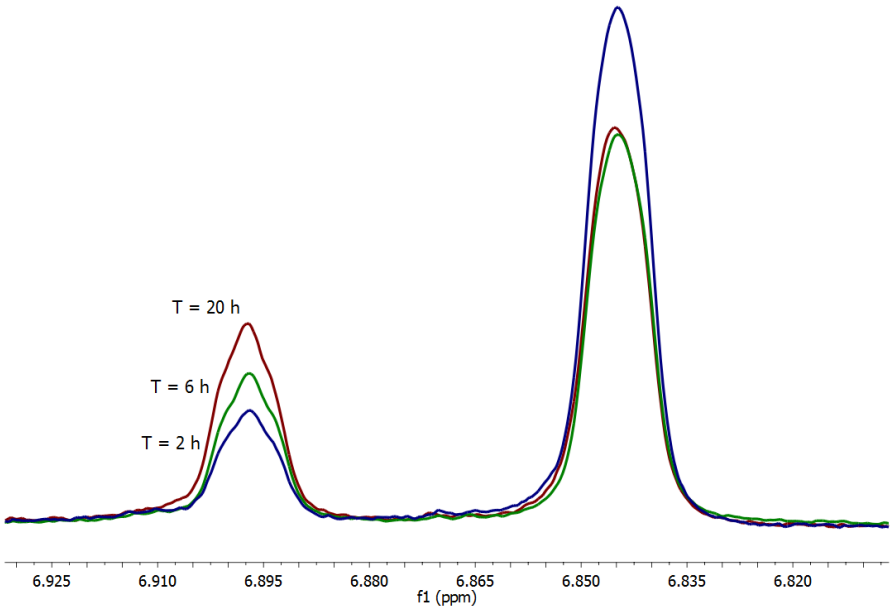

Figure 3.10: The interconversion of the two diastereoisomers of **3.21** occurs relatively rapidly at room temperature in donor solvents.

3.3 Conclusions

A number of factors must be considered when selecting a chiral directing group for the boron bridgehead in helically chiral complexes of tris(methimazolyl)borate ligands. Firstly, any donor must be sufficiently basic to substitute dimethylamine in **2.1** without causing ligand degradation through deprotonation of the $HNMe_2$ group. In addition, any potential donor group must be stable to attack by the nucleophilic methimazolyl sulphur atoms. Steric factors also play a critical role in successful chiral induction using a chiral boron substituent. The work presented in this chapter has shown that bulky donors (*e.g.* 6-Me-DBU) do not substitute the dimethylamine donor in **2.1** and may instead promote ligand degradation by deprotonation of this group, leading to the formation of a tetra(methimazolyl)borate salt. Despite this limiting factor, significant steric interaction between the chiral donor and the ligand arms is required for full stereodirection of the helix. Chiral imidazolines have been shown to coordinate to the boron centre successfully whilst also affecting the helical twist of the ligand arms upon complexation. However, the steric interaction of the substituents described herein with the methimazolyl ligand arms has been shown to be insufficient to induce the formation of a single helix conformation upon complexation. Generally, a ratio of stereoisomers of *ca.* 2:1 was observed in these complexes, therefore bulkier imidazoline substituents, such as *tert*-butyl, may be required in order to effect full stereodirection in these complexes and yield a single diastereoisomer complex; however, the increased steric bulk close to the donor nitrogen may preclude their coordination to the boron.

3.4 References

1. McCormack, C., PhD Thesis, University of Edinburgh, **2005**.
2. Bailey, P. J.; Dawson, A.; McCormack, C.; Moggach, S. A.; Oswald, L. D. H.; Parsons, S.; Rankin, D. W. H.; Turner, A., *Inorg. Chem.,* **2005**, *44*, 8884.
3. Bailey, P. J.; McCormack, C.; Parsons, S.; Rudolphi, F.; Sanchez-Perucha, A.; Wood, P., *Dalton Trans.,* **2007**, 476.
4. Perucha, A. S., PhD Thesis, University of Edinburgh, 2007.
5. Bailey, P. J.; Budd, L.; Cavaco, F. A.; Parsons, S.; Rudolphi, F.; Sanchez-Perucha, A.; White, F. J., *Chem. Eur. J.,* **2010**, *16*, 2819.
6. Kunz, K.; Bolte, M.; Wagner, M.; Lerner, H.-W., *Z. Anorg. Allg. Chem.,* **2009**, *635*, 1580.
7. Bailey, P. J.; Lorono-Gonzales, D.; McCormack, C.; Millican, F.; Parsons, S.; Pfeifer, R.; Pinho, P. P.; Rudolphi, F.; Sanchez Perucha, A., *Chem. Eur. J.,* **2006**, *12*, 5293.
8. Mauduit, M.; Clavier, H.; Boulanger, L.; Audic, N.; Toupet, L.; Guillemin, J.-C., *Chem. Comm.,* **2004**, 1224.
9. Casey, M.; Boland, N. A.; Hynes, S. J.; Matthews, J. W.; Smyth, M. P., *J. Org. Chem.,* **2002**, *67*, 3919.
10. Zhao, G.; Yang, Y. Q., *Chem. Eur. J.,* **2008**, *14*, 10888.
11. Dominianni, S. J.; Yen, T. T., *J. Med. Chem.,* **1989**, *32*, 2301.
12. Fieser, L. F.; Fieser, M. *Reagents for Organic Synthesis* **1967**, 581-595.

Chapter Four

"Twisted" Scorpionates: Lessons in the Requirements for Successful $B(L_2D)_3$ type Ligands

4.1 Introduction

The majority of trisubstituted borate ligands, such as Tp and Tm, coordinate in a tripodal (κ^3) mode, utilising three ligand donor 'arms' and leaving one uncoordinated boron substituent.[1,2] Hydrotris(methimazolyl)borate (Tm) differs from Tp in forming 8-membered chelate rings on metal complexation due to the presence of two atoms (N and C) linking the boron and sulfur donor atoms (*cf.* a single linking N atom in the Tp ligand). Never-the-less, Tm also commonly coordinates in the κ^3-mode and, as discussed in Chapter 1, such complexes exhibit C_3-helical chirality, contrasting with the achiral C_{3v}-Symmetry provided by the κ^3-Tp ligand. This chirality arises due to 'twisting' of the bicyclo[3.3.3] metal-ligand cage structure, which forms upon κ^3-complexation, in order to relieve angle strain (Figure 4.1).

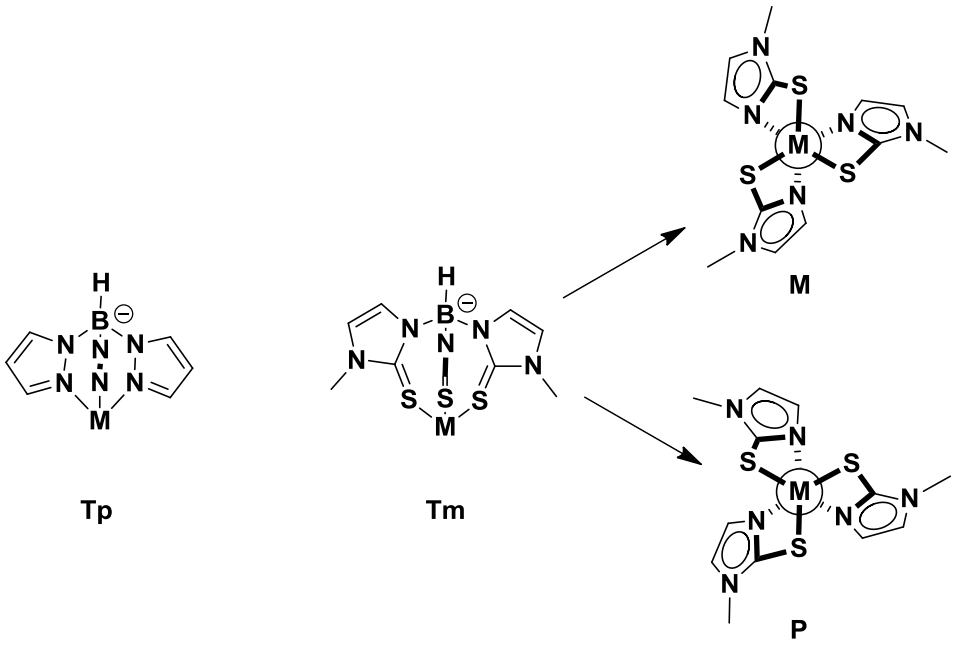

Figure 4.1: Hydrotris(methimazolyl)borate (Tm) exhibits C_3-helical chirality when coordinated to a metal.

The hydrotris(7-azindolyl)borate (Tai) ligand, which also forms 8-membered chelate rings on metal coordination, more commonly coordinates either in the κ²-[*N*,*N*] or κ³-[*N*,*N*,H] modes (Figure 4.2).[3,4] The complex [(Tai)ZnCl] contains the only reported example of this ligand coordinated in the κ³-[*N*,*N*,N] mode.[4] The coordination behaviour of this ligand therefore contrasts with that of Tm and its derivatives,[5] despite the topological equivalence of their κ³-[*N*,*N*,N] and κ³-[S,S,S] coordination modes.

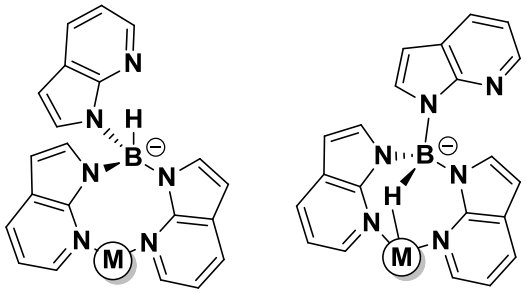

Figure 4.2: Common binding modes of the Tai ligand.

The Bailey group has sought to understand the coordination modes of these ligands in an effort to exploit the chirality of C_3-symmetric complexes in asymmetric catalysis. Analysis of the torsion angles around the sulfur donors in Tm complexes clearly indicates them to be sp^3 hybridised. The two lone pairs on an sp^2 thione sulfur are necessarily coplanar with the attached imidazole ring which would provide an ideal M-S-C-N torsion angle of 0° on metal complexation, and a C_{3v}-symmetric structure. However, torsion angles of between 60 and 70° are typically observed in Tm complexes of both octahedral and tetrahedral metal ions, and the M-S-C bond angles typically lay in the range 90-110° both of these parameters being consistent only with sp^3 sulfur.[7] It should be noted that the presence of sp^3 thiolate sulfur donors

in the Tm ligand and its derivatives is also entirely consistent with the donor properties of this ligand system.[6,7] In contrast, the involvement of the N-donor atoms in the Tai ligand in aromatic rings means that they can only provide sp^2 hybridised lone pairs in the plane of the pyridine rings (Figure 4.3). The resulting κ^3-coordinated Tai ligand in [(Tai)ZnCl] provides a highly strained C_{3v}-symmetric system in which the mean Zn-N-C-N torsion angle is just 3.6° and the mean angle at each of the nine 7-azaindolyl atoms involved in the chelate rings is 130.6°.[5] The evident angle strain in this system thus generally results in complexes in which only two of the 7-azaindolyl arms are coordinated to give either of the common coordination modes shown in Figure 4.2, although the structure of [(Tai)ZnCl] indicates that κ^3-coordination is not precluded.

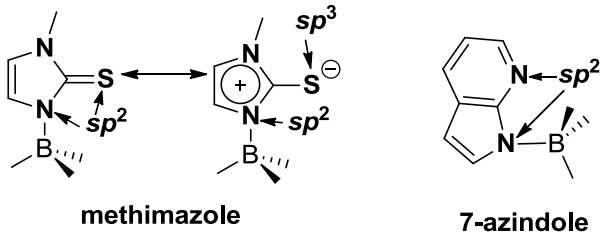

Figure 4.3: Resonance forms of methimazole and 7-azindole.

On considering the hybridisation issues in Tm and Tai it becomes apparent that C_3-symmetric tripodal (κ^3) coordination of this type of ligand requires that either the donor *or* the boron-bound atom of the donor group be sp^3 hybridised, and thus two possible hybridisation frameworks may be envisaged (Figure 4.4).

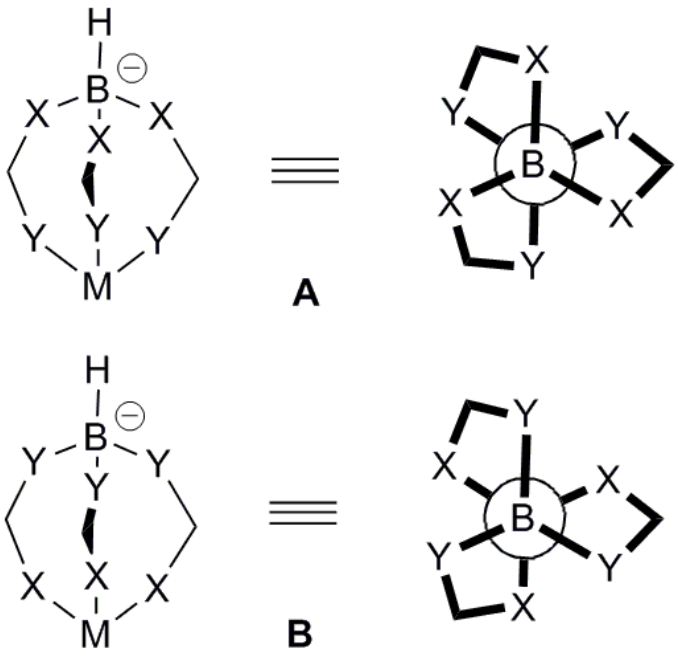

Figure 4.4: The two alternative hybridisation frameworks providing C_3-symmetric complexes. X = sp^2 hybridised atom, Y = sp^3 hybridised atom.

Seeking to design new ligands of both types **A** and **B** we have explored the synthesis of new scorpionates based on substituted pyridine heterocycles which have not been fully exploited in this field to date.

4.2 Results and Discussion

4.2.1 ZThp Synthesis

With the aim of developing a ligand with the alternative hybridisation type **B** (*i.e.* with sp^3 (**Y**) atoms bound to boron and sp^2 (**X**) donor atoms) the synthesis of a ligand incorporating 2-pyridonyl (derived from 2-hydroxypyridine) as the ligand arms was explored. It was rationalised that the hard sp^3-hybridised oxygen centre would preferentially bind to boron, leaving the pyridine nitrogen atoms available for metal coordination.

Following the synthetic methodology developed in the Bailey group (dimethylammonium)tris(2-pyridonyl)borate [($HNMe_2$)Thp] (**4.1**) was obtained from the reaction of 2-hydroxypyridine with tris(dimethylamino)borane in toluene (Scheme 4.1). Evolution of $HNMe_2$ ceased after 3 h under reflux and ^{1}H-NMR spectroscopy showed no evidence of starting materials. Four new resonances corresponding to the target material were present in the aromatic region of the spectrum at 6.71, 6.86, 7.42 and 8.01 ppm (each 3H). All of these resonances are shifted to higher frequency relative to those in free 2-hydroxypyridine; however, the resonance representing H_d shifts the least indicating binding of the exocyclic oxygen to the boron centre as expected by HSAB theory. In addition, a doublet at 2.84 ppm confirmed the retention of a single $HNMe_2$ group in this ligand. Mass spectrometry (EI) showed a molecular ion peak at m/z = 339.1 consistent with the anticipated structure.

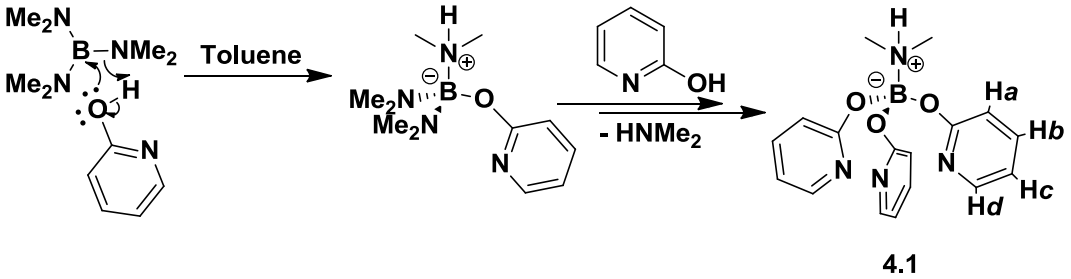

4.1

Scheme 4.1: Synthesis of (HNMe2)Thp (**4.1**).

Ligand **4.1** was found to be exteremely air-sentitive causing degradation to 2-hydroxypyridine within seconds upon exposure to air. This is likely due to hydrolysis of the B-O bonds by moisture in the air giving $B(OH)_3$. Alternate boron donors to replace the dimethylamine were therefore

sought in order to stabilise the boron centre to hydrolysis. The ligand in which the dimethylamine is replaced with 4-dimethylaminopyridine (DMAP) was constructed by reaction of 2-hydroxypyridine, $B(NMe_2)_3$ and DMAP (3:1:1) in toluene under reflux for 4 h (Scheme 4.2). The new adduct (**4.2**) was isolated as a colourless solid in 69% yield after workup and found to be slightly less moisture sensitive than **4.1**, although both ligands were handled in the glovebox or using Schlenk techniques throughout.

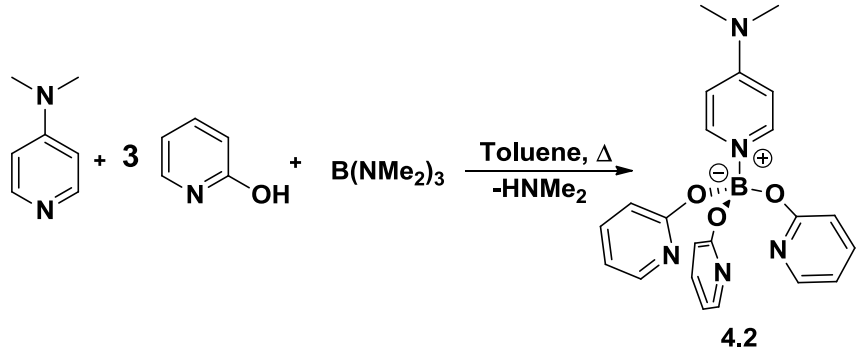

Scheme 4.2: Synthesis of (dimethylaminopyridinium)tris(2-pyridonyl)-borate **4.2**.

Two resonances at 6.52 (2H) and 8.78 (2H) ppm were visible in the ^{1}H-NMR spectrum of **4.2** and this, along with a singlet at 3.10 ppm (6H), indicated coordination of DMAP to the boron centre. Mass spectrometry (FAB^+) showed a molecular ion peak at m/z = 414.7 confirming the formulation of **4.2** as shown in Scheme 4.2.

Crystals suitable for X-ray diffraction were grown by slow diffusion of diethyl ether into a solution of the ligand in a DCM. The X-ray crystal structure of **4.2** confirms the expected binding of the 2-pyridonyl groups to boron through oxygen (Figure 4.5). The B-O-C angles are in the range 124-126° and the B-O-C-N torsion angles range from 7-28°. In contrast to ZTm, **4.2** does not exhibit axial chirality as a ligand. This appears to be a

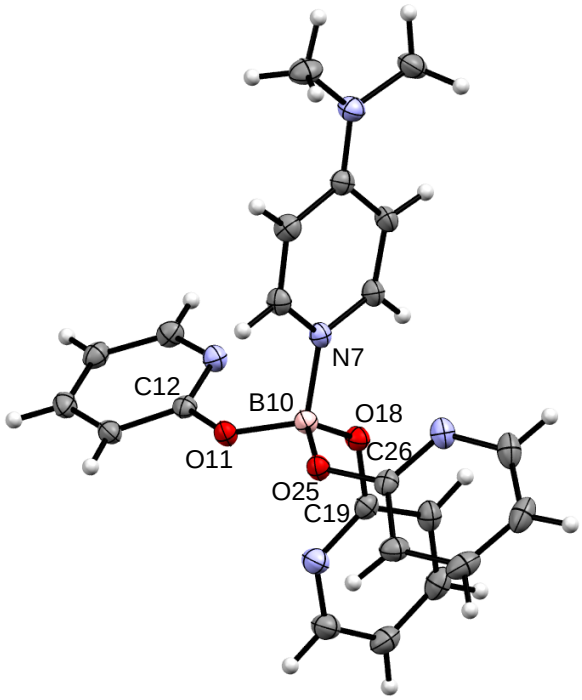

Figure 4.5: X-ray crystal structure of (DMAP)Thp **4.2**. Displacement elipsoids have been drawn at 50% probablility . Selected bond lengths and angles are provided in Table 6.12.

consequence of the increased conformational flexibility around the boron centre which is less sterically crowded than in ZTm. Hence, the 2-pyridonyl ligand arms are able to rotate about their B-O and O-C bonds freely without significant steric hindrance. In contrast the methimazole rings in **2.1** are closer to the central boron resulting in the free ligand adopting a chiral propeller-like arrangement in order to minimise steric repulsion (Chapter 2).

Complexation of the ligand **4.2** to copper(I) chloride in CH_2Cl_2 provided the yellow complex [{(DMAP)Thp}CuCl] (**4.3**). This was found to be insoluble in most common solvents, but the ^{1}H-NMR spectrum in d_6-DMSO showed three very broad resonances and a slightly sharper triplet for the pyridyl protons, each integrating for 3H. Two less broadened resonances corresponding to the DMAP ring protons are visible at 6.81ppm (2H) and 8.51 ppm (2H). A singlet appears at 3.10 ppm (6H) for the DMAP

dimethylamino protons. The ^{13}C-NMR also shows broadened resonances for three of the pyridine ring carbon atoms.

In pursuit of a more soluble Thp complex, **4.2** was reacted with $[(PPh_3)CuCl]_4$ with the expectation of forming the salt $[(DMAP)ThpCu(PPh_3)]Cl$. In order to test the viability of this route an initial test reaction was performed in a sealed NMR tube in $CDCl_3$ solvent. X-ray quality crystals of the product of this reaction grew serendipitously upon standing overnight and X-ray crystallography showed these to be the previously prepared chloro- complex **4.3**, thus demonstrating that the PPh_3, rather than the chloride, had been replaced by the Thp ligand.

The structure of **4.3** (Figure 4.6) confirms that the complex exhibits *pseudo*-C_3-Symmetry by forming a helically twisted complex of with hybridisation architecture **B** (Figure 4.7), the unit cell containing a racemic mixture of two pairs of complexes with *M* and *P* helicity. The B-O-C-N torsion angles (range 42.4 – 58.8°) clearly indicate sp^3 hybridisation of the O atoms. The B-O-C bond angles [avg. 128.2°] are larger than in **4.2** [avg. 125.3°] and deviate significantly from the ideal tetrahedral angle demonstrating that these oxygens experience significant angle strain upon complexation. There is also some strain within the metal-ligand cage evidenced by small deviations of the planes of the pyridyl rings from their N-Cu bonds (range 7.1 – 11.8°) leading to slight non-planarity at the N-atoms (sum of the angles at N range 358.8 – 359.6°). No corresponding distortions are observed in Tm metal complexes, in which the methimazolyl rings are found to be coplanar with their B-N bonds, and their origin would appear to be a result of the small size of oxygen (*cf.* sulfur), which results in an increase of the O-B-O angles on formation of the metal-ligand cage, and this strain is partially relieved by the observed distortions. The sum of the O-B-O angles in

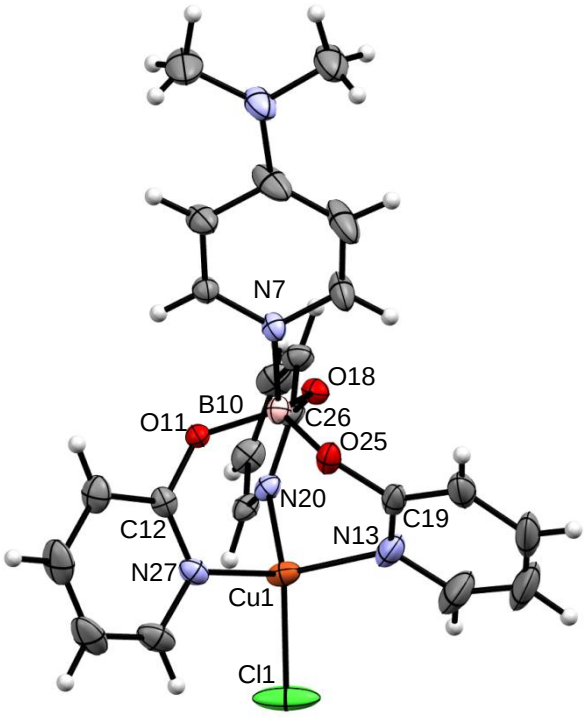

Figure 4.6: X-ray crystal structure of (DMAP)ThpCuCl (**4.3**). Displacement elipsoids have been drawn at 50% probablility .Selected bond lengths and angles are provided in Table 6.13.

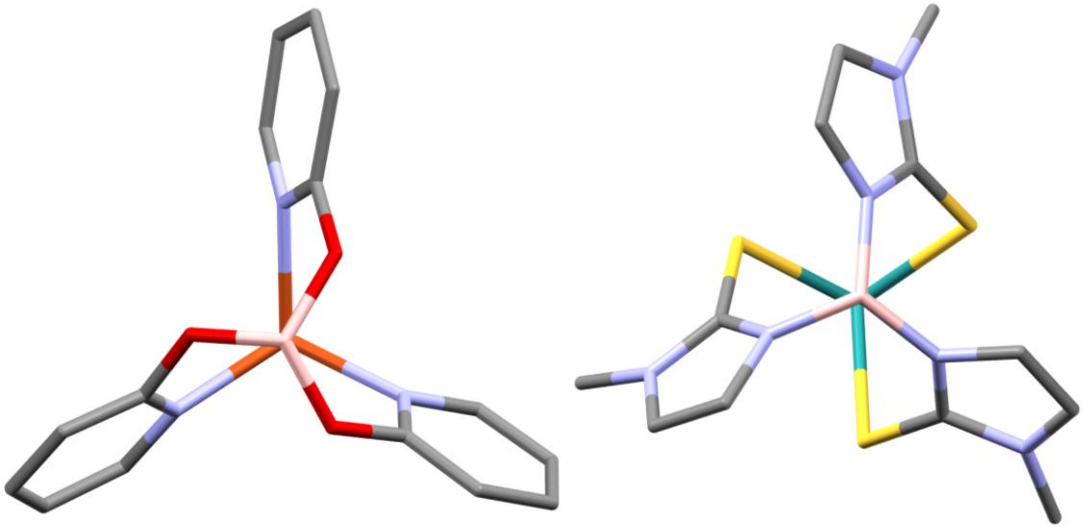

Figure 4.7: View down the Z-axis of the X-ray crystal structures of [{(DMAP)ZThp}CuCl] **4.3** and [{(N-MeImid)ZTm}Ru(*p*-cymene)] (**3.11**).

complex **4.3** and the free ligand are 342.4° and 333.0° respectively, values which should be compared with 329.0° for the sum of the N-B-N angles in the complex $TmCuPPh_3$ (*i.e.* almost ideal for tetrahedral boron).[8]

The helicity of complexes of the Tm ligand can be described using two parameters developed by Hill *et al*.[9] The first, θ, represents the N-B-M-S torsion angle in Tm complexes or more generally the X-B-M-Y torsion angle in complexes which have hybridisation framework **A** (Figure 4.4). This parameter implicitly includes a description of the chirality of the complex with $\theta > 0$ representing a P helix and $\theta < 0$ denoting an M helix. In complexes with the hybridisation framework **B** θ represents the Y-B-M-X torsion angle. The average O-B-Cu-N torsion angle (θ = -34.4°) in **4.3** signifies the M enantiomer although both enantiomers are present in the unit cell (Figure 4.7) which exhibits a smaller twist angle than in complexes of Tm (*ca.* 45-50°).

The second parameter (ω) describes the degree of displacement of the metal from the plane of the aromatic ring which is related to the 'twist' of the complex. The value ω is derived from the angle that the B-M vector makes with the normal to the plane of the aromatic ring. As such ω is inversely proportional to the displacement of the metal from the plane of the methimazolyl ring. In the case of **4.3**, which has the alternate hybridisation

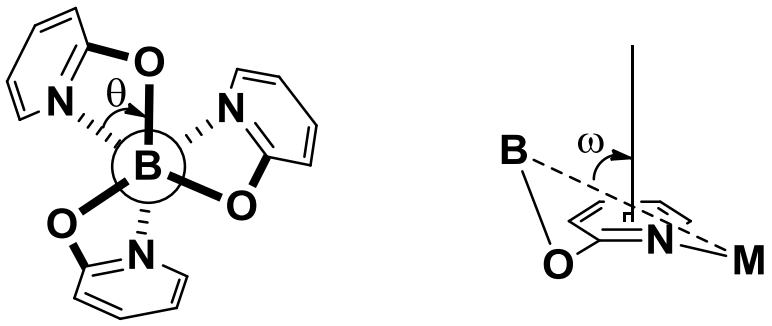

Figure 4.8: The parameters which describe helicity in complexes of ZThp.

framework **B**, this parameter is a measure of the displacement of the boron from the plane of the pyridine ring however this value still allows comparison of the relative helicity of complexes of ZThp with ZTm. The value in complex **4.3** (ω = 66.3°) is slightly larger than in complexes of Tm (*ca.* 55 - 59°) indicating that the ZThp ligand in **4.3** is less 'twisted' than Tm in similar complexes. A small twist angle (θ=27.1°, ω = 65.4°) was also observed in complexes of Parkin's Tio ligand which also contains oxygen **Y** atoms but has the same hybridisation framework as Tm (**A**).

The relative size of the twist angle in complexes of these ligands can be rationalised by analysis of the angles about the boron-bound atoms (**Y** in the type **B** ligand architechture – Figure 4.4). The difference in these angles in Tm, Thp and Tai is related to the nature of the **Y** atom in each system. Since oxygen is capable of forming strong π-bonds with carbon it may exhibit more sp^2-like behaviour,[vi] with relatively large B-O-C angles [avg. 128.2°] and short O-C bonds [avg. 1.345 Å *cf.* 1.43 (C-O) / 1.20 (C=O)]. Therefore, the Tio and ZThp ligands will exhibit a small helical twist. Sulfur, in contrast, has poor p_z-orbital overlap with carbon and thus will exhibit more sp^3-like character with smaller M-S-C angles (*ca.* 95°) and longer S-C bonds [*ca.* 1.73 Å *cf.* 1.82 (C-S) / 1.60 (C=S)]. This means that ligands with **Y** = S will exhibit larger helical twist angles compared with those with **Y** = O.

4.2.2 Exploration of synthetic routes to ZTmp

In 2009, Owen reported the synthesis of hydrotris(pyrid-2-thionyl)borate (Tmp) from reaction between 2-mercaptopyridine and potassium borohydride.[10] This ligand is the 2-mercaptopyridyl analogue of Tm and was synthesised by reaction of KBH_4 with 2-mercaptopyridine (mp)

[vi] Whilst VSEPR theory is helpful in approximating the hybridisation of the Y atom simplistically at this level of discussion MO theory is a more accurate descriptor of the nature of the orbitals in these complexes. Thus Y atom orbitals will be described as molecular orbitals with varying degrees of hybridised orbital character.

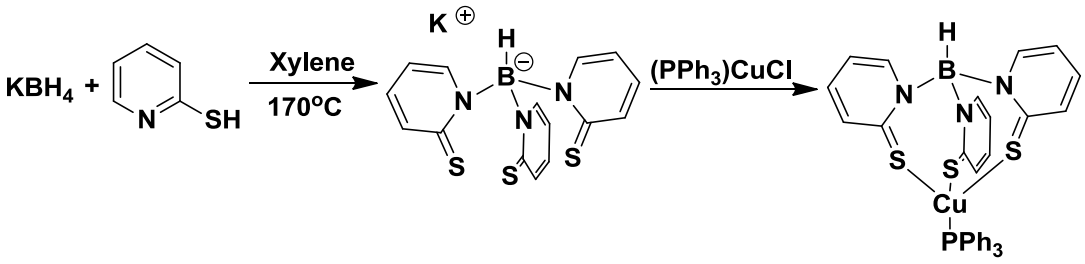

Scheme 4.3: Owen's synthesis and complexation of Tmp.

(Scheme 4.3). In the resulting ligand $HB(mp)_3$, (Tmp), the hard pyridine nitrogen (**X**) preferentially binds to the boron leaving the sulfur atoms (**Y**) as the tripod donors. This Tmp ligand is thought to exhibit a κ^3-[S,S,S] coordination to Cu(I) in the complex [(Tmp)Cu(PPh_3)], although no X-ray crystal structure has been reported; the helical twisting of the metal-ligand cage cannot therefore be assessed. Never-the-less, it is clear that the two ligands Thp and Tmp, which differ only in the identity of the pyridyl 2-substituent (O or S respectively) provide the two possible alternative architectures (**A** or **B**) through 'flipping' of the ligand arms.

Seeking to synthesise a zwitterionic analogue of Tmp, in order to assess its ability to adopt helicity upon complexation, 2-mercaptopyridine (3 eq.) was dissolved in dry toluene and tris(dimethylamino)borane (1 eq.) added. The yellow solution was heated to reflux for 4 hours after which time a sample of the reaction mixture was subjected to ^{1}H-NMR spectroscopy.

Four resonances in the aromatic region represent the mercaptopyridine protons and integrate for 1H each. The resonance representing H_d (Scheme 4.4) is shifted to lower frequency (7.31 ppm) from that of the same proton in free 2-mercaptopyridine (7.59 ppm). Those representing H_c and H_b are also shifted to lower frequency (7.21 and 6.67 ppm respectively) relative to the free heterocycle (7.38 and 6.78) whilst the shift of H_a remains the same (7.53 ppm). This is in contrast to the spectrum of Thp which saw high frequency shifts for all hydroxypyridine protons. A large singlet at 2.56 ppm integrates for 12H relative to the pyridine protons. The protons in tris(dimethylamino)borane appear at 2.51 ppm in $CDCl_3$ suggesting that this resonance belongs to two boron bound dimethylamine groups. Based on these data the formula of this species was assigned as $B(NMe_2)_2$(2-mp) (**4.4**). The binding mode (*i.e.* N or S) of the mercaptopyridine could not be unambiguously determined although HSAB theory would suggest a preference for the formation of a N-B bond over a S-B bond. The relative perturbation of the chemical shifts in the ^{1}H-NMR spectrum for H_a and H_d compared with the starting material also lends weight to this argument. Mass spectrometry (EI^+) showed a molecular ion peak at *m*/*z* =

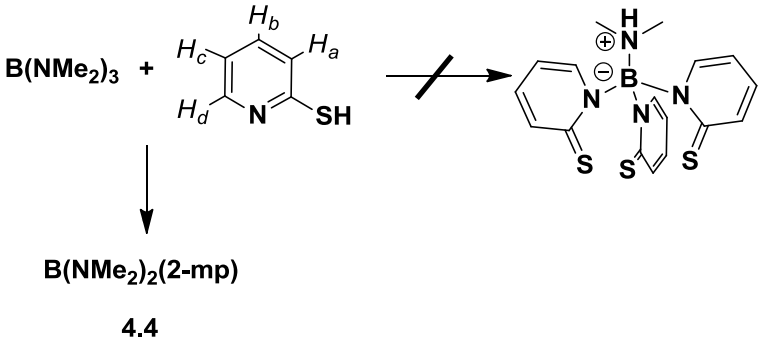

Scheme 4.4: Attempted synthesis of ZTmp from reaction of tris(dimethylamino)borane with 2-mercaptopyridine.

209.1 confirming the formulation of **4.4** as $B(NMe_2)_2(2\text{-mp})$. As with **4.1** and **4.2** this compound was found to be highly moisture-sensitive and was handled under nitrogen throughout.

Owen's successful synthesis of Tmp suggested that the ZTmp should be sterically feasible, therefore it was reasoned that higher temperatures were required to access $(HNMe_2)$ZTmp. With this in mind the 2-mercaptopyridine (3 eq.) was treated with tris(dimethylamino)borane (1 eq.) in dry xylene and heated to reflux (140°C). After 24 hours a black residue was visible in the reaction mixture. ^{1}H-NMR spectroscopy showed the presence of **4.4** as well as free mercaptopyridine. In addition a small set of resonances were present which correspond to the formation of 2,2′-dipyridyldisulfide (Figure 4.9).

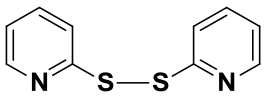

Figure 4.9: 2,2′-Dipyridyl disulfide which forms upon extended heating 2-mercaptopyridine.

The 2-mercaptopyrimidine analogue of **4.4** was expected to give greater insight into the nature binding in these compounds. If the heterocycle bound to boron through one of the ring nitrogens the inherent symmetry of this ring would be broken; however, in the case of sulfur binding the aromatic protons H_a were expected to be symmetry equivalent.

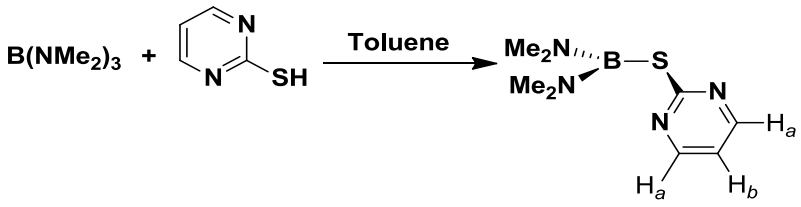

4.5

Scheme 4.5: Reaction of 2-mercaptopyrimidine with tris(dimethylamino)borane to give **4.5**.

Reaction between tris(dimethylamino)borane and 2-mercaptopyrimidine in refluxing toluene for 4 h yielded a bright yellow crystalline insoluble solid **4.5** upon workup (Scheme 4.5). Mass spectrometry (EI^+) suggested a similar product to **4.4** with a molecular ion peak at m/z = 209.1. ^{1}H-NMR spectroscopy showed two singlets at 3.27 (6H) and 3.09 (6H) ppm representing two inequivalent B(NMe_2) groups in contrast to **4.4** where these protons were equivalent in the NMR spectrum. Importantly, a doublet (2H) at 7.78 ppm and a triplet (1H) at 5.45 ppm represent the three pyrimidine ring protons H_a and H_b respectively. The symmetry equivalence of the H_a protons indicates that the exocyclic sulfur bonds to the boron centre rather than one of the nitrogen atoms.

Based on HSAB theory and the lower ability of sulfur to π-donate into the empty boron p_z orbital, nitrogen attack at the boron centre was expected to be preferred. None-the-less, this result provides a rationale for the failure to synthesise ($HNMe_2$)ZTmp from tris(dimethylamino)borane. The occupied p_z-orbital on the mercaptopyridine thiolate has poor overlap with the empty boron p_z-orbital. Therefore the B-N bonding in this species will be strengthened relative to $B(NMe_2)_3$. Substitution of one of these strongly bound dimethylamine groups would therefore be disfavoured (Scheme 4.6). Obviously, in this case the presence of a dimethylammonium substituent on

the boron does not lend sufficient electron density to compensate for the loss of π-electron density from the amine substituents.

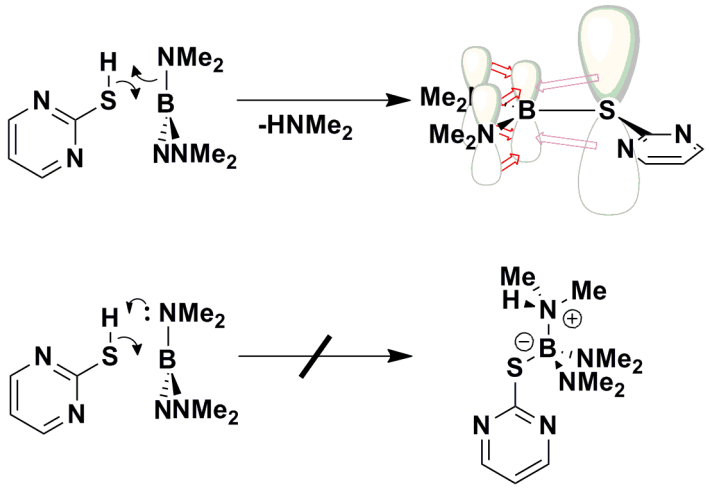

Scheme 4.6: The empty boron p_z-orbital is stabilised by the lone pairs of the two amine donors.

4.3 Conclusions

The results reported herein expand the range of zwitterionic charge-neutral tripodal borate ligands developed to date to include Thp which is based on 2-pyridonyl ligand arms. Comparison of the structure and common coordination modes of a complex of this ligand with those of Tm, Tai and Tio elucidates the hybridisation requirements for the formation of helically chiral complexes. The constraints of the bicyclo[3.3.3] cage architecture formed on κ^3-coordination of such ligands requires sp^3 hybridisation of either the boron-bound or donor atoms in order to reduce angle strain by twisting to form a C_3-symmetric helical structure. It is also evident that the size of the atoms incorporated into the L_2D arms has an impact on the angle strain within the cage. Therefore, ligands that incorporate sp^3 hybridised sulfur atoms in their donor groups exhibit a larger helical twist upon complexation than those containing sp^3 hybridised oxygen atoms.

Attempts to access a zwitterionic analogue of Owen's Tmp ligand by reaction between 2-mercaptopyridine and tris(dimethylamino)borane have proved unsuccessful, instead yielding $B(NMe_2)_2$(2-mp) (**4.4**). NMR spectra of the 2-mercaptopyrimidine analogue **4.5** suggests the exocyclic sulfur is bound to the boron in these molecules disfavouring the substitution of further dimethylamine groups which are required to stabilise the electron-deficient boron centre.

4.4 References

1. Trofimenko, S., *Chem. Rev.,* **1993**, *93*, 943.
2. Smith, J., *Comments Inorg. Chem.,* **2008**, *29*, 189.
3. Owen, G. R.; Tsoureas, N.; Hamilton, A.; Orpen, A. G., *Dalton Trans.,* **2008**, 6039.
4. Song, D. T.; Jia, W. L.; Wu, G.; Wang, S. N., *Dalton Trans.,* **2005**, 433.
5. Reglinski, J.; Spicer, M. D., *Eur. J. Inorg. Chem.,* **2009**, 1553.
6. Bailey, P. J.; Lorono-Gonzales, D. J.; McCormack, C.; Parsons, S.; Price, M., *Inorg. Chim. Acta,* **2003**, *354*, 61.
7. Bailey, P. J.; Budd, L.; Cavaco, F. A.; Parsons, S.; Rudolphi, F.; Sanchez-Perucha, A.; White, F. J., *Chem. Eur. J.,* **2010**, *16*, 2819.
8. Reglinski, J.; Dodds, C. A.; Garner, M.; Spicer, M. D., *Inorg. Chem.,* **2006**, *45*, 2733.
9. Hill, A. F.; Foreman, M. R. S. J.; White, A. J. P.; Williams, D. J., *Organometallics,* **2003**, *22*, 3831.
10. Owen, G. R.; Dyson, G.; Hamilton, A.; Mitchell, B., *Dalton Trans.,* **2009**, 6120

Chapter Five

Scorpionate Sandwiches: Ruthenium, Rhodium and Palladium Complexes of Charge-neutral Zwitterionic Tris(methimazolyl)borate Ligands

5.1 Introduction

'Half-sandwich' complexes of transition metals have been used to great effect in catalysis, and chiral analogues have been shown to catalyse a variety of asymmetric transformations with a high degree of stereoselectivity.[1-9] The chirality in these complexes is commonly conferred by use of a chiral mono- or bidentate ligand coordinated to a metal arene fragment (Figure 5.1).

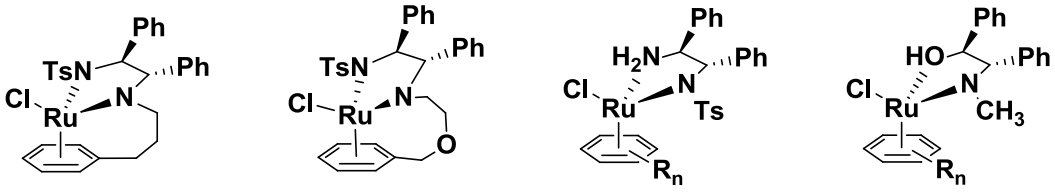

Figure 5.1: Ru(II) Half-Sandwich complexes which have shown high enantioselectivities as precatalysts for asymmetric transfer hydrogenation.

In his Nobel prize-winning work on chiral transfer-hydrogenation catalysis, Noyori developed a range of Ru(II) half-sandwich complexes.[5-8,10] In these systems, chirality is conferred by use of an enantiopure bidentate amino alcohol or diamine ligand. The mechanism for this process involves initial generation of a metal hydride 'half-sandwich' complex (Scheme 5.1).[11] Hydrogenation then occurs by "metal–ligand bifunctional catalysis" via a stable 6-membered transition state.

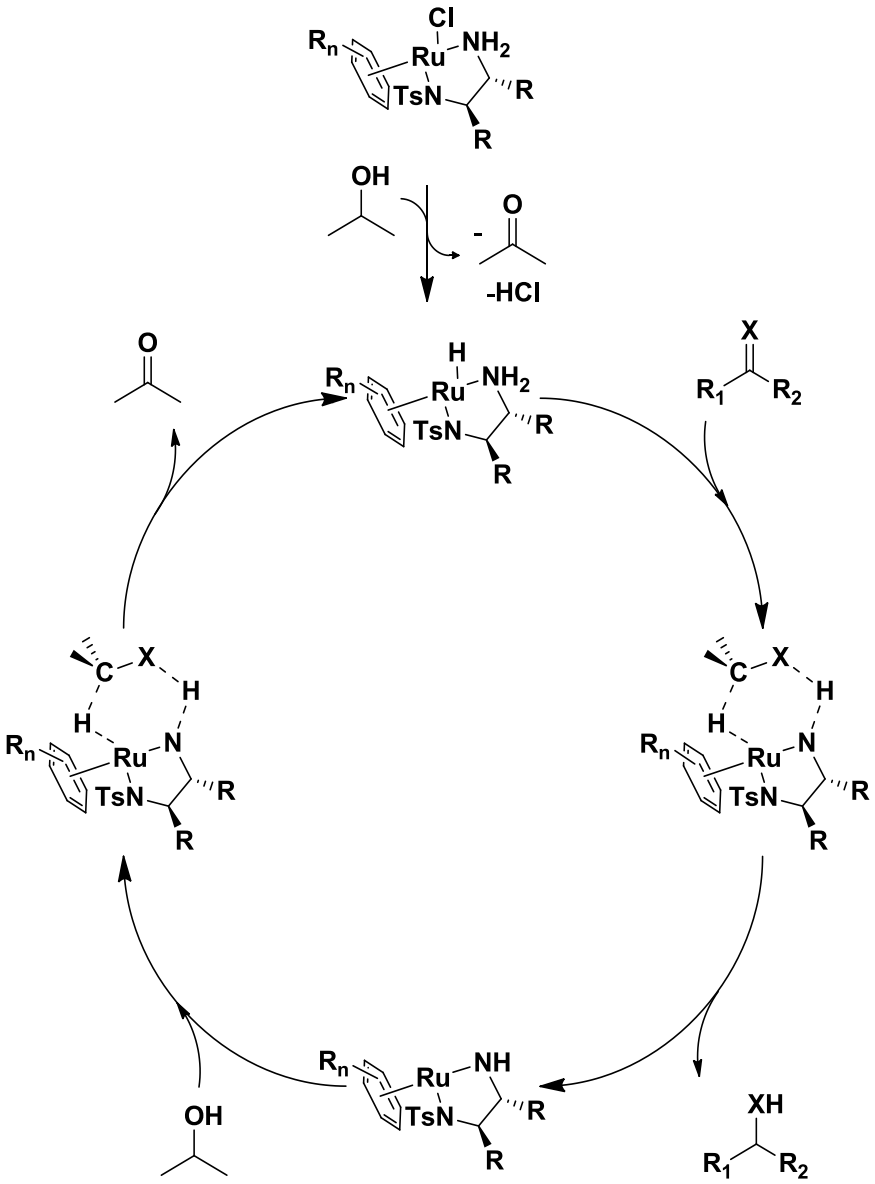

Scheme 5.1: Mechanism of asymmetric transfer hydrogenation with Noyoris Ru(II) 'Half-Sandwich' complexes. X = O, NR

As 6-electron donating face-capping ligands, anionic tripodal borate ligands (*e.g.* Tp, Tm) are often considered as analogues of cyclopentadienyl ligands.[12-14] A variety of 'mixed-sandwich' complexes of Tm and ZTm with metal arene or cyclopentadienyl fragments have been reported both in the published literature and in this work (Figure 5.2).[15-22] In all of these

complexes Tm coordinates in a κ^3-[*S,S,S*] mode although there is evidence for interconversion between the κ^3-[*S,S,S*] and the κ^3-[*H,S,S*] modes in solution.[23] Homoleptic 'sandwich' complexes of these ligands represent another commonly observed structural motif in which the ligand coordinates as a κ^3-[*S,S,S*] tripod.[12,24-26]

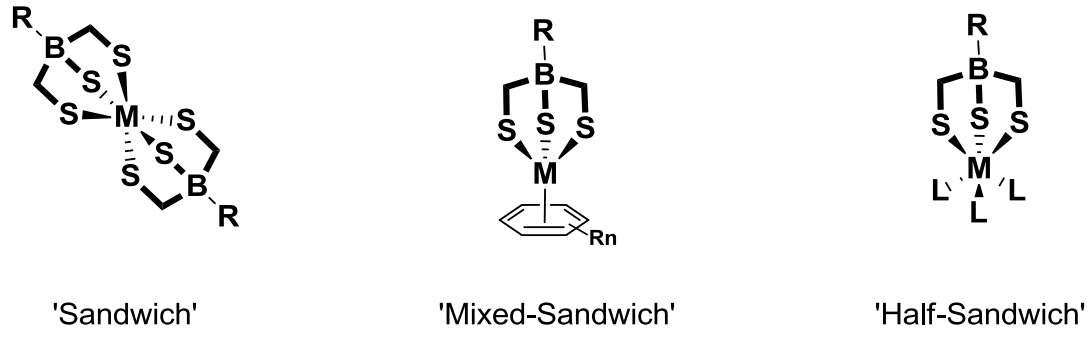

Figure 5.2: Tripod ligands are often compared with arene or cyclopentadienyl ligands and so the 'sandwich' terminology can be extended to these systems.

Pursuit of the corresponding heteroleptic 'half-sandwich' complexes of Tm which may be exploited in catalysis has been less fruitful. An initial study of the reaction between Na[Tm] and $RuCl_2[DMSO]_4$ in DCM isolated poor quality crystals which suggested the structure of the product of this reaction to be κ^3-[*S,S,S*]-TmRuCl[DMSO]$_2$ (**5.1**).[15] However, Hill *et al*. later isolated the similar complex κ^3-[*H,S,S*]-TmRuCl[DMSO]$_2$ (**5.2)** as the major product (90-95% yield by ^{1}H-NMR) by carrying out the reaction anaerobically in THF solvent.[27] This study found no evidence for presence of the κ^3-[*S,S,S*]-isomer in solution indicating **5.1** to be a minor side product.

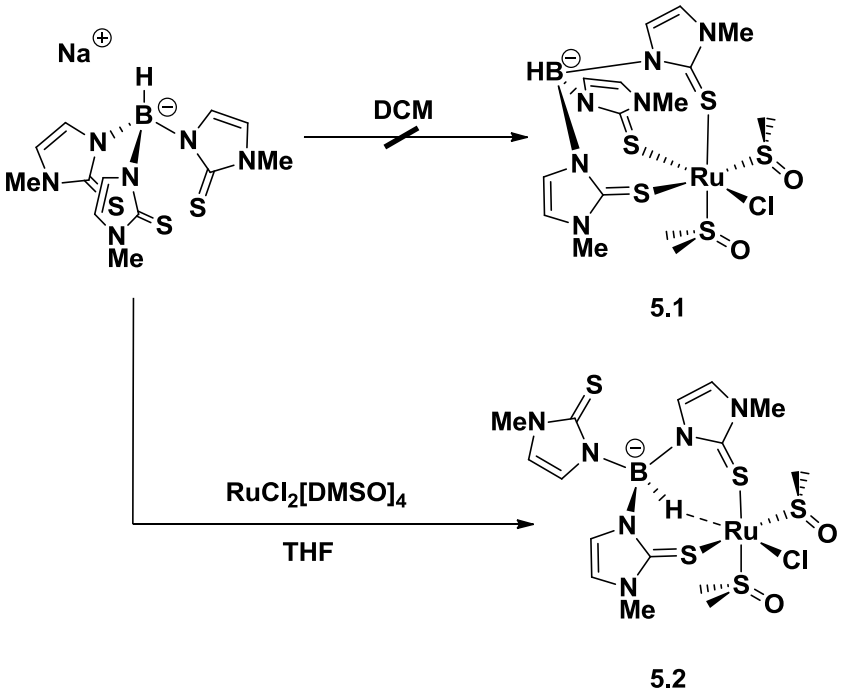

Scheme 5.2: Complexation of Tm to $RuCl_2[DMSO]_4$.

Earlier studies by the same group suggested the prevalence of the κ³-[*H,S,S*]-coordination mode over κ³-[*S,S,S*]- in other heteroleptic 'half-sandwich' complexes of Tm.[28] Reaction between Na[Tm] and $[RuR(CO)(NCMe)_2(PPh_3)_2]ClO_4$ or $[Ru(R)Cl(CO)(PPh_3)_3]$ yielded the complex [{κ³-[*H,S,S*]-Tm}Ru(R)(CO)PPh_3] (R = H, aryl, vinyl) (Scheme 5.3). Dissolution of this complex lead to the immediate formation of the corresponding metallaboratrane when R = aryl, vinyl. Similarly, Zhang demonstrated that

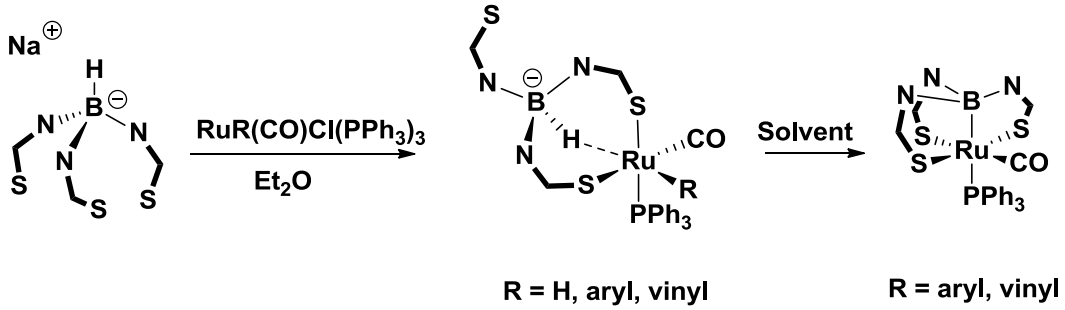

Scheme 5.3: Synthesis of ruthenaboratranes from heteroleptic complexes of Tm.

reaction of [Na{Tm}] with $RuCl_2(PPh_3)_3$ in THF under reflux yielded [{κ³-[*H,S,S*]-Tm}$RuCl(PPh_3)_2$] (Scheme 5.4).[29] Therefore, whilst Tm commonly coordinates to ruthenium in a κ³-[*S,S,S*] mode in 'mixed-sandwich' complexes, no examples of this coordination mode have been reported in ruthenium heteroleptic 'half-sandwich' type complexes.

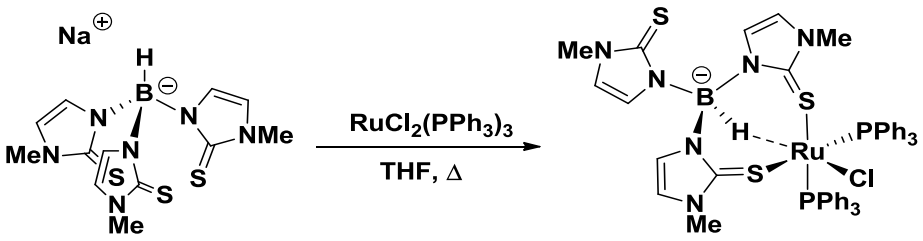

Scheme 5.4: Zhang demonstrated a κ³-[*H,S,S*] coordination mode for Tm upon reaction with $RuCl_2(PPh_3)_3$.

Given the "thiophilicity" of ruthenium this is particularly surprising and there is debate as to the basis of this favourability. Hill cites the geometric constraints of the bicyclo[3.3.3] cage being less favourable than a more compact bicyclo[1.3.3] arrangement arising from κ³-[*H,S,S*] coordination.[28] However, Reglinski and Spicer present a compelling argument that electronic effects play a larger role.[12] This stance takes into account the fact that the bis-ligand complex Tm_2Fe^{II} exhibits κ³-[*H,S,S*] coordination whilst the analogous Fe^{III} complex (with a smaller metal centre) exhibits κ³-[*S,S,S*] coordination. In addition, it was noted that many of the complexes containing a M···H-B interaction include relatively electron-rich d^n metals ($n \geq 6$) where the addition of a third π-donating sulfur may be disfavoured.

Rhodium catalysts are also used to great effect in asymmetric catalysis.[1,3] As with Rh(II), 'mixed-sandwich' Rh(III) complexes have been

reported previously,[30,31] along with the homoleptic bis-ligand 'sandwich' complex $[\{FB(mt)_3\}_2Rh]^+$.[32] A variety of complexes of Tm with d^8 Rh(I) are known where the metal adopts either square-planar or distorted trigonal-bipyramidal geometry with the ligand coordinating as either a bidentate or a fluxional tridentate donor.[32,33] There are no published examples of heteroleptic 'half-sandwich' Rh(III) complexes with Tm coordinating in a κ^3-[*S,S,S*] mode.

Since our charge-neutral zwitterionic (ZTm) ligands are unable to provide a B-H···M agostic bond, and may be considered neutral 6-electron donor analogues of arenes, mimicking the Tm/Cp relationship, it was of interest to study their reactivity towards ruthenium and rhodium precursors. In-keeping with the aim of exploiting the inherent helicity of Tm complexes for asymmetric catalysis, axially chiral complexes (*i.e.* with a κ^3-[*S,S,S*] ligand coordination mode) were required. Precatalysts were sought containing at least one labile ligand which could dissociate to allow attack of a catalytic substrate. Therefore, octahedral complexes of the form $[\{\kappa^3\text{-}[S,S,S]\text{-}(D)ZTm\}ML_nX_m]$ (M = Ru, Rh) were targeted.

5.2 Results and Discussion

5.2.1 Ruthenium(II) complexes

5.2.1.1 Unreactive Metal Precursors

Initially, a variety of commonly used ruthenium(II) precursors which were expected to yield heteroleptic complexes were screened for reactivity with the ligand (N-methylimidazolium)tris(methimazolyl)borate **5.3**. The complexes $RuClH(CO)(PPh_3)_3$, $RuH_2(PPh_3)_4$, $[RuCl_2(COD)]_n$ and $RuCl_2[MeCN]_4$ showed no reactivity with **5.3** even upon extended heating in a variety of solvents. Since most of these complexes contain only

monodentate ligands the fact that the tridentate **5.3** was unable to substitute even one or two of the labile donors was unexpected.

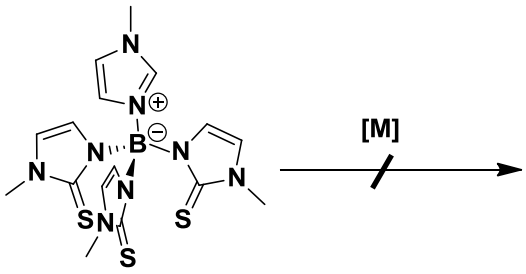

5.3

Scheme 5.5: Treatment of ligand **5.3** with [M]. ([M] = $RuClH(CO)(PPh_3)_3$, $RuH_2(PPh_3)_4$, $[RuCl_2(COD)]_n$, $RuCl_2[MeCN]_4$).

5.2.1.2 Reaction with $Ru(PPh_3)_3Cl_2$

$RuCl_2(PPh_3)_3$ contains a $16e^-$ ruthenium centre, stabilised by three bulky triphenylphosphine ligands, which was expected to dissociate one or two labile PPh_3 ligands and coordinate **5.3** in order to fill its coordination sphere.

1.1.1.1.1. Synthesis

(N-methylimidazolium)tris(methimazolyl)borate **5.3** (1 eq.) and $RuCl_2(PPh_3)_3$ (1 eq.) were stirred in dry methanol for 1 h at room temperature resulting in the formation of a deep blue solution. The solvent was reduced to half *in vacuo* yielding a dark precipitate. This precipitate was isolated by filtration and washed with methanol and diethyl ether giving a deep blue solid which was identified as complex **5.4a**. This complex could also be accessed more cleanly by reaction of 2 equivalents of **5.3** with $RuCl_2(PPh_3)_3$ under the same conditions, followed by salt-metathesis with excess ammonium hexafluorophosphate to precipitate **5.4b**, which exhibits analogous spectral properties to **5.4a**.

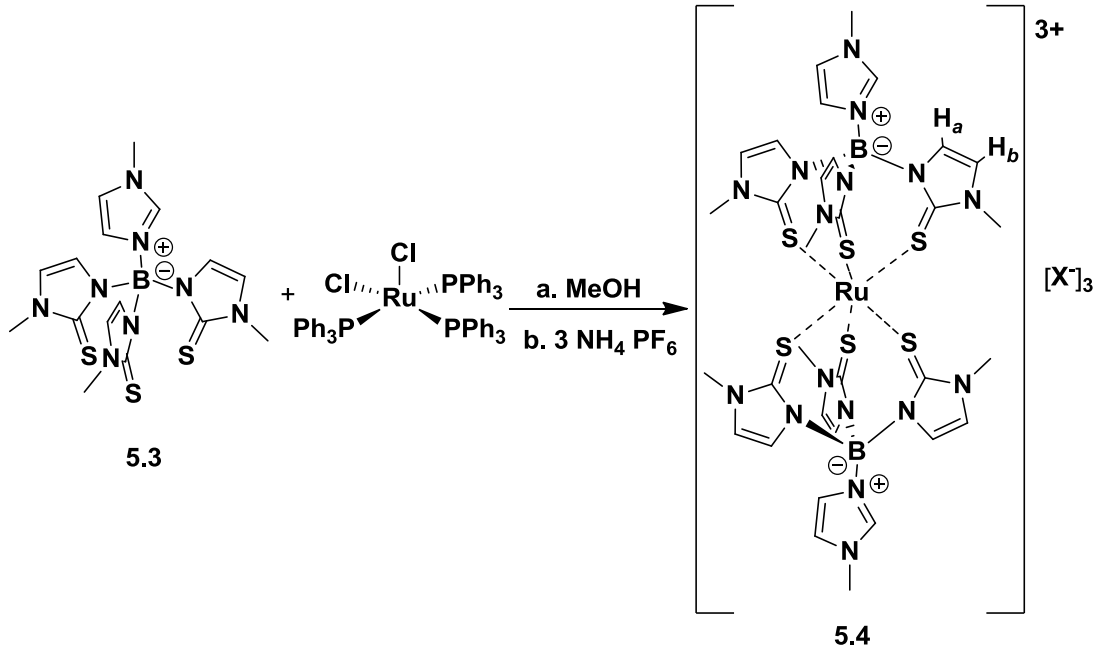

Scheme 5.6; Synthesis of bis{(N-methylimidazolium)tris(methimazolyl)borato}ruthenium dichloride (**5.4a** X = Cl; **5.4b** X = PF_6).

1.1.1.1.2. Characterisation

Mass spectrometry (ESI) of **5.4** displayed a molecular ion peak at *m*/*z* = 964 indicating the cation to be the homoleptic sandwich complex [{(N-methylimidazole)Tm}$_2$Ru]. An additional peak at *m*/*z* = 323 corresponds to [M^+/3] and suggested that this species exists as the 3^+ cation indicating oxidation of the Ru(II) centre during the synthesis. Whilst homoleptic sandwich complexes of Tm ligands have been synthesised with a variety of metals, there are no reports of the ruthenium analogue, and none with charge neutral ligands.[12]

The ^{1}H-NMR spectrum of **5.4** confirmed a κ^3-[*S*,*S*,*S*] ligand coordination mode with equivalent resonances for the methimazolyl aromatic protons (H_a/H_b), although these signals were shifted significantly to higher frequency (10.32 / 10.23 ppm). These resonances appear at *ca.* 6.65 ppm in the free ligand **5.3** and at 7.27 / 7.82ppm in the 'mixed-sandwich'

complex [{κ³-[*S,S,S*]-(N-MeImid)ZTm}Ru(II){*p*-cymene}] (**3.9**).[17] All other protons exhibit resonances in the expected regions based on other known complexes with the methimazolyl NCH_3 resonating at 3.44 ppm (3.49 ppm in **5.3** / 3.91 ppm in **3.9**). In contrast the ^{13}C-NMR spectrum shows the methimazolyl *C*H carbon atoms (120.2 / 119.4 ppm) within the expected shift region (*ca*. 105-125 ppm) although the resonances are shifted slightly to high frequency compared with **3.9** (114.3 / 106.2 ppm).[17] In this spectrum the NCH_3 carbon resonance appears at 86.9 ppm, which is dramatically shifted from the same resonance in **3.9** (30.4 ppm). The large paramagnetic shifts in this complex confirm the presence of a d^5 Ru(III) centre with one unpaired electron.

1.1.1.1.3. Electrochemistry

Chart 5.1: Cyclic Voltammogram of **5.4** (2.3 mM in DMF, Electrolyte: 0.3 M $[(Bu^t)_4N][BF_4]$) referenced to the ferrocene/ferrocinium couple (0 V).

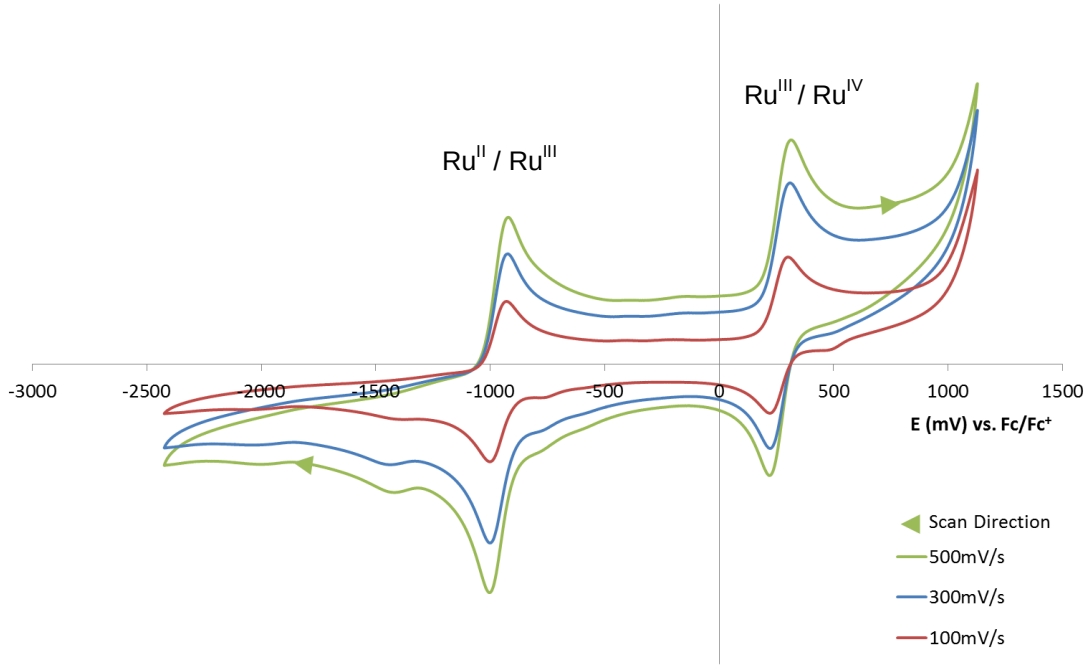

Electrochemical studies were carried out with the aim of rationalising the facile oxidation of the Ru(II) starting material to Ru(III) in this reaction. The cyclic voltammogram of **5.4** shows a single electron reversible reduction at -962 mV (*vs.* Fc/Fc^+) representing the Ru^{III}/Ru^{II} couple and a one electron reversible oxidation at +266 mV (*vs.* Fc/Fc^+) representing the Ru^{III}/Ru^{IV} couple. The large negative value of the reduction potential indicates that a strong reducing agent would be required to transfer an electron to the Ru(III) centre and demonstrates the strong electron donor properties of the ligand **5.3**. $[Tp_2Ru]$ has a reported Ru^{II}/Ru^{III} oxidation at -202 mV (*vs.* Fc/Fc^+) reflecting the weaker donor properties of a pyrazole nitrogen compared with the thiolate donors in **5.3**. These data correspond well with previous studies of the donor properties of ZTm, Tm and Tp in manganese tricarbonyl complexes using IR-spectroscopy which found Tm and ZTm to be stronger electron donors than Tp.[19] Chen recently reported the synthesis of a homoleptic Ru(III) complex with two tris(carbene)borate ligands which was

found to be more readily reduced (-630 mV) than **5.4** (-962 mV). This indicates that the thiolate donors in **5.4** are even stronger electron donors than N-heterocyclic carbene ligands.[34] Similarly, the lower oxidation potential of the Ru^{III}/Ru^{IV} couple in **5.4** (+266 mV) relative to Chen's complex (+600 mV) reflects the relative ease of oxidising a metal centre with strongly donating thiolate ligands rather than neutral carbene donors.

Therefore, oxidation from Ru(II) to Ru(III) in the synthesis of **5.4** likely occurs due to the presence of trace oxygen and is driven by the relatively high oxidation potential of the Ru(II) species. Upon carrying out this reaction under strict anaerobic conditions no reactivity was observed.

1.1.1.1.4. X-Ray Crystallography

The poor solubility of **5.4** lead to difficulty in the growth of X-ray quality crystals, therefore a more soluble analogue of the ligand was synthesised with N-*n*-butylimidazole, rather than N-methylimidazole, as the boron donor. Stirring of ligand **5.5** with $RuCl_2(PPh_3)_3$ in methanol for 1 h yielded a blue solution. Ammonium hexafluorophosphate was added, resulting in the precipitation of **5.6** as a dark blue solid.

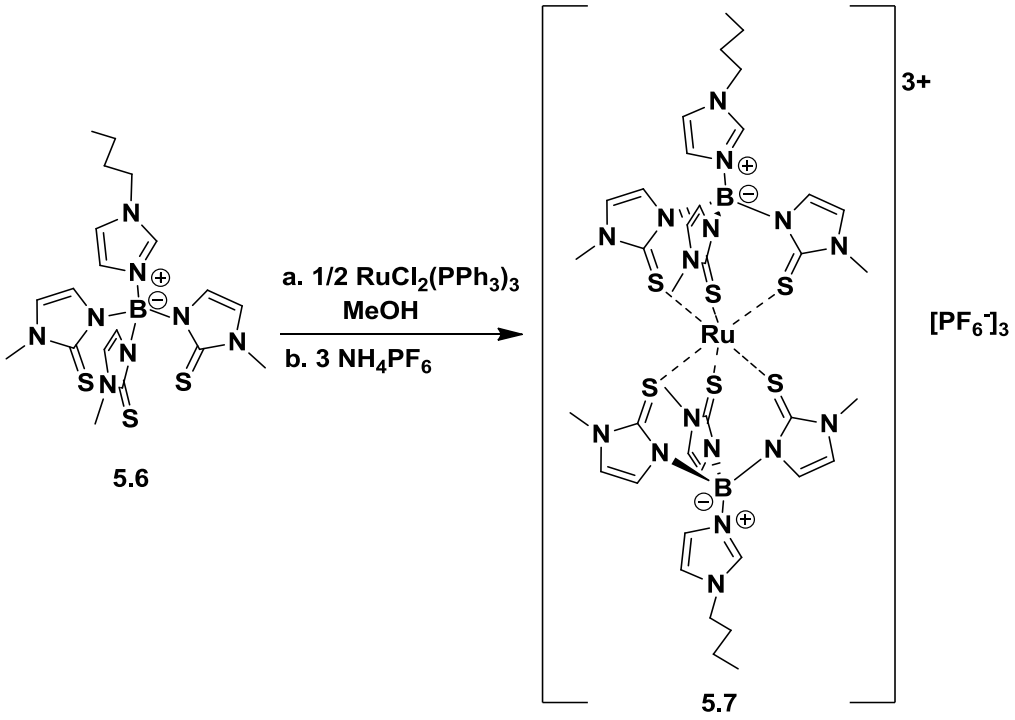

Scheme 5.7: Synthesis of the complex **5.6** from the soluble ligand **5.5**.

As expected, this complex showed very similar spectral properties to the less soluble analogue **5.4**. X-ray quality crystals were grown by slow diffusion of diethyl ether into a concentrated solution of **5.6** in acetonitrile, and the refined structure is shown in Figure 5.3. The average Ru-S bond length is shorter [avg. 2.402 Å] than that in the previously published Ru(II) mixed-sandwich complex [{κ^3-[*S,S,S*]-(N-MeImid)ZTm}Ru(II){*p*-cymene}] **3.9** [avg. 2.426 Å] indicative of a Ru(III) centre. The longest of these bonds, Ru-S5 [2.426(2) Å] and Ru-S7 [2.432(3) Å], lie along the z-axis while the shortest, Ru-S3 [2.380(2) Å] and Ru-S4 [2.377(3) Å], align with the x-axis. Since this system involves a d^5 metal centre, minor Jahn-Teller distortion may be anticipated. However, the bonds along the y-axis, Ru-S2 [2.397(2) Å] and Ru-S6 [2.399(3) Å], adopt an intermediate length between those aligning with the z- and x-axes; a feature which is not consistent with Jahn-Teller distortion. All other bonds in this structure are all similar to **3.9** within experimental error.

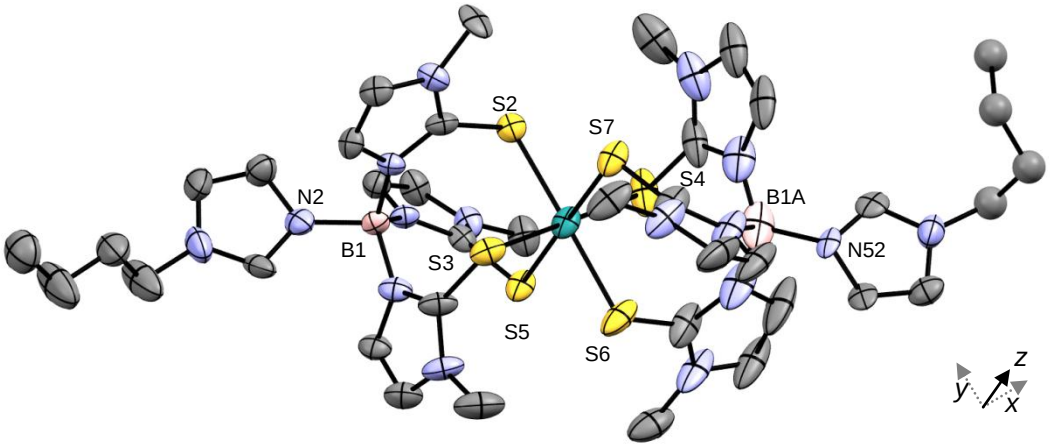

Figure 5.3: X-ray crystal structure of the cation of **5.6**. Hydrogen atoms, counterions and one acetonitrile molecule removed for clarity. Displacement elipsoids, where shown, have been drawn at 50% probablility . Selected bond lengths and angles are shown in Table 6.14.

1.1.1.1.5. Electronic Spectra

These homoleptic bis-ligand complexes also exhibit a strong blue colour both in solution and the solid phase. UV / visible spectroscopy of **5.4** showed an absorption at 580 nm with a molar absorption coefficient of *ca.* 3600 L mol^{-1} cm^{-1} as well as absorptions at 534 (ε = 2394 L mol^{-1} cm^{-1}), 454 nm (ε = 1305 L mol^{-1} cm^{-1}) and 673 nm (ε = 2277 L mol^{-1} cm^{-1}) (Chart 5.2).

Chart 5.2: UV/vis absorption spectrum of **5.4** at various concentrations.

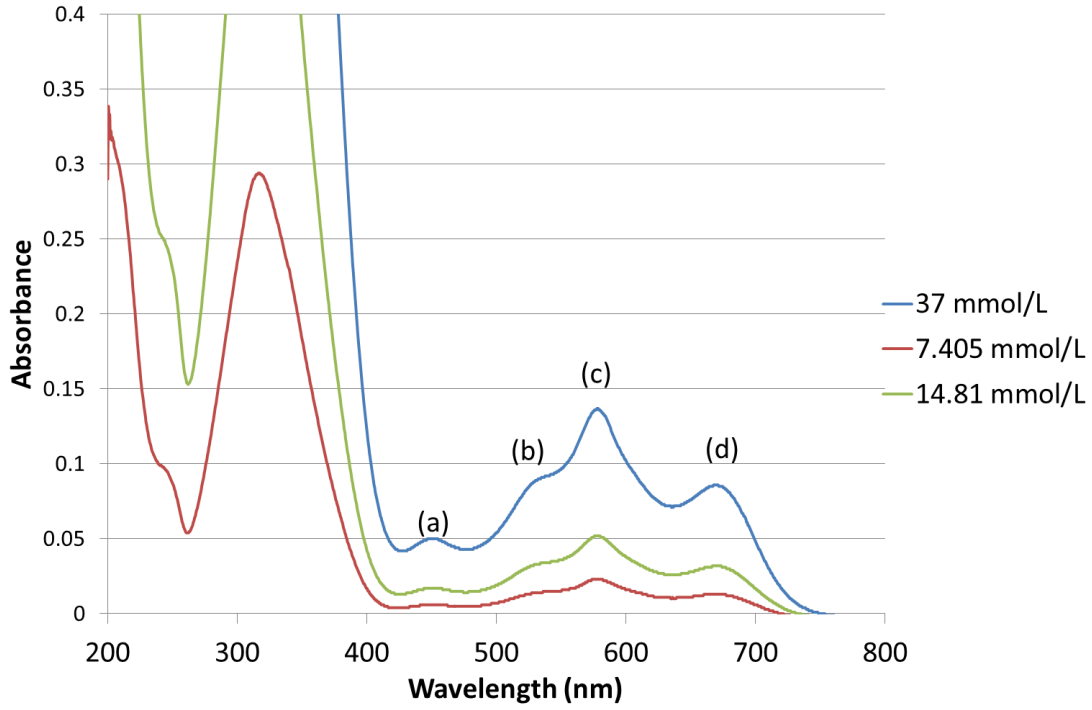

In order to gain a deeper insight into the origin of these absorptions, and thus the cause of the unusual blue colour of this complex, *ab initio* calculations were undertaken based on density functional theory (DFT) as approximated by the B3LYP functional and employing the 6-31G* basis set. These calculations showed the SOMO, HOMO and HOMO-1 to be part of a t_{2g}* anti-bonding set involving the sulfur p_z-orbitals and the ruthenium d_{xy}, d_{xz} and d_{yz} orbitals respectively (Figure 5.4). The LUMO was shown to be an anti-bonding orbital made up mostly of the ruthenium d_{z2} orbital whilst the LUMO+1 represents the d_{x2-y2} metal orbital. The orbitals below HOMO-1 are mostly ligand based and some key examples are shown in Figure 5.5.

These data make it possible to rationalise the unusual bond distortion seen in the X-ray crystal structure of **5.6** (Figure 5.3). The SOMO and HOMO (Figure 5.4) represent antibonding interactions along the y- and z-axis respectively. The additional electron density in the antibonding HOMO,

compared with the SOMO, results in an elongation of the S5–Ru [2.426(2) Å] and S7–Ru [2.432(3) Å] bonds along the z-axis compared with S2–Ru [2.397(2) Å] and S6–Ru [2.399(3) Å], which lie along the y-axis. Unlike the SOMO and HOMO, the HOMO-1 involves some bonding character between the metal and its sulfur ligands. Therefore the S3–Ru [2.380(2) Å] and S4–Ru [2.377(3) Å] bonds are the shortest in this complex.

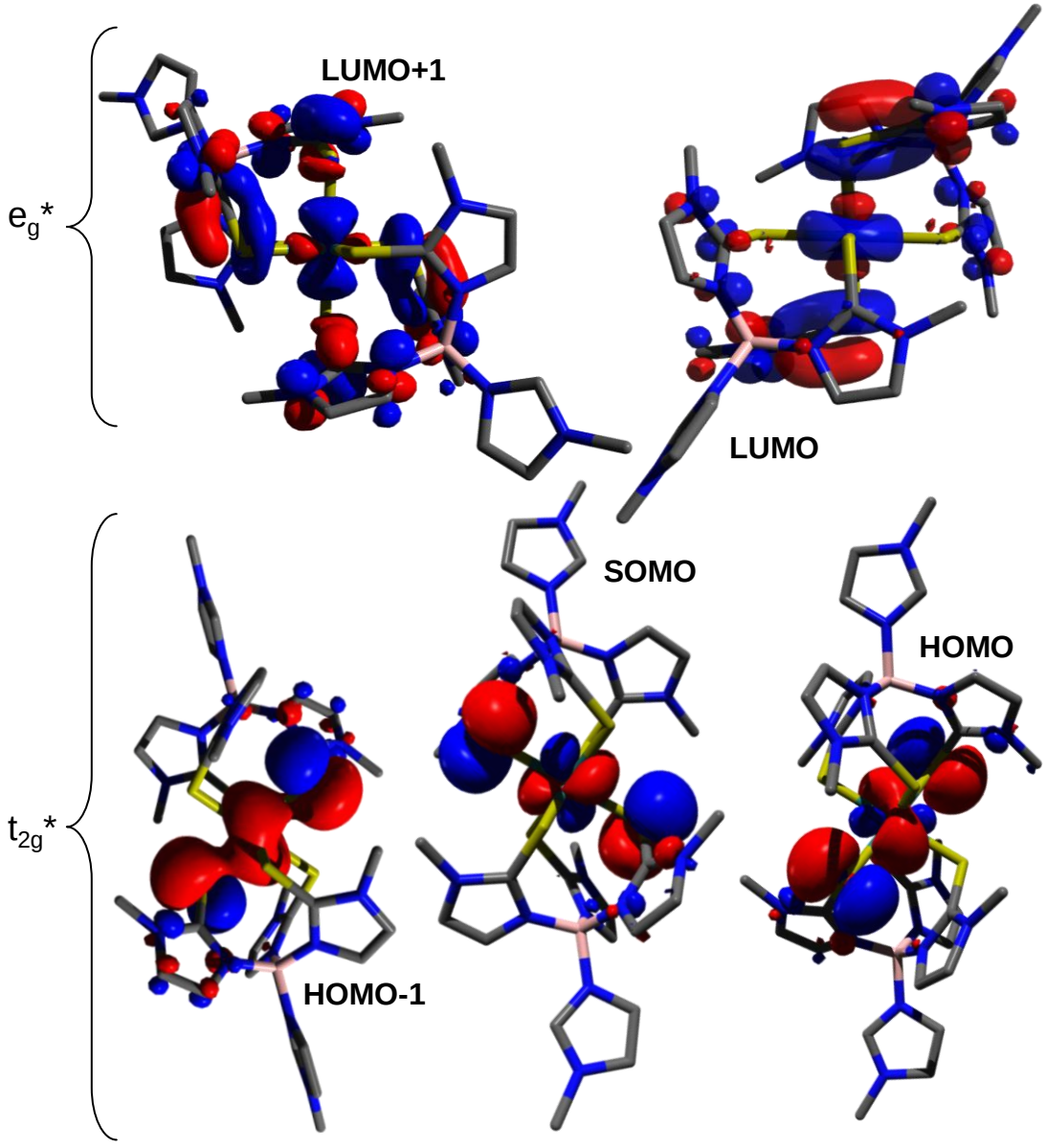

Figure 5.4: Frontier Molecular Orbitals calculated using DFT (B3LYP/6-31G*).

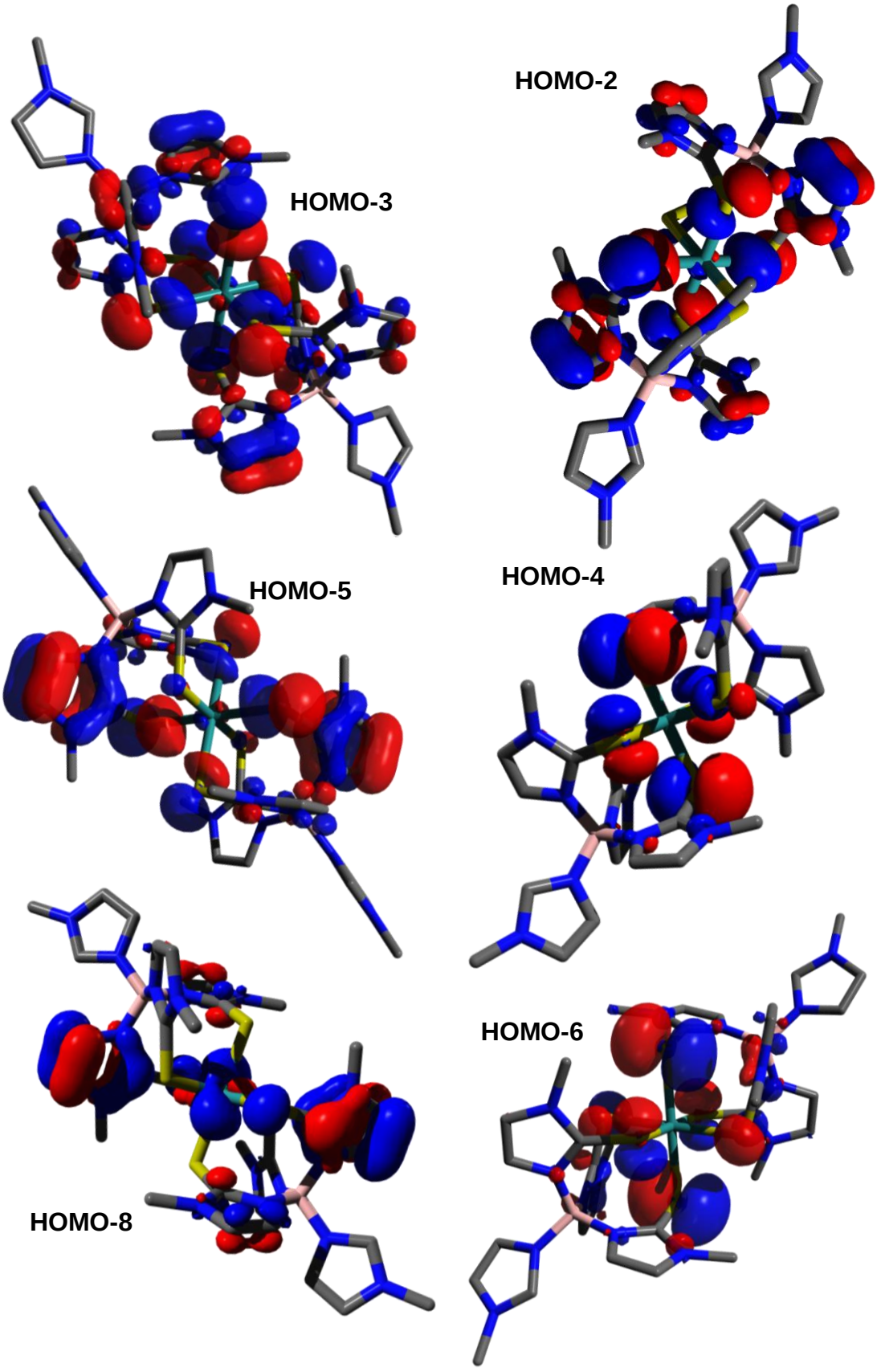

Figure 5.5: Occupied Molecular Orbitals calculated using DFT (B3LYP/6-31G*).

The molecular orbitals generated from these calculations show that the π-donor thiolate ligands mix with the t_{2g} set on ruthenium giving a high energy t_{2g}* set with one SOMO into which lower energy electrons may be

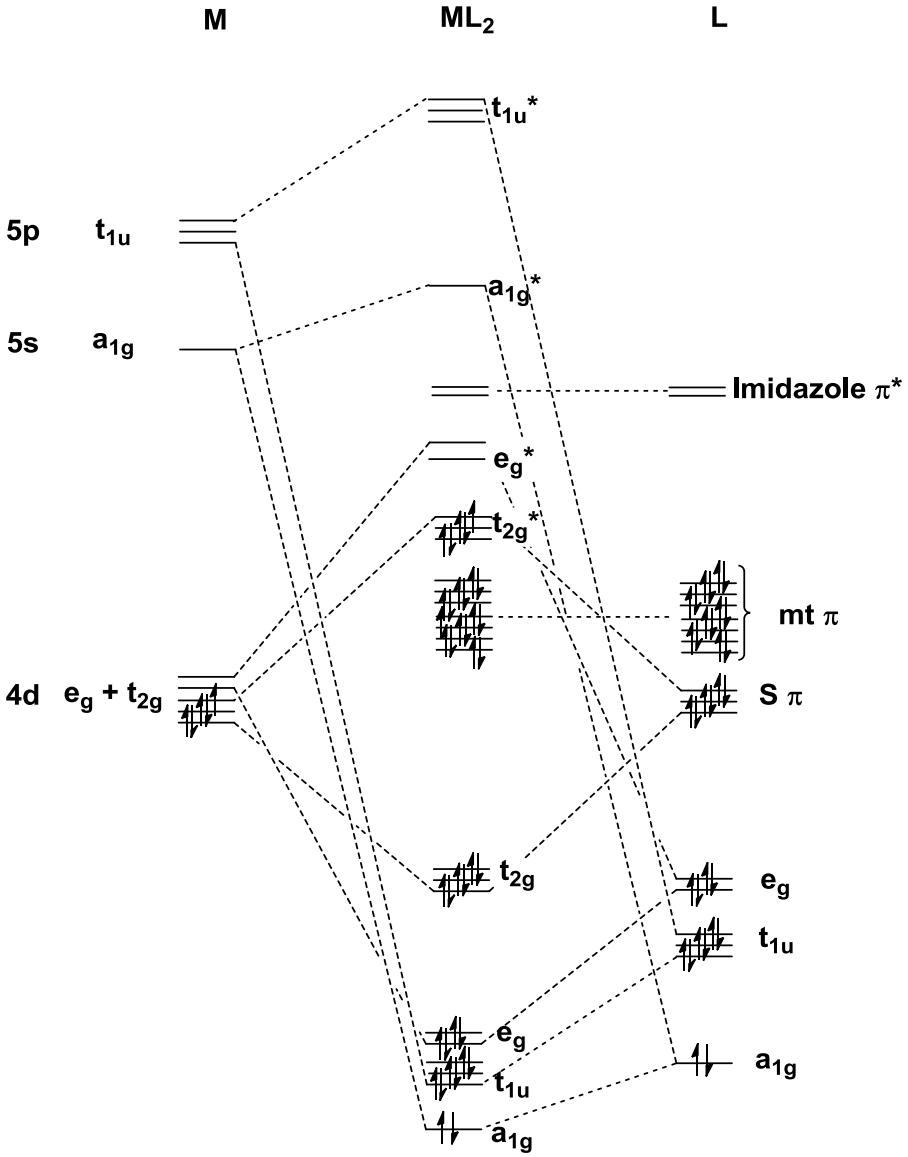

Figure 5.6: Simplified MO diagram for the interaction of **5.3** with Ru(III).

promoted (Figure 5.6).[vii] The presence of this SOMO means that **5.4** has a lower energy Δ_{oct} than if electrons were promoted to the LUMO.

Time dependant-DFT (TD-DFT) calculations were carried out in order to assign the main absorption bands (a-d) in the UV/vis spectrum (Chart 5.3). The low energy band (d) at 673 nm (ε = 2277 L mol^{-1} cm^{-1}) was assigned as the HOMO-3/4/5 – SOMO transition which can be classed as ligand-to-metal

Chart 5.3: Simulated and Experimental UV/vis spectrum based on TD-DFT calculations (B3LYP/6-31G*) along with a diagram showing the relative energies of the frontier molecular orbitals.

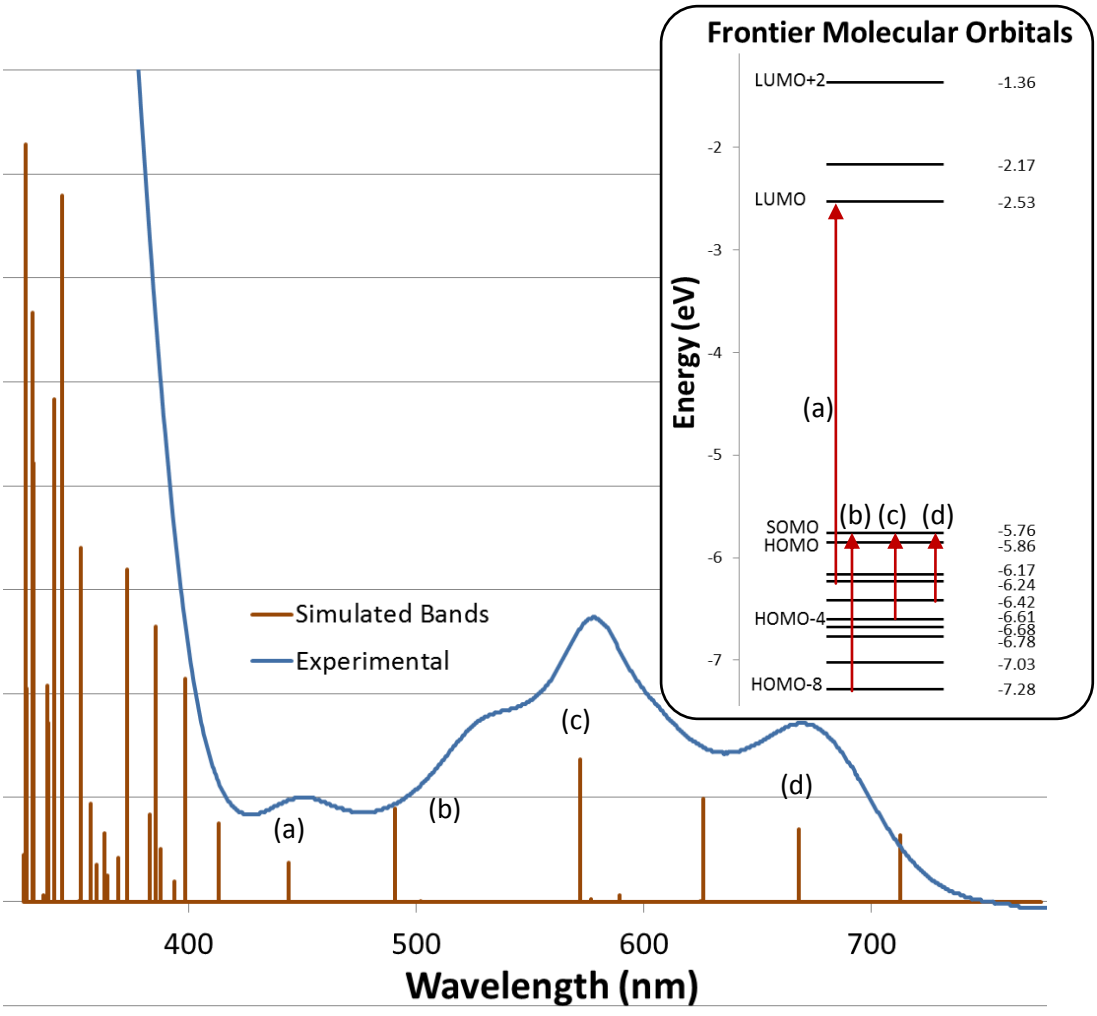

[vii] Whilst the Tm thiolate donor atoms have been commonly described as sp^3-hyrbidised in this work (Chapter Three) these calculations suggest the involvement of unhybridised p-orbitals in metal-ligand bonding. As discussed previously, at this level of complexity VSEPR theory is not an accurate model of the nature of bonding in these complexes however it remains useful to describe the thiolate donor atoms in Tm complexes as sp^3-hybridised as a simple representation of their geometry.

charge transfer (LMCT). The strongest band (c) also arises as a result of LMCT transitions, in this case, between the electrons of HOMO-5/6 to the SOMO hole. The high energy band (a) arises from the HOMO-2 – LUMO transition. Band (b) at 534 nm was not modelled as accurately as the others however a band at 490 nm appears to represent to this transition which corresponds to promotion from the HOMO-8 to the SOMO. These calculations therefore suggest that the unusual blue colour of **5.4** is a feature which arises as a result of the presence of a paramagnetic d^5 Ru(III) centre bound to six π-donor thiolate ligands and that neither the complexes $Tm_2Ru(II)$ or $Tp_2Ru(III)$ would be expected to exhibit these spectroscopic properties.

5.2.1.3 Bulky Ligands

Since the inclusion of steric bulk on the methimazolyl ligand arms was expected to prevent the formation of bis-ligand sandwich complexes a ligand with bulky tolyl substituents was designed. Reaction of three equivalents of N-(*p*-tolyl)-imidazol-2-thione with tris(dimethylamino)borane in the presence of N-*n*-butylimidazole gave the ligand (N-n-BuImid)ZTm^{Tol} (**5.7**). Mass spectrometry (ESI) showed a molecular ion peak at *m*/*z* = 702 indicating successful formation of (**5.7**. The ^{1}H-NMR spectrum of this ligand contains two singlets at 6.84 and 7.32 ppm corresponding to the aromatic methimazolyl C*H*'s.

Stirring of (**5.7** (1 eq.) with $RuCl_2(PPh_3)_3$ (1 eq.) in methanol for 72 h gave a turquoise-blue solution. Half of the solvent was removed *in vacuo* and addition of diethyl ether resulted in the precipitation of a dark aqua blue solid which was identified as **5.8a**. The clean synthesis of this complex could be achieved by reaction of 2 equivalents of (**5.7** with $RuCl_2(PPh_3)_3$ under the

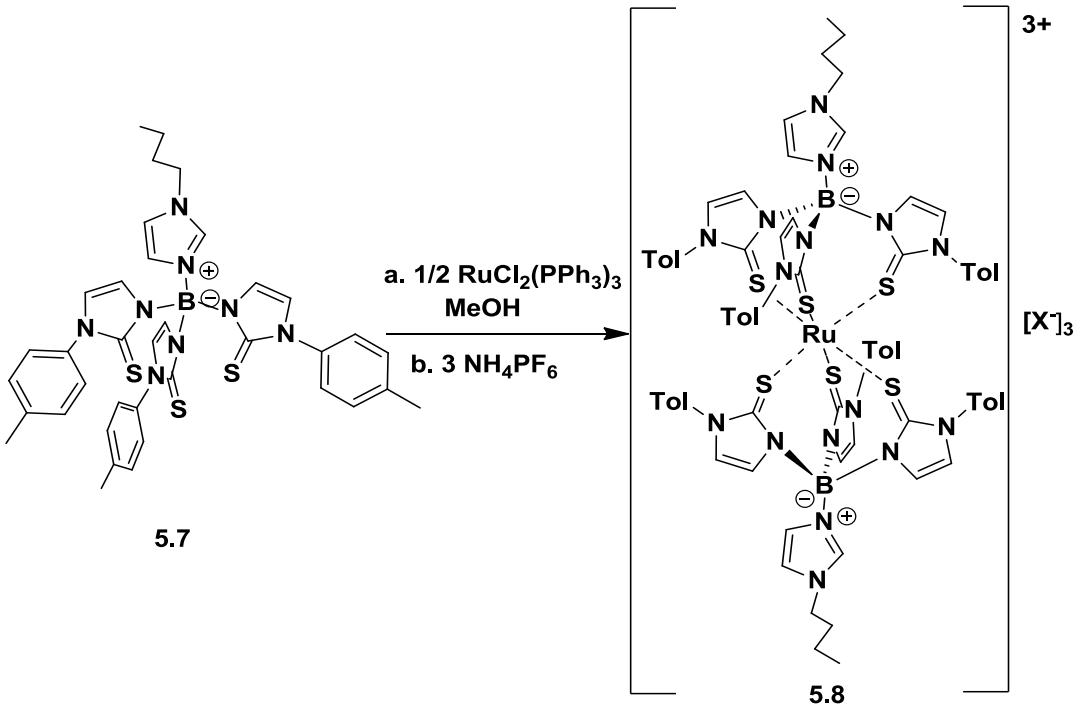

Scheme 5.8: Synthesis of the sandwich complex **5.8a** (X = Cl) and **5.8b** (X = PF_6) from ligand (5.7.

same conditions followed by salt metathesis with excess ammonium hexafluorophosphate yielding **5.8b**.

^{1}H-NMR spectroscopy of this complex shows that, as with **5.1** and **5.2,** the methimazolyl CH protons appear shifted to higher frequency (10.42 / 9.39 ppm) suggesting the formation of a paramagnetic Ru(III) sandwich complex. Mass spectroscopy (ESI) showed a molecular ion peak at *m*/*z* = 502 confirming the formulation of complex **5.8** as shown in Scheme 5.8.

X-ray quality crystals were grown by slow diffusion of diethyl ether into a concentrated solution of the ligand in acetonitrile. The structure of **5.8** confirms the formation of a bis-ligand species with the tolyl substituents on the ligand arms interlinking around the metal centre. Due to the steric crowding of the bulk tolyl groups the structure is fairly difficult to view in 2D. Therefore, a number of different views are shown in Figure 5.7 and Figure 5.8.

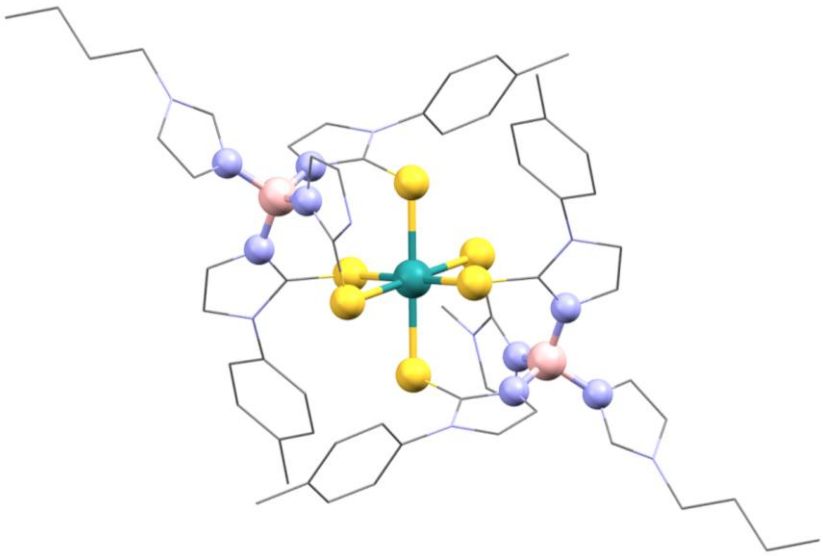

Figure 5.7: Ball and Stick plot of the X-ray crystal structure of the cation in **5.8**. Two tolyl substitutents have been removed for clarity along with the hydrogens and three [PF_6] counterions. Selected bond lengths and angles are shown in Table 6.15.

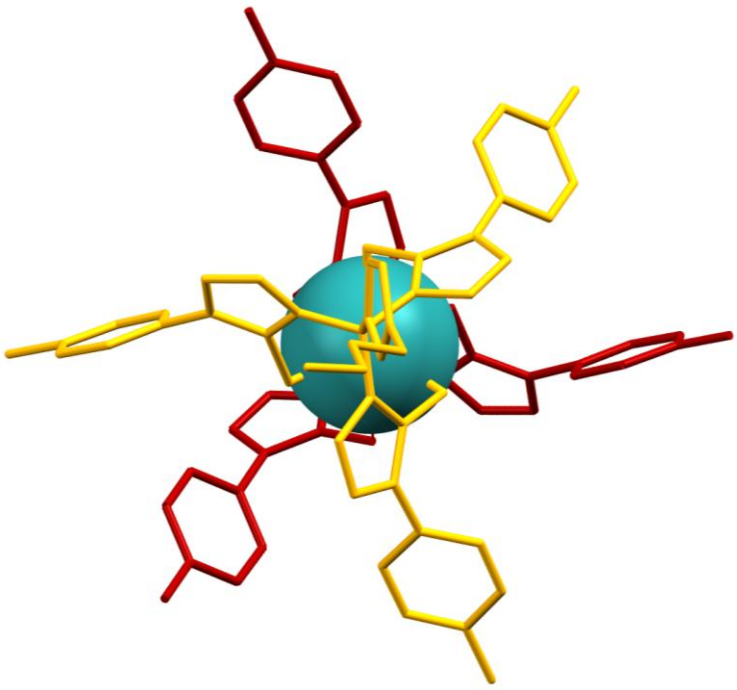

Figure 5.8: X-ray crystal structure of the cation of **5.8** showing the two ligand moieties with interlocking tolyl substituents. Hydrogens and counterions removed for clarity. Selected bond lengths and angles are shown in Table 6.15

From these results it appears a significant amount of steric bulk would be required prevent the formation of homoleptic sandwich complexes and encourage the formation of a heteroleptic 'half-sandwich' complex. Whilst tolyl groups are bulky in two dimensions, their planarity allows them to adopt a conformation in which their steric bulk is minimised. In contrast *tert*-butyl groups have steric bulk in three dimensions which was expected to prevent the formation of an interlocked bis-ligand complex.

N-*tert*-butylimidazole-2-thione was prepared by a published route and reacted with tris(dimethylamino)borane.[35] In this case, the *tert*-butyl groups were expected to solubilise any complexes therefore N-methylimidazole rather than N-*n*-butylimidazole was chosen as the boron donor to give the new ligand (N-MeImid)ZTm$^{t\text{Bu}}$ (**5.9)**. The effect of the additional steric bulk was evident in the ^{1}H-NMR spectrum of the free ligand where the protons in the ligand arms now appear inequivalent at room temperature. The aromatic methimazolyl CH protons appear as two sets of resonances in a ratio of 2:1 indicating that only two of the ligand arms are equivalent. The bulky *tert*-butyl groups obviously cause the ligand to adopt a different conformation to the pseudo-C_3-symmetric structure previously seen, although it is difficult to rationalise why this is the case as the *tert*-butyl groups are expected to be pointing away from the rest of the molecule.

Ligand **5.9** was stirred with $RuCl_2(PPh_3)_3$ in methanol for 5 days. The ^{1}H-NMR spectrum of a sample of the reaction mixture taken at this time showed no evidence for the formation of the homoleptic bis-ligand species although ligand degradation was noted. Therefore, whilst the additional steric bulk prevents the formation of the bis-ligand species it appears that the formation of the targeted hetereoleptic 'half-sandwich' species [{κ^3-[*S,S,S*]-

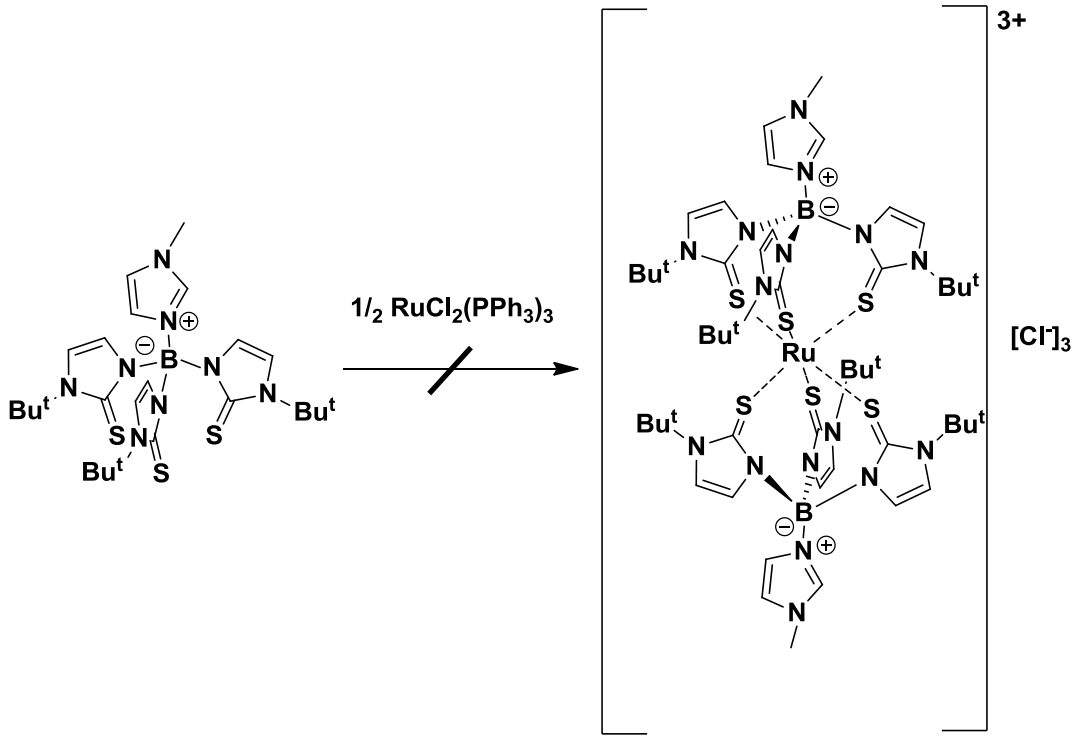

Scheme 5.9: Attempted synthesis of [{(N-MeImid)ZTm$^{Bu^t}$}$_2$Ru].

(N-MeImid)ZTm$^{Bu^t}$}RuCl$_2$(PPh$_3$)] is not favoured, possibly as a result of the steric bulk of the triphenylphosphine ligand.

5.2.1.4 Reactivity with Ruthenium (III) chloride

Since triphenylphosphine ligands appear to be too bulky to coordinate alongside a ZTm ligand, alternative ruthenium starting materials were investigated in order to access heteroleptic 'half-sandwich' complexes.

Displacement of the water ligands in ruthenium(III)chloride hydrate represents the most direct synthetic route to a complex of the form [{κ^3-[*S,S,S*]-(N-MeImid)ZTm}RuCl$_3$]. Thus, **5.3** was added to a suspension of ruthenium(III)chloride hydrate in methanol. After stirring the resulting dark brown suspension for 4 h, ^{1}H-NMR spectroscopy indicated the presence of two products in the reaction mixture.

The resonances of the minor product corresponded to those for the bis-ligand complex **5.4a** as a by-product. However, the spectrum of the major product (**5.10**) contained two sets of resonances corresponding to the methimazolyl CH protons in the ratio 2:1 indicating a κ^2-[*S,S*] coordination mode. Similarly, the methimazole NCH_3 protons appear as two singlets at 3.92 (6H) and 3.87 (3H). Therefore, the ruthenium metal centre is coordinated by three chloride ligands as well as two ZTm ligand arms. The sixth coordination site appears to be filled by a solvent molecule with a resonance at 3.43 ppm integrating for 3H. Mass spectrometry (ESI) showed a peak at m/z = 639 corresponding to $[M]^+$.

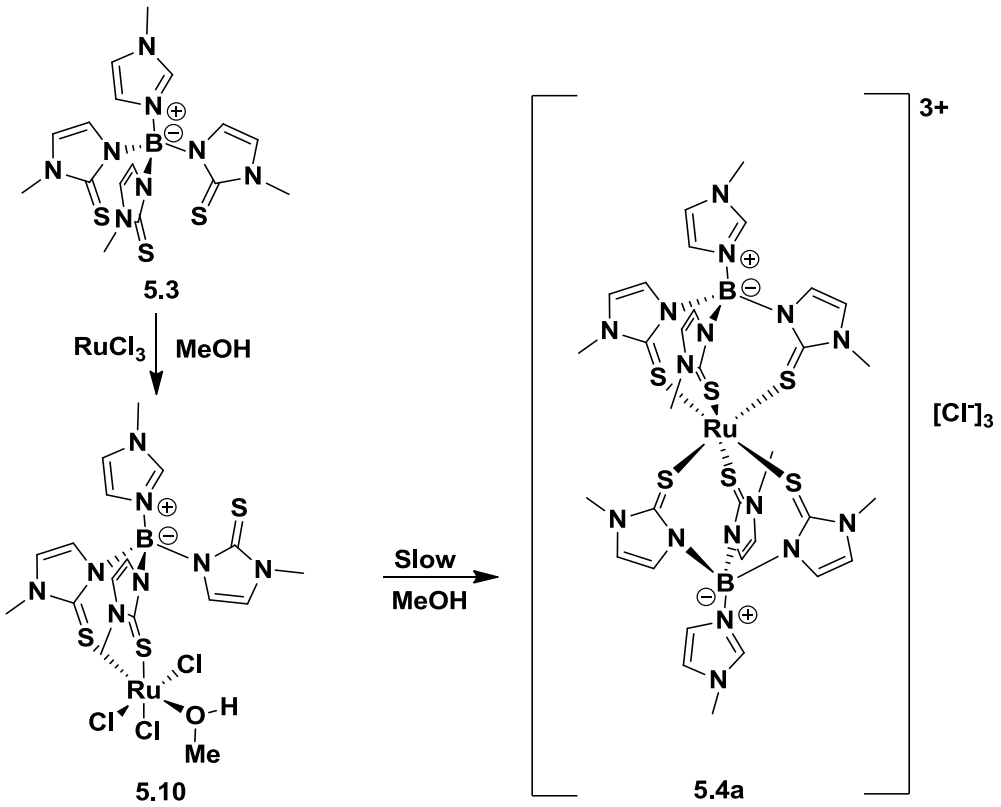

Scheme 5.10: Synthesis of [{κ^2-[*S,S*]-(N-MeImid)ZTm}$RuCl_3$(MeOH)] **5.10** and its conversion to **5.4** upon dissolution.

Unfortunately, X-ray quality crystals of this complex could not be grown despite multiple attempts using a variety of methods. It was noted that **5.10** was found to be very poorly soluble in organic solvents meaning that the choice of crystallisation medium was limited. In addition, the sandwich complex **5.4** formed slowly from **5.10** upon standing in solution at room temperature. Presumably, the mixture of compounds arising from this reaction hampered crystal growth.

Bidentate coordination (κ^2) of a ZTm ligand is unexpected, particularly in a complex containing a weakly bound methanol ligand, although it has been observed previously with anionic Tm.[32,36,37] The formation of **5.4** over time may suggest that attack at the metal centre of a second molecule of **5.3** is favoured over attack of the third ligand arm. However, the bis-ligand species **5.4** demonstrates that tridentate coordination is possible with minimal steric interaction between the ligands. In the absence of significant steric hindrance it must be concluded that the formation of [{κ^3-[*S,S,S*]-(N-methylimidazole)ZTmRuCl$_3$] is disfavoured for electronic reasons.

5.2.1.5 Reactivity with $RuCl_2[DMSO]_4$

Tetrakis(dimethylsulphoxido)ruthenium(II)chloride was stirred with **5.3** in methanol. The yellow suspension quickly darkened and after *ca.* 2 h a grey precipitate could be isolated upon workup. ^{1}H-NMR spectroscopy showed three sets of resonances relating to the methimazolyl CH protons in the region 6.39-7.50 ppm and three singlets (3.99, 3.87 and 3.76 ppm,) representing the methimazolyl NCH$_3$ protons. This indicates the presence of three inequivalent ligand arms. In addition, four singlets were present (3.62, 3.56, 3.26 and 2.93 ppm,) signifying the presence of two molecules of coordinated dimethylsulfoxide. The structure was therefore assigned as *cis*-

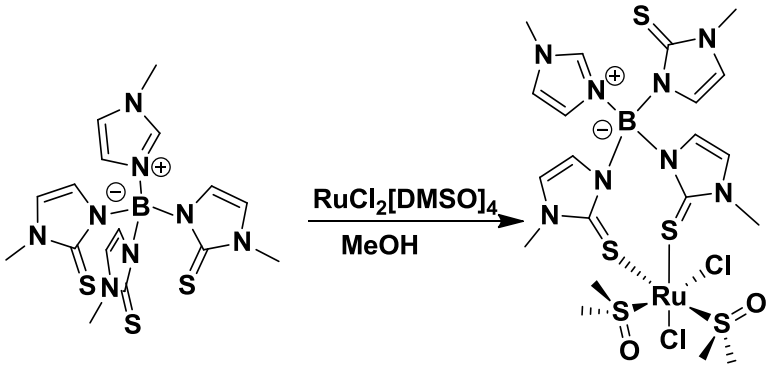

5.3 **5.11**

Scheme 5.11: Synthesis of *cis*-κ^2-[*S,S*]-(N-MeImid)ZTmRuCl$_2$[DMSO] (**5.11**)

κ^2-[*S,S*]-(N-MeImid)ZTmRuCl$_2$[DMSO] (**5.11**). In this structure the two coordinated arms are inequivalent due to the presence of different *trans*-substituents on the ruthenium, in contrast to the *trans* isomer where the ligand arms would be expected to be symmetry-equivalent by NMR spectroscopy. The dimethylsulfoxide ligands are also symmetry inequivalent in the *cis*-isomer but would be equivalent in the *trans*-isomer.

From these studies it appears that homoleptic sandwich complexes of the type [{ZTm}$_2$Ru^{III}] are highly stable and act as a 'thermodynamic sink' in many of these reactions. When bis-ligand species are inaccessible ZTm ligands may adopt κ^2-[*S,S*] coordination preferentially over κ^3-[*S,S,S*]. This also provides an explanation for the lack of reactivity with the metal precursors discussed in Section 5.2.1. For example, the complex [κ^2-[*S,S*]-**5.3**}RuHCl(CO)] is a 16e$^-$ species, however, addition of a triphenylphosphine ligand to this complex would be sterically unfavourable. As we have seen the formation of [κ^3-[*S,S,S*]-**5.3**}RuHCl(CO)] appears to be electronically disfavoured. The result of these opposing influences is that the metal precursor [RuHCl(CO)(PPh$_3$)$_3$] is unreactive towards **5.3**.

5.2.2 Rhodium (III) complexes

Rhodium complexes have also been used widely in asymmetric transfer hydrogenation [1,3,38-40] In light of the difficulties accessing heteroleptic 'half-sandwich' complexes of Ru(II), and noting that Rh(III) is isoelectronic with Ru(II), the reactivity of the ZTm ligand with Rh(III) was investigated.

(*N,N*-dimethylaminopyridinium)tris(methimazolyl)borate **5.12** was stirred in methanol with $RhCl_3 \cdot xH_2O$ for *ca.* 1 h. Mass spectroscopy (ESI) after this time showed a molecular ion peak at *m/z* = 349 corresponding to $[M^+/3]$, indicating the presence of the rhodium(III) analogue of the bis-ligand complex **5.13a**. Therefore, ammonium hexafluorophosphate was added to the reaction mixture and the orange precipitate which formed was isolated by filtration. (**5.13b**)

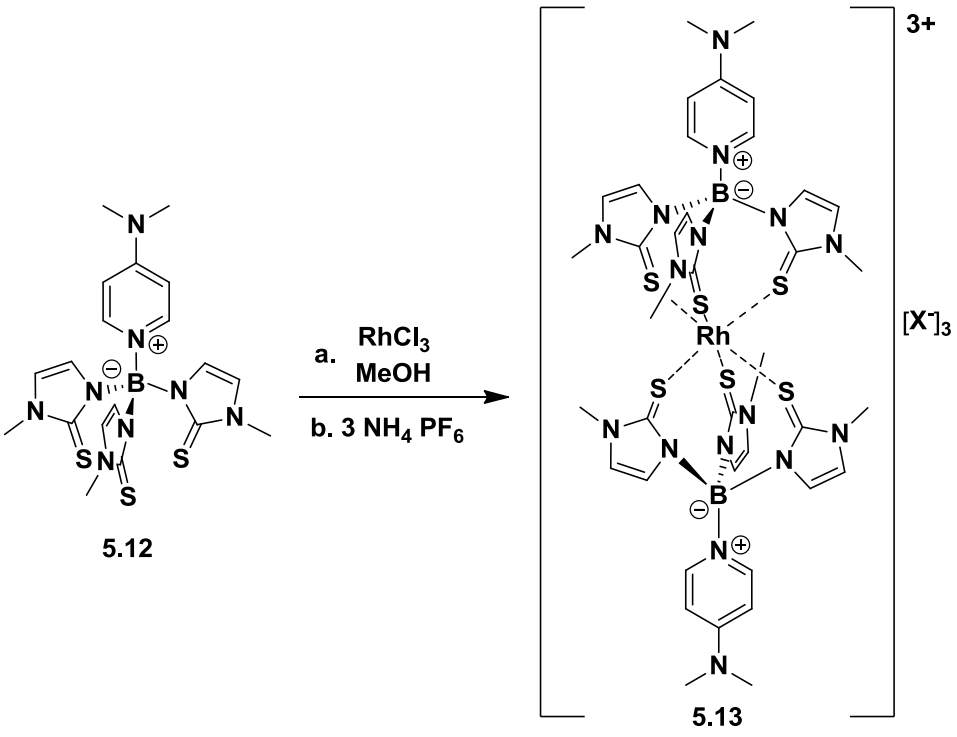

5.12 **5.13**

Scheme 5.12: Synthesis of the homoleptic sandwich complexes **5.13a** (X=Cl) and **5.13b** (X = PF_6).

^{1}H-NMR spectroscopy showed one set of resonances for the methimazolyl ligand arms (7.64 / 7.05 ppm) indicating κ^3-[*S,S,S*] coordination. These signals are shifted to lower frequency relative to the analogous Ru(III) complex **5.3** and well within the expected shift region (*ca.* 6-8 ppm) for complexes of diamagnetic metals. In addition, the methimazole NCH_3 protons appear at 3.73 ppm. In the ^{13}C-NMR spectrum the aromatic CH carbons appear at 122.7 and 123.6 ppm while the NCH_3 carbons appear at 36.7 ppm.

X-ray quality crystals of **5.13b** were grown by slow diffusion of diethyl ether into a concentrated solution of the complex in acetonitrile. The

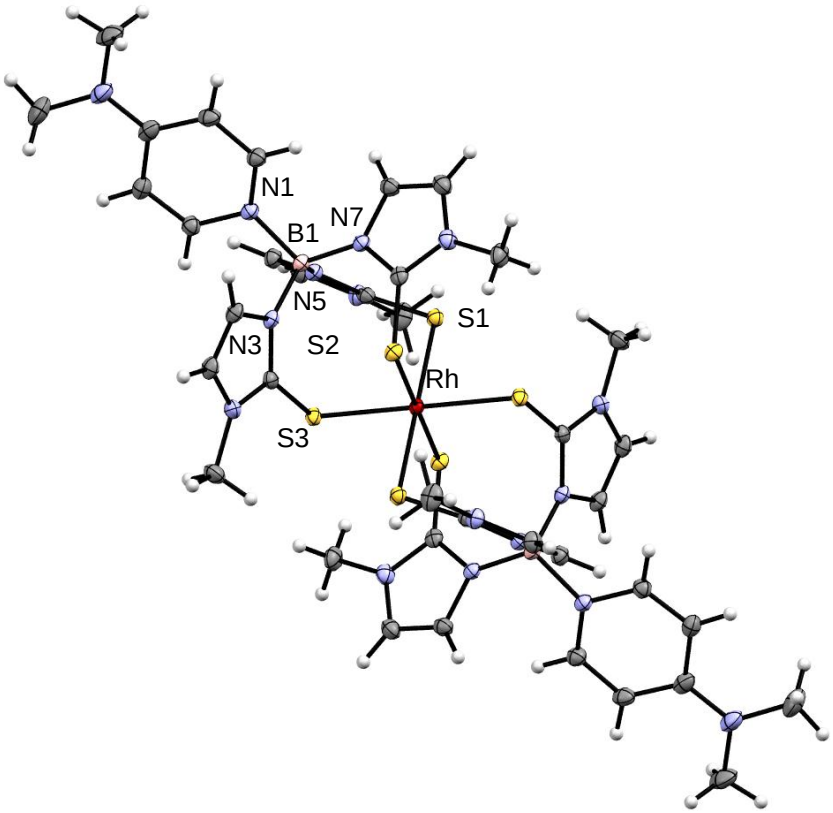

Figure 5.9: X-ray crystal structure of the cation of **5.13**. Hydrogens and counterions removed for clarity. Displacement elipsoids have been drawn at 50% probablility .Selected bond lengths and angles are shown in Table 6.16.

X-ray structure confirms the formulation of this complex as $[\{(DMAP)L\}_2Rh][PF_6]_3$. As with **5.6** there are three sets of dissimilar Ru-S bonds, Rh-S1 [2.3746(4) Å], Rh-S2 [2.3862(4) Å] and Rh-S3 [2.4021(4) Å], along the x-, y- and z- axes respectively,[viii] suggesting a similar electronic structure in both complexes, despite the fact that **5.13** contains no unpaired electrons. The average Rh-S bond length [2.3876 Å] in **5.13** is slightly longer than in the previously reported complex $\{FTm\}_2Rh$ [avg. 2.3828 Å]. Whilst this may indicate weaker binding of the charge-neutral, ligand M-S bond lengths in complexes of Tm and ZTm have been shown to vary widely even between two independent molecules in the same unit cell.[15,41] Previous studies have shown the donor properties of zwitterionic charge-neutral, Tm ligands to correspond closely to those of the anionic Tm ligand.[19]

5.2.3 Rhodium (I) complexes of Tm

As discussed in Chapter One, complexes of tripod ligands coordinated to square-planar metal centres have previously been shown to be highly active enantioselective catalysts in a number of asymmetric transformations. Therefore, the synthesis of Rh(I) complexes of substituted tris(methimazolyl)borate ligands was also investigated. In the future, oxidation of any Rh(I) complexes may yield octahedral heteroleptic Rh(III) 'half-sandwich' complexes where the ligand adopts κ^3-[*S,S,S*] coordination.

Based on the monocationic charge of the rhodium centre, the reaction between $[RhCl(COD)]_2$ and the anionic ligand $[H_2NMe_2][(NC)Tm]$ (**2.19)** was expected to yield a charge-neutral complex and the formation of the bis-ligand species $[(NC)Tm_2Rh]^-$ was expected to be disfavoured. Dissolution of **2.19** (2 eq.) with $[RhCl(COD)]_2$ (1 eq.) in CH_2Cl_2 gave a dark red solution.

[viii] The presence of an inversion centre in this structure means that both Ru-S bonds along a given axis are crystallographically equivalent.

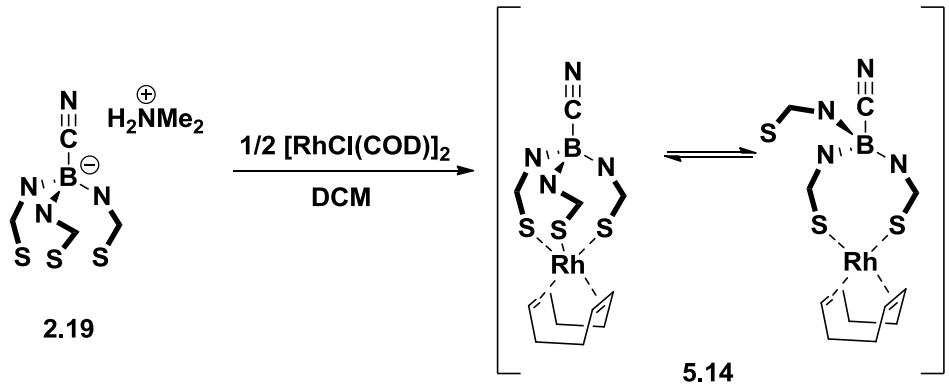

Scheme 5.13: Synthesis of 5.14 which exists as the fluxional κ^2/κ^3 complex in solution.

After stirring for 1 h, the solvent was removed from the reaction mixture and the residue extracted into toluene. The toluene was then reduced in volume by half *in vacuo* and addition of hexane gave a dark red precipitate which was isolated by filtration giving **5.14** as an orange solid (72%).

No resonances relating to the ligand cation $[H_2NMe_2]^+$ were present in the ^{1}H-NMR spectrum. Methimazolyl CH resonances at 6.96 and 6.86 ppm indicate the presence of metal-bound ligand, whilst three resonances in the aliphatic region (4.25, 2.30 and 1.82 ppm) confirm the presence of bound COD. Mass spectrometry (EI) displayed a molecular ion peak at m/z = 587 confirming the formulation of this complex as [{(NC)Tm}Rh(COD)] **5.14.** Despite the fact that the methimazolyl protons appear equivalent by NMR spectroscopy, there is ambiguity in the coordination mode of the ligand in this complex. TmRh(COD) was previously reported to exhibit κ^3-[*H,S,S*] coordination in the solid state. Contrastingly, in TpRh(COD) the metal adopts a distorted trigonal bipyramidal geometry with the ligand coordinated in a κ^3-[*N,N,N*] mode.[32] However, it was shown that a fine balance of sterics was at play with the complex Tp*Rh(COD) adopting κ^2-[*N,N*] coordination.[33] Tripod ligands are known to undergo fast exchange

between bound and unbound ligand arms in complexes of non-deltahedral metal centres in solution.[32,42] The equivalence of the methimazolyl protons in the ^{1}H-NMR spectrum of this complex suggests that in solution, at room temperature, exchange of the bound and unbound ligand arms is facile. However, X-ray quality crystals would be required to determine the solid state coordination mode of this ligand.

5.2.4 Palladium (II) complexes

Palladium complexes are also exploited in variety of asymmetric catalytic processes, some of which were the subject of the 2010 Nobel Prize in Chemistry.[43] Since Pd(II) is isoelectronic with Rh(I) it was of interest to investigate the reactivity of substituted tris(methimazolyl)borate ligands with palladium precursors.

Reaction between (NC)Tm (**2.19**)and $PdCl_2(MeCN)_2$ in CH_2Cl_2 yielded a dark red solution quickly upon dissolution of the reactants. After 1 h, a red precipitate formed which was filtered and washed with CH_2Cl_2 and diethyl ether yielding **5.15** as a red powder. ^{1}H-NMR spectroscopy of **5.15** showed only two resonances at 6.97 (6H) and 3.67 (9H) ppm; the former resonance represents both the methimazolyl CH protons while the latter denote the NCH_3 protons. Similarly to **5.14**, the equivalence the six ligand arms in this complex suggests that exchange of the ligand arms in this complex is fast on the NMR timescale.

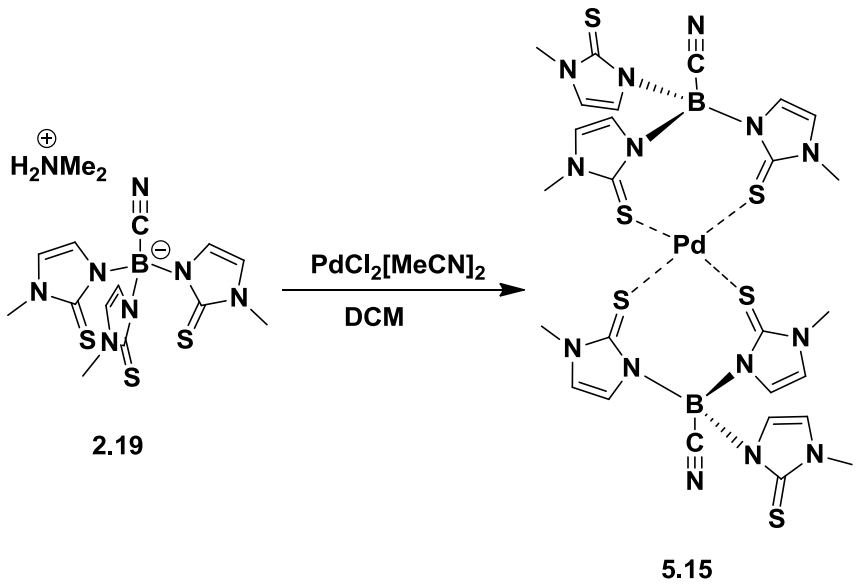

2.19 **5.15**

Scheme 5.14: Synthesis of the homoleptic bis-ligand species [{κ$_2$-[*S,S*]-(NC)Tm}2Pd] **5.15**.

X-ray quality crystals of **5.15** were grown serendipitously from an NMR sample in $CDCl_3$. The refined structure confirms the geometry around the metal centre to be square-planar with each ligand coordinated in a bidentate [S,S] fashion (Figure 5.10). The third ligand arm is twisted away from the metal centre so that the methimazolyl protons (H_a) are adjacent to the metal centre. The resulting Pd-H11 distance [3.051 Å] leaves a question as to the presence of a M···H-C interaction in this system (Figure 5.11).

There is still debate within the academic community as to the nature of M···H-C bonding opposed to M···H-N which is clearly defined as hydrogen bonding.[44] M···H-C bonding has been variously described as 2c-3e$^-$ (agostic) bonds and as 3c-4e$^-$ (hydrogen) bonds and are commonly referred to as preagostic or pregostic interactions. Others have described these interactions as the result of repulsion between the electron pair in the metal d_{z2} orbital and those of the C-H bond.[45,46] This argument takes into account the fact that many complexes which seemingly exhibit this interaction contain constrained ligand systems. Crabtree has investigated M···H-C bonds for a

variety of d^8 Pd(II) complexes.[47] In the reported structures the M-H distance was found to range between 2.3-2.93 Å, shorter than in **5.15**. In addition the M-H-C angle in **5.15** [98.2°] is much smaller than those reported which range between 140-171°.

Careful examination of the structure of **5.15** shows that rotation of the free methimazole ring about the B-N5 bond, reducing the C13-B-N5-C9 torsion angle [<55.4°] would move H11 closer to the palladium centre. This may be unfavourable as the C11-Pd distance [3.314 Å] is less than the sum of the Van der Waals radii of the two atoms [3.33 Å]. However the similar complex [{(AcO)Tm$^{Bu^t}$}$_2$Pd] contains an even shorter C-Pd distance [3.150 Å] due to its smaller O-B-N-C torsion angle [50.0°].[48] Increasing the C13-B-N5-C9 torsion angle [>55.4°] in order to move this proton further from the metal would involve unfavourable steric repulsion between the aromatic ring and

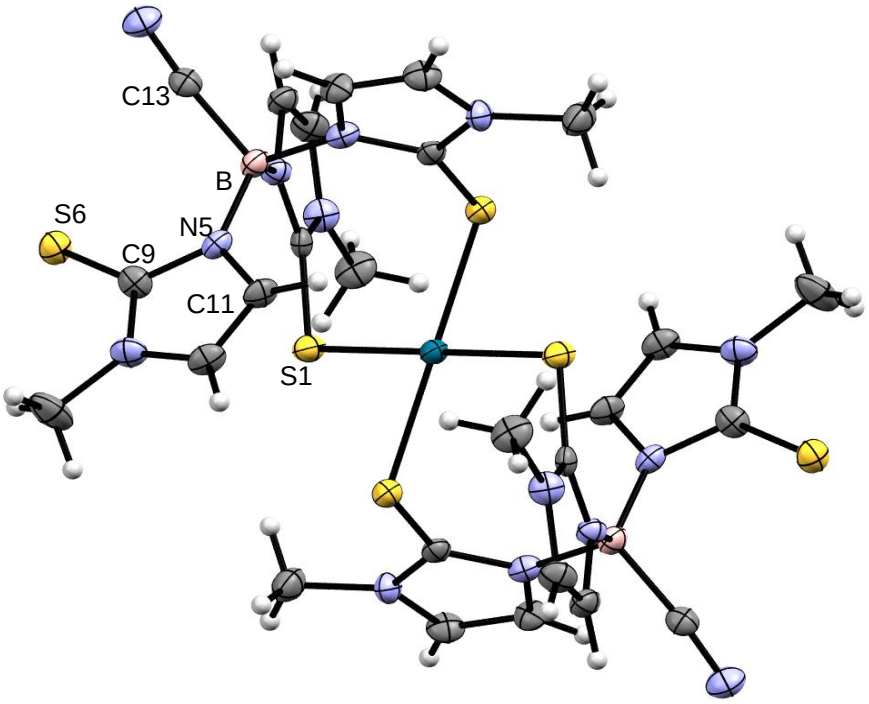

Figure 5.10: X-ray crystal structure of **5.15**. Displacement elipsoids have been drawn at 50% probablility .Selected bond lengths and angles are shown in Table 6.17.

S1. In fact the N5-S1 distance [3.174 Å] is also lower than the sum of the Van der Waals radii of the two atoms [3.35 Å] implying that the torsion of this ring may be close to the maximum in this structure. Therefore, the constraints of the tripod ligand system require that H11 occupies the position closest to the occupied d_{z^2} orbital of the Pd in order to minimise steric repulsion. However, this alone does not imply the presence of an interaction between these methimazolyl protons and the palladium centre in this system. This conclusion appears to be concordant with the observations of Lippard and Hoffman that these short M···H-C distances are a feature of constrained molecular systems.[45,46]

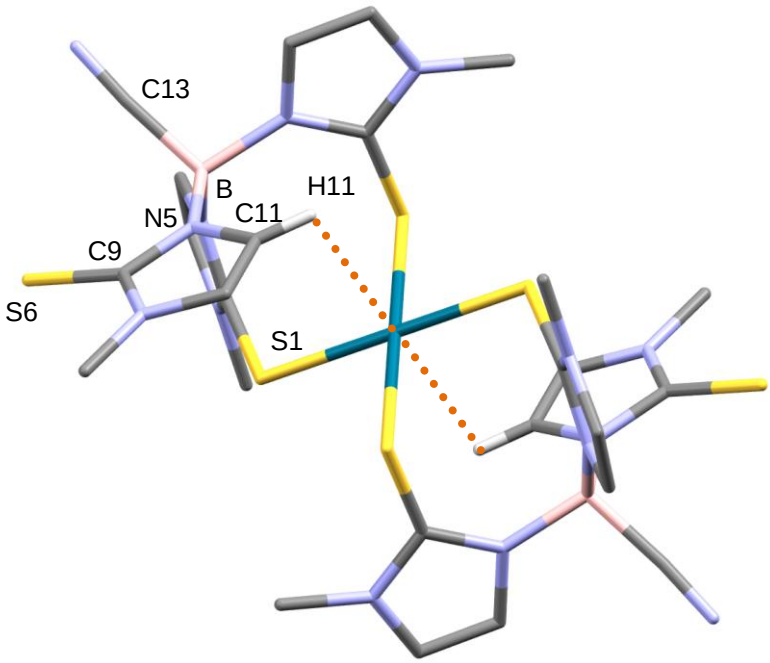

Figure 5.11: X-ray crystal structure of **5.15** showing a relatively short [3.051 Å] M···H-C distance.

5.3 Conclusions

This chapter has detailed efforts towards the synthesis of heteroleptic 'half-sandwich' ruthenium, rhodium and palladium complexes of substituted tris(methimazolyl)borate ligands. With all of these systems a preference for the formation of homoleptic 'sandwich' complexes was observed. However, in those complexes which did not immediately form bis-ligand species the κ^2-[*S,S*] coordination mode was found to be preferred over κ^3-[*S,S,S*]. Since there appears to be no geometric barriers to the coordination in the κ^3-[*S,S,S*] mode of at least some of these complexes (*i.e.* [{κ^3-[*S,S,S*]-(N-methylimidazole)ZTmRuCl$_3$]) it can be concluded that the former coordination mode is preferred for electronic reasons. The coordination mode of the heteroleptic complex [{(NC)Tm}Rh(COD)] in the solid state is undetermined, although it has been shown to be highly fluxional in solution. Oxidation of this d^8 Rh(I) species to Rh(III) may yield an octahedral complex containing a κ^3-[*S,S,S*] coordinated substituted Tm ligand. The palladium complex [{(NC)Tm}$_2$Pd] contains a relatively short M···H-C distance [3.051 Å] in the solid state, however, detailed study of the X-ray crystal structure of this complex suggests that this may result from ligand constraints rather than any M···H-C interaction.

5.4 References

1. Mashima, K.; Abe, T.; Tani, K., *Chem. Lett.*, **1998**, 1201.
2. Madrigal, C. A.; Garcia-Fernandez, A.; Gimeno, J.; Lastra, E., *J. Organomet. Chem.*, **2008**, *693*, 2535.
3. Ahlford, K.; Adolfsson, H., *Catal. Commun.*, **2011**, *12*, 1118.
4. Parekh, V.; Ramsden, J. A.; Wills, M., *Catal. Sci. Technol.*, **2012**, *2*, 406.
5. Uematsu, N.; Fujii, A.; Hashiguchi, S.; Ikariya, T.; Noyori, R., *J. Am. Chem. Soc.*, **1996**, *118*, 4916.
6. Takehara, J.; Hashiguchi, S.; Fujii, A.; Inoue, S.-i.; Ikariya, T.; Noyori, R., *Chem. Commun.*, **1996**, 233.
7. Fujii, A.; Hashiguchi, S.; Uematsu, N.; Ikariya, T.; Noyori, R., *J. Am. Chem. Soc.*, **1996**, *118*, 2521.
8. Noyori, R.; Hashiguchi, S., *Acc. Chem. Res.*, **1997**, *30*, 97.
9. Soni, R.; Collinson, J.-M.; Clarkson, G. C.; Wills, M., *Org. Lett.*, **2011**, *13*, 4304.
10. Hashiguchi, S.; Fujii, A.; Takehara, J.; Ikariya, T.; Noyori, R., *J. Am. Chem. Soc.*, **1995**, *117*, 7562.
11. Noyori, R.; Yamakawa, M.; Hashiguchi, S., *J. Org. Chem.*, **2001**, *66*, 7931.
12. Reglinski, J.; Spicer, M. D., *Eur. J. Inorg. Chem.*, **2009**, 1553.
13. Smith, J., *Comments Inorg. Chem.*, **2008**, *29*, 189.
14. Trofimenko, S., *Chem. Rev.*, **1993**, *93*, 943.
15. Bailey, P. J.; Lorono-Gonzales, D. J.; McCormack, C.; Parsons, S.; Price, M., *Inorg. Chim. Acta*, **2003**, *354*, 61.
16. Bailey, P. J.; Pinho, P.; Parsons, S., *Inorg. Chem.*, **2003**, 42, 8872.
17. Bailey, P. J.; Lorono-Gonzales, D.; McCormack, C.; Millican, F.; Parsons, S.; Pfeifer, R.; Pinho, P. P.; Rudolphi, F.; Sanchez Perucha, A., *Chem. Eur. J.*, **2006**, *12*, 5293.
18. Bailey, P. J.; McCormack, C.; Parsons, S.; Rudolphi, F.; Sanchez-Perucha, A.; Wood, P., *Dalton Trans.* **2007**, 476.
19. Bailey, P. J.; Budd, L.; Cavaco, F. A.; Parsons, S.; Rudolphi, F.; Sanchez-Perucha, A.; White, F. J., *Chem. Eur. J.*, **2010**, *16*, 2819.

20. Albers, M. O.; Oosthuizen, H. E.; Robinson, D. J.; Shaver, A.; Singleton, E., *J. Organomet. Chem.*, **1985**, *282*, c49.

21. Albers, M. O.; Robinson, D. J.; Shaver, A.; Singleton, E., *Organometallics*, **1986**, *5*, 2199.

22. Bailey, P. J.; Bell, N. L.; Nichol, G. S.; Parsons, S.; White, F., *Inorg. Chem.*, **2012,** *51*, 3677.

23. Kuan, S. L.; Leong, W. K.; Goh, L. Y.; Webster, R. D., *Organometallics*, **2005**, *24*, 4639.

24. Reglinski, J.; Garner, M.; Spicer, M. D.; Kennedy, A. R., *J. Am. Chem. Soc.*, **1999**, *121*, 2317.

25. Reglinski, J.; Slavin, P. A.; Spicer, M. D.; Kennedy, A. R., *Dalton Trans.*, **2000**, 239.

26. Garner, M.; Lewinski, K.; Pattek-Janczyk, A.; Reglinski, J.; Sieklucka, B.; Spicer, M. D.; Szaleniec, M., *Dalton Trans.*, **2003**, 1181.

27. Abernethy, R. J.; Hill, A. F.; Tshabang, N.; Willis, A. C.; Young, R. D., *Organometallics*, **2009**, *28*, 488.

28. Hill, A. F.; Foreman, M. R. S. J.; Owen, G. R.; White, A. J. P.; Williams, D. J., *Organometallics*, **2003**, *22*, 4446.

29. Wang, X.-Y.; Shi, H.-T.; Wu, F.-H.; Zhang, Q.-F., *J. Mol. Struct.*, **2010**, *982*, 66.

30. Jia, W.-G.; Jin, G.-X., *Wuji Huaxue Xuebao*, **2008**, *24*, 1242.

31. Jia, W.-G.; Huang, Y.-B.; Jin, G.-X., *J. Organomet. Chem.*, **2009**, *694*, 3376.

32. Lopez-Gomez, M. J.; Connelly, N. G.; Haddow, M. F.; Hamilton, A.; Orpen, A. G., *Dalton Trans.*, **2010**, *39*, 5221.

33. Adams, C. J.; Anderson, K. M.; Charmant, J. P. H.; Connelly, N. G.; Field, B. A.; Hallett, A. J.; Horne, M., *Dalton Trans.*, **2008**, 2680.

34. Chen, F.; Wang, G.-F.; Li, Y.-Z.; Chen, X.-T.; Xue, Z.-L., *Inorg. Chem. Commun.*, **2012**, *21*, 88.

35. Bedford, C. D.; Harris, R. N., III; Howd, R. A.; Goff, D. A.; Koolpe, G. A.; Petesch, M.; Koplovitz, I.; Sultan, W. E.; Musallam, H. A., *J. Med. Chem.*, **1989**, *32*, 504.

36. Melnick, J. G.; Parkin, G., *Dalton Trans.*, **2006**, 4207.

37. Dodds, C. A.; Reglinski, J.; Spicer, M. D., *Chem. Eur. J.*, **2006**, *12*, 931.

38. Canivet, J.; Suss-Fink, G.; Stepnicka, P., *Eur. J. Inorg. Chem.*, **2007**, 4736.

39. Blacker, A. J.; Duckett, S. B.; Grace, J.; Perutz, R. N.; Whitwood, A. C., *Organometallics*, **2009**, *28*, 1435.

40. Ito, M.; Endo, Y.; Tejima, N.; Ikariya, T., *Organometallics*, **2010**, *29*, 2397.

41. Bailey, P. J.; Dawson, A.; McCormack, C.; Moggach, S. A.; Oswald, L. D. H.; Parsons, S.; Rankin, D. W. H.; Turner, A., *Inorg. Chem.*, **2005**, *44*, 8884.

42. Gade, L. H.; Foltz, C.; Stecker, B.; Marconi, G.; Bellemin-Laponnaz, S.; Wadepohl, H., *Chem. Comm.*, **2005**, 5115.

43. Nobel Prize - Advanced Information; NobelPrize.org; http://www.nobelprize.org/nobel_prizes/chemistry/laureates/2010/advanced.html (Accessed: 21 Aug. 2012)

44. Brammer, L., *Dalton Trans.*, **2003**, 3145.

45. Sundquist, W. I.; Bancroft, D. P.; Lippard, S. J., *J. Am. Chem. Soc.*, **1990**, *112*, 1590.

46. Saillard, J. Y.; Hoffmann, R., *J. Am. Chem. Soc.*, **1984**, *106*, 2006.

47. Yao, W.; Eisenstein, O.; Crabtree, R. H., *Inorg. Chim. Acta*, **1997**, *254*, 105.

48. Pang, K.; Quan, S. M.; Parkin, G., *Chem. Comm.*, **2006**, 5015.

Chapter Six

Scorpionate Synthesis: *Experimental Chapter*

6.1 General Experimental

All reactions were carried out under an atmosphere of dry, oxygen–free dinitrogen, using standard Schlenk techniques or in a Saffron glovebox. Solvents were distilled and dried by standard methods or used directly from a Glass Contour solvent purification system. Mass spectra were recorded on a MAT 900 XP (EI/FAB), Thermo–Fisher LCQ Classic (ESI). NMR spectra were recorded either on a 400 MHz, 500 MHz or 600 MHz Bruker Advance III spectrometer. ^{1}H and ^{13}C chemical shifts are reported in ppm relative to $SiMe_4$ ($\delta = 0$) and were referenced internally with respect to the protio solvent impurity or the ^{13}C resonances respectively. Multiplicities and peak types are abbreviated: singlet, s; doublet, d; triplet, t; quartet, q, septet, spt; multiplet, m; broad, br. ^{11}B chemical shifts are reported in ppm relative to $BF_3.OEt_2$ ($\delta = 0$). Infra–red spectra were recorded from solution or a nujol mull using cells with CaF_2 windows on a Jasco FT–IR 410 spectrometer, or as neat solids using a Perkin–Elmer Spectrum 65. UV/vis spectra were recorded in quartz cells on a Shimadzu UV–1800 spectrometer. Electrochemical experiments were performed with an Autolab PGSTAT 302. A three compartment cell was used with an Ag/AgCl reference electrode, Pt foil counter electrode, and a Pt button working electrode. Freshly distilled and degassed DMF was used as the solvent with $[nBu_4N][BF_4]$ as the supporting electrolyte (0.2 M). Solutions contained 1 mmol of analyte in 10 mL of solvent. The measured potentials were corrected for junction potentials relative to ferrocenium/ferrocene (0.543 mV vs Ag/AgCl). All $E_{1/2}$ values were calculated from $(E_{pa} + E_{pc})/2$ at a scan rate of 300 mV/s. Elemental analyses were carried out at by Mr Stephen Boyer at London Metropolitan University.

The compounds [(HMe$_2$N)B(methimazolyl)$_3$] (**2.1**),[1] [PPN][SCN], [PPN][NCO], [PPN][N$_3$],[2] N–methylimidazoline,[3] [(*p*–cymene)RuCl$_2$],[4] [{(N–methylimidazolium)B(mt)$_3$}Ru(*p*–cymene)][PF$_6$]$_2$ (**3.9**),[1] RuCl$_2$(PPh$_3$)$_3$,[5] RuCl$_2$[DMSO]$_4$, RuCl$_2$[MeCN]$_4$, Ru(PPh$_3$)$_3$HCl(CO), [RuCl$_2$(COD)]$_n$, [RhCl(COD)]$_2$, N–tert–butylimidazol–2–thione[6] and N–p–tolylimidazol–2–thione[7] were synthesised according to the literature procedures. Piperazine and DABCO were sublimed *in vacuo* and stored under N$_2$ before use. Tris(dimethylamino)borane and N–methylimidazole were stored under N$_2$. All other chemicals were obtained from Sigma–Aldrich and used as received.

6.2 Chapter Two

6.2.1 (Piperidinium)tris(methimazolyl)borate (2.2)

Methimazole (499.8 mg, 4.38 mmol, 3 eq.) was suspended in toluene (20 cm^3). Piperidine (144 μL, 1.46 mmol, 1 eq.) and tris(dimethylamino)borane (256 μL, 1.46 mmol, 1 eq.) were added and the solution was heated to reflux for 6 h. After cooling half of the solvent was removed *in vacuo* and the precipitate which formed was filtered by cannula and washed with Et$_2$O (3 x 10 mL). The target material was isolated as a white powder (495.7 mg, 78%). X–ray quality crystals were grown from slow diffusion of Et$_2$O into a solution of the complex in DCM. MS (EI$^+$) *m*/*z* : 435.2 [M$^+$]; ^{1}H-NMR (400 MHz, CDCl$_3$) δ 8.81 (s, 1H, NH), 6.62 (d, *J* = 2.4 Hz, 3H, CH), 6.39 (br. s, 3H, CH), 4.42 (br. s, 1H, CH$_2$), 4.05 (br. s, 1H, CH$_2$), 3.53 (s, 9H, CH$_3$), 2.77 (br. s, 1H, CH$_2$), 2.27 (br. s, 1H, CH$_2$), 1.90–1.32 (m, 6H, CH$_2$CH$_3$CH$_2$) ppm; ^{13}C-NMR (125.8 MHz, CDCl$_3$) δ 165.3 (*C*=S), 120.7 (*C*H), 118.7 (*C*H), 52.3 (N*C*H$_2$), 50.2 (N*C*H$_2$), 34.9 (N*C*H$_3$), 25.9 (*C*H$_2$), 23.9 (*C*H$_2$), 22.5 (*C*H$_2$) ppm; ^{11}B-NMR (CDCl$_3$, 128.3 MHz) δ 2.2 ppm; Elemental analysis: expected for C$_{17}$H$_{26}$BN$_7$S$_3$ (435.44): C, 46.89; H, 6.02; N, 22.52; found: C, 46.76; H, 6.14; N, 22.62 %.

6.2.2 (Morpholinium)tris(methimazolyl)borate (2.3)

$[HNMe_2]B[methimazolyl]_3$ (509.8 mg, 1.29 mmol) was suspended in toluene (20 cm^3). Morpholine (110 μL, 1.26 mmol) was added and the solution was heated to reflux for 12 h becoming cloudy after 5 h. After cooling half of the solvent was removed *in vacuo* and the precipitate which formed was filtered by cannula and washed with Et_2O (3 x 10 mL). The target material was isolated as a white powder (410.0 mg, 74%). MS (EI^+) *m/z* : 437.2 [M^+] ^{1}H-NMR (500.1 MHz, $CDCl_3$) δ 9.54 (br. s, 1H, NH), 6.66 (d, 3H, CH), 6.43 (br. s, 3H, CH), 4.91 (br. m, 1H, NCH_2), 4.28 (br. m, 1H, NCH_2), 4.00 (m, 4H, OCH_2), 3.58 (s, 9H, NCH_3), 3.20 (br. m, 1H, NCH_2), 2.73 (br. m, 1H, NCH_2) ppm; ^{13}C-NMR (125.8 MHz, $CDCl_3$) δ 165.3 (*C*=S), 120.7 (*C*H), 119.0 (*C*H), 66.8 (OCH_2) 65.2 (OCH_2), 51.9 (NCH_2) 49.3 (NCH_2), 34.9 (NCH_3) ppm; ^{11}B-NMR (128.3 MHz, $CDCl_3$) δ 2.1 ppm; Elemental analysis: expected for $C_{16}H_{24}BN_7OS_3$ (437.41) : C, 43.93; H, 5.53; N, 22.42; found: C, 43.82; H, 5.45; N, 22.55 %.

6.2.3 (Ammonium)tris(methimazolyl)borate (2.5)

$Ca(OH)_2$ (*ca.* 5 g, 27 eq.) and NH_4Cl (*ca.* 1.8 g, 13 eq.) were mixed in a 2–necked round bottom flask equipped with a magnetic stirrer bar and heated to produce ammonia gas. One neck of the flask was attached to the Schlenk line whilst the other was attached to a Schlenk tube containing calcium oxide as a drying agent. After drying the ammonia gas was bubbled into the reaction flask through suspension of (dimethylammonium)tris(methimazolyl)borate (1 g, 2.53 mmol) in toluene (*ca.* 50 mL). Ammonia evolution was slow so a slight pressure of nitrogen was added to the first flask to drive the ammonia through the system at a rate of 1 bubble s^{-1}. The suspension was heated to reflux for 1 h. After cooling

a white precipitate formed in solution which was filtered and washed with toluene (3 x 10 mL) and diethyl ether (3 x 10 mL) to give the target material as a white solid. (205.3 mg, 22%). X–ray quality crystals were grown from slow diffusion of Et_2O into a solution of the complex in MeCN. MS (EI^+) *m*/*z*: 367.1 [M^+]; ^{1}H-NMR (500 MHz, $CDCl_3$) δ 8.58 (s, 3H), 6.72 (s, 3H), 6.05 (d, *J* = 0.9 Hz, 3H), 3.61 (d, *J* = 3.9 Hz, 9H) ppm; ^{13}C-NMR (126 MHz, $CDCl_3$) δ 164.0 (*C*=S), 119.4 (3 x *C*H), 119.0 (3 x *C*H), 34.7 (3 x N*C*H_3) ppm; ^{11}B-NMR (128 MHz, $CDCl_3$) δ –0.1 ppm; Elemental analysis: expected for $C_{12}H_{18}BN_7S_3$ (367.32) : C, 39.24; H, 4.94; N, 26.69; found: C, 39.17; H, 4.86; N, 26.56 %.

6.2.4 [PPN][(SCN)B(methimazolyl)$_3$] (2.7)

$(HNMe_2)$B(methimazolyl)$_3$ (**2.1**) (719.4 mg, 1.8 mmol) was dissolved in acetonitrile (20 cm^3). [PPN][SCN] (1.074 g, 1.8 mmol) was added and the solution was heated to reflux for 24 h. After this time half of the solvent was removed *in vacuo* and Et_2O was added (30 cm^3). The precipitate which formed was filtered by cannula and washed with Et_2O (3 x 10 mL) to give the target material as a white powder (683.3 mg, 51%). MS (ESI^+) *m*/*z*: 408 [M^+]; ^{1}H-NMR (500.1 MHz, $CDCl_3$) δ 7.71–7.63 (m, 6*H*, 6 x C*H*), 7.54–7.40 (m, 24H, 24 x C*H*), 6.84 (br. s, 3H, 3 x C*H*), 6.53 (d, *J* = 2.4 Hz, 3H, 3 x C*H*), 3.44 (s, 9H, 3 x NCH_3) ppm; ^{13}C-NMR (125.8 MHz, $CDCl_3$) δ 164.0 (*C*=S), 134.0 (3 x *C*H), 132.1 (6 x *C*H), 129.7 (6 x *C*H), 127.0 (d, *J* = 108 Hz, 2 x *C*–P), 122.5 (3 x *C*H), 116.3 (3 x *C*H), 34.6 (3 x N*C*H_3) ppm; ^{11}B-NMR ($CDCl_3$, 128.3 MHz) δ –3.5 ppm; Elemental analysis expected for $C_{49}H_{45}BN_8P_2S_4{\cdot}CHCl_3$ (1066.33): C, 56.32; H, 4.35; N, 10.51; found: C, 55.84; H, 4.55; N, 10.91 %; IR ($CHCl_3$): 2153 cm^{-1} (N=C=S).

6.2.5 [(SCN)B(methimazolyl)3Ru(p–cymene)] [BPh$_4$] (2.8)

[PPN][(SCN)B(methimazolyl)$_3$] (**2.7**) (100.0 mg, 0.20 mmol) and [Ru(*p*–cymene)Cl$_2$] (41.8 mg, 0.10 mmol) were dissolved in MeOH (5 cm^3) and stirred for 1 h. Sodium tetraphenylborate (91.5 mg, 0.40 mmol) was then added and a precipitate formed immediately. The precipitate was filtered and washed with MeOH (3 x 2 cm^3). The solvent was then half removed from the filtrate and ether added (*ca.* 5 cm^3). Red crystals precipitated which were filtered and washed with ether (3 x 5 cm^3). The target material was isolated as a red crystalline solid (57.8 mg, 30%). X–ray quality crystals were grown by slow diffusion of ether into a concentrated solution of the complex in chloroform. MS (ESI$^+$) *m*/*z*: 643.9 [M$^+$/2]; ^{1}H-NMR (500 MHz, CDCl$_3$) δ 7.45 (dd, *J* = 5.0, 3.6 Hz, 8H, 8 x C*H*), 7.05 (t, *J* = 7.4 Hz, 8H, 8 x C*H*), 6.98 (d, *J* = 2.0 Hz, 3H, 3 x C*H*), 6.86 – 6.94 (m, 4H, 4 x C*H*), 6.67 (d, *J* = 2.2 Hz, 3H, 3 x C*H*), 5.12 (t, *J* = 5.8 Hz, 2H, 2 x C*H*), 5.01 (d, *J* = 5.8 Hz, 1H, C*H*), 4.95 (d, *J* = 6.0 Hz, 1H, C*H*), 3.38 (s, 9H, 3 x NC*H*$_3$), 2.84 (spt, *J* = 6.9 Hz, 1H, C*H*), 2.04 (s, 3H, C*H*$_3$), 1.16 (t, *J* = 7.3 Hz, 6H, 2 x C*H*$_3$) ppm; ^{13}C-NMR (125.8 MHz, CDCl$_3$) δ 164.1 (q, *J* = 49 Hz, *C*–B), 157.2 (*C*=S), 136.8 (N*C*S), 136.3 (8 x *C*H), 125.6 (8 x *C*H), 121.7 (4 x *C*H), 121.5 (3 x *C*H), 121.3 (3 x *C*H), 107.0 (*C*$_q$), 101.0 (*C*$_q$), 85.1 (*C*H), 84.5 (*C*H), 84.3 (*C*H), 83.4 (*C*H), 35.1 (3 x NCH$_3$) 30.2 (*C*H), 22.9 (*C*H$_3$), 22.1 (*C*H$_3$), 18.8 (*C*H$_3$) ppm; ^{11}B-NMR (128.3 MHz, CDCl$_3$) δ –3.3 (*B*Mt$_3$), –6.5 (*B*Ph$_4$*)* ppm; Elemental analysis expected for C$_{47}$H$_{49}$B$_2$Cl$_3$N$_7$RuS$_4$ (1082.27): C, 58.63; H, 5.13; N, 10.18; found: C, 58.68; H, 5.23; N, 10.16 %; IR 2095 cm^{-1} (N=C=S).

6.2.6 (N,N–dimethylacetamidino)B(methimazolyl)$_3$ (2.10)

(HNMe$_2$)B(methimazolyl)$_3$ (**2.1**) (362 mg, 91.6 mmol) was dissolved in acetonitrile (20 cm^3) and the solution was heated to reflux for 3 h becoming cloudy after 1 h. The precipitate which formed upon cooling was filtered by

cannula and washed with Et_2O (3 x 10 mL). The target material was isolated as a white powder (288 mg, 72%). MS (EI^+) *m*/*z*: 436.1 [M^+]; ^{1}H-NMR (500.1 MHz, $CDCl_3$) δ 9.87 (s, 1H, 1 x N*H*), 6.66 (d, *J* = 2.3 Hz, 3H, 3 x C*H*), 6.24 (br. s, 3H, 3 x C*H*), 3.58 (s, 9H, 3 x NCH_3), 3.32 (s, 3H, NCH_3), 3.14 (s, 3H, NCH_3), 2.04 (s, 3H, CH_3) ppm; ^{13}C-NMR (125.8 MHz, $CDCl_3$) δ 167.4 (*C*=N), 164.0 (*C*=S), 120.4 (*C*H), 118.1 (*C*H), 41.3 (*C*H_3), 40.7 (*C*H_3), 34.7 (*C*H_3), 19.1 (*C*H_3) ppm; ^{11}B-NMR (128.3 MHz, $CDCl_3$) δ 0.3 ppm; Elemental analysis: expected for $C_{16}H_{25}BN_8S_3$ (436.15): C, 44.03; H, 5.77; N, 25.68; found: C, 44.14; H, 5.67; N, 25.73 %; IR (KBr) 1618 cm^{-1} (C=N).

6.2.7 *[(N,N–dimethylacetamidino)B(methimazolyl)$_3$Ru(p–cymene)][PF6]$_2$ (2.11)*

[(*N*,*N*–dimethylacetamidino)B(methimazolyl)$_3$] (**2.10**) (101.3 mg, 0.23 mmol) and [Ru(*p*–cymene)Cl_2]$_2$ (71.8 mg, 0.12 mmol) were dissolved in MeOH and stirred overnight. Ammonium hexafluorophosphate (75.5 mg, 0.46 mmol) was then added and a precipitate formed immediately. After stirring the precipitate was filtered and washed with MeOH (3 x 2 mL) and Et_2O (3 x 3 mL). The target material was isolated as a red solid (133.3 mg, 60%). X–ray quality crystals were grown by slow diffusion of ether into a concentrated solution of the complex in acetonitrile. MS (ESI^+) *m*/*z*: 335.86 [M^+]; ^{1}H-NMR (400 MHz, CD_3CN) δ 7.18 (d, *J* = 2.0 Hz, 3H, 3 x C*H*), 6.98 (br. s, 3H, 3 x C*H*), 5.99 (br. s, 1H, N*H*), 5.50 (s, 2H, 2 x C*H*), 5.34 – 5.43 (m, 2H, 2 x C*H*), 3.67 (s, 9H, 3 x NCH_3), 3.22 (d, *J* = 8.7 Hz, 6H, 2 x NCH_3), 2.94 (spt, *J* = 6.9 Hz, 1H, C*H*), 2.18 (s, 3H, CH_3), 1.96 (br. s, 3H, CH_3), 1.18 (dd, *J* = 6.9, 1.9 Hz, 6H, 2 x CH_3) ppm; ^{13}C-NMR (125.8 MHz, CD_3CN) δ 168.21 (C_q), 160.1 (*C*=S), 123.4 (3 x *C*H), 122.0 (3 x *C*H), 107.9 (C_q), 102.6 (C_q), 86.4 (*C*H), 86.1 (*C*H), 85.3 (*C*H), 84.3 (*C*H), 42.3 (N*C*H_3), 37.8 (N*C*H_3), 36.2 (3 x *C*H_3), 31.4 (*C*H), 23.0 (*C*H_3),

22.6 (CH_3), 20.7 (CH_3), 19.1 (CH_3) ppm; ^{11}B-NMR (CD_3CN, 128.3 MHz) δ 0.7 ppm; Elemental analysis: expected for $C_{26}H_{39}BF_{12}N_8P_2RuS_3$ (1046.58): C, 32.63; H, 4.26; N, 11.28 found: C, 32.57; H, 4.05 ; N, 11.58 %; IR (Nujol) 1632 cm^{-1}.

6.2.8 (N,N–dimethyl–Benzimidamide)B(methimazolyl)$_3$ (2.12)

$[HNMe_2]B[methimazolyl]_3$ (500 mg, 1.26 mmol) was dissolved in benzonitrile (10 cm^3) and the solution was heated to 110°C for 8 h. The precipitate which formed upon cooling was filtered by cannula and washed with toluene (3 x 10 mL) and Et_2O (3 x 10 mL). The target material was isolated as a white powder (336 mg, 53%). MS (EI^+) *m*/*z*: 498.2 [M^+]; ^{1}H-NMR (500.1 MHz, $CDCl_3$) δ 11.12 (s, 1 H, N*H*), 7.51 (m, 5H, 5 x C*H*), 6.82 (s, 3 H, 3 x C*H*), 6.36 (s, 3 H, 3 x C*H*), 3.54, (s, 3H, NCH_3), 3.42 (s, 9 H, 3 x CH_3), 2.79 (s, 3 H, NCH_3) ppm; ^{13}C-NMR (125.8 MHz, $CDCl_3$) 166.8 (C=S), 132.8 (CH), 132.2 (2 x CH), 131.2 (2 x CH), 127.8 (CH), 116.1 (CH), 41.9 (CH_3), 41.4(CH_3), 34.5 (CH_3) ppm; ^{11}B-NMR (128.3 MHz, $CDCl_3$) δ 0.1 ppm; Elemental analysis expected for $C_{21}H_{27}BN_8S_3$ (498.2): C, 50.60; H, 5.46; N, 22.48; found: C, 50.44; H, 5.37; N, 22.34 %; IR 1602 cm^{-1} (C=N).

6.2.9 [(N,N–dimethylbenzamidino)B(methimazolyl)$_3$Ru(p–cymene)] [PF$_6$]$_2$ (2.13)

[(*N*,*N*–Dimethylbenzamidino)B(methimazolyl)$_3$] (**2.12**) (101.3 mg, 0.20 mmol, 1 eq.) and [Ru(*p*–cymene)Cl_2]$_2$ (63.4 mg, 0.10 mmol, 0.5 eq.) were dissolved in MeOH and stirred for 1 h. Ammonium hexafluorophosphate (65.4 mg, 0.40 mmol, 2 eq.) was then added and a precipitate formed immediately. The precipitate was filtered and washed with MeOH (3 x 2 mL) and Et_2O (3 x 3 mL). The target material was isolated as a red solid (153.2 mg, 74%). X–ray quality crystals were grown by slow diffusion of ether into a concentrated solution of the complex in acetonitrile. MS (ESI^+) *m*/*z*: 367.23 [M^+/2]; ^{1}H-NMR

(500.1 MHz, d_6–DMSO) δ 7.49 (m, 5H, 5 x C*H*), 7.46 (s, 3H, 3 x C*H*), 7.27 (s, 3H, 3 x C*H*), 5.55 (m, 4H, 4 x C*H*) 3.56 (s, 9H, 3 x NCH_3), 2.94 (s, 3H, CH_3), 2.84 (spt, J = 6.9 Hz, 1H, C*H*), 2.10 (s, 3H, CH_3), 1.20 (dd, J = 6.9 Hz, 6H, 2 x CH_3) (Missing one CH_3 resonance: Under DMSO or H_2O peaks) ppm; ^{13}C-NMR (101 MHz, d_6–DMSO) δ 167.3 (C_q), 157.5 (*C*=S), 132.0 (*C*H), 128.9 (*C*H), 127.9 (*C*H), 122.6 (3 x *C*H), 121.6 (3 x *C*H), 105.8 (C_q), 100.9 (C_q), 85.1 (*C*H), 84.4 (*C*H), 83.7 (*C*H), 82.9 (*C*H), 44.0 (*C*H), 34.8 (3 x NCH_3), 30.0 (CH_3), 22.5 (NCH_3), 21.7 (NCH_3), 18.2 (2 x CH_3) ppm; ^{11}B-NMR (128.3 MHz, d_6–DMSO) δ –0.3 ppm; Elemental analysis: expected for $C_{31}H_{41}BF_{12}N_8P_2RuS_3$ (1023.72) C, 36.37; H, 4.04; N, 10.95; found C, 36.55; H, 3.90; N, 11.27 %; IR (Nujol) 1608 cm^{-1}.

6.2.10 (DMF)B(methimazolyl)$_3$ (2.14)

(HNMe$_2$)B(methimazolyl)$_3$ (**2.1**) (501.9 mg, 1.27 mmol) was suspended in toluene (20 cm^3). DMF (105 μL, 1.35 mmol) was added and the solution was heated to reflux for 6 h becoming cloudy after 1 h. After cooling the precipitate was filtered by cannula and washed with toluene (3 x 10 mL) and Et_2O (3 x 10 mL). The target material was isolated as a white powder (465 mg, 87%). MS (EI$^+$) *m*/*z*: 423.92 [M$^+$]; ^{1}H-NMR (500.1 MHz, $CDCl_3$) δ 8.67 (s, 1H, C(*H*)O), 6.66 (d, J = 2.3 Hz, 3H, 3 x C*H*), 6.44 (br. s, 3H, 3 x C*H*), 3.57 (s, 9H, 3 x CH_3), 3.33 (s, 3H, NCH_3), 3.23 (s, 3H, NCH_3) ppm; ^{13}C-NMR (125.8 MHz, $CDCl_3$) δ 165.0 (–*C*HO), 164.3 (*C*=S), 120.7 (*C*H), 118.3 (*C*H), 40.3 (*C*H_3), 36.3 (*C*H_3), 34.7 (*C*H_3) ppm; ^{11}B-NMR (128.3 MHz, $CDCl_3$) δ 2.3; Elemental analysis: expected for $C_{15}H_{22}BN_7OS_3$ (423.4): C, 42.55; H, 5.24; N, 23.16; found: C, 42.63; H, 5.16; N, 23.12 %; IR (MeCN): 1678 cm^{-1} (C=O).

6.2.11 3–Bis(methimazolyl)–2–(2,6–dimethylphenylimino)–7–methyl–[1,4,3]–thiazaborolo–[5,4–b]–imidazolium (2.15)

$(HNMe_2)B(methimazolyl)_3$ (**2.1**) (503.2 mg, 1.26 mmol) was suspended in toluene (20 cm^3). 2,6–dimethylphenylisonitrile (167 mg, 1.27 mmol) was added and the solution was heated to reflux for 96 h. After cooling half of the solvent was removed *in vacuo* and the precipitate which formed was filtered by cannula and washed with toluene (3 x 10 mL) and Et_2O (3 x 10 mL). The resultant white powder was recrystallised from $MeCN/Et_2O$ and the target material was isolated as a white powder (541.2 mg, 89%). X–ray quality crystals were grown from slow diffusion of diethyl ether into a concentrated solution of **2.15** in DCM. MS (EI^+) *m/z*: 481.2 [M^+]; ^{1}H-NMR ($CDCl_3$, 400MHz) δ 7.62 (br. s, 3H, 3 x C*H*), 6.93 – 7.11 (m, 3H, 3 x C*H*), 6.77 (d, *J* = 2.3 Hz, 3H, 3 x C*H*), 3.58 (s, 9H, 3 x NCH_3), 2.14 ppm (s, 6H, 2 x CH_3) ppm; ^{13}C-NMR (125.8 MHz, $CDCl_3$) δ 176.9 (br, C–B), 160.7 (*C*=S), 150.8 (*C*–NC), 128.5 (2 x *C*H), 126.7 (2 x *C*(CH_3)), 125.0 (*C*H), 122.6 (3 x *C*H), 119.3 (3 x *C*H), 34.8 (3 x NCH_3), 18.7 (2 x *C*H_3) ppm; ^{11}B-NMR (128.3 MHz, $CDCl_3$) δ –1.2 ppm; Elemental analysis: expected for $C_{21}H_{24}BN_7S_3$ (481.47): C, 52.39; H, 5.02; N, 20.36; found: C, 52.25; H, 5.09; N, 20.43 %; IR (Nujol) 1660 cm^{-1} (CN).

6.2.12 [{κ³–[N,S,S]–3–Bis(methimazolyl)–2–(2,6–dimethylphenylimino)–7–methyl–[1,4,3]–thiazaborolo–[5,4–b]–imidazolium}Ru(p–cymene)] [PF_6]$_2$ (2.16)

3–Bis(methimazolyl)–2–(2,6–dimethylphenyli*min*o)–7–methyl–[1,4,3]–thiazaborolo–[5,4–b]–imidazolium (**2.15**) (98.7 mg, 0.20 mmol) and [Ru(*p*–cymene)Cl_2]$_2$ (65.4 mg, 0.11 mmol) were dissolved in MeOH and stirred for 2 h. Ammonium hexafluorophosphate (67.7 mg, 0.42 mmol) was then added and an orange–red precipitate formed immediately. The precipitate was filtered and washed with MeOH (3 x 2 mL) and Et_2O (3 x 3 mL). The target material was isolated as a red solid (132.6 mg, 65%). X–ray quality crystals were grown by slow diffusion of ether into a concentrated solution of the

complex in acetonitrile. MS (ESI$^+$) *m/z*: 358.3 [M$^+$/2]. ^{1}H-NMR (400 MHz, CD_3CN) δ 7.48 (d, *J* = 2.1 Hz, 1H, C*H*), 7.42 (d, *J* = 2.1 Hz, 1H, C*H*), 6.08 – 7.38 (m, 7H, 7 x C*H*), 4.78 –5.10 (m, 2H, 2 x C*H*), 5.10–5.27 (m, 2H, 2 x C*H*), 3.76 (s, 6H, 2 x NCH_3), 3.55 (s, 3H, NCH_3), 3.03 (spt, *J* = 6.9 Hz, 1H, C*H*), 2.37 (br. s, 3H, CH_3), 2.01 (s, 3H, CH_3), 1.26 (d, *J* = 6.9 Hz, 6H, 2 x CH_3), 1.23 (br. s, 3H, CH_3) ppm; ^{13}C-NMR (125.8 MHz, CD_3CN) δ 196.4 (*C*–B), 158.14 (*C*=S), 148.5 (C_q), 131.5 (2 x *C*H), 130.7 (*C*H), 129.7 (C_q), 129.1 (2 x *C*H), 125.1 (*C*H), 123.3 (2 x *C*H), (One CH missing, most likely under H_3CCN resonance), 121.2 (C_q), 113.9 (C_q), 105.3 (C_q), 91.3 (2 x *C*H), 86.5 (2 x *C*H), 48.9 (CH), 36.8 (2 x N*C*H_3), 36.6 (N*C*H_3), 31.6 (*C*H_3), 22.9 (*C*H_3), 18.6 (*C*H_3), 18.0 (2 x *C*H_3) ppm; ^{11}B-NMR (128.3 MHz, CD_3CN) δ –2.4 ppm; Elemental analysis: expected for $C_{31}H_{38}BF_{12}N_7P_2RuS_3$ (1006.68) C, 36.99; H, 3.80; N, 9.74; found C, 37.14; H, 3.72; N, 9.73; IR (Nujol) 1567 cm^{-1}.

6.2.13 (N,N–dimethylaminoformamidine)B(methimazolyl)$_3$ (2.17)

SAFETY NOTE: There is a possibility of the formation of HCN in this reaction. Appropriate precautions should be taken when repeating this synthesis.

(HNMe$_2$)B(methimazolyl)$_3$ (**2.1**) (503.5 mg, 1.26 mmol) was suspended in toluene (20 cm^3). 1,1,3,3–tetramethylbutylisonitrile (222 μL, 1.26 mmol) was added and the solution was heated to reflux for 12 h. After cooling half of the solvent was removed *in vacuo* and the precipitate which formed was filtered by cannula and washed with Et_2O (3 x 10 mL). The resultant white powder was recrystallised from MeOH/Et_2O and the target material was isolated as a white powder (243.5 mg, 46%). MS (EI$^+$) *m/z*: 422.1 [M$^+$]; ^{1}H-NMR (500.1 MHz, $CDCl_3$) δ 10.02 (d, *J* = 15.5 Hz, 1H, N*H*), 7.94 (d, *J* = 15.5 Hz, 1H, C*H*), 6.68 (d, *J* = 2.1 Hz, 3H, 3 x C*H*), 6.06 (d, *J* = 1.7 Hz, 3H, 3 x C*H*), 3.59, (s, 9H, 3 x NCH_3), 3.18 (s, 3H, NCH_3), 3.07 (s, 3H, NCH_3) ppm; ^{13}C-NMR (125.8 MHz,

$CDCl_3$) δ 163.7 (*C*=S), 159.3 (*C*H), 119.8 (3 x *C*H), 118.5 (3 x *C*H), 42.8 (CH_3), 36.1 (CH_3), 34.6 (3 x CH_3) ppm; ^{11}B-NMR (128.3 MHz, $CDCl_3$) δ 0.7 ppm; Elemental analysis: expected for $C_{15}H_{23}BN_8S_3$ (422.40): C, 42.65; H, 5.49; N, 26.53; found: C, 42.72; H, 5.39; N, 26.43 %; IR (KBr) 1683 cm^{-1} (C=N).

6.2.14 [{(N,N–dimethylformamidino)B(methimazolyl)$_3$}Ru(p–cymene)][PF$_6$]$_2$ (2.18)

[(*N*,*N*–dimethylformamidino)B(methimazolyl)$_3$] (**2.17**) (96.2 mg, 0.23 mmol) and [Ru(*p*–cymene)Cl_2]$_2$ (72.5 mg, 0.12 mmol) were dissolved in MeOH and stirred overnight. Ammonium hexafluorophosphate (74.2 mg, 0.46 mmol) was then added and a precipitate formed immediately. The precipitate was filtered and washed with MeOH (3 x 2 mL) and Et_2O (3 x 3 mL). The target material was isolated as a red solid (114.7 mg, 53%). X–ray quality crystals were grown by slow diffusion of ether into a concentrated solution of the complex in acetonitrile. MS (ESI$^+$) *m*/*z*: 328.8 [M$^+$/2]; ^{1}H-NMR (500 MHz, d_6–DMSO) δ 8.24 (d, *J* = 12.5 Hz, 1H, N*H*), 7.73 (d, *J* = 1.9 Hz, 3H, 3 x C*H*), 7.54 (s, 3H, 3 x C*H*), 6.97 (d, *J* = 13.4 Hz, 1H, C*H*), 6.04 (d, *J* = 6.1 Hz, 2H, 2 x C*H*), 5.94 (dd, *J* = 13.6, 5.3 Hz, 2H, 2 x C*H*), 4.23 (s, 9H, 3 x NCH_3), 3.77 (s, 3H, NCH_3), 3.70 (s, 3H, NCH_3), 3.51 (spt, *J* = 7.0 Hz, 1H, C*H*), 2.22 (s, 3H, CH_3) 1.74 (d, *J* = 6.8 Hz, 6H, 2 x CH_3) ppm; ^{13}C-NMR (125.8 MHz, CD_3CN) δ 160.4 (*C*H), 158.6 (*C*=S), 123.1 (3 x *C*H), 122.6 (3 x *C*H), 107.9 (C_q), 102.5 (C_q), 86.2 (*C*H), 85.8 (*C*H), 85.2 (*C*H), 84.2 (*C*H), 44.9 (NCH_3), 37.1 (NCH_3), 36.0 (3 x *C*H_3), 31.4 (*C*H), 23.0 (*C*H_3), 22.6 (*C*H_3), 19.1 (*C*H_3) ppm; ^{11}B-NMR (128.3 MHz, CD_3CN) δ –0.5 ppm; Elemental analysis: expected for $C_{25}H_{37}BF_{12}N_8P_2RuS_3$ (947.62) C, 31.69; H, 3.94; N, 11.82; found C, 32.11; H, 3.38; N, 11.83 %; IR (Nujol) 1688 cm^{-1}.

6.2.15 [Dimethylammonium][(cyanato)B(methimazolyl)$_3$] (2.19)

SAFETY NOTE: There is a possibility of the formation of HCN in this reaction. Appropriate precautions should be taken when repeating this synthesis.

$(HNMe_2)B(methimazolyl)_3$ (**2.1**) (1.0094 g, 2.55 mmol) was suspended in toluene (20 cm^3). 1,1,3,3–tetramethylbutyllisonitrile (435 μL, 2.55 mmol) was added and the solution was heated to reflux for 4 h. After cooling, the resulting sticky solid was filtered and washed with toluene at 90°C (2 x 10 mL). After cooling the sticky solid was triturated with Et_2O to give a white powder. The resultant white powder could not be recrystallised from CH_2Cl_2/Et_2O, CH_2Cl_2/hexane, $MeCN/Et_2O$, THF/Et_2O or by cooling of solutions of the material. In each instance the product precipitated as a sticky solid or oil which could be converted back into a powder by trituration with Et_2O. The resultant precipitate was filtered, washed with Et_2O (3 x 10 mL) and dried *in vacuo* yielding a white powder (607.0 mg, 56%). MS (ESI^-) *m*/*z*: 376.04 [M^-]; ^{1}H-NMR (400 MHz, $CDCl_3$) δ 8.32 (br. s, 2H, N*H*$_2$), 6.68 (d, *J* = 2.27 Hz, 3H, 3 x C*H*), 6.55 (d, *J* = 1.77 Hz, 3H, 3 x C*H*), 3.58 (s, 9H, 3 x NC*H*$_3$), 2.69 (t, *J* = 5.43 Hz, 6H, N(C*H*$_3$)$_2$) ppm; ^{13}C-NMR (126 MHz, $CDCl_3$) δ 162.8 (*C*=S), 130.4 (q, *J* = 80 Hz, *C*–B), 121.0 (3 x *C*H), 118.1 (3 x *C*H), 35.2 (N(*C*H$_3$)$_2$), 34.7 (N*C*H$_3$) ppm; ^{11}B-NMR (128.3 MHz, $CDCl_3$) δ –6.7 ppm; Elemental analysis: expected for $C_{15}H_{23}BN_8S_3$ (422.40): C, 42.65; H, 5.49; N, 26.53; found: C, 42.75; H, 5.36; N, 26.36 %.

6.2.16 [N,N–dimethyl–N'–(1,1,3,3–tetramethylpropyl)formamidinium] [(cyanato)B(methimazolyl)$_3$] (2.20)

$(HNMe_2)B(methimazolyl)_3$ (**2.1**) (504.4 mg, 1.26 mmol) was suspended in toluene (20 cm^3). 1,1,3,3–tetramethylbutylisonitrile (434 μL, 2.55 mmol) was added and the solution was heated to reflux for 12 h. After cooling the resulting sticky solid was filtered and washed with toluene (2 x 10 mL) at

90°C. After cooling the sticky solid was triturated with Et_2O to give a white powder. The resultant white powder was could not be recrystallized by the methods described above for **2.19**. In each instance the product was obtained as a sticky solid or oil which could be converted back into a powder by trituration with Et_2O. The resultant precipitate was filtered, washed with Et_2O (3 x 10 mL) and dried *in vacuo* yielding a white powder (392 mg, 55%). MS (ESI^-) *m*/*z*: 376.1 [M^-], (ESI^+) 185.1 [M^+]; ^{1}H-NMR (400 MHz, $CDCl_3$) δ 8.52 (br. s, 1H, N*H*), 7.58 (d, 1H, C*H*), 6.62 (m, 6H, 6 x C*H*), 3.56 (s, 9H, 3 x CH_3), 3.24 (s, 6H, 2 x NCH_3), 1.73 (s, 2H, CH_2), 1.47 (s, 6H, 2 x CH_3), 0.97 (s, 9H, 3 x CH_3) ppm; ^{13}C-NMR (126 MHz, $CDCl_3$) δ 163.4 (*C*=S), 152.5 (N*C*(H)N), 129.3 (q, *J* = 84 Hz, *C*–B), 121.4 (3 x *C*H), 117.4 (3 x *C*H), 59.6 (NCH_3), 54.3 (NCH_3), 37.6 (*C*(CH_3)$_2$), 34.7 (3 x NCH_3), 31.7 (C(*C*H_3)$_2$), 31.6 (C(*C*H_3)$_3$), 29.6 (*C*H_2) ppm; ^{11}B-NMR (128.3 MHz, $CDCl_3$) δ: –6.7 ppm; Elemental analysis: expected for $C_{24}H_{40}BN_9S_3$ (561.64): C, 51.32; H, 7.18; N, 22.45; found: C, 51.18; H, 7.06; N, 22.61 %; IR 1694 cm^{-1} (C=N).

6.2.17 [(Cyano)B(methimazole)$_3$Ru(p–cymene)][PF$_6$] (2.21)

[*N*,*N*–dimethyl–N'–(1,1,3,3–tetramethylpropyl)formamidinium] [(cyano)B(methimazolyl)$_3$] (**2.19**) (102.7 mg, 0.18 mmol) and [Ru(*p*–cymene)Cl_2]$_2$ (54.2 mg, 0.09 mmol) were dissolved in MeOH and stirred overnight. Ammonium hexafluorophosphate (29.4 mg, 0.18 mmol) was then added and a precipitate formed immediately. The precipitate was filtered and washed with MeOH (3 x 2 mL) and Et_2O (3 x 3 mL). The target material was isolated as a red solid (88.9 mg, 65%). X–ray quality crystals were grown from vapour diffusion of Et_2O into a concentrated solution of the complex in acetonitrile. MS (ESI^+) *m*/*z*: 611.9 [M^+]; ^{1}H-NMR (400 MHz, $CDCl_3$) δ 7.19 (s, 3H, 3 x C*H*), 6.82 (d, *J* = 2.1 Hz, 3H, 3 x C*H*), 4.94 – 5.19 (m, 4H, 4 x C*H*), 3.49

(s, 9H, 3 x NCH_3), 2.87 (dt, *J* = 13.9, 7.10 Hz, 1H, C*H*), 2.07 (s, 3H, CH_3), 1.19 (t, *J* = 6.94 Hz, 6H, 2 x CH_3) ppm; ^{13}C-NMR (126 MHz, $CDCl_3$) δ 158.0, (*C*=S), 128.6 (q, *J* = 80 Hz, NC–B), 122.7 (3 x *C*H), 121.6 (3 x *C*H), 107.2 (C_q), 101.3 (C_q), 85.2 (*C*H), 84.6 (*C*H), 84.5 (*C*H), 83.6 (*C*H), 53.5 (CH), 35.2 (3 x *C*H_3), 30.3 (0.5 x *C*H_3), 29.7 (0.5 x *C*H_3), 22.9 (0.5 x *C*H_3), 22.1 (0.5 x *C*H_3), 18.9 (*C*H_3) ppm; ^{11}B-NMR (128.3 MHz, CD_3CN) δ: –5.0 ppm; Elemental analysis: expected for $C_{47}H_{49}B_2N_7RuS_3$ (930.83): C, 60.65; H, 5.31; N, 10.53, found: C, 60.78; H, 5.39; N, 10.54 %; IR 2218 cm^{-1} (C≡N).

6.3 Chapter Three

6.3.1 Starting Materials

6.3.1.1 6–Methyl–1,8–diazabicycloundec–7–ene (3.4)

A solution of 1,8–diazabicycloundec–7–ene (1.012 g, 6.65 mmol) in dry THF (10 mL) was cooled to –78°C in a dry ice/acetone bath under N_2 before addition of *n*–butyllithium (1.6 M in hexane, 4.1 mL, 1 eq.). The colourless solution immediately turned yellow and this solution was stirred at –78°C for 1h before addition of iodomethane (404 μL, 1 eq.). The solution was stirred for a further 1 h before the solution was allowed to return to ambient temperature. The reaction was quenched with NaOH (15% solution, 5 mL) and extracted with DCM (3 x 20 mL). The organic layer was dried over $MgSO_4$ and the solvent removed *in vacuo* to yield the crude product as a yellow oil which was purified by Kugelrohr distillation (100°C, 1.2 mbar) to yield the target material as a colourless oil (649 mg, 59%). HRMS (EI) Calcd. for $C_{10}H_{18}N_2$ (M^+) requires *m*/*z* = 166.14645, found *m*/*z* = 166.14643; ^{1}H-NMR (500 MHz, $CDCl_3$) δ 3.55 (dd, *J* = 14.8, 11.0 Hz, 1H), 3.48 – 3.35 (m, 1H), 3.35 – 3.12 (m, 4H), 2.92 (dd, *J* = 14.9, 5.5 Hz, 1H), 2.65 – 2.48 (m, 1H), 1.98 – 1.78 (m, 2H), 1.78 – 1.63 (m, 2H), 1.63 – 1.50 (m, 1H), 1.41 (tt, *J* = 12.6, 9.4 Hz, 2H), 1.14

(d, J = 6.9 Hz, 3H) ppm; ^{13}C-NMR (126 MHz, $CDCl_3$) δ 163.1 (C_q), 51.9 (NCH_2), 48.8 (NCH_2), 44.4 (NCH_2), 37.7 (CH), 34.6 (CH_2), 28.6 (CH_2), 27.9 (CH_2), 22.6 (CH_2), 19.4 (CH_3) ppm.

6.3.1.2 General route for the synthesis of 4–substituted imidazolines

1.1.1.1.6. Amino Acid Esterification:

The enantiopure *L*–amino acid (*ca.* 5 g) was suspended in ice–cooled methanol (50 mL) and thionyl chloride (1.1 eq.) was added slowly. The resulting solution was refluxed overnight. After cooling the solvent was removed *in vacuo* to give the amino acid methylester hydrochloride salt as a white solid which was used in the next step without further purification.

1.1.1.1.7. N–Methylamide synthesis:

The amino acid methylester hydrochloride salt was treated with methylamine (40% solution in water, *ca.* 15 mL) and heated to 40°C for *ca.* 4 h or until the ^{1}H-NMR spectrum of a sample of the reaction mixture indicated full conversion to the amino acid N–methylamide. The amide was then extracted with DCM (3 x 50 mL). The organic layer was dried over $MgSO_4$ and the solvent removed *in vacuo* to give the amino acid N–methylamide as a pale yellow oil which was used in the next step without further purification.

1.1.1.1.8. LAH reduction of the N–methylamide

To an ice–cooled suspension of $LiAlH_4$ (5 eq.) in THF (*ca.* 500 mL) was added the amino acid N–methylamide from Step 2. The suspension was heated to reflux for 72 h before cooling to rt. The reaction mixture was then treated according to the Feiser LAH workup procedure using H_2O (1 mL/gLAH), NaOH (15% solution, 1 mL/gLAH) and finally H_2O (3 mL/gLAH) with vigourous stirring. The reaction mixture was filtered and washed with THF

(3 x 200 mL). The filtrate was dried with $MgSO_4$, filtered and the solvent removed *in vacuo* to yield the N–methyldiamine as a pale yellow oil which was used in the next step without further purification.

1.1.1.1.9. Diamine cyclization:

DMF–dimethylacetal was added to a solution of the diamine (1 eq.) in THF (20 mL). The solution was heated to reflux for 8 h after which time the solvent was removed *in vacuo* and the residue purified by Kugelrohr distillation to give the target N–methylimidazoline.

6.3.1.3 1–Methyl–4–benzylimidazole (S-3.10)

Colourless oil (679.7 mg, 26%): bp 150°C, 1 mbar; HRMS (EI) Calcd. for $C_{11}H_{14}N_2$ [M^+] requires *m*/*z* = 174.11515, found *m*/*z* = 174.11505; ^{1}H-NMR (400 MHz, $CDCl_3$) δ 7.41 – 7.11 (m, 6H), 6.77 (d, *J* = 1.2 Hz, 1H), 4.47 – 4.22 (m, 1H), 3.19 (t, *J* = 9.5 Hz, 1H), 3.15 (dd, *J* = 13.6, 5.6 Hz, 1H), 2.87 (t, *J* = 8.8 Hz, 1H), 2.80 (s, 3H), 2.67 (dt, *J* = 16.1, 8.0 Hz, 1H) ppm; ^{13}C-NMR (126 MHz, $CDCl_3$) δ 157.5 (*C*H), 139.1 (C_q), 129.2 (2 x *C*H), 128.4 (2 x *C*H), 126.2 (*C*H), 68.6 (*C*H), 55.5 (CH_2), 42.4 (CH_2), 34.2 (NCH_3), 30.4 (*C*H) ppm.

6.3.1.4 1–Methyl–4–phenylimidazole (S-3.11)

Colourless oil (997.0 mg, 35%): bp 150°C, 3.1 mbar; HRMS (EI) Calcd. for $C_{10}H_{12}N_2$ [M^+] requires *m*/*z* = 160.09950, found *m*/*z* = 160.09951; ^{1}H-NMR (400 MHz, $CDCl_3$) δ 7.39 – 7.23 (m, 5H), 6.95 (d, *J* = 1.5 Hz, 1H), 5.18 (td, *J* = 10.2, 1.6 Hz, 1H), 3.68 (t, *J* = 9.0 Hz, 1H), 3.04 (t, *J* = 9.2 Hz, 1H), 2.88 (s, 3H) ppm; ^{13}C-NMR (101 MHz, $CDCl_3$) δ 158.1 (*C*H), 143.9 (C_q), 128.5 (2 x *C*H), 127.0 (2 x *C*H), 126.6 (*C*H), 70.4 (*C*H), 58.6 (CH_2), 34.2 (NCH_3), 30.4 (CH) ppm.

6.3.1.5 1–Methyl–4–isopropylimidazole (S-3.13)

Colourless oil (728.7 mg, 14%): bp 125°C, 30 mbar; HRMS (EI) Calcd. for $C_7H_{14}N_2$ [M^+] requires *m*/*z* = 126.11515, found *m*/*z* = 126.11525; ^{1}H-NMR (500 MHz, $CDCl_3$) δ 6.70 (d, *J* = 1.3 Hz, 1H), 3.86 – 3.69 (m, 1H), 3.26 (dd, *J* = 9.9, 9.2 Hz, 1H), 2.78 (s, 3H), 2.75 (t, *J* = 9.4 Hz, 1H), 1.78 – 1.60 (m, 1H), 0.97 (d, *J* = 6.7 Hz, 3H), 0.86 (d, *J* = 6.8 Hz, 3H) ppm; ^{13}C-NMR (126 MHz, $CDCl_3$) δ 157.1 (*C*H), 73.6 (*C*H), 53.6 (CH_2), 34.2 (NCH_3), 33.2 (*C*H), 19.1 (CH_3), 18.5 (CH_3) ppm.

6.3.1.6 1–Methyl–4–isobutylimidazole (S,S-3.12)

Colourless oil (958 mg, 18%): bp 137°C, 12 Torr; HRMS (EI) Calcd. for $C_8H_{16}N_2$ [M^+] requires *m*/*z* = 140.13863, found *m*/*z* = 141.13887; ^{1}H-NMR (400 MHz, $CDCl_3$) δ 6.72 (s, 1H), 3.91 (ddd, *J* = 10.0, 9.0, 4.0 Hz, 1H), 3.23 (t, *J* = 9.6 Hz, 1H), 2.79 (d, *J* = 0.9 Hz, 3H), 2.75 (t, *J* = 9.5 Hz, 1H), 1.72 – 1.49 (m, 1H), 1.29 – 1.12 (m, 1H), 0.92 (dd, *J* = 7.7, 6.9 Hz, 5H), 0.85 – 0.79 (m, 3H) ppm; ^{13}C-NMR (101 MHz, $CDCl_3$) δ 157.1 (*C*H), 72.2 (*C*H), 53.3 (CH_2), 39.7 (*C*H(CH_3)(C_2H_5)), 34.4 (NCH_3), 26.3 (CH_2), 14.7 (CH_3), 11.6 (CH_2CH_3) ppm.

6.3.2 Ligand Synthesis

6.3.2.1 [6–methyl–2,3,4,6,7,8,9,10–octahydropyrimido[1,2–a] azepinium][tetrakis(methimazolyl)borate] (3.6)

6–Methyl–1,8–diazabicycloundec–7–ene (238 μL, 1.46 mmol, 1 eq.) was added to a stirred suspension of methimazole (500.0 mg, 4.38 mmol, 3 eq.) in toluene. To this mixture was added tris(dimethylamino)borane (256 μL, 1.46 mmol 1 eq.) and the suspension heated to reflux for 72 h. After cooling to room temperature the precipitate which had formed was filtered and washed with hot toluene (3 x 10 mL, 50°C), diethyl ether (3 x 10 mL) and dried *in vacuo*. The target material was isolated as a pale blue solid (103 mg, 11%). MS (ESI$^+$) *m*/*z*: 630.7 [M^+], 463.1 [$B(mt)_4$], 167.3 [6–MeDBUH$^+$]; ^{1}H-NMR (500

MHz, d_6–DMSO) δ 8.83, (br. s, 1H), 6.83 (s, 4H), 6.67 (d, *J* = 1.9 Hz, 4H), 3.89 – 3.71 (m, 1H), 3.35 (m, 5H), 3.35 (s, 12H), 3.15 – 3.01 (m, 1H), 2.03 – 1.82 (m, 2H), 1.82 – 1.58 (m, 4H), 1.58 – 1.35 (m, 2H), 1.17 (d, *J* = 7.0 Hz, 3H) ppm; ^{13}C-NMR (126 MHz, d_6–DMSO) δ 167.3 (*C*=S), 164.1 (C_q), 124.2 (4 x *C*H), 115.0 (4 x *C*H), 54.9 (NCH_2), 52.8 (NCH_2), 48.6 (NCH_2), 38.1 (*C*H), 35.7 (CH_2), 33.8 (NCH_3), 31.4 (CH_2), 26.4 (CH_2), 25.34 (CH_2), 18.8 (CH_3) ppm; ^{11}B-NMR (128 MHz, $CDCl_3$) δ 0.8 ppm.

6.3.2.2 (1–Methylimidazolium)tris(methimazolyl)borate (3.7)

1–Methylimidazoline (106.4 mg, 1.26 mmol, 1 eq.) was added to a suspension of (dimethylammonium)tris(methimazolyl)borate (504.0 mg, 1.27 mmol, 1 eq.) in toluene (*ca.* 15 mL). The suspension was heated to reflux for 12 h before cooling to rt. The precipitate which formed was filtered and washed with hot toluene (3 x 10 mL, 50°C), diethyl ether (3 x 10 mL) and dried *in vacuo*. The target material was isolated as a pale green hygroscopic solid (196.8 mg, 46%). MS (EI$^+$) *m*/*z*: 434.0 [M$^+$]; ^{1}H-NMR (500 MHz, $CDCl_3$) δ 8.38 (s, 1H), 6.73 (br. s, 3H), 6.69 (d, 3H, *J* = 2.0 Hz), 4.29 (br. s, 1H), 4.01 – 3.70 (m, 3H), 3.50 (d, *J* = 10.4 Hz, 9H), 3.09 (s, 3H) ppm; ^{13}C-NMR (126 MHz, $CDCl_3$) δ 163.9 (*C*=S), 160.7 (*C*H), 122.2 (3 x *C*H), 117.5 (3 x *C*H), 50.8 (NCH_3), 49.3 (CH_2), 34.8 (3 x CH_3), 21.4 (CH_2) ppm; ^{11}B-NMR (128 MHz, $CDCl_3$) δ 0.3 ppm; Elemental analysis: expected for $C_{16}H_{23}BN_8S_3{\cdot}H_2O$ (452.43): C, 42.48; H, 5.57; N, 24.77, found: C, 42.14; H, 5.24; N, 24.78 %;

6.3.2.3 (1–Methyl–4–benylimidazolium)tris(methimazolyl)borate (3.14)

1–Methyl–4–benzylimidazoline (106.4 mg, 1.26 mmol, 1 eq.) was added to a suspension of (dimethylammonium)tris(methimazolyl)borate (504.0 mg, 1.27 mmol, 1 eq.) in toluene (*ca.* 15 mL). The suspension was heated to reflux for 12 h before cooling to rt. The precipitate which formed was filtered and

washed with hot toluene (3 x 10 mL, 50°C), diethyl ether (3 x 10 mL) and dried *in vacuo*. The target material was isolated as a white powder (354.6 mg, 54%). Analytically pure material was obtained by recrystallization from EtOH/Et_2O. MS (EI^+) *m*/*z*: 524.1 [M^+]; ^{1}H-NMR (500 MHz, $CDCl_3$) δ 7.76 (s, 1H), 7.48 – 7.15 (m, 5H), 7.15 (br. s, 1H), 6.88 (br. s, 1H), 6.72 (s, 3H), 6.17 (br. s, 1H), 4.61 (br. s, 1H), 3.63 (s, 10H), 3.37 (s, 1H), 3.14 (s, 3H), 2.94 (s, 1H), 2.37 (s, 1H) ppm; ^{13}C-NMR (126 MHz, $CDCl_3$) δ 164.6 (*C*=S), 163.9 (*C*H), 137.6 (C_i), 130.0 (2 x *C*H), 128.8 (2 x *C*H), 126.7 (*C*H), 122.0 (3 x *C*H), 117.8 (3 x *C*H), 62.3 (*C*H), 56.0 (CH_2), 37.6 (CH_2), 35.0 (CH_3), 32.6 (*C*H) ppm; Elemental analysis: expected for $C_{23}H_{29}BN_8S_3$·2EtOH (616.67): C, 52.59; H, 6.70; N, 18.17, found: C, 52.07; H, 6.81; N, 18.26 %.

6.3.2.4 (1–Methyl–4–phenylimidazolium)tris(methimazolyl)borate (3.15)

1–Methyl–4–phenylimidazoline (221 μL, 1.26 mmol, 1 eq.) and tris(dimethylamino)borane (256 μL, 1.26 mmol, 1 eq.) were added to a suspension of methimazole (503.7 mg, 4.4 mmol, 3 eq.) in toluene (*ca.* 15 mL). The suspension was heated to reflux for 12 h before cooling to rt. The precipitate which formed was filtered and washed with hot toluene (3 x 10 mL, 50°C), diethyl ether (3 x 10 mL) and recrystallized from MeOH/Et_2O. The pure material was washed with further diethyl ether (3 x 5 mL) and dried *in vacuo* to yield the target material as a white powder (313.3 mg, 42%). MS (EI^+) *m*/*z*: 510.1 [M^+]; ^{1}H-NMR (400 MHz, $CDCl_3$) δ 7.59 (s, 1H), 7.23 (tdd, *J* = 16.9, 12.6, 5.4 Hz, 5H), 6.51 (br. s, 6H), 4.31 (t, *J* = 11.0 Hz, 1H), 3.91 – 3.29 (br. m, 11H, 3 x N*CH*$_3$ and *CH*$_2$), 3.17 (s, 3H) ppm; ^{13}C-NMR (126 MHz, $CDCl_3$) δ 165.3 (*C*=S), 163.8 (*C*H), 140.2 (C_i), 128.9 (2 x *C*H), 127.7 (3 x *C*H), 127.6 (2 x *C*H), 126.5 (*C*H), 117.1 (3 x *C*H), 60.5 (*C*H), 53.7 (CH_2), 35.0 (NCH_3), 34.7 (3 x NCH_3) ppm; ^{11}B-NMR (128 MHz, $CDCl_3$) δ 0.8 ppm;

Elemental analysis: expected for $C_{22}H_{27}BN_8S_3$ (510.51): C, 51.76; H, 5.33; N, 21.95, found: C, 51.36; H, 5.20; N, 21.47 %.

6.3.2.5 (1–Methyl–4–isobutylimidazolium)tris(methimazolyl)borate (3.16)

1–Methyl–4–isobutylimidazoline (204.7 mg, 1.26 mmol, 1 eq.) and tris(dimethylamino)borane (256 μL, 1.26 mmol, 1 eq.) were added to a suspension of methimazole (506.6 mg, 4.4 mmol, 3 eq.) in toluene (*ca.* 15 mL). The suspension was heated to reflux for 12 h before cooling to rt. Half of the solvent was removed *in vacuo* and diethyl ether (*ca.* 5 mL) and hexane (*ca.* 5 mL) added. The solution was stored overnight at –30°C whereupon a white precipitate formed from the reaction mixture. The precipitate was filtered, washed with hexane (3 x 5 mL) and dried *in vacuo* to yield the target material as a white powder (472.3 mg, 42%). Analytically pure material was isolated by slow cooling of a DCM/hexane solution. MS (EI^+) *m*/*z*: 490.1 [M^+]; ^{1}H-NMR (400 MHz, $CDCl_3$) δ 8.08 (s, 1H), 6.68 (d, *J* = 2.3 Hz, 3H), 6.73 – 6.64 (m, 3H), 5.14 (br. s, 1H), 3.82 (t, *J* = 10.9 Hz, 1H), 3.58 (s, 9H), 3.45 (dd, *J* = 10.7, 4.4 Hz, 1H), 3.08 (s, 3H), 1.30 (m, 2H), 1.04 (d, *J* = 6.6 Hz, 3H), 1.00 – 0.91 (m, 1H), 0.72 (t, *J* = 7.3 Hz, 3H) ppm; ^{13}C-NMR (126 MHz, CDCl3) δ 165.1 (*C*H), 164.1 (*C*=S), 123.0 (3 x *C*H), 117.3 (3 x *C*H), 65.1 (*C*H), 52.2 (CH_2), 36.3 (*C*H), 34.9 (3 x NCH_3), 34.4 (NCH_3), 26.8 (CH_2), 12.5 (CH_3), 11.8 (CH_3) ppm; Elemental analysis: expected for $C_{20}H_{31}BN_8S_3 \cdot ½CH_2Cl_2$ (532.99): C, 46.20; H, 6.05; N, 21.02, found: C, 46.00; H, 6.13; N, 21.36 %.

6.3.2.6 (1–Methyl–4–isopropylimidazolium)tris(methimazolyl)borate (3.17)

1–Methyl–4–isopropylimidazoline (221 μL, 1.26 mmol, 1 eq.) and tris(dimethylamino)borane (256 μL, 1.26 mmol, 1 eq.) were added to a

suspension of methimazole (507.4 mg, 4.4 mmol, 3 eq.) in toluene (*ca.* 15 mL). The suspension was heated to reflux for 12 h before cooling to rt. The precipitate which formed was filtered and washed with hot toluene (3 x 10 mL, 50°C), diethyl ether (3 x 10 mL) and recrystallized from $MeOH/Et_2O$. The pure material was washed with further diethyl ether (3 x 5 mL) and dried *in vacuo* to yield the target material as a white powder (472.3 mg, 42%). MS (EI^+) *m*/*z*: 476.2 [M+]; ^{1}H-NMR (400 MHz, $CDCl_3$) δ 7.00 – 6.39 (m, 7H), 5.39 (br. s, 1H), 3.85 (t, *J* = 10.8 Hz, 1H), 3.61 (s, 9H), 3.47 (dd, *J* = 10.7, 4.4 Hz, 1H), 3.11 (s, 3H), 1.08 (d, *J* = 6.7 Hz, 3H), 0.89 (m, 1H), 0.81 (d, *J* = 7.0 Hz, 3H) ppm; ^{13}C-NMR (126 MHz, $CDCl_3$) δ 165.1 (*C*=S), 164.2 (*C*H), 122.5 (3 x *C*H), 117.4 (3 x *C*H), 65.4 (*C*H), 52.1 (CH_2), 34.9 (3 x NCH_3), 29.8 (NCH_3), 29.7 (*C*H), 19.6 (CH_3), 15.4 (CH_3) ppm; Elemental analysis: expected for $C_{19}H_{29}BN_8S_3$ (476.49): C, 47.89; H, 6.13; N, 23.52, found: C, 48.04; H, 6.24; N, 23.37 %.

6.3.3 Ligand Complexation

6.3.3.1 [{(1–Methylimidazolium)tris(methimazolyl)borate} ruthenium(II)(p–cymene)]bis(hexafluorophosphate) (3.8)

(1–Methylimidazolium)tris(methimazolyl)borate (65.0 mg, 0.15 mmol, 1 eq.) and $[Ru(p\text{–cymene})Cl_2]_2$ (45.8 mg, 0.75 mmol, 0.5 eq.) were dissolved in methanol (*ca.* 5 mL) and stirred for 1 h. Ammonium hexafluorophosphate was added (50 mg, 0.31 mmol, 2 eq.) causing immediate precipitation of an orange solid. The suspension was stirred for a further 1 h to ensure complete metathesis before the precipitate was filtered, washed with methanol (3 x 5 mL) and diethyl ether (3 x 5 mL). The orange solid was then dried *in vacuo* to give the target material as a orange–red powder (78.2 mg, 54%). X–ray quality crystals were grown from slow diffusion of diethyl ether into a concentrated solution of the complex in dichloromethane. MS (ESI^+) *m*/*z*:

335.1 [M^+]; ^{1}H-NMR (400 MHz, CD_3CN) δ 7.70 (s, 1H), 7.18 (d, *J* = 2.2 Hz, 3H), 6.91 (s, 3H), 5.59 – 5.22 (m, 4H), 4.30 – 4.11 (m, 1H), 4.10 – 3.84 (m, 3H), 3.67 (s, 9H), 3.12 (s, 3H), 2.93 (dt, *J* = 14.0, 7.0 Hz, 1H), 2.17 (s, 3H), 1.17 (d, *J* = 6.9 Hz, 6H) ppm; ^{13}C-NMR (101 MHz, CD_3CN) δ 163.0 (*C*=S), 161.1 (*C*H), 123.2 (3 x *C*H), 122.3 (3 x *C*H), 107.8 (C_q), 102.4 (C_q), 86.0 (*C*H), 85.5 (*C*H), 85.0 (*C*H), 83.9 (*C*H), 52.0 (NCH_3), 50.7 (CH_2), 36.0 (3 x NCH_3), 35.6 (CH_2), 31.4 (*C*H), 22.9 ($C(CH_3)_2$), 22.6 ($C(CH_3)_2$), 19.0 (CH_3) ppm; ^{11}B-NMR (128 MHz, CD_3CN) δ –0.1 ppm; Elemental analysis: expected for $C_{26}H_{37}BF_{12}N_8P_2RuS_3$ (959.63): C, 32.54; H, 3.89; N, 11.68, found: C, 32.39; H, 3.78; N, 11.77 %.

6.3.3.2 [{(1–Methyl–4–benylimidazolium)tris(methimazolyl)borate} ruthenium(II)(para–cymene)]bis(hexafluorophosphate) (3.18)

(1–Methyl–4–benzylimidazolium)tris(methimazolyl)borate (108.6 mg, 0.21 mmol, 1 eq.) and [Ru(*p*–cymene)Cl_2]$_2$ (58.4 mg, 0.10 mmol, 0.5 eq.) were dissolved in methanol (*ca.* 5 mL) and stirred for 1 h. Ammonium hexafluorophosphate was added (62.2 mg, 0.38 mmol, 2 eq.) causing immediate precipitation of an orange solid. The suspension was stirred for a further 1 h to ensure complete metathesis before the precipitate was filtered, washed with methanol (3 x 5 mL) and diethyl ether (3 x 5 mL). The orange solid was then dried *in vacuo* to give the target material as an orange–red powder (181.5 mg, 84%). MS (ESI$^+$) *m*/*z*: 379.9 [M^+/2]; ^{1}H-NMR (400 MHz, CD_3CN) δ 7.82 (m, 1H, *maj*), 7.77 (m, 1H, *min*), 7.41–7.13 (m, 8H), 7.05 (s, 1H, *min*), 7.03 (s, 2H, *maj*), 5.53 (d, *J* = 6.1 Hz, 2H), 5.42 (s, 2H), 5.03 – 4.84 (m, 1H), 3.93 – 3.78 (m, 1H), 3.71 (s, 9H), 3.70 – 3.61 (m, 1H), 3.61 – 3.50 (m, 2H), 3.21 (s, 2H, *maj*), 3.18 (s, 1H, *min*), 3.04 – 2.92 (m, 1H), 2.92 – 2.81 (m, 1H), 2.81 – 2.69 (m, 1H), 2.21 (s, 3H), 1.21 (d, *J* = 6.9 Hz, 6H) ppm; ^{13}C-NMR (126 MHz, CD_3CN) δ 162.8 (CH_{min}), 162.3 (CH_{maj}), 161.5 (*C*=S), 135.8 (C_{imaj}), 135.6

(*C*$_{imin}$), 130.5 (*C*H$_{maj}$), 130.3 (*C*H$_{min}$), 130.0 (*C*H$_{min}$), 129.9 (*C*H$_{maj}$), 128.5 (*C*H$_{min}$), 128.4 (*C*H$_{maj}$), 123.4 (3 x *C*H$_{min}$), 123.2 (3 x *C*H$_{maj}$), 122.4 (3 x *C*H), 107.9 (*C*H$_{min}$), 107.9 (*C*H$_{maj}$), 102.5 (*C*H$_{min}$), 102.4 (*C*H$_{maj}$), 86.0 (*C*H$_{maj}$), 85.9 (*C*H$_{min}$), 85.4 (*C*H$_{maj}$), 85.4 (*C*H$_{min}$), 85.0 (*C*H$_{maj}$), 84.9 (*C*H$_{min}$), 84.0 (*C*H$_{maj}$), 83.9 (*C*H$_{min}$), 63.4 (*C*H$_{maj}$), 63.0 (*C*H$_{min}$), 56.0 (*C*H$_{2maj}$), 55.8 (*C*H$_{2min}$), 39.6 (*C*H$_{2maj}$), 38.9 (*C*H$_{2min}$), 36.1 (3 x NCH$_{3maj}$), 36.1 (3 x NCH$_{3min}$), 36.1 (NCH$_{3maj}$), 35.9 (NCH$_{3min}$), 31.4 (*C*H(CH$_3$)$_{2min}$), 31.4 (CH(*C*H$_3$)$_{2maj}$), 23.0 (CH(*C*H$_3$)$_2$), 22.6 (CH(CH$_3$)$_{2min}$), 22.6 (CH(*C*H$_3$)$_{2maj}$), 19.1 (*C*H$_3$), 19.1 (*C*H$_3$) ppm; ^{11}B-NMR (128 MHz, CD$_3$CN) δ 0.1 ppm; Elemental analysis: expected for $C_{33}H_{43}BF_{12}N_8P_2RuS_3$ (1049.75): C, 37.76; H, 4.13; N, 10.67, found: C, 37.70; H, 4.24; N, 10.58 %.

6.3.3.3 [{(1–Methyl–4–phenylimidazolium)tris(methimazolyl)borate} ruthenium(II)(para–cymene)]bis(hexafluorophosphate) (3.19)

(1–Methyl–4–phenylimidazolium)tris(methimazolyl)borate (103.1 mg, 0.2 mmol, 1 eq.) and [Ru(*p*–cymene)Cl$_2$]$_2$ (61.8 mg, 0.10 mmol, 0.5 eq.) were dissolved in methanol (*ca.* 5 mL) and stirred for 1 h. Ammonium hexafluorophosphate was added (68.0 mg, 0.42 mmol, 2 eq.) causing immediate precipitation of an orange solid. The suspension was stirred for a further 1 h to ensure complete metathesis before the precipitate was filtered, washed with methanol (3 x 5 mL) and diethyl ether (3 x 5 mL). The orange solid was then dried *in vacuo* to give the target material as a red powder (159.6 mg, 77%). MS (ESI$^+$) *m*/*z*: 372.7 [M$^+$/2]; ^{1}H-NMR (400 MHz, CD$_3$CN) δ 8.03 (s, 1H, *maj*), 7.99 (s, 1H, *min*), 7.51 – 7.22 (m, 5H), 7.13 (dd, *J* = 31.4, 2.3 Hz, 3H), 7.06 (s, 3H), 5.68 – 5.26 (m, 4H), 4.50 (dd, *J* = 27.5, 15.8 Hz, 1H), 3.82 – 3.62 (m, 2H), 3.70 – 3.62 (m, 9H), 3.21 (d, *J* = 6.6 Hz, 3H), 3.01 – 2.85 (m, 2H), 2.18 (d, *J* = 2.3 Hz, 3H), 1.25 – 1.16 (m, 6H) ppm; ^{13}C-NMR (126 MHz, CD$_3$CN) δ 164.1 (*C*H$_{min}$), 163.2 (*C*H$_{maj}$), 160.4 (*C*=S), 160.3 (*C*=S), 140.5 (*C*$_{imaj}$),

140.5 (C_{imin}), 129.8 (2 x CH_{min}), 129.5 (2 x CH_{maj}), 129.1 (2 x CH_{min}), 128.7 (2 x CH_{maj}), 125.8 (CH_{min}), 125.5 (CH_{maj}), 122.1 (3 x CH_{min}), 122.0 (3 x CH_{maj}), 121.6 (3 x CH), 106.9 (C_{qmin}), 106.9 (C_{qmaj}), 101.4 (C_{qmaj}), 101.4 (C_{qmin}), 84.9 (CH_{maj}), 84.9 (CH_{min}), 84.4 (CH_{maj}), 84.3 (CH_{min}), 83.9 (CH), 82.9 (CH_{min}), 82.8 (CH_{maj}), 64.4 (CH_{min}), 62.9 (CH_{maj}), 60.9 (CH_{2maj}), 60.1 (CH_{2min}), 35.1 (3 x NCH_3), 35.0 (NCH_{3maj}), 34.9 (NCH_{3min}), 30.4 ($CH(CH_3)_2$), 22.0 (CH_{3min}), 21.9 (CH_{3maj}), 21.6 (CH_{3maj}), 21.5 (CH_{3min}), 18.1 (CH_{3min}), 18.0 (CH_{3maj}) ppm; ^{11}B-NMR (128 MHz, $CDCl_3$) δ 0.6 ppm; Elemental analysis: expected for $C_{32}H_{41}BF_{12}N_8P_2RuS_3$ (1035.73): C, 37.11; H, 3.99; N, 10.82, found: C, 37.04; H, 4.09; N, 10.71 %.

6.3.3.4 [{(1–Methyl–4–isobutylimidazolium)tris(methimazolyl)borate} ruthenium(II)(para–cymene)]bis(hexafluorophosphate) (3.20)

(1–Methyl–4–isobutylimidazolium)tris(methimazolyl)borate (99.1 mg, 0.20 mmol, 1 eq.) and [Ru(*p*–cymene)Cl_2]$_2$ (63.8 mg, 0.10 mmol, 0.5 eq.) were dissolved in methanol (*ca.* 5 mL) and stirred for 1 h. Ammonium hexafluorophosphate was added (67.9 mg, 0.42 mmol, 2 eq.) effecting precipitation of an orange solid after *ca.* 5 mins. The suspension was stirred for a further 1 h to ensure complete metathesis before the precipitate was filtered, washed with methanol (3 x 5 mL) and diethyl ether (3 x 5 mL). The orange solid was then dried *in vacuo* to give the target material as a red powder (101.5 mg, 50%). MS (ESI$^+$) *m*/*z*: 362.5 [M$^+$/2]; ^{1}H-NMR (500 MHz, $CDCl_3$) δ 7.72 (s, 1H), 7.18 (d, *J* = 2.1 Hz, 3H), 6.87 (s, 1H, *min*), 6.82 (s, 2H, *maj*), 5.51 – 5.32 (m, 4H), 4.63 – 4.49 (m, 1H), 4.00 – 3.84 (m, 1H), 3.82 – 3.71 (m, 1H), 3.67 (d, *J* = 1.9 Hz, 9H), 3.15 (s, 2H, *maj*), 3.12 (s, 1H, *min*), 2.93 (dt, *J* = 13.8, 6.9 Hz, 1H), 2.17 (s, 3H), 1.70 – 1.56 (m, 1H), 1.29 (tdd, *J* = 19.3, 13.5, 7.3 Hz, 1H), 1.20 – 1.15 (m, 6H), 0.86 (ddd, *J* = 15.2, 14.2, 6.9 Hz, 6H) ppm; ^{13}C-NMR (126 MHz, $CDCl_3$) δ 163.4 (CH_{min}), 163.2 (CH_{maj}), 161.7 (C=S_{maj}),

161.4 (*C*=S*min*), 123.3 (3 x *C*H*min*), 123.2 (3 x *C*H*maj*), 122.4 (3 x *C*H*min*), 122.3 (3 x *C*H*maj*), 107.9 (*C*q*min*), 107.8 (*C*q*maj*), 102.4 (*C*q), 85.9 (*C*H*maj*), 85.8 (*C*H*min*), 85.4 (*C*H*maj*), 85.3 (*C*H*min*), 84.9 (*C*H*maj*), 84.8 (*C*H*min*), 83.9 (*C*H*maj*), 83.8 (*C*H*min*), 66.1 (*C*H*min*), 65.1 (*C*H*maj*), 53.0 (*C*H$_2$*maj*), 52.2 (*C*H$_2$*min*), 37.8 (*C*H(CH$_3$)(CH$_2$CH$_3$)*maj*), 37.6 (*C*H(CH$_3$)(CH$_2$CH$_3$)*min*), 36.1 (3 x NCH$_3$*maj*), 36.0 (3 x NCH$_3$*min*), 35.6 (NCH$_3$*maj*), 35.3 (NCH$_3$*maj*), 31.4 (*C*H(CH$_3$)$_2$*min*), 31.4 (*C*H(CH$_3$)$_2$*maj*), 26.4 (*C*H$_2$*min*), 26.1 (*C*H$_2$*maj*), 22.9 (CH(*C*H$_3$)$_2$*min*), 22.9 (CH(*C*H$_3$)$_2$*maj*), 22.6 (CH(*C*H$_3$)$_2$*min*), 22.6 (CH(*C*H$_3$)$_2$*maj*), 19.1 (*C*H$_3$*min*), 19.0 (*C*H$_3$*maj*), 12.0 (*C*H$_3$*min*), 11.7 (*C*H$_3$*maj*), 11.6 (*C*H$_3$*maj*), 11.4 (*C*H$_3$*min*) ppm; Elemental analysis: expected for $C_{30}H_{45}BF_{12}N_8P_2RuS_3$ (1001.71): C, 35.47; H, 4.47; N, 11.03, found: C, 35.50; H, 4.48; N, 11.13 %.

6.3.3.5 [{(1–Methyl–4–isopropylimidazolium)tris(methimazolyl)borate} ruthenium(II)(para–cymene)]bis(hexafluorophosphate) (3.21)

(1–Methyl–4–isopropylimidazolium)tris(methimazolyl)borate (100.8 mg, 0.21 mmol, 1 eq.) and [Ru(*p*–cymene)Cl_2]$_2$ (61.8 mg, 0.10 mmol, 0.5 eq.) were dissolved in methanol (*ca.* 5 mL) and stirred for 1 h. Ammonium hexafluorophosphate was added (68.4 mg, 0.42 mmol, 2 eq.) effecting precipitation of an orange solid after *ca.* 5 mins. The suspension was stirred for a further 1 h to ensure complete metathesis before the precipitate was filtered, washed with methanol (3 x 5 mL) and diethyl ether (3 x 5 mL). The orange solid was then dried *in vacuo* to give the target material as a red powder (139.6 mg, 66%). MS (ESI$^+$) *m*/*z*: 355.5 [M$^+$/2]; ^{1}H-NMR (500 MHz, CD_3CN) δ 7.75 (s, 1H), 7.21 (d, *J* = 2.2 Hz, 3H), 6.90 (s, 1H, *min*), 6.85 (s, 2H, *maj*), 5.63 – 5.22 (m, 4H), 4.64 – 4.44 (m, 1H), 3.96 (dt, *J* = 26.6, 11.6 Hz, 1H), 3.88 – 3.73 (m, 1H), 3.73 – 3.62 (m, 9H), 3.19 (s, 2H, *maj*), 3.15 (s, 1H, *min*), 2.96 (dt, *J* = 13.8, 6.9 Hz, 1H), 1.92–1.81 (m, 1H), 1.24 – 1.16 (m, 6H), 0.91 (dd,

J = 6.8, 4.5 Hz, 2H, *min*), 0.86 (dd, *J* = 13.1, 6.9 Hz, 4H, *maj*) ppm; ^{13}C-NMR (126 MHz, CD_3CN) δ 162.3 (C=S_{min}), 162.2 (C=S_{maj}), 160.7 (CH_{maj}), 160.5 (CH_{min}), 122.3 (3 x CH_{maj}), 122.2 (3 x CH_{min}), 121.4 (3 x CH_{min}), 121.2 (3 x CH_{maj}), 106.9 (C_{qmin}), 106.9 (C_{qmaj}), 101.4 (C_{qmin}), 101.4 (C_{qmaj}), 84.9 (CH_{maj}), 84.8 (CH_{min}), 84.4 (CH_{maj}), 84.3 (CH_{min}), 84.0 (CH_{maj}), 83.8 (CH_{min}), 82.9 (CH_{maj}), 82.8 (CH_{min}), 65.6 (CH_{min}), 64.7 (CH_{maj}), 51.6 (NCH_{3maj}), 50.8 (NCH_{3min}), 35.1 (3 x NCH_{3maj}), 35.1 (3 x NCH_{3min}), 34.6 (CH_{2maj}), 34.4 (CH_{2maj}), 30.4 ($CH(CH_3)_{2min}$), 30.4 ($CH(CH_3)_{2maj}$), 30.4 ($CH(CH_3)_{2maj}$), 30.3 ($CH(CH_3)_{2min}$), 22.0 (CH_{3min}), 21.9 (CH_{3maj}), 21.6 (CH_{3min}), 21.6 (CH_{3maj}), 18.1 (CH_{3min}), 18.1 (CH_{3maj}), 17.6 (CH_{3min}), 17.0 (CH_{3maj}), 13.8 (CH_{3min}), 13.2 (CH_{3maj}) ppm; Elemental analysis: expected for $C_{29}H_{43}BF_{12}N_8P_2RuS_3$ (1001.71): C, 34.77; H, 4.33; N, 11.19, found: C, 34.76; H, 4.24; N, 11.11 %.

6.4 Chapter Four

6.4.1 (Dimethylammonium)tris(pyrid–2–onyl)borate (4.1)

2–Hydroxypyridine (400.6 mg, 4.21 mmol, 3 eq.) was suspended in toluene (20 mL). Tris(dimethylamino)borane (245 μL, 1.40 mmol) was added and the reaction mixture refluxed for 4 h evolving a basic gas after 15 min. The reaction mixture was allowed to cool to ambient temperature before half of the solvent was removed *in vacuo*. The precipitate which formed was filtered by cannula, washed with toluene (3 x 5 mL) and diethyl ether (3 x 10 mL) and dried *in vacuo* to give the target material as a white powder (286 mg, 60.3%); MS (EI) *m*/*z* = 339.1 [M^++1]; ^{1}H-NMR ($CDCl_3$, 400 MHz) δ 8.01 (dd, *J* = 8.3 Hz, 3H), 7.81 (s, 1H), 7.42 (td, *J* = 2.1, 7.7 Hz, 3H), 6.86 (d, *J* = 8.2 Hz, 3H), 6.71 (td, *J* = 1.5, 13.0 Hz, 3H), 2.84 (d, *J* = 4.8 Hz, 6H) ppm; ^{13}C-NMR (126 MHz, $CDCl_3$) δ 163.4 (C_q), 147.2 (CH_{Ar}), 138.5 (CH_{Ar}), 116.6 (CH_{Ar}), 113.7 (CH_{Ar}), 36.8 ($N(CH_3)_2$) ppm. ^{11}B-NMR ($CDCl_3$, 400 MHz) δ 2.2 ppm.

Elemental analysis: expected for $C_{17}H_{19}BN_4O_3$ (338.17): C, 60.38; H, 5.66; N, 16.57, found: C, 60.23, H, 5.50, N, 16.46 %.

6.4.2 (Dimethylaminopyridinium)tris(pyrid–2–onyl)borate (4.2)

2–Hydroxypyridine (1.0033 g, 10.55 mmol, 3 eq.) was suspended in toluene (15 mL). Tris(dimethylamino)borane (616 μL, 3.52mmol, 1 eq.) was added and the reaction mixture was heated to reflux evolving a basic gas after 15 min.. After four hours DMAP (431.1 mg, 3.53 mmol, 1 eq.) was added to the reaction mixture and the reaction was refluxed for a further 6 h during which time a white precipitate formed. The precipitate was filtered by cannula and washed with toluene (3 x 5 mL) and Et_2O (3 x 10 mL) to give the target material as a white solid (1.005 g, 69%); Analytically pure samples were prepared by recrystallization of the ligand from chloroform and diethyl ether. Crystals suitable for X–ray structure determination were obtained by slow diffusion of diethyl ether into a concentrated solution of the ligand in DCM. MS (FAB$^+$) *m*/*z* = 414.7 [M$^+$–1]; ^{1}H-NMR ($CDCl_3$, 400 MHz) δ 8.78 (d, *J*= 7.4 Hz, 2H), 8.04 (dd, *J* = 1.6, 4.9 Hz, 3H), 7.38 (td, *J* = 2.2, 7.4 Hz, 3H), 6.98 (d, *J* = 8.2 Hz, 3H), 6.65 (td, *J* = 1.0, 5.9 Hz, 3H), 6.52 (d, *J* = 7.6 Hz, 2H), 3.10 (s, 6H) ppm; ^{13}C-NMR (126 MHz, $CDCl_3$) δ 39.6 (N(CH_3)$_2$), 105.5 (CH_{DMAP}), 144.3 (CH_{DMAP}), 156.2 (C_{qDMAP}), 113.0 (CH_{Ar}), 115.8 (CH_{Ar}), 138.3 (CH_{Ar}), 147.8 (CH_{Ar}), 162.9 (C_{qAr}) ppm; ^{11}B-NMR ($CDCl_3$, 400 MHz) δ 2.5 ppm; Elemental analysis: expected for $C_{22}H_{22}BN_5O_3 \cdot ½CHCl_3$ (573.94): C, 56.90; H, 4.78; N,14.75; found: C, 56.53, H, 4.60, N, 14.98 %.

6.4.3 [{(Dimethylaminopyridinium)tris(pyrid–2–onyl)borate}copper(I)chloride] (4.3)

(DMAP)B(2–pyridonyl)$_3$ (250 mg, 0.6 mmol) and copper (I) chloride (59.6 mg, 0.6 mmol) were suspended in DCM yielding a yellow suspension

immediately. The suspension was stirred for 2 h before the precipitate was filtered and washed with DCM (3 x 5 mL) and Et_2O (3 x 5 mL) and dried *in vacuo* to give the target material as an insoluble yellow solid (100 mg, 33%).^{1}H-NMR (500 MHz, d_6–DMSO) δ 8.51 (d, *J* = 6.78 Hz, 2 H), 7.77 – 8.21 (br. s., 3 H), 7.50 (t, *J* = 7.1 Hz, 3 H), 6.86 (d, *J* = 7.25 Hz, 3 H), 6.81 (d, *J* = 6.80 Hz, 2 H), 6.76 (br. s., 3 H), 3.10 (s, 6 H) ppm; ^{13}C-NMR (126 MHz, d_6–DMSO) δ 39.2 (N(CH_3)$_2$), 106.0 (CH_{DMAP}), 112.8 (CH_{Ar}), 116.0 (CH_{Ar}), 138.4 (CH_{Ar}), 142.9 (CH_{DMAP}), 147.4 (CH_{Ar}), 155.9 (C_{qDMAP}), 162.3 (C_{qAr}) ppm; Elemental analysis: expected for $C_{22}H_{22}BClCuN_5O_3$ (514.25): C, 51.38; H, 4.31; N, 13.62; found: C, 51.28, H, 4.42, N, 13.76 %.

6.4.4 Attempted synthesis of [(DMAP)ThpCuPPh$_3$][Cl]

(DMAP)B(2–pyridonyl)$_3$ (50 mg, 0.12 mmol) and copper (I) chloride triphenylphosphine (44 mg, 0.12 mmol) were suspended in $CDCl_3$. The NMR tube was left at room temperature overnight and a few small crystals formed at the bottom of the NMR tube. X–ray crystallography confirmed these to be crystals of [(DMAP)B(2–pyridonyl)$_3$CuCl] (**4.3**).

6.4.5 Attempted synthesis of (HNMe$_2$)ZTmp (4.4)

Tris(dimethylamino)borane (1.59 mL, 9.08 mmol, 1 eq.) was added to a solution of 2–mercaptopyridine (1.0096 g, 9.08 mmol, 1 eq.) in toluene (*ca.* 15 mL). The reaction mixture was heated to reflux for 4 h forming a yellow precipitate after *ca.* 1 h. After cooling to room temperature the precipitate was filtered, washed with toluene (3 x 5 mL) and diethyl ether (3 x 5 mL) and dried *in vacuo* to give a yellow crystalline solid (1.17 g, 62%). MS (EI$^+$) *m*/*z* = 209.1 [M$^+$]; ^{1}H-NMR (500 MHz, CDCl3) δ 7.53 (dd, *J* = 8.7, 0.9 Hz, 1H, H*a*), 7.31 (dd, *J* = 6.2, 0.8, 1H, H*d*), 7.21 (ddd, *J* = 8.7, 6.9, 1.8 Hz, 1H, H*c*), 6.67

(dd, *J* = 6.8, 1.2 Hz, 1H, H*b*), 2.56 (s, 12H, 2 x N(CH_3)$_2$) ppm; ^{11}B (128.3 MHz, $CDCl_3$) δ 25.1 ppm.

6.4.6 Attempted synthesis of (HNMe$_2$)ZTmpm (4.5)

Tris(dimethylamino)borane (781 μL, 4.46 mmol, 1 eq.) was added to a solution of 2–mercaptopyrimidine (500.6 g, 4.46 mmol, 1 eq.) in toluene (*ca.* 15 mL). The reaction mixture was heated to reflux for 4 h forming a yellow precipitate after *ca.* 1 h. After cooling to room temperature the precipitate was filtered, washed with toluene (3 x 5 mL) and diethyl ether (3 x 5 mL) and dried *in vacuo* to give a yellow crystalline solid (311.6 mg, 35%). MS (EI$^+$) *m*/*z* = 209.1 [M$^+$–1]; ^{1}H-NMR (400 MHz, d_6–DMSO) δ 7.78 (d, *J* = 9.0 Hz, 2H), 5.45 (t, *J* = 11.6 Hz, 1H), 3.26 (d, *J* = 8.0 Hz, 6H), 3.08 (d, *J* = 8.1 Hz, 6H) ppm; ^{13}C-NMR (126 MHz, d_6–DMSO) δ 183.9 (C_q), 162.8 (*C*H), 90.0 (2 x *C*H), 45.7 (N(CH_3)$_2$), 37.9 (N(CH_3)$_2$) ppm.

6.5 Chapter Five

6.5.1 Ligand Synthesis

6.5.1.1 (N–(n–butyl)imidazolium)tris(methimazolyl)borate (5.5)

N–*n*–Butylimidazole (1.15 mL, 8.75 mmol, 1 eq.) and tris(dimethylamino)borane (1.5 mL, 8.57 mmol, 1 eq.) were added to a suspension of methimazole (3.0186 g, 26.4 mmol, 3 eq.) in toluene (*ca.* 15 mL). The mixture was heated to reflux whereupon the methimazole dissolved giving a green solution after *ca.* 30 mins. After 4 h $HNMe_2$ evolution slowed and the reaction mixture was cooled to rt. The precipitate which formed was washed with hot toluene (2 x 10 mL) at *ca.* 50℃ and cold diethyl ether (3 x 15 mL) and dried *in vacuo* to give the target material as a white powder (3.0115 g, 74%): MS (EI$^+$) *m*/*z*: 474.3 [M$^+$]; ^{1}H-NMR (400 MHz, $CDCl_3$) δ 9.04 (s, 1H), 6.98 (s, 2H), 6.88 (s, 3H), 6.66 (d, *J* = 2.3 Hz, 3H), 4.01

(dd, *J* = 7.6, 6.4 Hz, 2H), 3.56 (s, 9H), 1.84 (q, *J* = 7.6 Hz, 2H), 1.39 (qt, *J* = 7.5, 7.4, 7.4 Hz, 2H), 0.94 (t, *J* = 7.4 Hz, 3H) ppm; ^{13}C-NMR (126 MHz, $CDCl_3$) δ 164.5 (*C*=S), 142.1 (*C*H), 124.2 (*C*H), 122.0 (*C*H), 119.9 (3 x *C*H), 117.7 (3 x *C*H), 49.3 (CH_2), 34.9 (3 x NCH_3), 32.2 (CH_2), 19.7 (CH_2), 13.5 (CH_3) ppm; ^{11}B-NMR (128 MHz, $CDCl_3$) δ 0.5 ppm. Elemental analysis: expected for $C_{19}H_{27}BN_8S_3$ (474.48): C, 48.10; H,–5.74; N, 23.62; found: C, 47.90; H, 5.70; N, 23.50 %.

6.5.1.2 (N–(n–butyl)imidazolium)tris(N–p–tolyl–imidazolyl–2–thione) (5.8)

N–*n*–butylimidazole (230 μL, 1.75 mmol, 1 eq.) and tris(dimethylamino)borane (307 μL, 1.75 mmol, 1 eq.) were added to a solution of N–*p*–tolyl–imidazolyl–2–thione (1.0050 g, 5.28 mmol, 3 eq.) in toluene and the solution was heated to reflux. After 48 h $HNMe_2$ evolution slowed and the reaction mixture was cooled to rt. Half of the solvent was removed from the reaction mixture and Et_2O added resulting in the precipitation of a pink solid. This was washed with cold toluene (2 x 10 mL) and ether (3 x 15 mL) and dried *in vacuo* to give the target material as a white powder (928.0 mg, 75%): MS (EI$^+$) *m*/*z*: 702.2 [M$^+$]; ^{1}H-NMR (400 MHz, CDCl3) δ 9.22 (s, 1H), 7.61 – 7.43 (m, 7H), 7.36 (s, 3H), 7.27 (s, 4H), 7.07 (s, 2H), 6.85 (d, *J* = 2.4 Hz, 3H), 6.72 – 6.39 (m, 1H), 4.05 (td, *J* = 7.3, 3.3 Hz, 2H), 2.41 (s, 9H), 1.93 – 1.77 (m, 2H), 1.41 (dd, *J* = 15.0, 7.5 Hz, 2H), 0.95 (t, *J* = 7.4 Hz, 3H); ^{13}C-NMR (126 MHz, $CDCl_3$) δ 162.0 (*C*=S), 141.7 (*C*H), 137.9 (C_q), 136.6 (C_q), 129.8 (*C*H), 129.5 (*C*H), 126.8 (*C*H), 125.7 (*C*H), 125.7 (3 x *C*H), 118.4 (3 x *C*H), 49.3 (CH_2), 32.2 (CH_2), 21.2 (3 x CH_3), 19.6 (CH_2), 13.4 (CH_3) ppm;^{11}B-NMR (128 MHz, $CDCl_3$) δ 0.9 ppm; Elemental analysis: expected for

$C_{37}H_{38}BN_8S_3$ (702.77): C, 63.24; H,–5.59; N, 15.94; found: C, 63.30; H, 5.50; N, 15.84 %.

6.5.1.3 (N–(Methyl)imidazolium)tris(N–tert–butyl–imidazolyl–2–thione) (5.9)

N–methylimidazole (116.5 mL, 1.46 mmol, 1 eq.), and tris(dimethylamino)borane (256 μL, 1.46 mmol, 1 eq.) were added to a solution of N–*tert*–butylimidazolyl–2–thione (685.2 mg, 4.38 mmol, 3 eq.) in toluene. The solution was heated to reflux for 24 h before $HNMe_2$ evolution slowed. Half of the solvent was removed *in vacuo* and Et_2O (*ca.* 20 mL) added giving a white precipitate which was filtered, washed with Et_2O (3 x 10 mL) and dried *in vacuo* to give the target material as a white powder (711.9 mg, 87%). MS (EI^+) *m*/*z*: 558.2 [M^+]; ^{1}H-NMR (400 MHz, $CDCl_3$) δ 9.22 (s, 1H), 7.07 (s, 2H), 6.94 (s, 1H), 6.82 (s, 1H), 6.78 (s, 2H), 6.71 (s, 1H), 6.30 (s, 1H), 3.81 (s, 3H), 1.78 (s, 27H) ppm; ^{13}C-NMR (126 MHz, $CDCl_3$) δ 166.1 (*C*=S), 163.9 (*C*=S), 163.6 (*C*=S), 142.8 (*C*H), 124.7 (*C*H), 124.2 (*C*H), 122.2 (*C*H), 121.0 (*C*H), 119.3 (*C*H), 114.3 (2 x *C*H), 113.8 (*C*H), 58.6 (*C*$(CH_3)_3$), 58.4 (*C*$(CH_3)_3$), 58.2 (*C*$(CH_3)_3$), 35.8 (NCH_3), 28.8 – 27.9 (3 x NC(*C*$H_3)_3$) ppm; ^{11}B-NMR (128 MHz, $CDCl_3$) δ 0.6 ppm; Elemental analysis: expected for $C_{25}H_{39}BN_8S_3$ (558.64): C, 53.75; H, 7.04; N, 20.06; found: C, 53.66; H, 6.93; N, 19.86 %.

6.5.2 Ruthenium Complexes

6.5.2.1 Attempted Synthesis of [{κ³–[S,S,S]–(N–MeImid)ZTm}$RuCl_2(PPh_3)$]

(N–methylimidazolium)tris(methimazolyl)borate (114.8 mg, 0.27 mmol, 1.1 eq.) and ruthenium(II)dichloridetris(triphenylphosphine) (229.9 mg, 0.24 mmol, 1 eq.) were dissolved in methanol (*ca.* 5 mL) and stirred for 1h. After this time the reaction mixture had turned from brown to blue. Half of the solvent was removed *in vacuo* and Et_2O added to precipitate out the product.

The precipitate was filtered, washed with toluene (3 x 5 mL) and Et_2O (3 x 5 mL) and dried *in vacuo* to give the product as a deep blue powder which was identified as **5.4a**: MS (ESI$^+$) *m*/*z*: 964.0 [M$^+$–2], *m*/*z:* 322.5 [M$^+$/3]; ^{1}H-NMR (500 MHz, CD_3CN) δ 10.32 (s, 3H), 10.23 (s, 3H), 9.56 (s, 1H), 7.88 (s, 1H), 7.70 (s, 1H), 4.14 (s, 3H), 3.44 (s, 9H) ppm.

6.5.2.2 [{κ³–[S,S,S]–(N–MeImid)ZTm}$_2$Ru][PF$_6$]$_3$ (5.4b)

(N–methylimidazolium)tris(methimazolyl)borate (499.2 mg, 1.15 mmol) and tris(triphenylphosphine)ruthenium(II)dichloride (0.555 g, 0.58 mmol) were dissolved in methanol (*ca.* 5 mL) and stirred for 1h. After this time the reaction mixture had turned from brown to blue. Ammonium hexafluorophosphate (381.5 mg, 2.3 mmol) was added resulting in the formation of a dark precipitate. The precipitate was filtered, washed with toluene (3 x 5 mL) and Et_2O (3 x 5 mL) and dried *in vacuo* to give the product as a deep blue powder (493.1 mg, 61%): MS (ESI$^+$) *m*/*z*: 964.0 [M$^+$–2], *m*/*z:* 322.5 [M$^+$/3]; ^{1}H-NMR (500 MHz, CD_3CN) δ 10.32 (s, 3H), 10.23 (s, 3H), 9.56 (s, 1H), 7.88 (s, 1H), 7.70 (s, 1H), 4.14 (s, 3H), 3.44 (s, 9H) ppm; ^{13}C-NMR (126 MHz, d_6–DMSO) δ 143.4 (*C*H), 126.2 (*C*H), 124.9 (*C*H), 120.2 (3 x *C*H), 119.4 (3 x *C*H), 86.9 (3 x *C*H$_3$), 36.4 (N*C*H$_3$) ppm; ^{11}B-NMR (128.3 MHz, $CDCl_3$) –3.9 ppm; Elemental analysis: expected for $C_{32}H_{42}B_2F_{18}N_{16}P_3RuS_6$ (1400.76): C, 27.44; H, 3.02; N, 16.00; found: C, 27.45; H, 3.09; N, 15.97 %.

6.5.2.3 [{κ³–[S,S,S]–(N– n–Bu–Imid)ZTm}$_2$Ru][PF$_6$]$_3$ (5.6)

(N–*n*–butylimidazolium)tris(methimazolyl)borate (100.5 mg, 0.21 mmol) and tris(triphenylphosphine)ruthenium(II)dichloride (102.4 mg, 0.11 mmol) were dissolved in methanol (*ca.* 5 mL) and stirred for 1h. After this time the reaction mixture had turned from brown to blue. Ammonium hexafluorophosphate (51.8 mg, 0.32 mmol) was added and a blue product

precipitated from solution. The precipitate was filtered, washed with toluene (3 x 5 mL) and Et_2O (3 x 5 mL) and dried *in vacuo* to give the product as a deep blue powder (78 mg, 55%). X–ray quality crystals were grown from slow diffusion of Et_2O into a solution of the complex in a MeCN/MeOH mixture. MS (ESI^+) *m*/*z*: 524.5 [M^+/2]; ^{1}H-NMR (400 MHz, CD_3CN) δ 10.19 (s, 6H), 10.19 (s, 6H), 9.01 (s, 2H), 7.91 (s, 2H), 7.72 (s, 2H), 4.38 (t, *J* = 7.3 Hz, 4H), 3.46 (s, 18H), 2.09 – 1.98 (m, 4H), 1.52 (dq, *J* = 14.9, 7.4 Hz, 4H), 1.07 (t, *J* = 7.4 Hz, 6H) ppm; ^{13}C-NMR (126 MHz, d_6–DMSO) δ 207.0 (*C*=S), 142.1 (*C*H), 126.6 (3 x *C*H), 123.1 (3 x *C*H), 119.7 (*C*H), 118.8 (*C*H), 86.6 (NCH_3), 48.8 (CH_2), 31.6 (CH_2), 19.2 (CH_2), 13.6 (CH_3) ppm; ^{11}B-NMR (128 MHz, d_6–DMSO) δ –3.9 ppm; Elemental Analysis: $C_{38}H_{54}B_2F_{12}N_{16}P_2RuS_6$ (1484.92): C, 30.74; H, 3.67; N, 15.09; found: C, 30.66; H, 3.64; N, 14.98 %;

6.5.2.4 Attempted Synthesis of [{κ³–[S,S,S]–(N–n–Bu–Imid)ZTm^{Tol}}RuCl$_2$(PPh$_3$)]

(N–butylimidazole)tris(1–*p*–tolylimidazol–2–thionyl)borate (104.0 mg, 0.15 mmol, 1.1 eq.) and tris(triphenylphosphine)ruthenium(II)dichloride (136.4 mg, 0.14 mmol, 1 eq.) were dissolved in methanol (*ca.* 5 mL) and stirred for 1h. After this time the reaction mixture had turned from brown to greenish–blue. Half of the solvent was removed *in vacuo* and Et_2O added to precipitate out the product. The precipitate was filtered, washed with toluene (3 x 5 mL) and Et_2O (3 x 5 mL) and dried *in vacuo* to give the product as a deep blue powder which was identified as **5.8a**. MS (ESI) *m*/*z:* 502.0 [M^+/3]; ^{1}H-NMR (500 MHz, CD_3CN) δ 10.42 (s, 3H), 9.39 (s, 3H), 9.03 (s, 1H), 8.12 (s, 1H), 7.77 (s, 1H), 7.31 (d, *J* = 7.9 Hz, 6H), 6.61 (d, *J* = 7.4 Hz, 6H), 4.40 (t, *J* = 7.3 Hz, 2H), 2.18 (s, 9H), 2.12 – 2.02 (m, 2H), 1.66 – 1.45 (m, 2H), 1.10 (t, *J* = 7.4 Hz, 3H).

6.5.2.5 [{κ³–[S,S,S]–(N–n–Bu–Imid)ZTm^{Tol}}$_2$Ru][PF$_6$]$_3$ (5.8b)

(N–*n*–butylimidazole)tris(1–*p*–tolylimidazol–2–thionyl)borate (97.0 mg, 0.14 mmol, 2 eq.) and tris(triphenylphosphine)ruthenium(II)dichloride (68.2 mg, 0.07 mmol, 1 eq.) were dissolved in methanol (*ca.* 5 mL) and stirred for 1h. After this time the reaction mixture had turned from brown to blue. Ammonium hexafluorophosphate (40 mg, 0.25 mmol) was added and the mixture stirred for a further 1 h. Half of the solvent was removed *in vacuo* and Et_2O added to precipitate out the product. The precipitate was filtered, washed with toluene (3 x 5 mL) and Et_2O (3 x 5 mL) and dried *in vacuo* to give the product as a deep blue powder (46.8 mg, 34%). X–ray quality crystals were grown from slow diffusion of Et_2O into a solution of the complex in a MeCN/MeOH mixture. MS (ESI) *m*/*z*: 502.0 [M^+/3]; ^{1}H-NMR (500 MHz, CD_3CN) δ 10.42 (s, 3H), 9.39 (s, 3H), 9.03 (s, 1H), 8.12 (s, 1H), 7.77 (s, 1H), 7.31 (d, *J* = 7.9 Hz, 6H), 6.61 (d, *J* = 7.4 Hz, 6H), 4.40 (t, *J* = 7.3 Hz, 2H), 2.18 (s, 9H), 2.12 – 2.02 (m, 2H), 1.66 – 1.45 (m, 2H), 1.10 (t, *J* = 7.4 Hz, 3H) ppm; ^{13}C-NMR (126 MHz, CD_3CN) δ 167.6 (*C*=S), 142.4 (C_q), 140.40 (C_q), 138.9 (*C*H), 131.4 (*C*H), 130.1 (*C*H), 127.7 (*C*H), 124.3 (*C*H), 120.7 (3 x *C*H), 119.8 (3 x *C*H), 50.5 (CH_2), 32.6 (CH_2), 21.2 (3 x CH_3), 20.2 (CH_2), 13.8 (CH_3) ppm; ^{11}B-NMR (128 MHz, CD_3CN) δ 0.7 ppm; Elemental Analysis expected for $C_{74}H_{78}B_2F_{12}N_{16}P_2RuS_6$ (1796.34): C, 49.47; H, 4.38; N, 12.47; found: C, 49.40; H, 4.46; N, 12.36 %.

6.5.2.6 [{κ²–[S,S]–(N–MeImid)ZTm}RuCl₃(MeOH)] (5.10)

(N–methylimidazolium)tris(methimazolyl)borate (63.0 mg, 0.24 mmol) was stirred with ruthenium(III)trichloride hydrate (102.4 mg, 0.24 mmol) in methanol (*ca.* 5 mL). A precipitate formed after 1h which was filtered and washed with cold MeOH (2 x 5 mL) and $E_{t2}O$ (3 x 5 mL) to give the target material a brownish solid (142 mg, 87%). MS (ESI^+) *m*/*z*: 638.7 [M^+–MeOH] ;

^{1}H-NMR (500 MHz, d_6–DMSO) δ 9.00 (s, 1H), 7.97 (s, 2H), 7.81 (s, 1H), 7.62 (s, 2H), 7.49 (s, 1H), 7.30 (s, 1H), 6.52 (s, 1H), 3.92 (s, 6H), 3.87 (s, 3H), 3.43 (s, 3H) ppm; ^{13}C-NMR (126 MHz, d_6–DMSO) δ 166.1 (*C*=S), 141.7 (*C*=S), 137.5 (*C*H), 127.5 (*C*H), 126.2 (2 x *C*H), 126.0 (2 x *C*H), 124.1 (*C*H), 121.7 (*C*H), 119.7 (*C*H), 37.4 (2 x N*C*H$_3$), 36.2 (N*C*H$_3$), 35.3 (N*C*H$_3$) ppm; ^{11}B-NMR (128 MHz, d_6–DMSO) δ –0.8 ppm; Elemental analysis: expected for $C_{18}H_{24}BCl_3N_9RuS_3$ (680.88): C, 31.75; H, 3.55; N, 18.51; found: C, 31.86; H, 3.60; N, 18.42 %;

6.5.2.7 [{κ^2–[S,S]–(N–MeImid)ZTm}RuCl$_2$(DMSO)$_2$] (5.11)

(N–Methylimidazolium)tris(methimazolyl)borate (99.9 mg, 0.23 mmol) and tetrakis(dimethylsulphoxido)ruthenium(II)chloride (112.3 mg, 0.23 mmol) were stirred in methanol (*ca.* 10 mL). The yellow solution turned brown after *ca.* 15 mins. After 4 h half of the solvent was removed *in vacuo* and the precipitate was filtered and washed with Et_2O (3 x 5 mL) to give the product as a brown solid (153.0 mg, 87%). MS (ESI$^+$) *m/z:* 723.6 [M–Cl]$^+$; ^{1}H-NMR (400 MHz, CDCl3) δ 10.19 (s, 1H), 7.54 (s, 1H), 7.50 (d, *J* = 2.0 Hz, 1H), 7.30 (s, 1H), 7.15 (d, *J* = 2.1 Hz, 1H), 7.04 (d, *J* = 2.0 Hz, 1H), 7.00 (d, *J* = 2.0 Hz, 1H), 6.84 (d, *J* = 2.0 Hz, 1H), 6.39 (d, *J* = 2.0 Hz, 1H), 4.27 (s, 3H), 3.99 (s, 3H), 3.87 (s, 3H), 3.76 (s, 3H), 3.62 (s, 3H), 3.56 (s, 3H), 3.26 (s, 3H), 2.93 (s, 3H) ppm; ^{13}C-NMR (126 MHz, $CDCl_3$) δ 166.3 (C_q), 163.5 (C_q), 163.0 (C_q), 141.6 (*C*H), 125.2 (*C*H), 123.7 (*C*H), 122.4 (*C*H), 122.2 (*C*H), 122.0 (*C*H), 121.8 (*C*H), 121.7 (*C*H), 120.7 (*C*H), 46.2 (CH_3), 46.1 (CH_3), 45.3 (CH_3), 43.6 (CH_3), 37.7 (CH_3), 37.0 (CH_3), 36.3 (CH_3), 35.5 (CH_3) ppm;^{11}B-NMR (128 MHz, CD_3CN) δ 0.7 ppm; Elemental analysis: expected for $C_{20}H_{33}BCl_2N_8O_2RuS_5$ (760.64): C, 31.58; H, 4.37; N, 14.73; found: C, 31.87; H, 4.39; N, 14.64 %;

6.5.3 Rhodium Complexes

6.5.3.1 [{κ³–[S,S,S]–(DMAP)ZTm}$_2$Rh][PF6]$_3$ (5.13)

(*N,N*–Dimethylaminopyridinium)tris(methimazolyl)borate (101.4 mg, 0.21 mmol, 2 eq.) and rhodium(III)chloride hydrate (52.0 mg, 0.21 mmol, 1 eq.) were dissolved in methanol (*ca.* 5 mL) and stirred for 4h. Ammonium hexafluorophosphate (100 mg, 0.20 mmol, 3 eq.) was added forming an orange precipitate almost immediately. The solution stirred for another 1h before the precipitate was filtered, washed with MeOH (2 x 5 mL) and Et_2O (3 x 5 mL) and dried *in vacuo* to give the target material as a red solid (102.0 mg, 66%). X–ray quality crystals were grown from slow diffusion of Et_2O into a solution of the complex in a MeCN/EtOH mixture. MS (ESI$^+$) *m/z:* 349.07 [M$^+$]; ^{1}H-NMR (400 MHz, d_6–DMSO) δ 8.30 (d, *J* = 7.5 Hz, 2H), 7.64 (d, *J* = 2.2 Hz, 3H), 7.05 (d, *J* = 2.2 Hz, 3H), 7.01 (d, *J* = 7.8 Hz, 2H), 3.73 (s, 9H), 3.25 (s, 6H); ^{13}C-NMR (126 MHz, d_6–DMSO) δ 160.3 (*C*=S), 156.5 (C_i), 145.0 (2 x *C*H), 123.6 (3 x *C*H), 122.7 (3 x *C*H), 107.8 (2 x *C*H), 36.7 (3 x N*C*H$_3$) ppm, Missing one 2 x NCH$_3$ resonance under d_6–DMSO solvent residual signal; ^{11}B-NMR (128 MHz, d_6–DMSO) δ 1.7 ppm; Elemental analysis: expected for $C_{38}H_{50}B2F_{15}N_{16}P_3RuS_6$ (1482.72): C, 30.78; H, 3.40; N, 15.11; found: C, 30.72; H, 3.25; N, 14.95 %;

6.5.3.2 [{κ³–[S,S,S]–(NC)Tm}Rh(COD)] (5.14)

[Dimethylammonium][(cyano)tris(methimazolyl)borate] (100 mg, 0.24 mmol, 2 eq.) and [RhCl(COD)]$_2$ (58.4 mg, 0.12 mmol, 1 eq.) were dissolved in MeOH (*ca.* 5 mL) forming a red solution which was stirred for *ca.* 1 h. After this time the solvent was completely removed *in vacuo* and toluene (*ca.* 5 mL) added to the residue. The resulting precipitate was filtered and washed with toluene (3 x 2 mL), hexane (3 x 5 mL) and dried *in vacuo* to yield the target material as an orange solid (87.3 mg, 72%): MS (EI$^+$) *m/z:* 586.8 [M$^+$]; ^{1}H-NMR

(400 MHz, $CDCl_3$) δ 6.96 (s, 3H), 6.86 (s, 3H), 4.25 (s, 4H), 3.71 (s, 9H), 2.30 (s, 4H), 1.82 (d, *J* = 7.9 Hz, 4H) ppm; ^{13}C-NMR (126 MHz, $CDCl_3$) δ 161.0 (C=S), 127.6 (q, *J* = 82.0 Hz, *C*–B), 121.9 (3 x *C*H), 120.1 (3 x *C*H), 81.1 (d, *J* = 11.4 Hz, 4 x *C*H), 35.4 (4 x CH_2), 31.3 (3 x NCH_3) ppm; Elemental analysis: expected for $C_{21}H_{27}BN_7RuS_3$ (587.40): C, 42.94; H, 4.63; N, 16.69; found: C, 42.83; H, 4.77; N, 16.66 %.

6.5.4 Palladium Complexes

6.5.4.1 Synthesis of [{κ²–[S,S]–(NC)Tm}₂Pd] (5.15)

[Dimethylammonium][(cyano)tris(methimazolyl)borate] (100.4 mg, 0.24 mmol, 2 eq.) and $PdCl_2(MeCN)_2$ (30.71 mg, 0.12 mmol, 1 eq.) were dissolved in DCM (*ca.* 5 mL) forming a red solution which was stirred for *ca.* 1 h. After this time half of the solvent was removed *in vacuo* and diethyl ether added to precipitate the product. This precipitate was filtered and washed with DCM (3 x 2 mL), diethyl ether (3 x 5 mL) and dried *in vacuo* to yield the target material as a red solid (51.5 mg, 23%). X–ray quality crystals were grown from slow cooling of a solution in $CDCl_3$. MS (EI$^+$) *m/z:* 858.0 [M$^+$]; ^{1}H-NMR (500 MHz, $CDCl_3$) δ 6.97 (s, 6H), 3.67 (s, 9H) ppm; ^{13}C-NMR (126 MHz, $CDCl_3$) δ 159.0 (*C*=S), 129.5 (br. s, *C*–B), 122.2 (br., 3 x *C*H), 120.5 (br., 3 x *C*H), 35.5 (br., 3 x NCH_3) ppm; Elemental analysis: expected for $C_{26}H_{30}B_2Cl_2N_{14}PdS_6$ (859.04): C, 36.35; H, 3.52; N, 22.83; found: C, 36.46; H, 3.59; N, 22.97 %.

6.6 X–ray crystallography.

Crystal data for the structures described within are presented in Table 6.18. Structures **2.8**, **2.11** and **4.2** were collected with with graphite–monochromated Mo–Kα radiation (λ= 0.71073 Å) on a Bruker SMART APEX II CCD diffractometer. Absorption corrections were carried out using the multi–scan procedure *SADABS*.[8] All other data sets were collected on a Agilent Technologies SuperNova diffractometer with Cu–Kα radiation (λ= 1.5418 Å) and X–ray mirror optics. Absorption corrections were carried out using the multi–scan procedure CrysAlisPro.[9] All datasets were collected at 100 K. Structure **2.21** was solved by SIR92[10] and refined by Olex2.[11] All other structures were solved by SHELXS and refined by full–matrix least squares against F^2 using SHELXL.[12] All non–hydrogen atoms were refined anisotropically, while hydrogen atoms were placed in calculated positions, constrained to ride on their parent atom with group U_{iso} values assigned [U_{iso}(H)= 1.2U_{iso} for aromatic carbons and 1.5U_{iso} for methyl atoms]. In structure **2.2** H1 (on N1) was found as a peak in the Fourier Difference map while all other hydrogens were placed as above.

Structure **2.11** contains MeCN disordered over two sites. The occupancies of each component were fixed at 0.5 after competitive refinement.

Structure **2.21** contained a disordered PF_6 moiety. The occupancies of each component were refined to approximately 0.6:0.4. The largest residual electron density peak in **2.21** is 1.42 e/Å^3 high and resides 3.065 Å from N1AA.

Structure **4.3** contains two disordered chloroform molecules in the structure both of which are modelled over two sites each. The occupancies in

each component were set at 0.5 after competitive refinement. Restraints were used to maintain sensible anisotropic displacement parameters.

Structure **5.6** was obtained from data collected from a weakly diffracting crystal (0.9 Å). The refined structure contains one *n*–butyl imidazole substituent disordered over two sites. The occupancies in each component were competitively refined to 0.54 : 0.46. The *n*–butyl chains containing C51–C54 and C51′–C54′ were refined isotropically due to severe disorder common in long alkyl chains. This structure also contains three PF_6 anions two of which are disordered over two sites. The occupancies of the sites containing P1 were set at 0.5 after competitive refinement. The occupancies of the sites containing P2 were competitively refined to 0.54 : 0.46.

Structures **2.13, 2.16, 5.6, 5.8** and **5.13** contained disordered solvent regions which were treated using the SQUEEZE routine of PLATON.[13] In **2.13** the number of electrons treated equates to 1 MeCN per formula unit. In **2.16** the number equates to 2 molecules of Et_2O and 1.5 molecules of MeOH per formula unit. The values of F(000), D, M and mu are all calculated on this assumption. In **5.6** the number of electrons removed equates to 2 molecule of MeOH and 0.75 molecules of MeCN per formula unit. In **5.8** the number of electrons removed equates to 0.625 molecules of MeOH and 0.125 molecules of MeCN per formula unit. In **5.13** the number of electrons removed equates to 1 molecule of EtOH per formula unit.

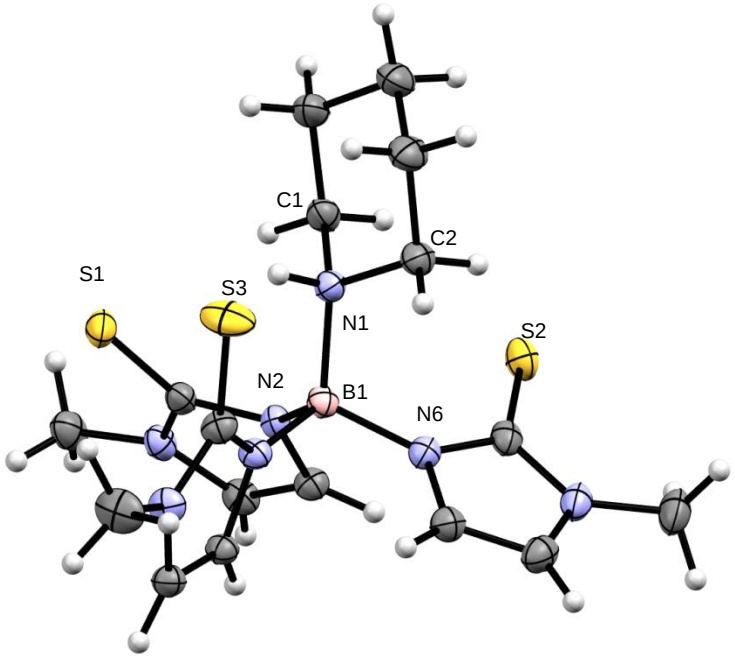

Figure 6.1: X–ray crystal structure of (piperidinium)tris(methimazolyl)borate **2.2**. Selected bond lengths and angles are provided in Table 6.1.

Table 6.1: Selected Bond lengths (Å) and Angles (°) for **2.2**.

2.2			
N1—B1	1.605 (2)	N2—B1—N6	110.19 (15)
N2—B1	1.543 (2)	N2—B1—N4	105.78 (14)
N4—B1	1.557 (3)	N6—B1—N4	106.83 (15)
N6—B1	1.552 (2)	N2—B1—N1	112.13 (15)
N1—C1	1.512 (2)	N6—B1—N1	111.59 (15)
N1—C2	1.510 (2)	N4—B1—N1	110.03 (15)
S2—C14	1.688 (2)		
S3—C10	1.6930 (19)		
S1—C6	1.6901 (19)		

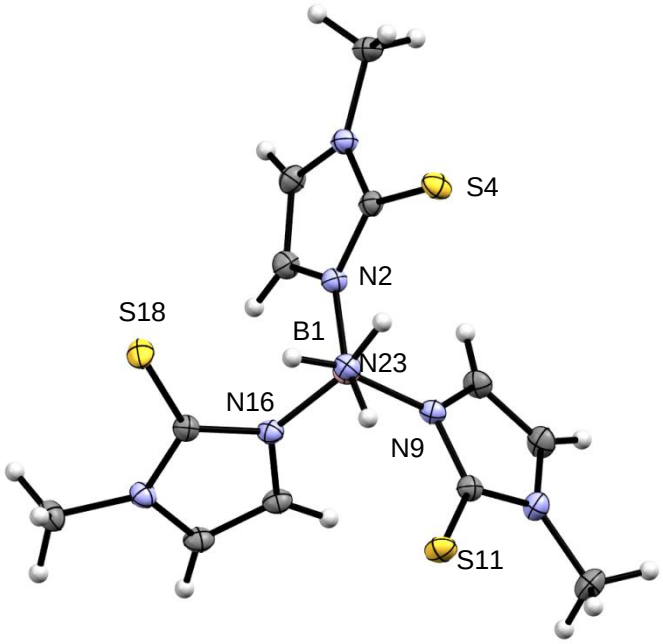

Figure 6.2: X–ray crystal structure of (ammonium)tris(methimazolyl)borate (**2.5**). One acetonitrile molecule removed for clarity. Selected bond lengths and angles are provided in

.

Table 6.2: Selected Bond lengths (Å) and Angles (°) for **2.5**.

2.5			
B1—N2	1.541 (2)	N2—B1—N9	109.62 (12)
B1—N9	1.5410 (19)	N2—B1—N16	109.34 (12)
B1—N16	1.5481 (19)	N9—B1—N16	108.57 (11)
B1—N23	1.558 (2)	N2—B1—N23	111.11 (12)
C3—S4	1.6961 (15)	N9—B1—N23	109.79 (12)
C10—S11	1.7018 (15)	N16—B1—N23	108.35 (12)
C17—S18	1.7035 (15)		

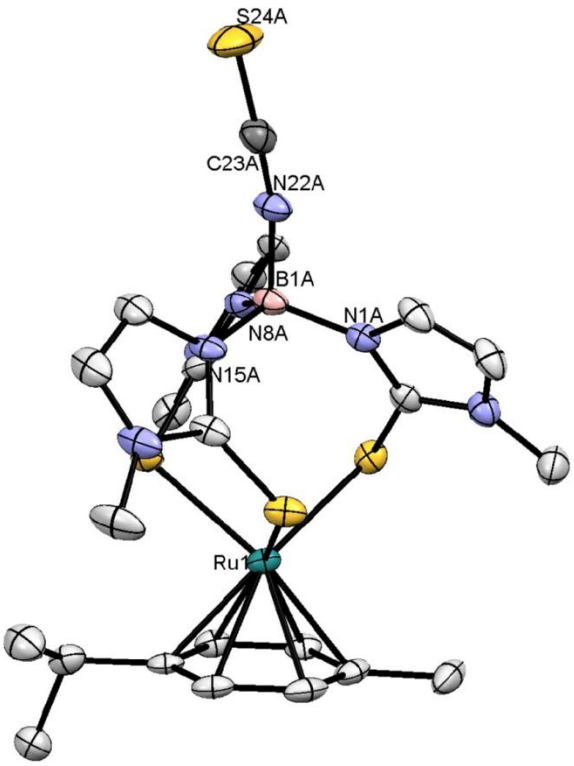

Figure 6.3. Structure of [{κ^3–[S,S,S]–(thiocyanate)–B(methimazolyl)$_3$}Ru(*p*–cymene)] (**2.8**). Hydrogen atoms and counter ion omitted for clarity. Selected bond lengths and angles are provided in Table 6.3.

Table 6.3: Selected Bond lengths (Å) and Angles (°) for **2.8**.

2.8			
Ru(1)—S(10A)	2.4208 (7)	S(10A)–Ru(1)–S(17A)	90.84 (2)
Ru(1)—S(17A)	2.4318 (6)	S(10A)–Ru(1)–S(3A)	91.67 (2)
Ru(1)—S(3A)	2.4387 (7)	S(17A)–Ru(1)–S(3A)	90.66 (2)
N(1A)—B(1A)	1.542 (4)	N(22A)–B(1A)–N(8A)	107.4 (2)
B(1A)—N(22A)	1.518 (3)	N(22A)–B(1A)–N(1A)	107.4 (2)
B(1A)—N(8A)	1.536 (4)	N(22A)–B(1A)–N(15A)	106.87 (19)
B(1A)—N(15A)	1.545 (3)	N(8A)–B(1A)–N(15A)	113.5 (2)
N(22A)—C23A)	1.156 (3)	N(1A)–B(1A)–N(15A)	110.2 (2)
C23A)—S(24A)	1.597 (3)	C(23A)–N(22A)–B(1A)	167.2 (3)
		N(22A)–C(23A)–S(24A)	178.2(3)

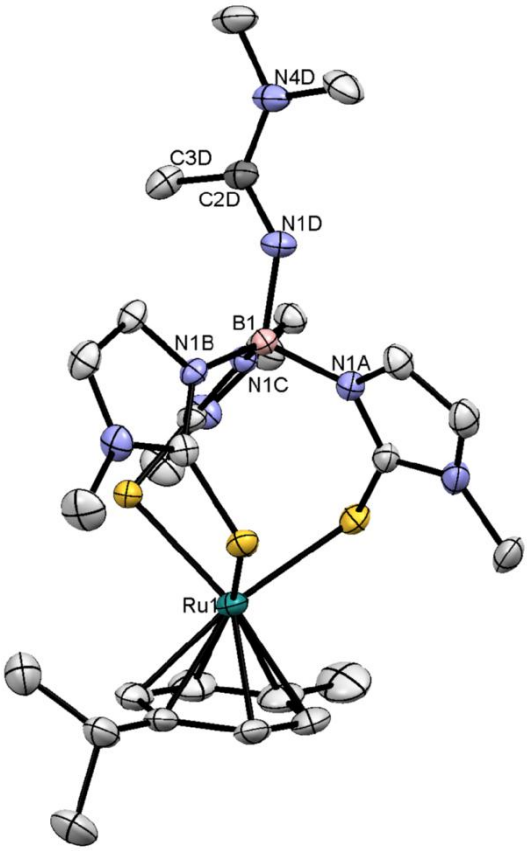

Figure 6.4. Structure of [κ^3–[S,S,S]–(*N,N*–dimethyl–acetamidine)B(methimazolyl)$_3$Ru(*p*–cymene)][PF_6]$_2$ (**2.11**). Hydrogens omitted for clarity. Selected bond lengths and angles are provided in Table 6.5.

Table 6.4: Selected Bond lengths (Å) and Angles (°) for **2.11**.

2.11			
Ru(1) S(1A)	2.4258(7)	S(1B)–Ru(1)–S(1C)	88.95(2)
Ru(1) S(1B)	2.4218(7)	S(1B)–Ru(1)–S(1A)	90.38(2)
Ru(1) S(1C)	2.4257(6)	S(1C)–Ru(1)–S(1A)	94.11(2)
B(1) N(1C)	1.541(3)	N(1C)–B(1)–N(1D)	108.64(19)
B(1) N(1D)	1.545(3)	N(1C)–B(1)–N(1A)	109.46(19)
B(1) N(1A)	1.558(3)	N(1D)–B(1)–N(1A)	105.94(19)
B(1) N(1B)	1.560(3)	N(1C)–B(1)–N(1B)	115.12(19)
N(1D) C(2D)	1.337(3)	N(1D)–B(1)–N(1B)	108.94(19)
C(2D) C(3D)	1.496(4)	N(1A)–B(1)–N(1B)	108.35(18)
C(2D) N(4D)	1.315(3)	C(2D)–N(1D)–B(1)	132.9(2)
N(4D) C(6D)	1.468(4)	N(1D)–C(2D)–C(3D)	121.5(2)
N(4D) C(5D)	1.471(4)	N(4D)–C(2D)–N(1D)	119.7(2)
		N(4D)–C(2D)–C(3D)	118.9(2)
		C(2D)–N(4D)–C(6D)	120.7(2)
		C(2D)–N(4D)–C(5D)	122.3(3)
		C(6D)–N(4D)–C(5D)	117.0(2)

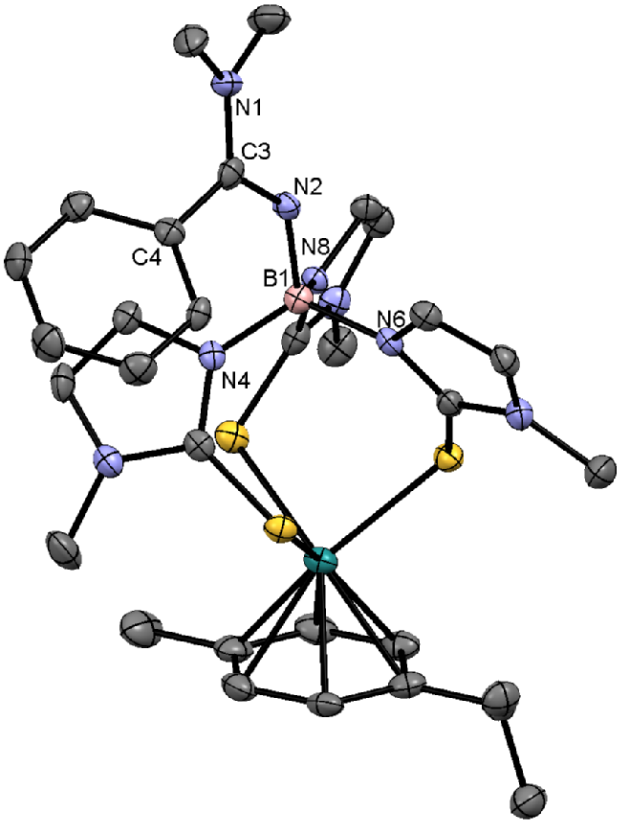

Figure 6.5: Structure of the dication in [κ^3–[S,S,S]–(*N,N*–dimethylbenzamidine)B(methimazolyl)$_3$Ru(*p*–cymene)][PF_6]$_2$ (**2.13**). PF_6 counterions and MeCN solvent omitted for clarity. Selected bond lengths and angles are provided in Table 6.4.

Table 6.5: Selected Bond lengths (Å) and Angles (°) for **2.13**.

2.13			
Ru(1)–S(3)	2.4111(11)	S(3)–Ru(1)–S(2)	88.51(4)
Ru(1)–S(2)	2.4143(11)	S(3)–Ru(1)–S(1)	95.19(4)
Ru(1)–S(1)	2.4373(11)	S(2)–Ru(1)–S(1)	89.92(4)
B(1)–N(4)	1.525(6)	N(4)–B(1)–N(2)	109.8(3)
B(1)–N(2)	1.544(5)	N(4)–B(1)–N(8)	108.0(3)
B(1)–N(8)	1.567(6)	N(2)–B(1)–N(8)	108.5(3)
B(1)–N(6)	1.580(6)	N(4)–B(1)–N(6)	117.0(3)
N(2)–C(3)	1.340(5)	N(2)–B(1)–N(6)	106.1(3)
C(3)–C(4)	1.473(6)	N(8)–B(1)–N(6)	107.3(3)
N(1)–C(3)	1.326(5)	C(3)–N(2)–B(1)	135.4(3)
N(1)–C(2)	1.461(5)	N(1)–C(3)–N(2)	118.6(4)
N(1)–C(1)	1.472(5)	N(1)–C(3)–C(4)	118.1(4)

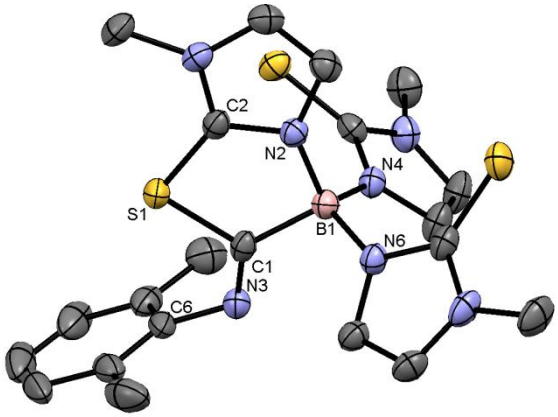

Figure 6.6: Structure of 3–bis(methimazolyl)–2–(2,6–dimethylphenylimino)–7–methyl–[1,4,3]–thiazaborolo[5,4–*b*]imidazolium (**2.15**). Hydrogen atoms omitted for clarity. Selected bond lengths and angles are provided in Table 6.6.

Table 6.6: Selected Bond lengths (Å) and Angles (°) for **2.15**.

2.15			
S1—C1	1.835 (2)	C1—S1—C2	89.37 (11)
S1—C2	1.721 (3)	C2—N2—B1	116.5 (2)
S2—C14	1.700 (3)	C4—N2—B1	136.5 (2)
S3—C18	1.686 (3)	C1—N3—C6	120.6 (2)
N1—C2	1.331 (3)	C18—N6—B1	127.2 (2)
N2—C2	1.342 (3)	C20—N6—B1	125.0 (2)
N2—B1	1.547 (3)	S1—C1—N3	120.39 (18)
N3—C1	1.255 (3)	S1—C1—B1	112.56 (17)
N3—C6	1.431 (3)	N3—C1—B1	126.8 (2)
N4—B1	1.535 (4)	S1—C2—N1	129.47 (19)
N6—B1	1.537 (3)	S1—C2—N2	120.32 (19)
C1—B1	1.652 (3)	N2—B1—C1	101.23 (19)
		N4—B1—C1	108.1 (2)
		N6—B1—C1	111.36 (19)

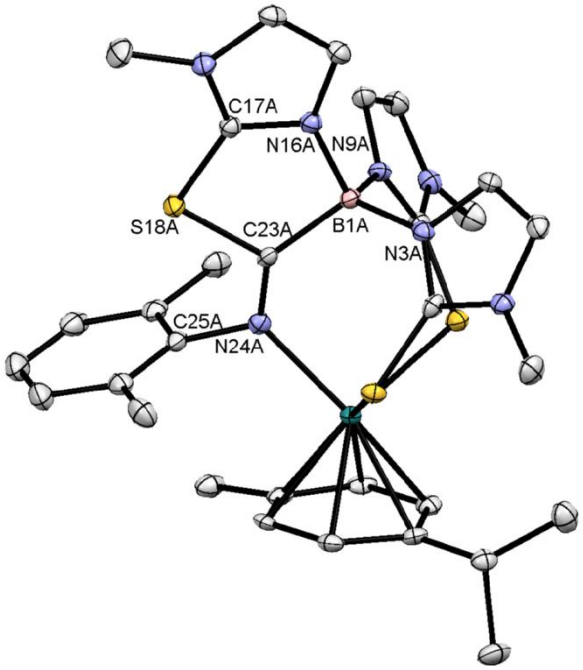

Figure 6.7: Structure of the dication in [{κ^3[N,S,S]–3–bis(methimazolyl)–2–(2,6–dimethylphenylimino)–7–methyl–[1,4,3]–thiazaborolo[5,4–*b*]imidazolium}Ru(*p*–cymene)] $[PF_6]_2$ (**2.16**). Hydrogen atoms and PF_6^- counterions omitted for clarity. Selected bond lengths and angles are provided in Table 6.7.

Table 6.7: Selected Bond lengths (Å) and Angles (°) for **2.16**.

2.16			
Ru(1)–N(24A)	2.1127(19)	N24A–Ru1–S4A	83.15(6)
Ru(1)–S(4A)	2.4147(6)	N(24A)–Ru(1)–	95.17(5)
Ru(1)–S(11A)	2.4156(6)	S(4A)–Ru(1)–S(11A)	95.15(2)
B(1A)–N(9A)	1.533(3)	N(9A)–B(1A)–N(3A)	109.67(18)
B(1A)–N(3A)	1.535(3)	N(9A)–B(1A)–	109.42(19)
B(1A)–N(16A)	1.561(3)	N(3A)–B(1A)–	109.57(19)
B(1A)–C(23A)	1.658(3)	N(9A)–B(1A)–	105.43(19)
N(16A)–C(17A)	1.325(3)	N(3A)–B(1A)–	120.62(19)
C(17A)–S(18A)	1.731(2)	N(16A)–B(1A)–	1 01.54(17)
S(18A)–C(23A)	1.791(2)	C(17A)–N(16A)–	115.40(19)
C(17A)–N(19A)	1.322(3)	C17A–N16A–C22A	106.77(19)
C(23A)–N(24A)	1.283(3)	C23A–N24A–Ru1	125.60(16)
N(24A)–C(25A)	1.452(3)	C25A–N24A–Ru1	118.07(14)
		N24A–C23A–B1A	130.5(2)
		C23A–N24A–C25A	115.70(19)
		N19A–C17A–S18A	129.07(18)
		C17A–S18A–C23A	90.30(11)

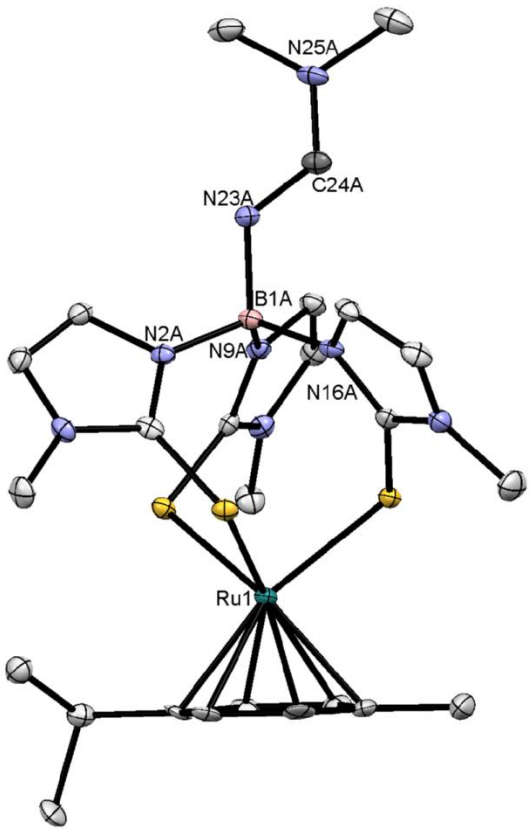

Figure 6.8: Structure of the dication in [κ^3–[S,S,S]–(*N,N*–dimethylformamidine)B(methimazolyl)$_3$Ru(*p*–cymene)][PF_6]$_2$ (**2.18**). PF_6 counterions and MeCN solvent omitted for clarity. Selected bond lengths and angles are provided in Table 6.8.

Table 6.8: Selected Bond lengths (Å) and Angles (°) for **2.18**.

2.18			
Ru(1)–S(11A)	2.4224(10)	S(11A)–Ru(1)–	92.18(4)
Ru(1)–S(18A)	2.4296(11)	S(11A)–Ru(1)–S(4A)	89.53(4)
Ru(1)–S(4A)	2.4351(11)	S(18A)–Ru(1)–S(4A)	91.28(4)
B(1A)–N(16A)	1.536(6)	N16A–B1A–N2A	110.5(4)
B(1A)–N(2A)	1.546(6)	N16A–B1A–N23A	107.2(3)
B(1A)–N(23A)	1.549(6)	N2A–B1A–N23A	107.5(4)
B(1A)–N(9A)	1.556(6)	N16A–B1A–N9A	112.2(4)
N(23A)–C(24A)	1.323(6)	N2A–B1A–N9A	110.8(3)
C(24A)–N(25A)	1.306(6)	N23A–B1A–N9A	108.4(3)
N(25A)–C(26A)	1.463(6)	C24A–N23A–B1A	125.5(4)
N(25A)–C(27A)	1.466(6)	N25A–C24A–N23A	125.0(4)
		C24A–N25A–C26A	121.3(4)
		C24A–N25A–C27A	120.9(4)
		C26A–N25A–C27A	117.7(4)

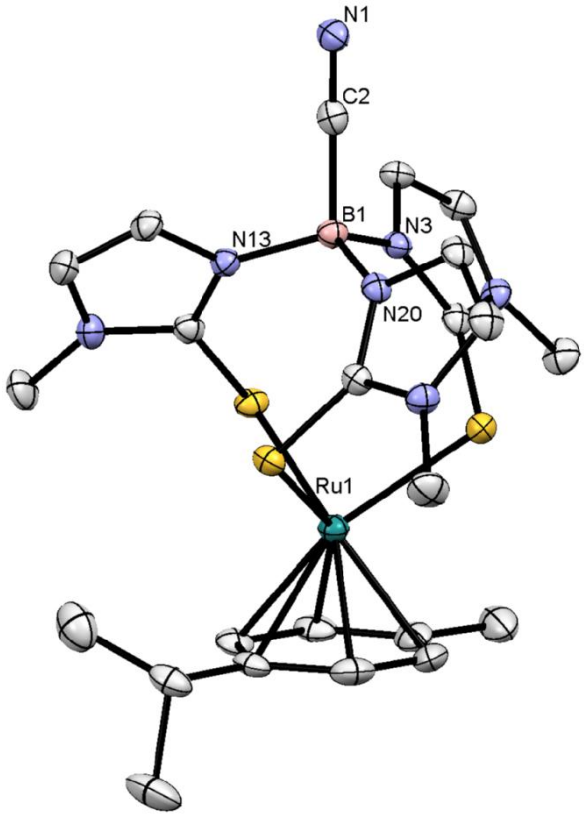

Figure 6.9: X–ray crystal structure of [κ^3–[S,S,S]–(cyano)B(methimazolyl)$_3$Ru(*p*–cymene)] [PF_6] (**2.21**). Hydrogens and an acetonitrile molecule removed for clarity. Selected bond lengths and angles provided in Table 6.9.

Table 6.9: Selected Bond lengths (Å) and Angles (°) for **2.21**.

2.21			
Ru(1) – S(12)	2.4331 (9)	S12–Ru1–S26	91.85 (3)
Ru(1) – S(19)	2.4356 (9)	S26–Ru1–S19	91.88 (3)
Ru(1) – S(26)	2.4340 (9)	S12–Ru1–S19	91.08 (3)
B(1)–C(2)	1.624 (5)	N3–B1–N13	111.3 (3)
B(1)–N(3)	1.535 (4)	N3–B1–N20	111.9 (3)
B(1)–N(13)	1.540 (4)	N13–B1–N20	113.0 (3)
B(1)–N(20)	1.551 (4)	N3–B1–C2	106.3 (3)
N(1)–C(2)	1.143 (4)	N13–B1–C2	107.1 (3)
		N20–B1–C2	106.8 (3)
		N1–C2–B1	178.5 (3)

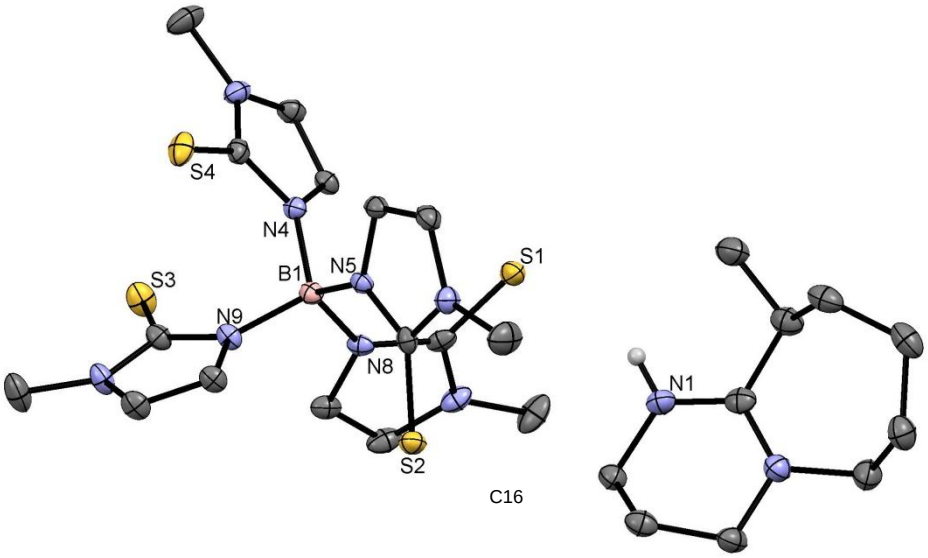

Figure 6.10: X–ray crystal structure of $[6\text{–MeDBUH}]^{+}[B(mt)_4]^{-}$ (**3.6**). All hydrogens except H1 removed for clarity. Selected bond lengths and angles shown in Table 6.10.

Table 6.10: Selected Bond lengths (Å) and Angles (°) for **3.6**.

3.6			
S1—C16	1.703 (2)	N4—B1—N9	109.75 (18)
S2—C13	1.694 (2)	N4—B1—N5	109.79 (17)
S3—C21	1.693 (2)	N9—B1—N5	110.38 (17)
S4—C12	1.693 (2)	N4—B1—N8	108.01 (17)
N4—B1	1.550 (3)	N9—B1—N8	108.77 (17)
N5—B1	1.557 (3)	N5—B1—N8	110.10 (18)
N8—B1	1.558 (3)		
N9—B1	1.550 (3)		

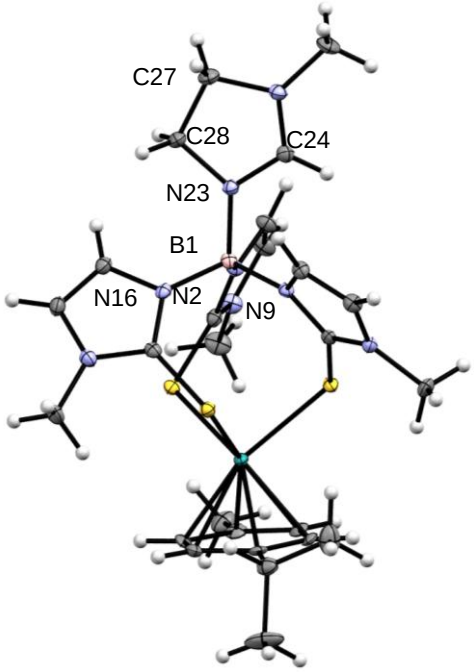

Figure 6.11: X–Ray crystal structure showing the cation of **3.8**. Hydrogens, counter ions and one DCM molecule excluded for clarity. Selected bond lengths and angles shown in Table 6.11.

Table 6.11: Selected Bond lengths (Å) and Angles (°) for **3.8**.

3.8			
Ru1—S4	2.4172 (6)	S4—Ru1—S11	89.93 (2)
Ru1—S11	2.4266 (6)	S4—Ru1—S18	91.28 (2)
Ru1—S18	2.4544 (6)	S11—Ru1—S18	92.86 (2)
B1—N23	1.551 (3)	N23—B1—N9	104.61 (19)
B1—N9	1.552 (3)	N23—B1—N2	108.7 (2)
B1—N2	1.557 (3)	N9—B1—N2	113.5 (2)
B1—N16	1.559 (3)	N23—B1—N16	110.9 (2)
C3—S4	1.732 (3)	N9—B1—N16	111.0 (2)
C10—S11	1.726 (3)	N2—B1—N16	108.1 (2)
		B1 —N23 —C24	123.7 (2)
		B1 —N23 —C28	128.7(2)

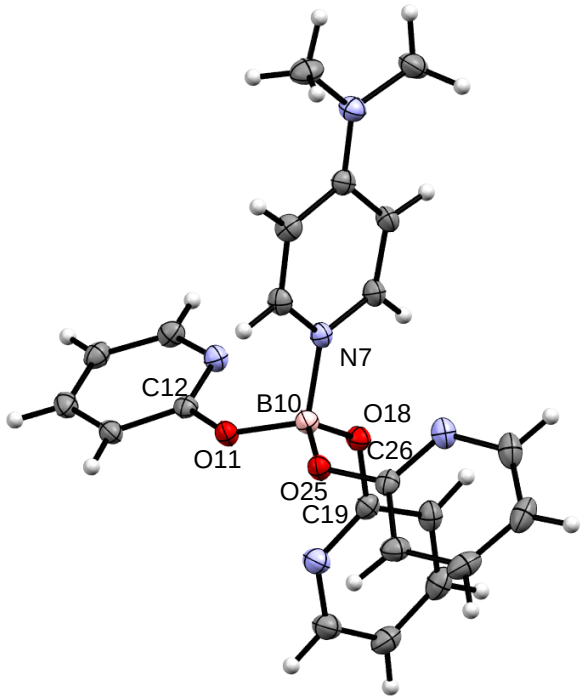

Figure 6.12: X–ray crystal structure of (DMAP)Thp (**4.2**). Selected bond lengths and angles shown in Table 6.12.

Table 6.12: Selected Bond lengths (Å) and Angles (°) for **4.2**.

4.2			
N7—B10	1.5928 (16)	O18—B10—O11	118.00 (10)
B10—O18	1.4518 (15)	O18—B10—O25	113.93 (10)
B10—O11	1.4578 (15)	O11—B10—O25	101.09 (9)
B10—O25	1.4641 (15)	O18—B10—N7	104.58 (9)
		O11—B10—N7	108.93 (9)
		O25—B10—N7	110.27 (9)
		C12—O11—B10	126.56 (9)
		C19—O18—B10	125.13 (9)
		C26—O25—B10	124.14 (9)

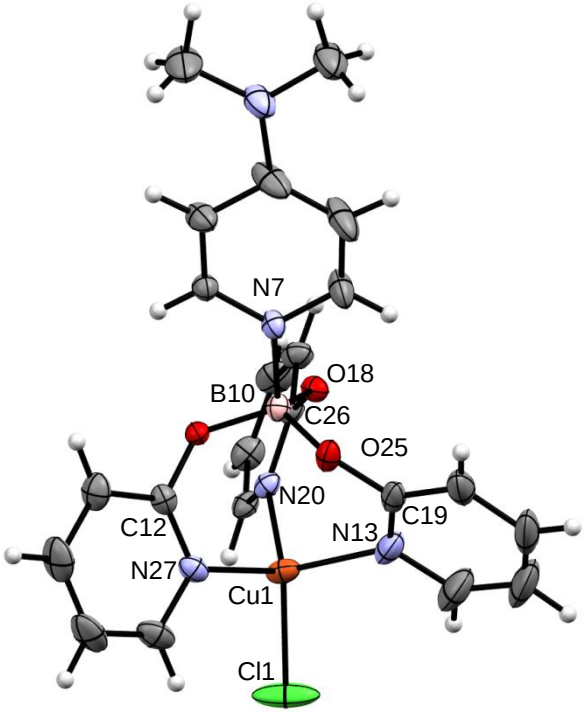

Figure 6.13: X–ray crystal structure of (DMAP)ThpCuCl (**4.3**). Selected bond lengths and angles shown in Table 6.13**.**

Table 6.13: Selected Bond lengths (Å) and Angles (°) for **4.3**.

4.3			
N7—B10	1.609 (4)	O18—B10—O11	113.5 (2)
B10—O18	1.461 (3)	O18—B10—O25	113.3 (2)
B10—O11	1.457 (4)	O11—B10—O25	115.6 (2)
B10—O25	1.443 (4)	O18—B10—N7	104.9 (2)
Cu1—Cl1	2.3033 (9)	O11—B10—N7	103.2 (2)
Cu1—N13	2.034 (3)	O25—B10—N7	104.7 (2)
Cu1—N20	2.036 (2)	C12—O11—B10	127.9 (2)
Cu1—N27	2.025 (2)	C19—O18—B10	128.2 (2)
		C26—O25—B10	128.4 (2)
		Cl1—Cu1—N13	109.52 (9)
		Cl1—Cu1—N20	111.94 (7)
		N13—Cu1—N20	105.58 (10)
		Cl1—Cu1—N27	107.77 (8)
		N13—Cu1—N27	112.36 (11)
		N20—Cu1—N27	109.72 (10)

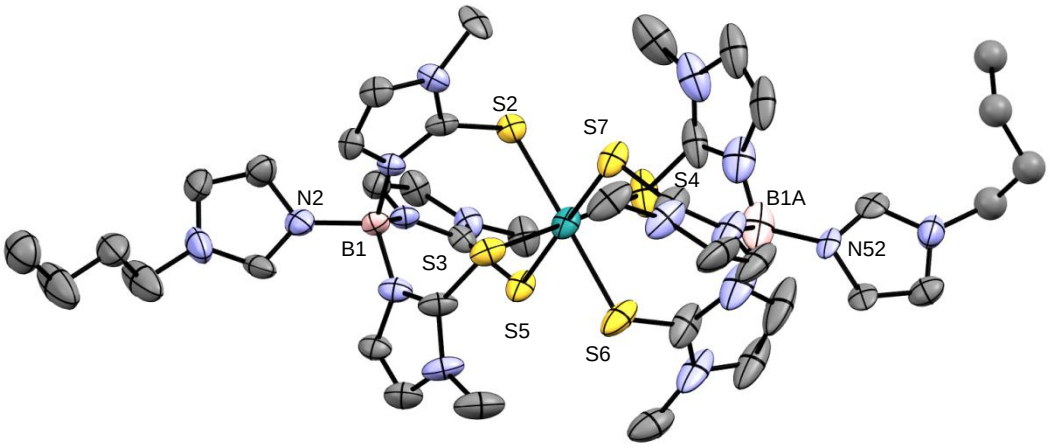

Figure 6.14: X–ray crystal structure of the cation of **5.6**. Hydrogens, counterions and one acetonitrile molecule removed for clarity. Selected bond lengths and angles are shown in Table 6.14.

Table 6.14: Selected Bond lengths (Å) and Angles (°) for **5.6**.

5.6			
S2—Ru	2.397 (2)	S4—Ru—S2	89.04 (8)
S3—Ru	2.380 (2)	S3—Ru—S2	90.86 (8)
S4—Ru	2.377 (3)	S4—Ru—S6	91.26 (9)
S5—Ru	2.426 (2)	S3—Ru—S6	88.86 (9)
S6—Ru	2.399 (3)	S4—Ru—S5	84.26 (9)
S7—Ru	2.432 (3)	S3—Ru—S5	96.89 (9)
N3—B1	1.548 (12)	S2—Ru—S5	96.90 (8)
N5—B1	1.544 (12)	S6—Ru—S5	82.23 (10)
N7—B1	1.527 (12)	S4—Ru—S7	95.53 (9)
B1—N2	1.574 (12)	S3—Ru—S7	83.31 (9)
N9—B1A	1.55 (2)	S2—Ru—S7	82.71 (10)
B1A—N52	1.534 (18)	S6—Ru—S7	98.16 (12)
B1A—N13	1.584 (19)	N7—B1—N5	107.5 (7)
B1A—N52'	1.66 (2)	N7—B1—N3	112.9 (7)
B1A —N11	1.549(17)	N5—B1—N3	115.7 (7)
		N7—B1—N2	111.4 (7)
		N5—B1—N2	106.7 (7)
		N3—B1—N2	102.5 (7)
		N52—B1A—N9	120.0 (13)
		N52—B1A—N11	99.4 (11)
		N9—B1A—N11	115.2 (11)
		N52—B1A—N13	101.8 (11)
		N9—B1A—N13	107.2 (10)
		N11—B1A—N13	112.6 (13)
	– –	N9—B1A—N52'	93.2 (13)
		N11—B1A—N52'	109.4 (13)
		N13—B1A—N52'	117.9 (13)

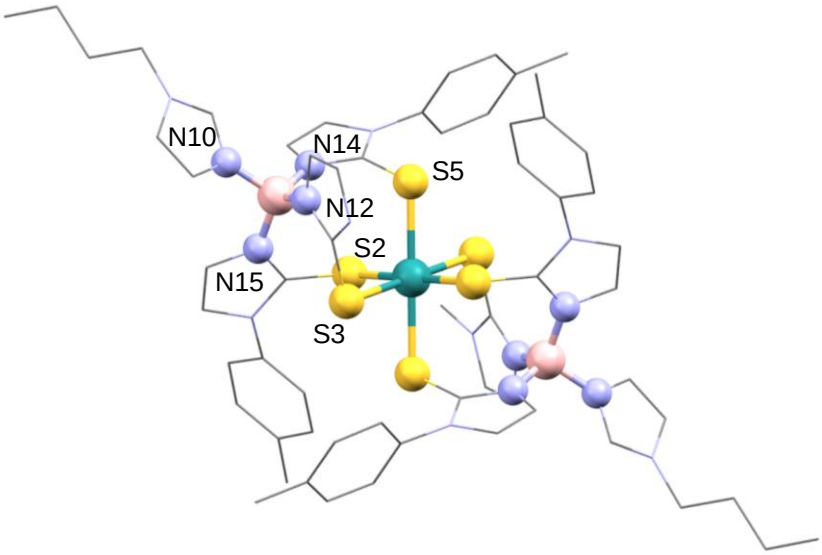

Figure 6.15: Ball and Stick plot of the X–ray crystal structure of the cation in **5.8**. Two tolyl substitutents have been removed for clarity along with the hydrogens and three [PF_6] counterions. Selected Bond lengths and angles are shown in Table 6.15.

Table 6.15: Selected Bond lengths (Å) and Angles (°) for **5.8**.

		5.8	
Ru—S2	2.3460 (9)	S2—Ru—S3^{i}	86.13 (3)
Ru—S3	2.4191 (10)	S2—Ru—S3	93.87 (3)
Ru—S5	2.4539 (10)	S2^{i}—Ru—S5	87.22 (3)
N10—B55	1.587 (6)	S2—Ru—S5	92.78 (3)
N12—B55	1.549 (6)	S3—Ru—S5	98.32 (3)
N14—B55	1.534 (6)	S3—Ru—S5^{i}	81.68 (3)
N15—B55	1.564 (6)	N14—B55—N12	112.0 (4)
		N14—B55—N15	108.3 (3)
		N12—B55—N15	116.8 (4)
		N14—B55—N10	109.7 (3)
		N12—B55—N10	102.0 (3)
		N15—B55—N10	107.7 (4)

Symmetry code(s): (i) $-x, -y, -z$.

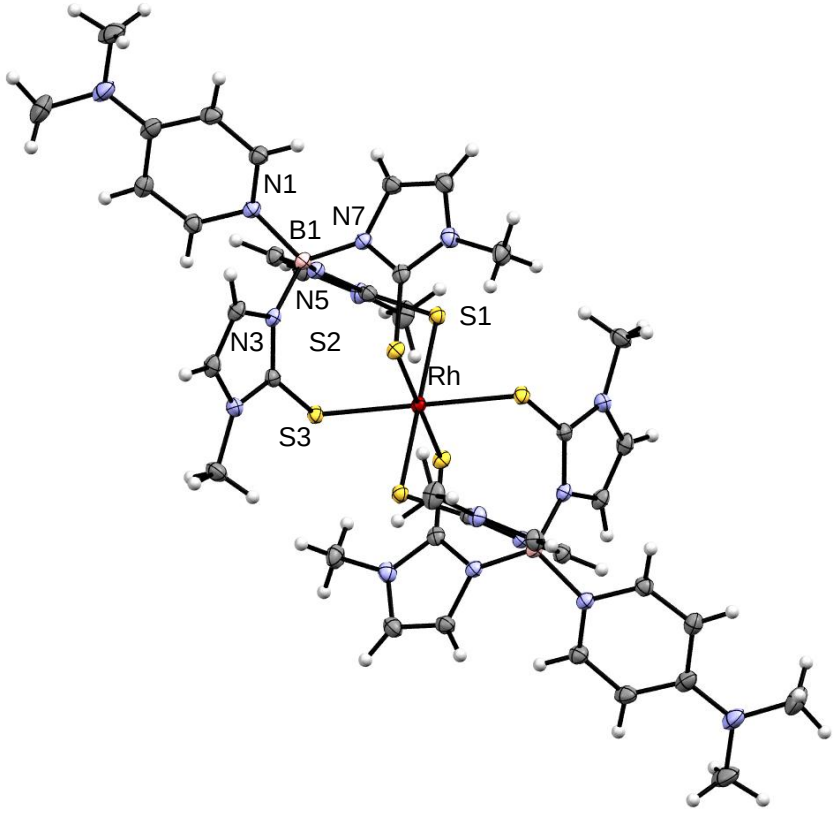

Figure 6.16: X–ray crystal structure of the cation of **5.13**. Hydrogens and counterions removed for clarity. Selected bond lengths and angles are shown in Table 6.16.

Table 6.16: Selected Bond lengths (Å) and Angles (°) for **5.13**.

5.13			
Rh01—S1	2.3746 (4)	S1—Rh01—S2	92.554 (15)
Rh01—S2	2.3862 (4)	S1—Rh01—S2^{i}	87.446 (15)
Rh01—S3	2.4021 (4)	S1^{i}—Rh01—S3^{i}	95.963 (15)
S2—C12	1.7199 (19)	S1—Rh01—S3^{i}	84.037 (15)
S3—C8	1.7320 (19)	S2—Rh01—S3^{i}	82.572 (15)
S1—C16	1.7316 (19)	S1^{i}—Rh01—S3	84.038 (15)
N3—B1	1.535 (2)	S1—Rh01—S3	95.962 (15)
N7—B1	1.562 (3)	S2^{i}—Rh01—S3	82.572 (15)
N1—B1	1.593 (2)	S2—Rh01—S3	97.428 (15)
N5—B1	1.547 (2)	N3—B1—N5	112.83 (15)
		N3—B1—N7	108.01 (15)
		N5—B1—N7	114.12 (15)
		N3—B1—N1	110.32 (14)
		N5—B1—N1	102.37 (14)
		N7—B1—N1	109.05 (14)

Symmetry code(s): (i) −*x*, −*y*, −*z*.

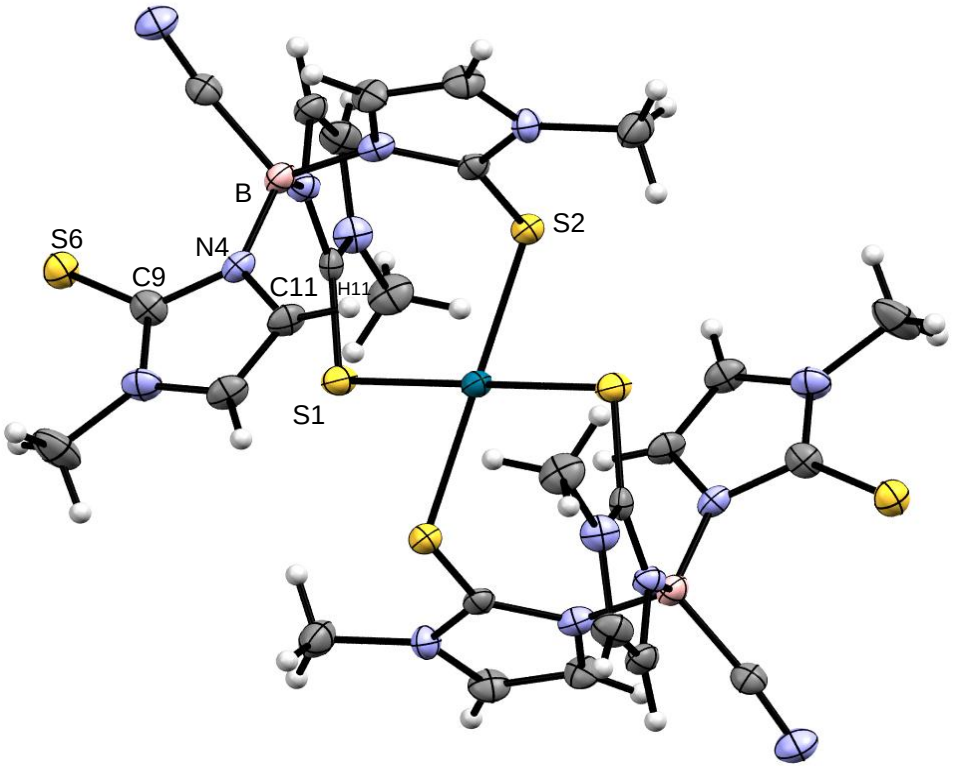

Figure 6.17: X–Ray crystal structure of **5.15**. Solvent molecules omitted for clarity. Selected bond lengths and angles shown in Table 6.17.

Table 6.17: Selected Bond lengths (Å) and Angles (°) for **5.15**.

5.15			
C9—S6	1.698 (4)	C1—S1—Pd	104.84 (14)
C13—N7	1.143 (5)	C5—S2—Pd	102.10 (15)
C13—B	1.622 (7)	S1—Pd—S2	84.87 (4)
N1—B^{i}	1.548 (7)	S1^{i}—Pd—S2	95.13 (4)
N3—B	1.571 (6)	S1^{i}—Pd—S2^{i}	84.87 (4)
N5—B	1.526 (6)	N5—B—N1^{i}	115.5 (4)
S1—Pd	2.3330 (11)	N5—B—N3	108.0 (3)
Pd—S1^{i}	2.3330 (11)	N1^{i}—B—N3	110.5 (4)
Pd—S2^{i}	2.3389 (11)	N5—B—C13	111.5 (4)
B—N1^{i}	1.548 (7)	N1^{i}—B—C13	105.8 (3)
		N3—B—C13	105.1 (3)

Symmetry code(s): (i) −*x*, −*y*, −*z*.

Table 6.18: X–Ray crystallography experimental details.

	2.2	**2.5**	**2.8**	**2.11**
Chemical formula	$C_{17}H_{26}BN_7S_3$	$C_{14}H_{21}BN_8S_3$	$C_{57}H_{77}B_2O_4N_7RuS_4$	$C_{28}H_{47}BF_{12}N_9P_2RuS_3$
M_r	435.44	408.38	1159.16	1001.70
Crystal system	Orthorhombic	Monoclinic	Monoclinic	Monoclinic
Space Group	$P2_12_12_1$	$P2_1/c$	I2/a	$P2_1/c$
a (Å)	10.6912 (2)	12.57438 (13)	16.1020 (4)	16.72141 (12)
b (Å)	13.2418 (2)	7.13533 (9)	25.7120 (7)	12.89427 (8)
c (Å)	14.9781 (2)	22.1766 (2)	27.9161 (9)	20.16553 (14)
β (°)	–	97.6823 (9)	105.768 (1)	95.5773 (7)
V (Å^3)	2120.46 (6)	1971.88 (4)	11122.8 (5)	4327.31 (5)
Z	4	4	8	4
μ (mm^{-1})	3.34	3.57	0.48	0.67
T_{min}, T_{max}	0.565, 0.871	0.525, 1.0	0.657, 0.746	0.943, 1.0
Ind. Refl.	4377	4092	12310	11145
R_{int}	0.023	0.031	0.064	0.027
R[$F^2 > 2\sigma(F^2)$],	0.022	0.032	0.042	0.042
wR(F^2),	0.060	0.086	0.096	0.111
S	1.04	1.08	1.09	1.05
Δ_{max},Δ_{min}(e Å^{-3})	0.18, –0.18	0.39, –0.27	0.89, –0.85	1.21, –1.11
	2.13	**2.15**	**2.16**	**2.18**
Chem. formula	$C_{68}H_{91}B_2F_{24}N_{19}P_4Ru_2S_6$	$C_{21}H_{24}BN_7S_3$	$C_{31}H_{38}BF_{12}N_7P_2RuS_3$	$C_{25}H_{37}BF_{12}N_8P_2RuS_3$
M_r	2170.60	481.46	1006.68	947.63
Crystal system	Monoclinic	Orthorhombic	Monoclinic	Triclinic
Space Group	$P2_1/c$	$P2_12_12_1$	$P2_1/n$	$P\bar{1}$
a (Å)	17.0566 (3)	10.8256 (2)	13.5789(4)	12.72(2)
b (Å)	13.0618 (2)	13.4721 (3)	14.2055(5)	17.0209(3)
c (Å)	19.9834 (3)	16.4802 (3)	19.7712(8)	18.7739(3)
α(°)	–	–	–	110.562(2)
β(°)	91.993 (1)	–	90	1.114(1)
γ(°)	–	–	–	97.616 (1)
V (Å3)	4449.41 (12)	2403.53 (8)	3813.7(2)	3662.46(10)
Z	2	4	4	4
μ (mm^{-1})	0.66	3.01	6.53	6.75
T_{min}, T_{max}	0.678, 0.745	0.687, 0.9	0.832, 1.0	0.829, 1.0
Ind. Refl.	9083	4854	7570	14453
R_{int}	0.074	0.067	0.042	0.058
R[$F^2 > 2\sigma(F^2)$]	0.051	0.039	0.029	0.039
wR(F^2)	0.126	0.102	0.080	0.108
S	1.04	1.04	1.05	1.06
Δ_{max}, Δ_{min} (eÅ^{-3})	1.57, –0.87	0.35, –0.31	0.58, –0.67	1.42, –1.37

	2.21	**3.6**	**3.8**
Chemical formula	$C_{48}H_{61}B_2F_{12}N_{15}P_2Ru_2S_6$	$C_{26}H_{39}BN_{10}S_4$	$C_{27}H_{39}BCl_2F_{12}N_8P_2RuS_3$
M_r	1554.18	630.72	1044.56
Crystal system	Triclinic	Monoclinic	Triclinic
Space Group	$P\bar{1}$	$P2_1/n$	$P\bar{1}$
a (Å)	10.0598(3)	11.4406 (2)	12.4715 (4)
b (Å)	16.6932(4)	20.0212 (4)	12.7829 (4)
c (Å)	19.9429(5)	13.7498 (3)	14.8288 (3)
α(°)	76.356(1)	–	66.864 (2)
β(°)	85.925(1)	91.550 (1)	88.916 (2)
γ(°)	75.842(1)	–	66.201 (3)
V (Å^3)	3155.34(14)	3148.30 (11)	1961.48 (10)
Z	2	4	2
μ (mm^{-1})	0.84	0.34	7.60
T_{min}, T_{max}	0.811, 0.923	0.875, 0.977	0.569, 1.0
Ind. Refl.	12924	6337	8187
R_{int}	0.045	0.046	0.067
$R[F^2 > 2\sigma(F^2)]$	0.040	0.042	0.037
$wR(F^2)$	0.101	0.108	0.097
S	1.03	1.06	1.05
Δ_{max}, Δ_{min} (e Å^{-3})	1.44, –0.58	0.42, –0.31	1.48, –0.99

	4.2	**4.3**	**5.6**
Chemical formula	$C_{22}H_{22}BN_5O_3$	$C_{24}H_{24}BCl_7CuN_5O_3$	$C_{40}H_{57}B_2F_{18}N_{17}P_3RuS_6$
M_r	415.26	753.01	1525.98
Crystal system	Monoclinic	Monoclinic	Monoclinic
Space Group	$P2_1/n$	$P2_1/c$	$P2_1/c$
a (Å)	11.5746 (2)	8.5238 (2)	21.6714 (7)
b (Å)	10.6207 (2)	16.9403 (5)	18.3557 (6)
c (Å)	16.5475 (3)	21.7245 (6)	17.4348 (5)
β(°)	93.599 (1)	91.247 (3)	95.030 (2)
V (Å^3)	2030.18 (6)	3136.17 (16)	6908.7 (4)
Z	4	4	4
μ (mm^{-1})	0.09	6.78	5.01
T_{min}, T_{max}	0.886, 0.985	0.35, 0.50	0.624, 0.877
Ind. Refl.	5167	6197	9923
R_{int}	0.037	0.051	0.097
$R[F^2 > 2\sigma(F^2)]$	0.039	0.057	0.089
$wR(F^2)$	0.1	0.144	0.270
S	1.07	1.	1.07
Δ_{max}, Δ_{min} (e Å^{-3})	0.29, –0.24	1.20, –1.15	2.24, –1.04

	5.8	**5.13**	**5.15**
Chemical formula	$C_{74}H_{78}B_2F_{18}N_{16}P_3RuS_6$	$C_{42}H_{56}B_2F_{18}N_{18}P_3RhS_6$	$C_{32}H_{36}B_2Cl_{18}N_{14}PdS_6$
M_r	1941.49	1564.85	1575.29
Crystal system	Monoclinic	Triclinic	Monoclinic
Space Group	$P2_1/n$	$P\bar{1}$	$P2_1/n$
a (Å)	10.4293 (2)	9.7354 (3),	15.2678 (5),
b (Å)	25.9269 (4)	9.9613 (3)	11.8506 (4),
c (Å)	17.5308 (3)	16.6355 (7)	17.0134 (8)
α(°)	–	99.986 (3)	–
β(°)	102.999 (2)	91.995 (3)	92.756 (4)
γ(°)	–	90.774 (3)	–
V (Å^3)	4618.84 (14)	1587.55 (10)	3074.7 (2)
Z	2	1	2
μ (mm^{-1})	3.88	5.65	1.33
T_{min}, T_{max}	0.574, 1.0	0.139, 0.601	0.923, 1.136
Independent	9297	6197	5626
R_{int}	0.077	0.0264	0.087
$R[F^2 > 2\sigma(F^2)]$	0.075	0.028	0.047
$wR(F^2)$	0.225	0.075	0.107
S	1.05	1.05	1.02
Δ_{max}, Δ_{min} (e Å^{-3})	2.82, –0.99	0.68, –1.02	0.87, –0.71

6.7 References

1. Bailey, P. J.; Lorono-Gonzales, D.; McCormack, C.; Millican, F.; Parsons, S.; Pfeifer, R.; Pinho, P. P.; Rudolphi, F.; Sanchez Perucha, A., *Chem. Eur. J.,* **2006**, *12*, 5293.
2. Martinsen, A.; Songstad, J., *Acta Chem. Scand. A,* **1977**, *31*, 645.
3. Dominianni, S. J.; Yen, T. T., *J. Med. Chem.,* **1989**, *32*, 2301.
4. Jensen, S. B.; Rodger, S. J.; Spicer, M. D., *J. Organomet. Chem.,* **1998**, *556*, 151.
5. Komiya, S.; Hurano, M. *Synthesis of Organometallic Compounds*; 1 ed.; John Wiley and Sons: London, 1997; Vol. 1.
6. Bedford, C. D.; Harris, R. N., III; Howd, R. A.; Goff, D. A.; Koolpe, G. A.; Petesch, M.; Koplovitz, I.; Sultan, W. E.; Musallam, H. A., *J. Med. Chem.,* **1989**, *32*, 504.
7. Matsuda, K.; Yanagisawa, I.; Isomura, Y.; Mase, T.; Shibanuma, T., *Synth. Commun.,* **1997**, *27*, 3565.
8. Lan-Chang, L., *Coord. Chem. Rev,* **2006**, *250*, 1152.
9. CrysAlis PRO, Oxford Diffraction Ltd. UK, 2007..
10. Altomare, A.; Cascarano, G.; Giacovazzo, C.; Guagliardi, A. J., *Appl. Cryst. ,* **1993**, *26*, 343.
11. Dolomanov, O. V.; Bourhis, L. J.; Gildea, R. J.; Howard, J. A. K.; Puschmann, H., *J. Appl. Cryst.,* **2009**, *42*,.
12. SHELXL, G. M. Sheldrick, 1998
13. Spek, A. L.; Sluis, P. v. d., *Acta Cryst. A,* **1990**, *46*, 194.